

Design and optimization of naturally inspired enzymatic cascades for the synthesis of platform chemicals from C1-compounds and biomass sources

Vivian Pascal Willers

Vollständiger Abdruck der von dem TUM Campus Straubing für Biotechnologie und Nachhaltigkeit der Technischen Universität München zur Erlangung eines

Doktors der Naturwissenschaften (Dr. rer. nat.)

genehmigten Dissertation.

Vorsitz: Prof. Dr. Bastian Blombach

Prüfende der Dissertation:

1. Prof. Dr. Volker Sieber
2. Prof. Dr. Henrike Niederholtmeyer
3. Prof. Dr. Harald Gröger

Die Dissertation wurde am 26.01.2024 bei der Technischen Universität München eingereicht und durch den TUM Campus Straubing für Biotechnologie und Nachhaltigkeit am 03.09.2024 angenommen.

*"In der grossen Verkettung von Ursachen und Wirkungen darf
kein Stoff, keine Thätigkeit isolirt betrachtet werden."*

Alexander von Humbold

Ideen zu einer Geographie der Pflanzen nebst einem Naturgemälde der
Tropenländer, mit A. Bonpland, Cotta, Tübingen 1807, S. 39

Übernommen aus Wikiquote (letzte Aktualisierung 06.06.2023)

Table of Contents

List of Publications	iv
Summary.....	v
Zusammenfassung	vii
Acknowledgements	ix
1. Introduction	1
1.1. Future resources for chemistry and energy supply	1
1.1.1. Chemicals and fuels from lignocellulosic biomass	2
1.1.2. Carbon dioxide as a resource	5
1.2. Chemical industry of the future: transformation from petroleum based to bio-based processes	8
1.2.1. Comparison of <i>in vitro</i> and <i>in vivo</i> enzyme cascades as tools for industrial chemical production	8
1.1.1. Enzymes in industrial application	10
1.3. Cell-free multi-enzyme cascades as proof of concept for the production of platform chemicals	12
1.3.1. The concept of <i>in vitro</i> multi-enzymatic cascade systems	12
1.3.2. From scratch to trial: Enzymatic pathway design	13
1.3.3. Enzyme specificity vs. promiscuity	15
1.4. Aim of this work	17
1.4.1. Development of an enzymatic cascade for the utilization of xylose and CO ₂ for biofuel production	18
1.4.2. Development of an enzymatic cascade for the utilization of CO ₂ for L-Alanine production	18
2. Materials and Methods	20
2.1. Materials	20
2.1.1. Devices	20
2.1.2. Software and Databases	25
2.1.3. Chemicals	26
2.1.4. Buffers and Media	29
2.1.5. Kits	29
2.1.6. Commercial enzymes used for enzymatic assays	30
2.1.7. Commercial enzymes used for molecular biology and purification	31
2.1.8. Bacterial strains	32
2.1.9. Oligonucleotides	34
2.1.10. Plasmids	36
2.2. Methods	40
2.2.1. DNA manipulation methods	40
2.2.2. Protein production	47

2.2.3.	Enzymatic activity determination via NAD(P)H detection.....	56
2.2.4.	Enzyme kinetic measurements	60
2.2.5.	Enzyme thermostability analysis	61
2.2.6.	Enzyme stability with the addition of formaldehyde and isobutanol	63
2.2.7.	Enzyme regulation and inhibition measurements.....	65
2.2.8.	Thermodynamics pathway analysis using eQuilibrator.....	66
2.2.9.	Cascade reactions	66
2.2.10.	Quantification via gas chromatography.....	66
2.2.11.	Quantification via HPLC.....	67
2.2.12.	Quantification via chemical assays.....	69
3.	Results	71
3.1.	Cell-free enzyme cascades — application and transition from development to industrial implementation	71
3.2.	Integrating Carbohydrate and C1 Utilization for Chemicals Production	72
3.3.	Cell-free enzymatic L-alanine synthesis from green methanol	73
4.	Discussion and Outlook.....	74
4.1.	Cell-free enzymatic cascades for the production of amino acids and biofuels from C1-chemicals: From proof of concept to industrial application	74
4.1.1.	Optimizing the efficiency of enzymatic proof of concept cascades.....	74
4.1.2.	Optimizing the yield of enzymatic proof of concept cascades.....	75
4.2.	Enzymatic cascade design and optimization for the production of commodity chemicals.....	77
4.2.1.	Enzymatic stability in enzyme cascades.....	77
4.2.2.	Cofactor regeneration systems in enzymatic cascades	79
4.2.3.	Cross-talk between components in enzyme cascades.....	81
4.3.	Methanol assimilation through formaldehyde condensing enzymes.....	82
4.3.1.	Natural- and synthetic formaldehyde fixation in enzyme cascades	83
4.4.	<i>In vitro</i> vs <i>In vivo</i> C1-valorization to various chemicals.....	86
4.4.1.	Integration of new to nature and natural methanol utilizing pathway to create synthetic methylotrophs vs <i>in vitro</i> applications	87
4.5.	Sustainable chemical production from renewable resources by the use of enzymatic cascades	90
5.	References	93
6.	Appendices	105
7.	Abbreviations	181
8.	List of Tables	186
9.	List of Figures.....	187
10.	List of Formulas	188

List of Publications

1. Teshima, M., Willers, V.P. & Sieber, V. Cell-free enzyme cascades — application and transition from development to industrial implementation. *Curr. Opin. Biotechnol.* 79, 102868 (2023)
2. Willers, V. P., Beer, B. & Sieber, V. Integrating Carbohydrate and C1 Utilization for Chemicals Production *ChemSusChem*, 16, e202202122 (2023)
3. Willers, V.P., Döring, M., Beer, B. & Sieber, V. Cell-free enzymatic L-alanine synthesis from green methanol. *Chem Catal.* 3, 100502 (2023)

Summary

Looming climate change, the depletion of many species' habitats, and the scarcity of fossil resources as demand and population increase are prompting us to think about how we need to adapt the production of chemicals and food in the future, and how we can shift our polluting lifestyles toward sustainability, recycling, and climate-friendly living. Biocatalysis is a powerful tool based on the properties of enzymes that catalyze all kinds of chemical reactions and could replace or complement conventional chemical synthesis for fine chemicals, platform chemicals, and food and feed. It has always been considered environmentally friendly and sustainable, since the reactions mostly take place in aqueous solvents at ambient temperature, the substrates for the enzymes can be based on renewable sources, and there is the possibility to extend the range of substrates to different waste streams and to recycle them. While enzymes and multi-enzyme cascades are already used in the production of pharmaceuticals, their use in the production of low-cost bulk chemicals is still in development. Enzymatic cascades are being developed for the production of biofuels, food additives and other platform products, but high cost, low titers and small scale make them uncompetitive with cheap fermentative or chemical routes. Nevertheless, proof-of-principle systems are gradually going through a transition phase in which process parameters are optimized and these systems are prepared for the leap into the industrial phase with high scale and high product titers. A new “megatrend” is the use of cell-free multi-enzyme cascades for the direct production of various chemicals from C1-compounds such as methanol, formaldehyde or formic acid and CO₂. Carbon elongation reactions as C-C bond coupling by key enzymes such as formolase play a crucial role in the synthesis of higher carbon precursor molecules such as dihydroxyacetone.

In this thesis, this trend was taken up and an enzymatic cascade was designed for the production of the amino acid L-alanine as a potential food and feed additive or nutritional supplement from the C1-compound methanol. The design of the cascade is based on the formolase-driven formose reaction for carbon elongation, lower glycolysis for cofactor regeneration and the natural L-alanine synthesis pathway for L-alanine production. With an intrinsic ATP and NAD⁺ regeneration system, the entire cascade is cofactor neutral and can be separated into three modules to provide variability in product output. To optimize this system for L-alanine, all cascade enzymes were characterized based on their kinetic properties and their interaction with cascade compounds. The toxic effects of formaldehyde as well as the inactivating effects of cascade additives were investigated and the findings implemented in the system. A final addition of extra oxygen could increase the final L-alanine titer up to 3.9 g L⁻¹, corresponding to a yield of 88%. To further exploit C1-compounds as a resource in the second part of the studies, a cascade for the production of the most common biofuel ethanol and the biofuel

alternative or drop-in biofuel isobutanol was designed and brought to proof-of-concept. This system combined two waste streams and added the C1-compound methanol to the C5 compound xylose, one of the major components of lignocellulosic biomass. In this way, an enzymatic cascade based on the natural xylulose monophosphate pathway, lower glycolysis and the natural valine pathway was designed. This system also demonstrated modularity that was used to produce ethanol instead of isobutanol. Similar to the L-alanine cascade, cofactor neutrality could be generated for an intrinsic NADP⁺ and ATP recycling system. To optimize the system, the key enzymes transketolase, dihydroxyacetone kinase and alcohol dehydrogenase were characterized and the most suitable candidates in terms of activity and cascade compatibility were used in the final system. In addition, pH and buffer optimization of the cascade was used to increase conversion and final yield. Once the optimal cascade conditions were established, a final titer of 2 g L⁻¹ isobutanol and 3 g L⁻¹ ethanol could be produced.

Zusammenfassung

Der sich abzeichnende Klimawandel, die Zerstörung der Lebensräume vieler Arten und die Verknappung fossiler Rohstoffe einhergehend mit einer steigenden Nachfrage und Bevölkerungszahl veranlassen uns, darüber nachzudenken, wie wir die Produktion von Chemikalien und Lebensmitteln in der Zukunft anpassen können und wie wir unseren umweltbelastenden Lebensstil in Richtung Nachhaltigkeit, Recycling und klimafreundliches Leben ändern können. Die Biokatalyse ist eine Technologie, die auf der Umsetzung von verschiedenen Ausgangssubstanzen zu einer breiten Produktpalette auf der Basis von Enzymen beruht, die alle Arten von chemischen Reaktionen katalysieren und die herkömmliche chemische Synthese für Feinchemikalien, Plattformchemikalien sowie Lebens- und Futtermittel ersetzen oder ergänzen könnte. Sie gilt seit jeher als umweltfreundlich und nachhaltig, da die Reaktionen meist in wässrigen Lösungsmitteln bei Umgebungstemperatur ablaufen, die Substrate für die Enzyme auf erneuerbaren Quellen basieren können und die Möglichkeit besteht, die Palette der Substrate auf verschiedene Abfallströme auszudehnen und diese zu recyceln. Während Enzyme und Multienzymkaskaden bereits bei der Herstellung von Arzneimitteln eingesetzt werden, befindet sich ihr Einsatz bei der Produktion von kostengünstigen Plattformchemikalien noch in der Entwicklung. Enzymkaskaden werden für die Herstellung von Biokraftstoffen, Lebensmittelzusatzstoffen und anderen Plattformprodukten entwickelt, sind aber aufgrund der hohen Kosten, der niedrigen Titer und des kleinen Maßstabs nicht konkurrenzfähig mit kostengünstigeren fermentativen oder chemischen Verfahren. Dennoch durchlaufen die Proof-of-Principle-Systeme allmählich eine Übergangsphase, in der die Prozessparameter optimiert und diese Systeme auf den Sprung in die industrielle Phase mit hohem Maßstab und hohen Produkttitern vorbereitet werden. Ein neuer „Megatrend“ ist der Einsatz von zellfreien Multienzymkaskaden zur direkten Herstellung verschiedener Chemikalien aus C1-Verbindungen wie Methanol, Formaldehyd oder Ameisensäure sowie CO₂. Kohlenstoffverlängerungsreaktionen wie die C-C-Bindungskopplung durch Schlüsselenzyme wie die Formolase spielen eine entscheidende Rolle bei der Synthese von kohlenstoffreicheren Vorläufermolekülen wie Dihydroxyaceton.

In dieser Arbeit wurde dieser Trend aufgegriffen und eine enzymatische Kaskade zur Herstellung der Aminosäure L-Alanin als potenzieller Lebens- und Futtermittelzusatzstoff oder Nahrungsergänzungsmittel aus der C1-Verbindung Methanol konzipiert. Das Design der Kaskade basiert auf der Formolase-getriebenen Formosereaktion zur Kohlenstoffverlängerung, der unteren Glykolyse, gekoppelt mit dem natürlichen L-Alanin-Syntheseweg. Mit einem intrinsischen ATP- und NAD⁺-Regenerationssystem ist die gesamte Kaskade kofaktorneutral und kann in drei Module aufgeteilt werden, um eine Variabilität der Produktausgabe zu

ermöglichen. Um dieses System für L-Alanin zu optimieren, wurden die Kaskadenenzyme auf der Grundlage ihrer kinetischen Eigenschaften und ihrer Interaktion mit Kaskadenverbindungen charakterisiert. Die toxische Wirkung von Formaldehyd sowie die inaktivierende Wirkung von Kaskadenenzuzusätzen wurden untersucht und die Ergebnisse in das System implementiert. Eine abschließende Zugabe von zusätzlichem Sauerstoff konnte den endgültigen L-Alanin-Titer auf bis zu $3,9 \text{ g L}^{-1}$ erhöhen, was einer Ausbeute von 88 % entspricht. Zur weiteren Nutzung der C1-Verbindungen als Ressource wurde im zweiten Teil der Studien eine Kaskade zur Herstellung des gebräuchlichsten Biokraftstoffs Ethanol und der Biokraftstoff-Alternative bzw. des Drop-in-Biokraftstoffs Isobutanol konzipiert und zum Proof-of-Concept gebracht. In diesem System wurden zwei Abfallströme kombiniert und die C1-Verbindung Methanol mit der C5-Verbindung Xylose, einer der Hauptbestandteile der lignozellulosehaltigen Biomasse, umgesetzt. Auf diese Weise wurde eine enzymatische Kaskade auf der Grundlage des natürlichen Xylulosemonophosphatwegs, der unteren Glykolyse und des natürlichen Valinwegs erstellt. Dieses System zeigte auch eine Modularität, die zur Herstellung von Ethanol anstelle von Isobutanol verwendet wurde. Ähnlich wie bei der L-Alanin-Kaskade konnte Kofaktorneutralität für ein intrinsisches NADP^+ - und ATP-Recycling-System erzeugt werden. Zur Optimierung des Systems wurden die Schlüsselenzyme Transketolase, Dihydroxyacetonkinase und Alkoholdehydrogenase charakterisiert und die hinsichtlich Aktivität und Kaskadenkompatibilität am besten geeigneten Kandidaten im endgültigen System verwendet. Darüber hinaus wurden pH-Wert und Puffer der Kaskade optimiert, um den Umsatz und die endgültige Ausbeute zu erhöhen. Sobald die optimalen Kaskadenbedingungen festgelegt waren, konnte ein Endtiter von 2 g L^{-1} Isobutanol und 3 g L^{-1} Ethanol hergestellt werden.

Acknowledgements

First of all, I would like to express my sincere thanks to my supervisor Prof. Volker Sieber. Thank you for your continuous support, your advice and the many discussions and conversations. It was great to have the opportunity to follow my own ideas, guided by your expertise, advice and encouragement.

In addition to my supervisor, I would also like to thank the other professors on my doctoral committee, Prof. Dr. Bastian Blombach, who chaired the defense, Prof. Dr. Henricke Niederholtmeyer as second examiner and Prof. Dr. Harald Gröger as third examiner.

I would like to thank Dr. Barbara Beer to supervise me during my first years of the PhD and proofreading my dissertation. With your expertise, advice and motivation, you helped me to build a good foundation for my research and PhD career, which I was able to expand in the following years.

I would like to thank my mentor Dr. Helge Jochens for his time, advice, and motivation. Furthermore, I would like to thank Prof. John Woodley and his group at DTU to give me the opportunity to do a research internship, as well as the Funding from IGSSE, which made this stay possible, supported by Deutsche Forschungsgemeinschaft (DFG) through TUM International Graduate School of Science and Engineering (IGSSE), GSC 81. Together with that the work was supported by Bundesministerium für Bildung und Forschung (BMBF), Förderkennzeichen:031B0351C.

Thanks to all my colleagues in the Department of Chemistry of Biogenic Resources for their support and help, which made my stay at CBR a great experience.

For the good atmosphere in our office, the fun and the discussions I would like to thank Benjamin Begander, Ammar Al-Shameri, Enrique Raga Carbajal, Jan Grundheber and Mahdi.

I would like to thank Lena Würstl, Magdalena Haslbeck, Petra Lommes and Manuel Döring for their help in the lab, as well as Broder Rühmann and Anja Schmidt for their advice and help with the analytics. Thank you to André Pick and Enrico Hupfeld for great discussions and advises.

Thanks to my Lab Red colleagues: Samuel Sutiono, Samed Güner, Zinnia Dsouza, Renan Miyamoto, Mariko Teshima and Marcel Mayer for discussing, energizing, and keeping each

Acknowledgements

other company late into the night. Thanks to Tatjana Laudage, Tristan Rath, Luca Schmermund, Alexander Fuchs and Mathilde Steinmaßl for their friendship and the great time during and after our time in CBR.

Thank you to my friends from my studies in Düsseldorf: Anne Pfitzer, Nora Bitzenhofer, Lea Sundermeyer, Leonie Windeln, Alexander Fejzagic, Manuel Anlauf, Florestan Bilsing, Niklas Peters and Maurice Tust for the fun and enjoyable past and coming years.

Finally, I would like to thank my family:

Nicky, Kamini, Michael, Brigitte, Sean, Ken, Nanni, Chandra, Hannelore, Horst, Estelle and Erik, who have supported me throughout my life and are always there for me, and Mariko, who is my motivation, encouragement and support in every way.

1. Introduction

1.1. Future resources for chemistry and energy supply

In recent years, the unsustainable lifestyle of industrialized nations has exceeded the earth's capacity, leading to the depletion of fossil resources. A simplified representation of how Earth's population overuses Earth's resources is the Earth Overshoot Day. This day was calculated by the Global Footprint Network based on ecological footprint and bio-capacity data since 1961 and is intended to be a measure of the day on which the population has used all the resources that should last for an entire year. Since the beginning of recording, this day has been moved forward and is already dated the 2nd of August for 2023 ¹ (Figure 1). However, in certain countries such as Germany, this date is even earlier than calculated for the Earth. If the world's population lived the way Germans do, resources for 2023 would have been exhausted by the 4th of May 2023 ². Nevertheless, the German Overshoot Day tends to be shifted backward since 1971 in contrast to the Earth Overshoot Day. To counteract this overuse and with that shortage of resources, a rethink must take place, and sustainable as well as resource-saving alternatives are needed that not only replace fossil raw materials and energy sources but also have to be significantly more climate-friendly in order to be able to mitigate climate change.

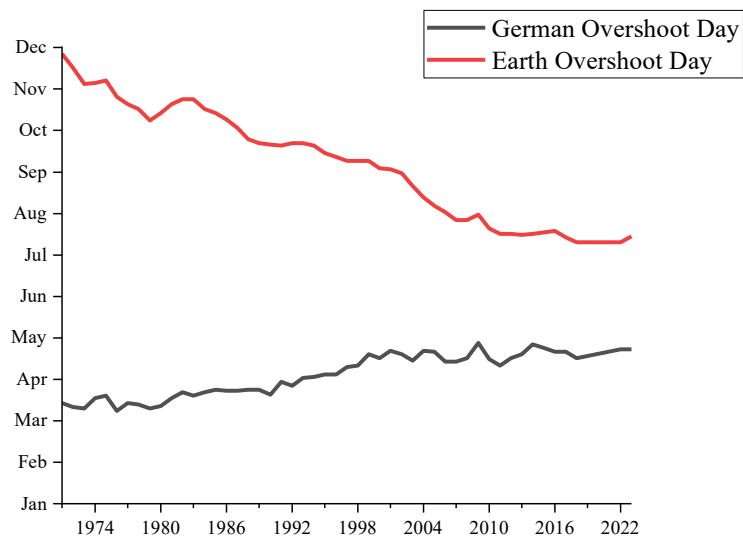


Figure 1: Comparison of Earth Overshoot Days and German Overshoot Days continuous between 1971 and 2018 plus the dates for 2022 and 2023. Thereby the dates for the German Overshoot Days were calculated based on day numbers extracted from the public data package of National Footprint and Bio-capacity Accounts 2022 Public Data Package and the data for 2023. Earth Overshoot Days were extracted from overshootdays.com based on National Footprint and Bio-capacity Accounts 2022 dataset* and the data for 2023¹⁻⁵.*

In the following chapters, various available sources that could act as future resources are reviewed and possible ways to lead the chemical industry to a more sustainable and bio-based future are discussed. By evaluating different concepts of biomanufacturing, the focus will be on the valorization of different waste streams and sustainable resources through the application of cell-free enzymatic cascades for the sustainable and ecological production of chemicals and to what extent they can be a substitute for the previous fossil-based methods.

1.1.1. Chemicals and fuels from lignocellulosic biomass

Lignocellulosic biomass is the most abundant biomass resource on Earth and has an enormous potential as a renewable alternative to fossil resources for producing sustainable chemicals and fuels⁶. Lignocellulose is seen as second-generation feedstock and mainly consists of the two main polysaccharides cellulose (30-50%) and hemicellulose (25-30%) as well as the aromatic polymer lignin (15-20%). Thereby, cellulose consists of glucose subunits that are connected via a beta-1,4-glycosidic bond. Hemicellulose is a mixture of glucose, xylose and other sugars, with a complex branched arrangement⁷⁻¹⁰. To release the monomeric sugar units, lignocellulosic biomass is first pretreated, whereas the lignocellulosic structure is destroyed using biological, chemical, mechanical and thermal processes^{11, 12}. Afterward, the resulting cellulose and hemicellulose need to be hydrolyzed. The main methods for hydrolyzation of cellulose and

hemicellulose are acid hydrolysis and enzymatic treatment. Hemicellulose can easily be split into its monomeric composition, whereas cellulose needs harsher treatments due to its highly cross-linked structure ¹³.

After the degradation of these polymers, the sugar units are usually further processed by fermentation. Since ethanol is one of the most common biofuels used as a substitute for gasoline, intensive research is being conducted to produce ethanol from lignocellulosic biomass ¹⁴. High yields from lignocellulosic biomass for ethanol range between 23- and 24 g L⁻¹ from different biomass sources like pinewood, timothy grass, or wheat straw ¹⁵. Besides ethanol, more valuable chemicals and fuels can be derived from lignocellulosic biomass. Higher alcohols as butanol or isobutanol have a higher energy density, higher octane number and lower hygroscopicity and more similar properties to gasoline ¹⁶. Isobutanol is seen as an advanced biofuel and together with that, is used in industry for perfumes, lubricants, coatings, antiseptics, or drug precursors ^{17, 18}. Elevated 1-butanol titers have previously been obtained with *Clostridium tyrobutyricum* and various carbon sources such as cassava bagasse hydrolysate, soluble starch, or paper mill sludge and ranged from 15- to 17 g L⁻¹ ¹⁹. While the highest reported titer for isobutanol using *Escherichia coli* is 22 g L⁻¹ on glucose, only lower yields are reported for other carbon sources such as glycerol (0.75 g L⁻¹) or xylose (3.1 g L⁻¹ from *Saccharomyces cerevisiae* strain) ¹⁹. While glucose is the most abundant sugar in nature and is already used in various approaches, xylose, the second most common sugar, is not yet used as intensively ²⁰.

Glucose can easily be taken up from common industrial microorganisms like *Saccharomyces cerevisiae* or *Zymomonas mobilis* ²¹. However, these organisms are inefficient at converting xylose and other pentoses to ethanol ²². Different approaches are being pursued to find a solution for the more difficult xylose utilization. Naturally, xylose can be converted by pentose-fermenting yeasts such as *Scheffersomyces stipites*, *Kluyveromyces marxianus* *Candida shehatae* or *Pachysolen tannophilus*, but also bacteria such as *Clostridium* strains or *Lactobacillus pentoses* ^{20, 21, 23, 24}. However, natural xylose-consuming strains lack genetic tools and require a more sophisticated environment than classical fermentation strains ²¹.

One way to utilize xylose is to adapt common fermentative hosts to utilize xylose. Therefore, two different pathways are mainly integrated, the xylose isomerase pathway (XI pathway) and the xylose reductase/xylose dehydrogenase pathway (XR/XDH pathway) ²⁵. Unlike ethanol, producing higher alcohols such as isobutanol or n-butanol from xylose is challenging and besides the need to adapt the host to utilize xylose, the higher toxicity of these alcohols compared to ethanol significantly reduces the final yield ²⁶.

As alternative cell-free enzyme cascades are applied to utilize xylose for the production of various chemicals and biofuels.

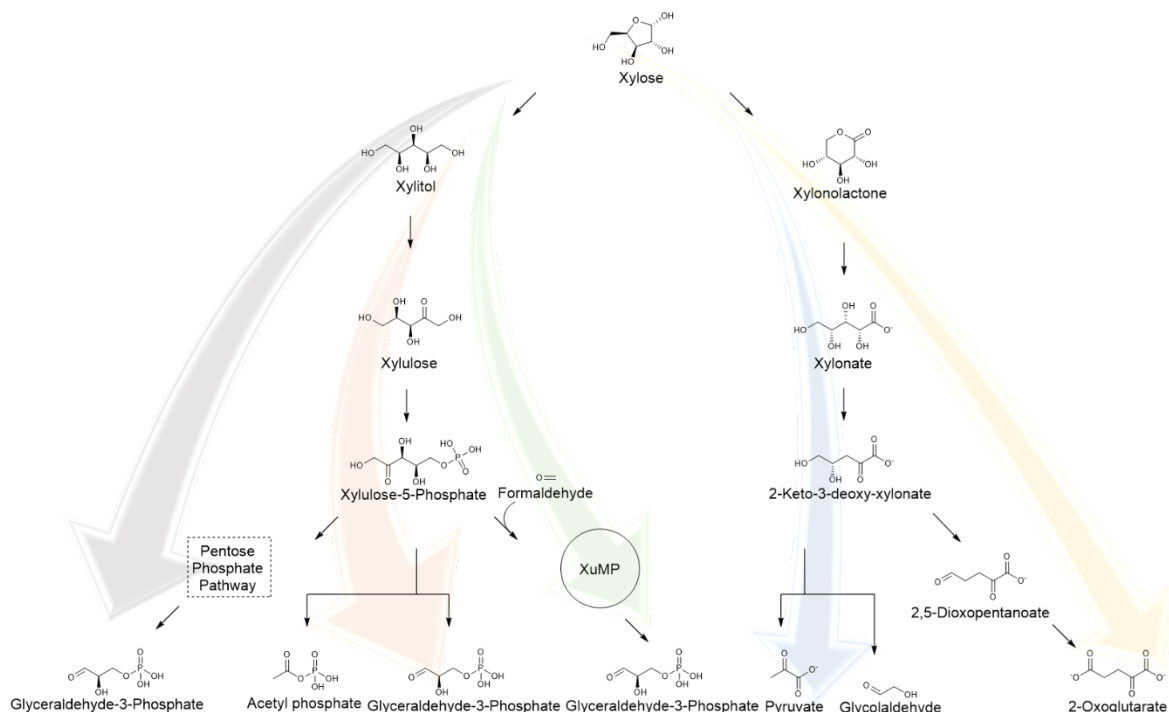


Figure 2: Natural pathways of xylose utilization adapted from Zhao et al. ¹⁰. The gray arrow indicates the metabolism of xylose via the pentose phosphate pathway. The red arrow indicates the metabolism of xylose via the phosphoketolase reaction. The green arrow indicates the metabolism of xylose via the xylulose monophosphate pathway (XuMP) involving formaldehyde. The blue arrow indicates the metabolism of xylose via the Dahms pathway and the yellow arrow indicates the metabolism of xylose via the Weimberg pathway.

Xylose is utilized by several different pathways (Figure 2). One possibility is an analogous pathway to the non-phosphorylative Entner-Doudoroff pathway ^{27, 28}. Xylose is first oxidized to xylonolactone by xylose reductase. Xylonolactonase converts xylonolactone to xylonate, which is then dehydrated by xylonate dehydratase. The resulting 2-keto-3-deoxy-xylonate is cleaved by aldolase to glycolaldehyde and pyruvate. Glycolaldehyde and pyruvate can then be further processed into chemicals via different pathways. Alternatively, different phosphorylation pathways can be used to utilize xylose to produce different chemicals. Xylose is either isomerized to xylulose by xylose isomerase or first reduced to xylitol by xylitol reductase and then oxidized to xylulose by xylose reductase. Xylulose is further phosphorylated to xylulose-5-phosphate by xylulokinase. Xylulose-5-phosphate is an intermediate of the pentose phosphate pathway and can be further utilized. Alternatively, xylulose 5-phosphate can

be converted directly to glyceraldehyde-3-phosphate and acetyl phosphate and enter the TCA cycle ²⁹. In addition to these common pathways, other natural or synthetic xylose degradation pathways are used as entry points for xylose into the metabolism. By introducing xylulose-1-phosphate (X1P) kinase and X1P aldolase, xylose can be converted to dihydroxyacetone phosphate, which enters glycolysis and glycolaldehyde. Mainly, these pathways or parts of these pathways are used to produce various chemicals, including alcohols such as butanediol or ethylene glycol, organic acids such as glycolic acid, or even other biochemicals such as myo-inositol from xylose or mixed sugars *in vitro* ³⁰⁻³⁵. These examples of cell-free xylose utilization demonstrate the high flexibility of cell-free cascades with different types of platform chemicals as products with high yields and titers.

1.1.2. Carbon dioxide as a resource

Carbon dioxide (CO₂) is considered as the strongest driving force of climate change and its emission from energy and industrial processes increases steadily. Projection from the International Energy Agency (IEA) shows that from the year 1990 energy and industrial processes related CO₂ emission increased by 14.8 Gt to 36.2 Gt in the year 2021 ³⁶. For this reason, not only the reduction of CO₂ emissions, but also its use as a building block for the production of chemicals or fuels could have a direct impact on achieving climate change mitigation goals.

Biological carbon sequestration directly binds CO₂ and couples it to various chemical compounds. Plants and algae can fix carbon dioxide, for example, through the Calvin cycle, which produces triose phosphates that can enter glycolysis and be further processed into chemicals ³⁷. Alternatively, bacterial pathways as the reverse TCA cycle or 3-hydroxypropionate pathway fix CO₂ directly and produce acetyl-CoA or glyoxylate as important building blocks, which can then be further metabolized ³⁸⁻⁴⁰.

Furthermore, CO₂ can be fixed indirectly via formaldehyde by methylotrophic organisms. There are several formaldehyde assimilation pathways that use formaldehyde to produce important metabolites, such as glyceraldehyde-3-phosphate or acetyl-CoA, which can be further processed into chemicals ⁴¹. Here the main pathways are the xylulose monophosphate pathway (XuMP) in methylotrophic yeast, the ribulose monophosphate pathway (RuMP), and the serine cycle in methylotrophic bacteria. In the XuMP and RuMP pathways, formaldehyde is added to a sugar phosphate, whereas in the serine cycle, formaldehyde is added to glycine as methylene tetrahydrofolate ^{42, 43}. Together with these natural pathways, synthetic formaldehyde fixation pathways open the way to produce even more chemicals from CO₂. Here prominent examples are based either on the serine cycle ⁴⁴, the RuMP pathway ⁴⁵ or even novel synthetic

pathways as the formolase pathway ⁴⁶, where the key enzyme formolase can condensate three formaldehyde molecules to dihydroxyacetone, a precursor of glycolysis intermediate dihydroxyacetone phosphate, without carbon loss. Nevertheless, formaldehyde is a toxic compound and can harm organisms already at millimolar (mM) concentrations ⁴⁷.

As a promising usage of CO₂, recently the production of methanol from CO₂ gained a lot of attention ⁴⁸. Methanol has emerged as an attractive carbon feedstock for biotechnological applications, because it is abundant, inexpensive, less toxic than formaldehyde, and cannot be used as a food or feed ⁴⁹. For the reduction of CO₂ to methanol different routes were developed (Figure 3). Among them are the reduction via electro catalysis, chemical hydrogenation (heterogeneous-/homogenous catalysis), photo catalysis and biocatalysis ⁵⁰. The enzymatic reduction of CO₂ to methanol is a challenging multi-enzymatic process in which CO₂ is first converted to formate, then formate is reduced to formaldehyde, and finally formaldehyde is reduced to methanol ^{51, 52}. However, low methanol yields and a high cofactor demand make these systems cost intensive and unsuitable for larger applications. ⁵³.

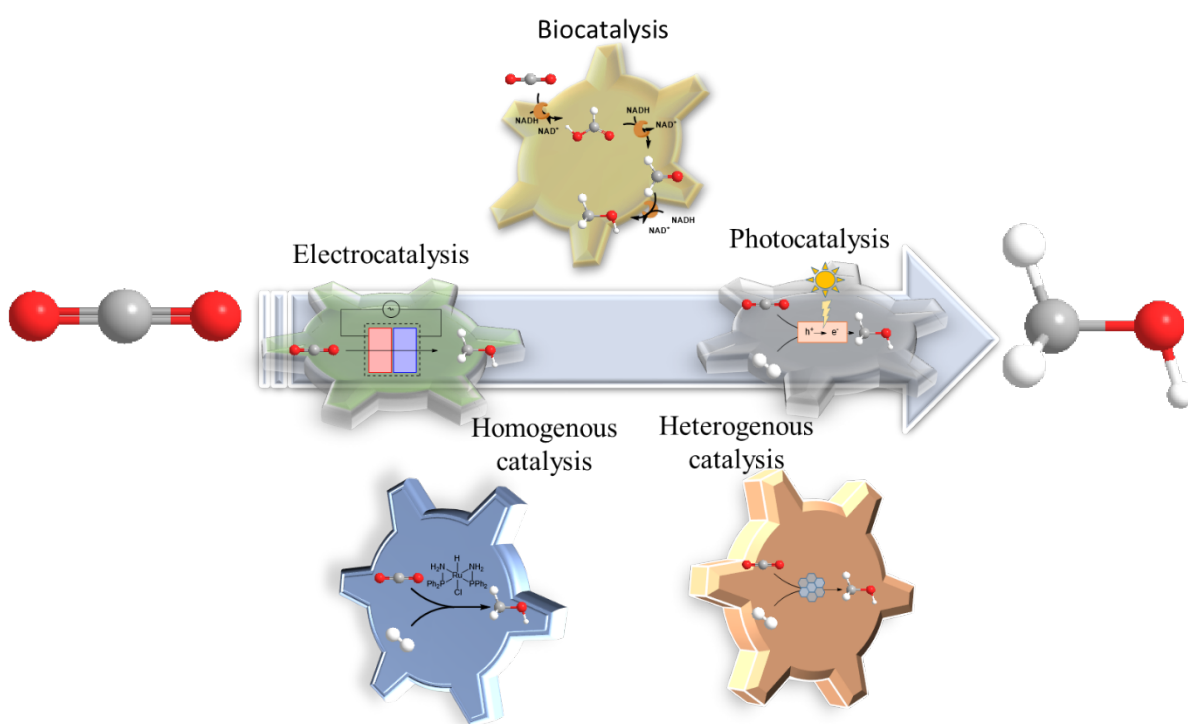


Figure 3: Schematic representation of concepts of biocatalysis, electrocatalysis, photocatalysis, homogenous- and heterogenous-catalysis for the production of methanol from CO₂. Adapted from Navarro-Jaén et al. ⁵⁰.

In heterogeneous-catalysis, CO₂ is commonly hydrogenated with Cu-ZnO catalysts. This type of catalyst was developed in the mid-20th century and relies on the activity of Cu in conjunction with the important ZnO promoter to enhance system activity ⁵⁴. These catalysts are already on

the market and have high stability and good performance.⁵⁵ Together with that, a direct coupling to renewable energy sources is possible⁵⁶. However, further development of these catalysts regarding CO₂ to methanol conversion have the potential to increase their sustainability and applicability⁵⁷.

Alternatively to the two methods described above and among others, electrochemical reduction of CO₂ to methanol gains attention due to its possible direct coupling to renewable energy sources⁵⁸. Depending on the catalyst material and the reaction medium, many different products can be formed, such as CO, formate, methanol or formaldehyde, as well as oxalate, methane, ethylene or ethanol. Due to the large variety of products, the main challenge is to efficiently and unambiguously convert CO₂ to methanol and to find a selective and active catalyst material capable of performing the specific reduction of CO₂ to methanol^{58, 59}. Although much research is still needed to further develop methanol production processes from CO₂ and make them more scalable and sustainable, methanol's versatile properties as a fuel, fuel additive, energy source or chemical precursor offer an opportunity for the next step towards a non-fossil resource dependent economy.

1.2. Chemical industry of the future: transformation from petroleum based to bio-based processes

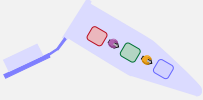
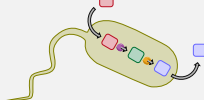
To lead industry into a renewable and sustainable future, the German government proposed a biological transformation of manufacturing. To achieve this transformation in manufacturing, three key elements have been introduced: bio-inspiration, bio-integration and bio-intelligence.⁶⁰ Miehe et al. describe these key elements as modes of evolution, where inspiration transfers a natural phenomenon and creates a bioinspired value chain; the integration mode uses existing processes and extends, complements, modifies, replaces, or even completely renews them. The third mode is the final evolution to bio-intelligent manufacturing by combining information, technical and biological systems to create self-sufficient and new production technologies and structures⁶¹⁻⁶³. In the chemical industry, a potential shift to sustainable chemical production will require the integration of various biologically based concepts, such as whole-cell fermentation and biocatalysis, but also electrobiocatalysis and photobiocatalysis. The integration of these processes will transform petrochemical refineries into biorefineries. In these biorefineries, the hydrocarbon feedstocks from petroleum or methane used so far will have to be replaced by more renewable feedstocks in the future⁶⁴. Furthermore, the switch to biotechnological or biocatalytic processes brings significant changes in terms of process design. Biocatalytic approaches are usually performed under mild reaction conditions regarding temperature, pressure and solvents and are dependent on the biocatalyst or microorganism. Fermentative *in vivo* processes use sugars derived from biomass or even syngas or CO₂ as feedstock for various chemicals. Together with that, biocatalysis with cell-free enzymes is gaining momentum due to its ability to catalyze a wide variety of chemical reactions that generate various complex molecular structures⁶⁵.

1.2.1. Comparison of *in vitro* and *in vivo* enzyme cascades as tools for industrial chemical production

Although new approaches, such as combining benefits from *in vitro* and *in vivo* systems, are emerging⁶⁶, there are still significant differences between these two systems (Table 1). Whole-cell based systems use the intracellular metabolism of the particular host organism to produce products of choice. To set up a system, a microorganism must be found that naturally produces a specific product of interest, fermentation conditions must be established, and then the host must be able to produce the product from cheap substrates such as sugars⁶⁷. To broaden the scope of the host to the utilization of various substrates and the production of different products, different strategies were investigated and applied. Through genetic and metabolic engineering, the flux from a substrate to the product of choice can be manipulated by switching specific

genes on or off, introducing artificial enzymes, or overexpress certain genes⁶⁸. However, this approach can often be tedious and requires a deep understanding of the microorganism and specific engineering tools. When metabolic engineering is used, there is an overlap between the newly created metabolic pathways and the intrinsic metabolism, which can lead to imbalances in the organism and thus lower productivity. However, the main advantage of *in vivo* biocatalysis is the low cost of production. Due to the intrinsic protein production and cofactor regeneration of the microorganisms, expensive purification of enzymes and cofactors is avoided. In addition, the cell membrane is an intrinsic barrier between the enzymes and the external environment. This barrier protects, for example, enzymes that are unstable or sensitive to oxygen⁶⁹. However, together with all the positive effects, the biggest challenge in whole-cell biocatalysis is product purity and downstream processing⁷⁰. As mentioned earlier, due to natural metabolism, flow to a specific product is problematic, and intermediates can be diverted to different cellular products. Also, the substrates are consumed not only to produce the product but also to secure the viability of the microorganism itself, leading to a loss of efficiency in product production⁷¹. Since toxic intermediates or end-products occur in several pathways, the efficiency of those processes is harmed by growth inhibition, cell viability, or detoxification routes, which might interrupt the pathway^{72,73}. In contrast to the whole-cell approach, cell-free enzyme cascades need to be created from scratch. All enzymes and compounds for a pathway are artificially applied to the system and in the optimal case, intrinsic cofactor regeneration systems need to be created. However, this is still associated with high cost⁷⁴. Nevertheless, the artificial nature of cell-free systems gives freedom to the pathways used to produce a specific product from substrates. Enzymes derived from different metabolic pathways of different microorganisms can be easily combined, resulting in shorter and more efficient pathways^{75,76}. While most enzymes can operate in aqueous buffer solutions, site reactions and their optima in terms of pH and temperature might hamper the construction of these cascades^{77,78}. The concentration of enzymes can be easily varied, and computational tools can guide and calculate which parts of the system need to be changed to generate high efficiency and product yield⁷⁹⁻⁸¹. In contrast to whole cell systems, cell-free enzymatic systems are prone to have high product titers without loss in substrate to the microorganism. All substrates, which are used, can directly be channeled to the product of choice⁸². Together with that, a broad variety of conditions can be applied as different temperatures, buffer systems, pH, solvents, or metabolite concentrations^{33,83,84}. With this variability, reactions and pathways are possible that cannot be established in a microbial system. Finally, toxic compounds, which would harm the viability of the host, can be applied in higher concentrations due to the higher tolerance of cell-free enzymatic systems.

Table 1: Differences between *in vitro* and *in vivo* enzymatic cascade reactions

	<i>In vitro</i> enzyme cascade	<i>In vivo</i> enzyme cascade
Reaction host		
Reaction environment	<ul style="list-style-type: none"> ✓ Precise control over all components (enzymes, temperature, buffer, salts, cofactor, additives) 	<ul style="list-style-type: none"> ✗ Predefined conditions due to the microorganism of choice (Media composition, temperature, oxygen supply, pH)
Pathway design	<ul style="list-style-type: none"> ✓ Flexible design with the possibility of shortcut pathways without interference with metabolism ✗ Cofactor balance through intrinsic or exogenous regeneration systems 	<ul style="list-style-type: none"> ✓ Already established pathways through metabolism as the backbone ✓ Intrinsic cofactor supply ✗ Interference of pathways through metabolism
Yield and Productivity	<ul style="list-style-type: none"> ✓ No byproduct formation ✓ High efficiency and productivity 	<ul style="list-style-type: none"> ✓ High titers ✗ Byproducts through metabolism ✗ Branching off substrates for viability ✗ Boundaries in substrate and product channeling through membranes
Downstream processing	<ul style="list-style-type: none"> ✓ Immobilization for ease of enzyme separation ✓ Application of in situ product removal through phase separation 	<ul style="list-style-type: none"> ✓ Easy separation of cells ✗ Problem to purify single compounds out of the fermentation broth
Tolerance to toxicity, inhibition, inactivation	<ul style="list-style-type: none"> ✓ Higher tolerance towards toxic compounds ✓ Broad range of metabolite concentrations ✓ Enzyme immobilization for stabilization ✗ Enzyme stability 	<ul style="list-style-type: none"> ✓ Protection of labile enzymes through a barrier ✓ Natural compartmentalization ✗ Low tolerance towards toxic compounds
Cost	<ul style="list-style-type: none"> ✗ Need for enzyme purification or lysate preparation ✗ External cofactor supply ✗ Costly scale up 	<ul style="list-style-type: none"> ✓ Intrinsic cofactor supply ✓ Low production cost

1.1.1. Enzymes in industrial application

Nowadays, enzymes are well established as biocatalysts in the chemical industry and are applied in various industries such as the food, pharmaceutical, cosmetic, and agricultural

industries ⁸⁵. However, to establish a sustainable biocatalytic process, several requirements must be fulfilled. The economic potential of a process is often determined by the difference in value between the substrate and the product. For example, a high concentration of a cheap substrate can lead to a low titer of a valuable product, that requires subsequent separation. Woodley describes this problem in terms of the downstream process, where low product concentrations make the downstream process uneconomic due to higher purification and waste costs ⁸⁶. With this in mind, reasonable product titers required for industrial application are between 10- and 50 g L⁻¹ for high priced products and above 100 g L⁻¹ for low priced products ^{86, 87}. Besides a decent activity and tolerance to a substrate and product inhibition, enzyme stability is a major property needed to drive enzymatic conversion in the above-mentioned range. Here different stabilities such as thermal stability or solvent stability can be addressed. Several methods, including enzyme engineering, immobilization, or the use of thermostable enzymes, were developed to raise the reusability of a biocatalyst, its solvent stability and volumetric activity ⁸⁷⁻⁸⁹. One measure of enzyme performance is the total turnover number (TTN), which gives the expected yield in moles of a given product in relation to the moles of catalyst required over its lifetime. Industrially relevant TTNs range from 1 to 10 million ⁹⁰. When developing an industrial process, it is necessary to identify the above factors and evaluate whether the enzymes used meet these criteria and could be of interest to industry. Today, enzymes can be engineered more and more easily for industrial applications. However, the application of complex multi-enzyme cascades is still under development, but the number of developed cascades is increasing ⁹¹. These complex cascades may have a bright future in industrial applications thanks to new technologies such as machine learning-guided enzyme engineering, reaction modeling, and pathway discovery tools ⁹². However, due to the brief nature of this introduction, a detailed analysis of the development of enzyme cascades and how these cascades manage the transition phase from laboratory scale to industry would be beyond the scope. This will be explored in more detail in Section 3.1.

1.3. Cell-free multi-enzyme cascades as proof of concept for the production of platform chemicals

1.3.1. The concept of in vitro multi-enzymatic cascade systems

In contrast to single enzymatic systems, multi-enzymatic systems with at least two reaction steps can be classified as enzymatic cascade reactions⁹³. Enzymatic cascades can be distinguished in their appearance and are divided into linear, orthogonal, parallel, and cyclic cascades⁹⁴. A major advantage common to all these cascades is the avoidance of stepwise synthesis with isolation and purification of sometimes unstable intermediates to achieve greater atom economy, higher yields, and a reduction in cost and waste⁹⁵.

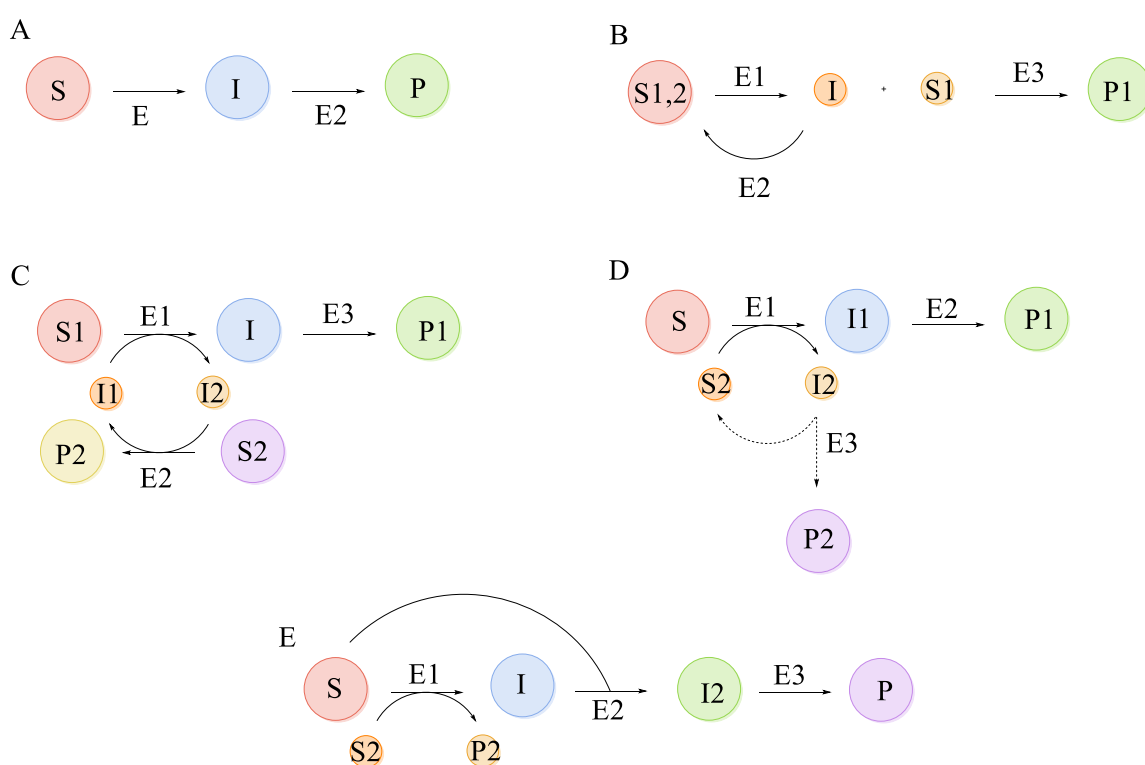


Figure 4: Concepts of enzymatic cascade systems adapted from Benítez-Mateos et al.⁹³, whereby S is the substrate, I is an intermediate, P is the product and E is an enzyme. A: Linear cascade. B: Cyclic cascade. C: Parallel cascade. D: Orthogonal cascade. E: Triangular cascade

Linear cascades consist of a sequence of reaction steps that convert a substrate to an intermediate that directly serves as the substrate for the next reaction step. Using this principle, thermodynamically unfavorable reactions can be combined with favorable reactions to direct the reaction to a product of choice⁹⁶. Orthogonal and parallel cascades are designed for product formation in the presence of a co-substrate that is converted to a specific by-product. The difference between these two concepts lies mainly in the value of the by-products. Whereas in

orthogonal cascades, a relevant reaction is coupled with another to facilitate the production of the main product, the by-product tends to be discarded. In parallel concepts, valuable by-products are produced and both the by-product and the main product are purified^{97,98}. Concepts of parallel cascade design often address the problem of cofactor regeneration. Parallel cascades achieve redox neutrality by combining two reactions. Typical examples are the combination of a kinetic resolution of an alcohol coupled to asymmetric reduction⁹⁹. Orthogonal cascade designs can be used to shift the equilibrium of a desired reaction efficiently. This concept is often used in the case of transaminase reactions whereby the byproduct, e.g. pyruvate can be withdrawn from the reaction *in situ* to reach higher conversion to the main product¹⁰⁰. In contrast, cyclic cascade designs form either a by-product through a reaction that reenters the cascade as a substrate of the cascade. A common application of this system is the deracemization for preparing enantiopure amines or alcohols. In this process, one enantiomer is selectively converted to an intermediate, which is then converted back to the racemic substrate, enriching the unreacted enantiomer and yielding the pure final product^{95, 101}. Together with the classical concepts described above also, more rare concepts are possible as a triangular cascade design¹⁰². Here, an intermediate product is usually recycled either in combination with a substrate to produce a new product or as a substrate⁹³.

1.3.2. From scratch to trial: Enzymatic pathway design

Since cell-free enzyme cascades are artificial systems that do not have access to the metabolism of an organism, the first step in their construction is to carefully evaluate the key parameters required for an efficient cell-free enzyme cascade. The product and substrate of choice, a cofactor regeneration system, and operating conditions play a critical role in the initial assessment of whether naturally occurring pathways are available that already meet the requirements or whether a *de novo* approach leading to non-natural pathways is needed to produce a specific product. In addition, chemoenzymatic cascade approaches are possible in which chemical catalysts are used to catalyze a specific reaction in a multi-enzyme cascade¹⁰³. When using parts of an existing pathway as a blueprint, primary metabolism or secondary metabolic pathways can be considered. Primary metabolic pathways often start with low-cost initial substrates, whereas secondary pathways often produce high-value products⁷⁷. These concepts have existed for more than three decades, with an early example by Welch and Scopes describing the *in vitro* reconstruction of the *Saccharomyces cerevisiae* Embden-Meyerhof pathway for the production of ethanol from glucose by the use of 13 purified enzymes¹⁰⁴. As alternative tailor-made synthetic pathways can be developed *de novo*, which brings the benefit of producing a specific compound that may not be easily accessible through known pathway.

However, creating such a metabolic pathway is a challenging process. Recently, computational synthesis planning tools, already used by organic chemists or in synthetic biology, are gaining attention for cell-free enzymatic metabolic planning. A prominent example is the RetroBioCat tool provided by Finnigan et al., which supports the user with knowledge about enzyme-catalyzed reactions or usable metabolic modules¹⁰⁵. This tool considers pathways to target products from suitable starter substrates, using both native and modified enzymes. In addition, different pathways are analyzed and the most effective ones are selected. However, due to the novelty of this program, the range of reactions and enzymes is still limited to a small subset of enzymatic reactions.

Nowadays, many cell-free enzymatic pathways are based on combinations of primary and secondary metabolism and consist of different enzymes derived from different host organisms. This concept of chimeric enzyme cascades can often lead to advantages such as cofactor regeneration, inhibition prevention, or shortening of naturally occurring pathways⁷⁷. Attempts to combine primary and secondary pathways are shown by various research groups which designed pathways up to 54 enzymes in one pot^{80, 106-108}. However, demonstrating that an enzymatic system can produce the product of choice does not mean that it already shows the efficiency and yields which are aimed as stated before (Section 1.2.1). Different parameters need to be addressed and optimized to tune a cascade to be attractive for industrial applications. The success and efficiency of a multi-enzymatic system, thereby, is affected by mostly enzyme activities, the reaction mixture, and the reaction conditions⁷⁷. It is important to note that these parameters are not just affected by the properties of one enzyme and its interaction with the environment but by interactions of many different enzymes with supposedly very different optimal conditions with the cascade enzymes and the system^{109, 110}. Therefore, for the cascade to function, a tolerable environment must be created, which is most likely a compromise. Finding this "window" requires a detailed study of the individual enzymes, evaluating the effects of, e.g., temperature, pH, metal ions, intermediates, or cofactors for each individual enzyme. After assessing the effect on individuals, the most promising parameters' impact needs to be evaluated in the whole reactions system^{77, 111, 112}. To optimize their *in vitro* systems, many different research groups went through a set of optimization steps to improve their productivity, titer, or efficiency. Many of the above key parameters are varied in elaborate experiments¹¹³. To reduce the workload, especially in systems with a large number of enzymes, more and more data-driven model-based tools have been developed recently¹¹⁴⁻¹¹⁶. Unlike kinetic modeling, these models do not require a sophisticated understanding of each individual enzyme in the cascade. They can capture the complexity and synergistic effects of dynamically acting enzyme cascades with multiple components involved, because they model the relationship between independent variables (e.g., concentrations or pH).

An important parameter in addition to the parameters described above is the cofactor regeneration. Because cofactor regeneration is critical in *in vitro* systems and sometimes intrinsic cofactor regeneration is not possible due to the characteristics of the pathway, an additional cofactor regeneration system can be added to the cascade as described above. It is important to note that a second product or substrate needed to balance the cofactor supply, such as NAD(P)⁺/NAD(P)H, ATP, or the provision of S-adenosyl-methionine (SAM) or coenzyme A (CoA), does not interfere with the system itself ¹¹⁷⁻¹²⁰. A prominent NAD(P)H regeneration system is glucose dehydrogenase, with the cheap substrate glucose and a high stability and activity ¹²¹. Still, a difficulty of using glucose dehydrogenase is the production of gluconate and with that, a shift in pH which need to be regulated ¹²². Other elegant systems using NADH oxidase or hydrogenases to balance NAD⁺/NADH ratios by producing hydrogen or water as by-product ^{123, 124}. To balance the reverse reaction, one option used frequently is formate dehydrogenase, which can balance NAD⁺/NADH ratios by producing CO₂ from formate ¹²⁵. Several ATP regeneration systems can regenerate ATP by using by-products such as phosphoenol pyruvate (PEP), creatine phosphate, or polyphosphate ¹²⁶. However, in all cases, issues occur, e.g., due to the cost of the co-substrate for PEP but also inhibition by using polyphosphate ¹²⁷.

1.3.3. Enzyme specificity vs. promiscuity

Enzymes are widely known for their high substrate specificity, enantioselectivity and mild working conditions, making them highly suitable for white biotechnology ¹²⁸. However, this ideal image of enzymes is contradicted by the fact that enzymes are not always specific and can be highly promiscuous. Promiscuous biocatalysts can lead to more by-products and thus lower yields of the target product. In addition, it makes the downstream process more difficult to remove unwanted products. However, promiscuity can also provide a greater degree of flexibility in biocatalytic systems, which, if properly exploited, can be valuable in biotechnology ¹²⁹.

Enzyme promiscuity can be classified as substrate, condition, or catalytic promiscuity. Conditional promiscuity represents enzyme activity under different reaction conditions, with varying pH, temperature, or media. Substrate promiscuity describes enzymatic activity for a wider range of substrates, and catalytic promiscuity describes a variety of chemical transformations performed by an enzyme ¹³⁰.

In multi-enzymatic cascade reactions, enzyme promiscuity can have both beneficial and detrimental effects on the success of the cascade. On the one hand, substrate-specific enzymes are needed to prevent side reactions that can lead to the accumulation of unwanted or toxic by-

products, cofactor imbalances, and thus a sudden stop of the cascade. On the other hand, substrate promiscuity can be a critical factor in the process. Assuming that a single enzyme can catalyze similar reactions with different intermediates in the cascade, intelligent cascade design can reduce the number of enzymes and thus costs and variables. In addition, greater flexibility in substrates and intermediates can be achieved since unnatural substrates or intermediates can be converted due to promiscuity. The concept of targeted use of substrate promiscuity in a cascade has been demonstrated for several enzyme cascades^{35,75}. However, the final step must be specific to produce one product rather than lead to product mixtures. This means that having promiscuous enzymes in a multi-enzymatic system can be very advantageous, but these reactions must be controlled to direct the intermediates to a single product.

1.4.Aim of this work

The utilization of waste streams and renewable and sustainable compounds from biomass will be the challenge of the chemical industry in the coming decades. In order to drive the biological transformation of the chemical industry, new concepts need to be developed that will be the starting point for a sustainable future. Biocatalysis can play a crucial role in this transformation as it encompasses many aspects to support this transformation, being clean, versatile and bio-based. Recently, biocatalytic utilization of cheap renewable substrates into chemicals has received new impetus, with important work involving the production of biofuels from sugar and starch from CO₂. To expand the biocatalytic production of biofuels and chemicals using CO₂ and biomass, new cascades need to be developed to expand the scope and use of this greenhouse gas.

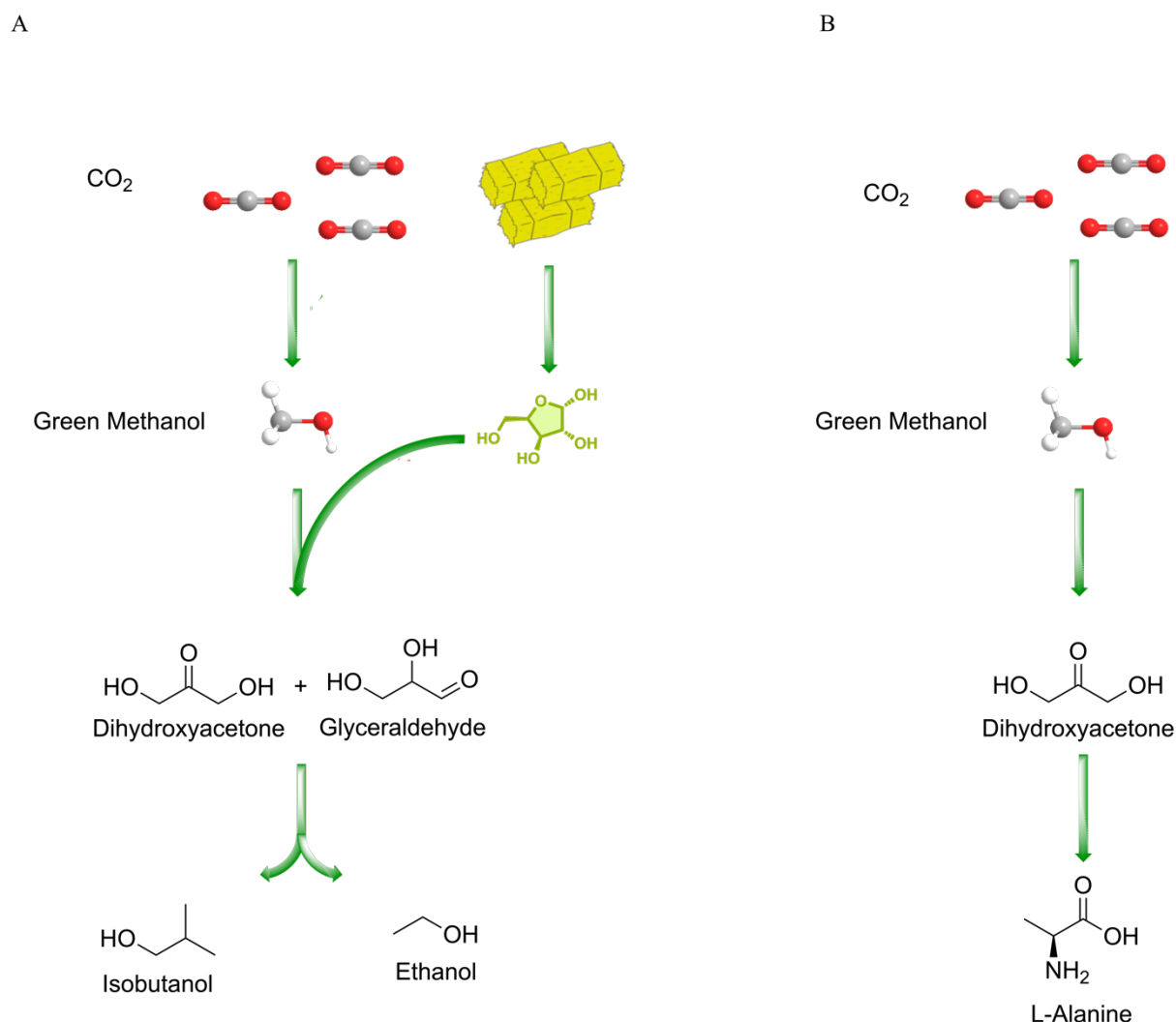


Figure 5: Schematic representation of the production of biofuels from CO₂ and lignocellulosic biomass (A) as well as L-alanine production from CO₂ (B).

1.4.1. Development of an enzymatic cascade for the utilization of xylose and CO₂ for biofuel production

Cell-free production of ethanol and isobutanol as biofuels from glucose from biomass has been enabled in several experiments by using different cascades inspired by the blueprints of natural glucose utilization pathways. These pathways show impressive titers of up to 275 g L⁻¹ ¹³¹. However, no *in vitro* cascade addresses the production of biofuels from xylose. Since xylose is the second most abundant sugar in nature, sustainable biofuel production is only possible if not only glucose but also xylose is converted. To expand the biocatalytic production of biofuels, an enzymatic cascade capable of efficiently utilizing xylose and producing biofuels should be developed as an extension of the already developed pathways. To realize this cascade, first biosynthetic xylose utilization pathways should be investigated and suitable pathways should be examined for implementation and possible combination of already existing biofuel production modules. One focus by the valorization of xylose should be on methylotrophic C1-fixation pathways using xylose to fix a molecule of formaldehyde via the key enzyme dihydroxyacetone synthase. As a possible “drop in solution”, formaldehyde, which can be derived from CO₂, could be added to a xylose-containing system to artificially mimic a glucose or C6-molecule. The conversion of formaldehyde as a C1-molecule and xylose as a C5-molecule thus creates two C3-molecules, which are essential for the efficient production of biofuels from xylose. This C3-molecule to biofuel route could be similarly applied to glucose as by its degradation via glycolysis also two triose phosphates are derived. Together with that the utilization of an additional carbon derivable from CO₂ offers the possibility of the valorization of two different waste streams to one specific product. After developing a cascade based on a blueprint, suitable enzyme candidates for the sugar guided formaldehyde fixation should be screened for the realization of the key reaction. In a final stage the cascade should run as a proof-of-principle cascade to produce biofuels from xylose and CO₂ derived formaldehyde in small scale.

1.4.2. Development of an enzymatic cascade for the utilization of CO₂ for L-Alanine production

Amino acids are the building blocks of proteins and have wide-ranging applications, e.g. as a health product or as a dietary supplement for animals ^{132, 133}. Recently, the biocatalytic synthesis of L-alanine based on glucose has been demonstrated ¹³⁴. However, considering the loss of biodiversity due to agriculture and land reclamation, new resources need to be developed to produce amino acids sustainably and ecologically. Due to the new possibilities of using CO₂-derived green methanol as a carbon source for the production of longer chain molecules, there

are new opportunities for the use of methanol for the production of chemicals. The production of dihydroxyacetone from methanol could be shown recently via the oxidation of methanol and the formolase guided formose reaction of formaldehyde ⁴⁶. Using this initial carbon expansion reaction, dihydroxyacetone should serve as the starting point for a newly developed enzyme cascade for the amino acid L-alanine, with the goal of producing L-alanine directly from methanol. To realize this project, the dihydroxyacetone assimilation from the already developed pathway to biofuels from xylose and formaldehyde should be adapted and reformed for L-alanine. To generate a knowledge of the enzymes of the system, all enzymes from dihydroxyacetone to L-alanine should be kinetically characterized. Based on these data, the proof-of-principle system should be optimized with respect to the L-alanine titer. Due to the complexity of the system, further optimizations should be determined and optimized based on the interactions between the metabolic pathways.

2. Materials and Methods

The materials and methods used in the context of the dissertation are presented in this chapter. The methods used were taken from the literature, the standard operating procedures (SOP) of the Chair of Chemistry of Biogenic Resources at TUM, or adapted based on the SOPs.

2.1. Materials

2.1.1. Devices

Devices used for the studies are listed below (Table 2)

Table 2: List of devices

Device category	Device	Manufacturer
Autoclave	Varioklav 135S	Thermo Fischer Scientific
	Sorvall Lynx 6000	Thermo Fischer Scientific
Centrifuges and rotor	F9-6x1000 LEX	Thermo Fischer Scientific
	F12-6x500 LEX	Thermo Fischer Scientific
	A27-8x50	Thermo Fischer Scientific
	Sorvall RC 6 Plus	Thermo Fischer Scientific
	Rotor F10-6x500y	Piramoont Technologies Inc,
	Rotor F9-4x1000y	Piramoont Technologies Inc,
	Rotor SS-34	Thermo Fischer Scientific
	Galaxy MiniStar	VWR
	Heraus Frisco 21	Thermo Fischer Scientific
	Heraus Pico 17	Thermo Fischer Scientific
Freezer	Rotanta 460R	Hettich Lab Technology
	Freezer -20 °C	Liebherr-Hausgeräte
	Freezer -80 °C Forma 906 - 86°C ULT	Thermo Fischer Scientific
	Freezer -80 °C CryoCube F740hi	Eppendorf®
Gel documentation	Gel iX Imager	Intas Science Imaging Instruments GmbH

Device category	Device	Manufacturer
Transilluminator	DR 46B	Clara Chemical Research
Gel electrophoresis	Mini-sub® cell GT system	Bio-Rad Laboratories GmbH
	Wide Mini-Sub® Cell GT Cell	Bio-Rad Laboratories GmbH
	SDS electrophoresis chambers	Bio-Rad Laboratories GmbH
	Mini-PROTEAN®-Tetra Cell casting	Bio-Rad Laboratories GmbH
	Mini-Protean®-3Multi-Casting Chamber	Bio-Rad Laboratories GmbH
	Power supply PowerPac™ Basic	Bio-Rad Laboratories GmbH
Biological safety cabinets	MSC-Advantage™	Thermo Fischer Scientific
Sonicator and sonotrode	Ultrasonic processor UIS 250 V	Hielscher Ultrasonics
	LS24d10	Hielscher Ultrasonics
	LS24d3	Hielscher Ultrasonics
	VialTweeter	Hielscher Ultrasonics
Incubation cabinets	Climate chamber KBF 240 E5.1/C	BINDER GmbH,
	Heraus B12	Thermo Fischer Scientific
	Heraus Kelvitron kp	Thermo Fischer Scientific, Heraeus
Incubation shakers and general shakers	HAT Minitron	Infors AG,
	New Brunswick™ Innova® 44/44R	Eppendorf AG
	IKA KS 4000 ic central	IKA Laboratory Equipment
	MaxQ 2000	Thermo Fischer Scientific
	TiMix 5 control	Edmund Bühler GmbH, Hechingen
	Rocking platform	VWR International GmbH
Thermoblock and thermoshakers	Tmix	Analytik Jena
	Eppendorf ThermoMixer® C	Eppendorf®
	SLG digital dry bath	Süd-Laborbedarf GmbH
Fast protein liquid chromatography (FPLC)	ÄKTA™ purifier UPC 900	GE Healthcare Europe GmbH

Device category	Device	Manufacturer
	Pump P-900	GE Healthcare Europe GmbH
	Sample pump UP-960	GE Healthcare Europe GmbH
	Control unit UPC-900	GE Healthcare Europe GmbH
FPLC Columns	HisTrap FF Crude 1 mL, 5 mL	Cytiva
	HisTrap FF 5 mL	Cytiva
	HiTrap Desalting HiPrep 26/10 Desalting	Cytiva
High-performance liquid chromatography (HPLC)	UltiMate 3000 RS and LC System	Thermo Fischer Scientific, Dionex
	Degasser SRD 3400	Thermo Fischer Scientific, Dionex
	Pump module 3400RS	Thermo Fischer Scientific, Dionex
	Pump module 3400 RD	Thermo Fischer Scientific, Dionex
	Autosampler WPS 3000TRS	Thermo Fischer Scientific, Dionex
	Autosampler WPS 3000TSL	Thermo Fischer Scientific, Dionex
	Column compartment TCC3000RS	Thermo Fischer Scientific, Dionex
	Ultimate 3000 Photodiode Array Detector	Thermo Fischer Scientific, Dionex
HPLC detectors	Refractive Index Detector	Shodex
	DAD 3000RS Diode Array Detector	Thermo Fischer Scientific, Dionex
	Evaporative light scattering detector (ELSD), Varian 380-LC	Varian
	RezexROA-Organic Acid H ⁺ (8%)	Phenomenex
Columns	Triat Diol-Hilic 1,9 µm 100 mm 2 mm	YMC
	GromSil OPA-3 3 µm, 125 mm, 4.0 mm	Dr. Maisch
	Trace GC 2000 with Ultra Trace	Thermo Fischer Scientific
Gas chromatography (GC)	GC-autosampler TriPlus Autosampler	Thermo Fischer Scientific
	Flame ionization detector (FID)	Thermo Fischer Scientific

Device category	Device	Manufacturer
GC-Columns	Stabilwax	Restek
Magnetic stirrer	MR 3001 K	Heidolph Instruments GmbH & Co.KG,
	VMS-C7	VWR International GmbH
Microliter pipets, electric	Transferpette® S -8 electronic 10-200 µL	BRAND GmbH & Co. KG
	Research pro 8x 1200 µL	Eppendorf®
	Research pro 12x 300 µL	Eppendorf®
Microliter pipets, manual	Transferpette® S : 0.1-10,000 µL	BRAND GmbH & Co. KG
	Microliter syringe, 25 µL	Hamilton AG
PCR thermocyclers	MJ Mini™ Personal Thermo Cycler	Bio-Rad Laboratories GmbH
	MyCycler™ Thermal Cycler	Bio-Rad Laboratories GmbH
	CFX96 Touch Real-Time PCR Detection System	Bio-Rad Laboratories GmbH
	C1000 Touch Thermal Cycler	Bio-Rad Laboratories GmbH
	Dual 48/48 Fast Reaction Module	Bio-Rad Laboratories GmbH
	Q-POD Milli-Q Waterbath ED-33	JULABO Labortechnik GmbH
Water systems, Water bath and ultrasonic devices	CC1 Compatible Control Microprocessor Control MPC	Huber
	Ultrasonic Cleaner	VWR International GmbH
	FiveGo™	Mettler-Toledo GmbH,
	FiveEasy™	Mettler-Toledo GmbH,
pH meter and electrodes	pH Elektrode LE438	Mettler-Toledo GmbH,
	InLab® Micro Pro pH 0-14 ; 0-100 °C	Mettler-Toledo GmbH,
	Microscales Pioneer™	Ohaus Europe GmbH,
Balances	TE6101	Sartorius AG
	TE1502S	Sartorius AG
	AW320	Shimadzu Corporation
	Epoch 2	BioTek Instruments, Inc.
Plate reader, spectrophotometer	Varioskan	Thermo Fischer Scientific
	NanoPhotometer® P-Class	Implen,

Device category	Device	Manufacturer
Vacuum pump	Vacuum pump PC 2004 VARIO	VACUUBRAND GmbH & Co. KG
Vortex mixer	Vortex Genie	Scientific Industries Inc,
Microwave	Microwave MH 25 ED	ECG

2.1.2. Software and Databases

Software and databases used during studies are listed in Table 3

Table 3: Software and databases used in this study

Software	Supplier	Version number/ Reference
UniProt	European Bioinformatics Institute, UK; Schweizer Institut für Bioinformatik, Schweiz; Protein Information Ressource, US	135
Braunschweig Enzyme Database (BRENDA)	<i>Technische Universität</i> Braunschweig, Institut für Biochemie und Biotechnologie, http://www.brenda-enzymes.info/	136
NCBI	National Center for Biotechnology Information, http://www.ncbi.nlm.nih.gov/	137
Basic Local Alignment Search Tool BLAST	National Center for Biotechnology Information	138
Benchling	Benchling, Inc (benchling.com)	Benchling [Biology software] (2020 - 2023)
Expasy translate tool	Swiss Institute of Bioinformatics	139
Expasy ProtParam	Swiss Institute of Bioinformatics	140
Multalin	Plateforme Bioinformatique Genotoul	5.4.1 ¹⁴¹
Clone Manager 9	Scientific & Educational Software	9.5.1
eQuilibrator	Weizmann Institute in Rehovot, Israel	3.0 ¹⁴²
eQuilibrator pathway analysis	Weizmann Institute in Rehovot, Israel	143
Bio-Rad CFX Manager	Bio-Rad Laboratories GmbH	3.1
Intas	Intas Science Imaging Instruments GmbH	3.9.3
YASARA	YASARA Biosciences GmbH	15.11.18
Chromeleon	Thermo Fischer Scientific	6.8

Software	Supplier	Version number/ Reference
ChemDraw	PerkinElmer	17.0
Chem3D	PerkinElmer	17.0
OriginPro	Originlab	2021b
PyMol	Schrodinger, LLC	2.5.2
CopasiUI	Copasi.org	4.4
Clustal Omega	Conway Institute, UCD	1.2.4
Xcalibur™	Thermo Fisher Scientific	2.0.7
Unicorn	GE Healthcare	7.3
Gen	BioTek	5.3.1 and 2.09.1
Skanit	Thermo Fisher Scientific	2.4.3
Office 2016	Microsoft	Professional Plus 2016

2.1.3. Chemicals

Chemicals used in the studies are listed in Table 4

Table 4: Chemicals used in this study

Chemicals	Supplier/Manufacturer	Catalogue number
Tris(hydroxymethyl)aminomethane (Tris Base)	Carl Roth	AE15.2
Ethylenediaminetetraacetic acid (EDTA)	Carl Roth	8040.2
Acetic acid	Carl Roth	6755.1
Glycerol 99.5%	Fisher Bioreagents	12144481
Sodium hydroxide (NaOH)	Carl Roth	6771.2
Xylene cyanol	VWR(Serva)	SERA38505.01
Bromophenol blue	Merck	108122
Agarose	Biozym	840004
DNA Stain Clear G	VWR(Serva)	SERA39804.02
Agar-Agar	Carl Roth	5210.4
Yeast extract	Carl Roth	2363.5
Peptone/Tryptone	Carl Roth	8952.5

Chemicals	Supplier/Manufacturer	Catalogue number
Sodium chloride (NaCl)	Carl Roth	P029.3
Potassium chloride (KCl)	Carl Roth	6781.2
Magnesium chloride hexahydrate (MgCl ₂ * 6H ₂ O)	Carl Roth	2189.1
Magnesium sulfate heptahydrate (MgSO ₄ * 7H ₂ O)	Carl Roth	8283.2
α -D-glucose monohydrate	Carl Roth	6887,5
4-(2-hydroxyethyl)-1-piperazineethanesulfonic acid (HEPES)	Carl Roth	HN78.3
Calcium chloride (CaCl ₂)	Carl Roth	5239.1
Potassium hydroxide (KOH)	Carl Roth	6751.1
Manganese chloride tetrahydrate MnCl ₂ * 4H ₂ O	Merck	M3634
Dimethyl sulfoxide (DMSO)	Carl Roth	4720.1
DMSO for molecular biology	Sigma	D8418
Liquid nitrogen (N ₂)	Linde	
Monopotassium phosphate (KH ₂ PO ₄)	Carl Roth	3904.3
Dipotassium phosphate (K ₂ HPO ₄)	Carl Roth	P749.3
Ammonium sulfate ((NH ₄) ₂ SO ₄)	VWR	A1032.5000
Disodium phosphate (Na ₂ HPO ₄)	VWR	1.065.862.500
α -Lactose monohydrate	Carl Roth	6868.1
Isopropyl β -D-1-thiogalactopyranoside (IPTG)	Carl Roth	CN08.3
Ampicillin sodium salt	Carl Roth	K029.2
Kanamycin sulfate	Carl Roth	T832.3
Imidazole	Merck	1047161000
Hydrochloric acid (HCl)	Carl Roth	4625.2
Glycine	Carl Roth	3790.2
Sodium dodecyl sulfate	VWR (Serva)	SERA20760.02
Tris(hydroxymethyl)aminomethane (Tris-HCl)	Carl Roth	9090.3
Ammonium persulfate	VWR	1.01201.0500
Coomassie G250	VWR (Serva)	(0472) 443283M

Chemicals	Supplier/Manufacturer	Catalogue number
β-Mercaptoethanol	Merck	805740
Rotiphorese® Gel 30 (37,5:1)	Carl Roth	3029.1
Tetramethylethylenediamine (TEMED)	Carl Roth	2367.3
Sulfuric acid (H₂SO₄)	Carl Roth	4623.4
Acetonitrile	VWR	83640.320
Formic acid	Sigma (Fluka)	06440
Monosodium phosphate (NaH₂PO₄ * H₂O)	Sigma Aldrich	71496
Boric acid	Sigma	B7901
OPA-Reagent	Dr-Maisch	9800600
Fluorescamin	VWR	43749.MB
L-norvaline	Dr-Maisch	9041901
L-Alanine	Sigma-Aldrich	A7627
Acetylacetone	VWR	8.000.230.005
Ammonium acetate	Carl Roth	7869.2
37% Formaldehyde	Carl Roth	4979.2
Diphenylamine	Merck	8205280100
Dihydroxyacetone	VWR	8204820025
Methanol	VWR	83638320
Acetaldehyde	Carl Roth	3004.1
Ethanol	Sigma	32221-M
Isobutanol	Sigma	1.00984
2,2'-Azino-di(3-ethylbenzthiazolin-6-sulfonsäure), ABTS	Sigma	10102946001 Sigma (Roche)
SYPRO™ Orange protein gel stain	Sigma	S5692
β-Nicotinamidadenindinucleotid (NAD⁺)	Carl Roth	AE11.2
β-Nicotinamidadenindinucleotidphosphat (NADP⁺)	Carl Roth	AE13.1
β-Nicotinamidadenindinucleotid (NADH)	Carl Roth	AE12.1

Chemicals	Supplier/Manufacturer	Catalogue number
β-		
Nicotinamidadeninucleotidphosphat (NADPH)	Carl Roth	AE14.2
Adenosine-5'-triphosphate (ATP)	Carl Roth	HN35.4
Adenosine-5'-diphosphate (ADP)	VWR (Serva)	SERA10800.02
Thiamine pyrophosphate (TPP)	Sigma	C8754-5G
Glucose-1-Phosphate	Alfa Aesar	A12064.06
Glyceraldehyde D/L	Sigma	G5001
Dihydroxyacetone phosphate	Santa Cruz	sc-214896A
Glyceraldehyde 3-phosphate	Sigma	G5251
3-Phosphoglycerate	Santa Cruz	sc-214793A
2-Phosphoglycerate	Sigma	79470
Phosphoenolpyruvate	(VWR) Alfa Aesar	B20358.06
Pyruvate	Carl Roth	8793.1
Xylose	Carl Roth	5537.3
Fructose-1.6-bisphosphate	Sigma	F6803
Xylulose	Cayman Chemicals	Cay20830-50
Xylulose 5-Phosphate	Carbosynth	MX29090
2,3-Dihydroxyisovalerate	Sigma	39693
2-Ketoisovalerate	Sigma	W386901
Isobutyraldehyde	Sigma	418110

2.1.4. Buffers and Media

Media compounds were weight in and diluted in Milli-Q water. Afterward, heat-stable media were sterilized through an autoclave for 20 minutes at 121 °C and ~200 kPa. Heat-unstable media, buffers and solutions were sterilized through a syringe with a 0.2 µm sterile filter (VWR). Buffers for HPLC were prepared in 1- or 2 L volumetric flasks for precise preparation. All buffers were filtered before usage with a 0.2 µm filter membrane (regenerated Celluloseacetat Labsolute®).

2.1.5. Kits

Commercial kits used for the studies are listed in Table 5

Table 5 Commercial Kits

Kit	Manufacturer	Catalog number
DNeasy® Ultra Clean® Microbial Kit	Qiagen	12224-50
GeneJET Plasmid Miniprep Kit	Thermo Fisher Scientific	K0503
NucleoSpin Gel and PCR Clean-up Mini Kit	Macherey-Nagel	740609.250

2.1.6. Commercial enzymes used for enzymatic assays

Commercial enzymes used in this study for assays or in the cascades are listed below (Table 6).

Table 6: Commercial enzymes for assays used in this study

Enzyme	Origin	Application	Manufacturer	Catalog number
Pyruvate Kinase/Lactate dehydrogenase mix	Rabbit muscle	Enzymatic assays for activity determination of ATP, dependent reactions or activity determination of enzymes from lower glycolysis (2.2.3)	Sigma	P0294
Lactate dehydrogenase	Rabbit muscle	Activity determination of pyruvate kinase (2.2.3.9)	Carl Roth	6060.1
Alcohol oxidase	<i>Pichia pastoris</i>	Methanol oxidation in cascade reactions (2.2.9)	Sigma	A2404
Catalase	<i>Corynebacterium glutamicum</i>	H ₂ O ₂ detoxification in cascade reactions (2.2.9)	Sigma	02071
Glyceraldehyde 3-Phosphate dehydrogenase	Rabbit muscle	Activity determination of triose phosphate isomerase (2.2.3.5)	Sigma	G2267
Aldolase	Rabbit muscle	Activity determination of Glyceraldehyde 3-phosphate dehydrogenases (2.2.3.4)	Sigma	A2714
3-Phosphoglycerate-phosphokinase	Yeast	Activity determination of triose phosphate isomerase (2.2.3.5)	Sigma	P7634

2.1.7. Commercial enzymes used for molecular biology and purification

Enzymes which were used for molecular biology applications as gene cloning, polymerase chain reaction etc. are listed in Table 7.

Table 7: Commercial Enzymes used in this study

Enzyme	Manufacturer	Catalogue number	Application
DNase I	AppliChem	A3778,0500	Purification, DNA cleavage
Taq DNA Polymerase	Promega	M166A	Molecular biology, PCR reaction
Phusion High-Fidelity DNA-Polymerase	NEB	M0530L	
CIP, Alkaline Phosphatase	NEB	M0290S	Hydrolyzation of free phosphate groups
T4 DNA Ligase	NEB	M0203S	DNA ligation
NdeI	NEB	R0111S	Restriction enzyme
SacI-HF	NEB	R3156S	Restriction enzyme
BamHI-HF	NEB	R3136S	Restriction enzyme
XhoI	NEB	R0146S	Restriction enzyme

2.1.8. Bacterial strains

Escherichia coli NEB Turbo (NEB) and *Escherichia coli* DH5 α (DH5 α TM F- ϕ 80lacZ Δ M15 Δ (lacZYA-argF) U169 recA1 endA1 hsdR17 (rK-,mK+) phoA supE44 λ - thi-1 gyrA96 relA1) (Invitrogen/ Thermo Fisher Scientific) were used as cloning strains. *Escherichia coli* BL21 (DE3) (F- ompT gal dcm lon hsdSB(rB- mB-) λ (DE3 [lacI lacUV5-T7 gene 1 ind1 sam7 nin5])) (Novagen) was used as the expression strain.

Microorganisms carry genes of interest and are used for cloning genes of interest for usage in the studies are listed in Table 8.

Table 8: Microorganisms carry genes of interest

Microorganism	Strain	Origin
<i>Escherichia coli</i>	TOP10	Invitrogen
<i>Geobacillus</i> <i>stearothermophilus</i>	ATCC 7953	Merk Kit Sterikon® plus Bioindikator
<i>Meiothermus ruber</i>	21	DSMZ 1279
<i>Clostridium cellulovorans</i>	743B	DSMZ 3052
<i>Kozakia baliensis</i>	SR-745	Chair of Chemistry of Biogenic Resources
<i>Variovorax paradoxus</i>	EPS	RUB - LS für Biologie der Mikroorganismen

2.1.9. Oligonucleotides

Oligonucleotides used to amplify genes via PCR were purchased from Eurofins Scientific and are listed in Table 9.

Table 9: Oligonucleotides used in this study. The highlighted segment represents the cutting site for the restriction enzymes used. The annealing temperature (T_a) of oligonucleotides was calculated via the NEB T_m Calculator web application for Phusion® High-Fidelity DNA Polymerase with Phusion® High-Fidelity DNA Polymerase buffer (HF-Buffer) and an oligonucleotide concentration of 500 nM.

Name	Sequence	Application	T_a
Mut_fw-lac_2	GAATTG TGAGC GGATAA CAATTCCC	Colony PCR standard primer and amplification of flsm3 full gene	64
Mut_rev_2	CTTTGT TAGCAG CCGG ATCTC	Colony PCR standard primer and amplification of flsm3 full gene	
FW_gsTPI_NdeI	GCCATATG AGAAAACCG ATCATTG CAGGCAA CTGGAAAATGC	Amplification of gsTPI gene from genomic DNA	72
RV_gsTPI_SacI	AAGAGCTC TTACTCAT GACGCCCG CCTCCACC	Amplification of gsTPI gene from genome	
FW_mrTktA_NdeI	GCCATATG ACCCAGATA CCCCC ATTGCAAAAAGC	Amplification of mrTktA gene from genome	72
RV_mrTktA_BamHI	GAGGATCC TCAAACC CCCAAC AGGACTT CACCTCG	Amplification of mrTktA gene from genome	
FW_gsPgmI_NdeI	ATACATATG AGTAAAAA ACCGTTG CGCTCA TCATTTTAG	Amplification of gsPgmI gene from genome	69
RV_gsPgmI_SacI	AGAGCTC TTATTGACA ATCAACGAT TTCCCGTCATTTC	Amplification of gsPgmI gene from genome	
FW_ccGapN_NdeI	ATCATATG TTAAAAA TCTTTGT AATGAGG AAAAAATA	Amplification of ccGapN gene from genome	61
RV_ccGapN_SacI	AAGAGCTC TTAAATATCTA AATTCATAACA ATAACCTTATGTC	Amplification of ccGapN gene from genome	
FW_kbDhaK_NdeI	CCCATATG AAGCGCT TTTATAATCAT CGCGATA CTATTGTGAGC	Amplification of kbDhaK gene from genome	72
RV_KbDhaK_XhoI	GACTCGAG TCAAACCA GCCCTTC CAGGAGCCG	Amplification of kbDhaK gene from genome	

Name	Sequence	Application	T _a
FW_vpTK1_Nhis_NdeI	GCCATATG GCAAAC CACGC CCTGATGGC	Amplification of vpTK1 gene from genome	72
RV_vpTK1_Nhis_XhoI	CGCTCGAG TCAGTCC CGCAGC GCCGCTTC	Amplification of vpTK1 gene from genome	
FW_ecTK1_Nhis_NdeI	GCGCATATG TCCTCACGT AAAGAGCTTGC	Amplification of ecTK1 gene from genome	65
RV_ecTK1_Nhis_XhoI	CGCTCGAG TTACAGC AGTTCTTTT GCTTTCGC	Amplification of ecTK1 gene from genome	
Flanking T7mut_RV	GCAGGCCAAACA GATGTTT TACGCCAGC	Amplification of gene section of FLS gene for overlap extension PCR	
I28L_Formolase	CTGTTTGGCCTG CATGGCCTGCA TATTGA CACCATTTTC	Amplification of gene section of FLS gene for overlap extension PCR	
N283H_Formolase	GGGTGCTCG TTTCGGTCTG CATACCGGT CATGGTTCCGG	Amplification of gene section of FLS gene for overlap extension PCR	
RV_I28L_Overhang_T90L	CGTTCG CGATCGGC GTAACGGC	Amplification of gene section of FLS gene for overlap extension PCR	
RV_T90L_Overhang_N283H	CGAAACGAG CACCCA GCATCAGTACC AGGTCCGGAGC	Amplification of gene section of FLS gene for overlap extension PCR	
T90L_Formolase	GCCGATC GCGAAC GCTAGGCTGG ATCGCACTCCG	Amplification of gene section of FLS gene for overlap extension PCR	

2.1.10. Plasmids

Plasmids used or generated are listed in Table 10

Table 10: Plasmids used in this study

Plasmid	Description	Reference
pET28a	Empty vector for cloning	Novagen
pET24a	Empty vector for cloning	Novagen
pJET1.2	Empty vector for cloning	pJET Cloning Kit, Thermo
pET28a_ecTk1_nHis	Expression vector for transketolase gene of <i>Escherichia coli</i> with N-terminal His ₆ Tag	Created in this study
pET28a_vpTK_Nhis	Expression vector for transketolase gene of <i>Variovorax paradoxus</i> with N-terminal His ₆ Tag	Created in this study
pET28a_ecXylB	Expression vector for xylulokinase gene of <i>Escherichia coli</i> with N-terminal His ₆ Tag	Provided by André Pick
pET28a_kbDHAK	Expression vector for dihydroxyacetone kinase gene of <i>Kozakia baliensis</i> with N-terminal His ₆ Tag	Created in this study
pJET1.2_tk_GAPN	cloning vector with codon-optimized glyceraldehyde 3-phosphate dehydrogenase gene of <i>Thermococcus kodakarensis</i> for further cloning	Gene string bought from Geneart; blunt end ligation with pJet1.2
pET28a_tkGAPN	Expression vector for codon-optimized glyceraldehyde 3-phosphate dehydrogenase gene of <i>Thermococcus kodakarensis</i> with N-terminal His ₆ Tag	Created in this study
pET28a_ccGapN	Expression vector for glyceraldehyde 3-phosphate dehydrogenase gene of <i>Clostridium cellulovorans</i> with N-terminal His ₆ Tag	Created in this study
pET28a_tkGAPN_NO	Expression vector for non-codon-optimized glyceraldehyde 3-phosphate	Plasmid bought from Twist

Plasmid	Description	Reference
	dehydrogenase gene of <i>Thermococcus kodakarensis</i> with N-terminal His ₆ Tag	Bioscience (non-codon optimized gene)
pET28a_Nhis_GsKARI-	Expression vector for Ketoacid reductoisomerase gene of <i>Geobacillus stearothermophilus</i> with N-terminal His ₆ Tag	Created in this study
pET28a_gsIpgM_Nhis	Expression vector for phosphoglycerate mutase gene of <i>Geobacillus stearothermophilus</i> with N-terminal His ₆ Tag	Created in this study
pET28a_mrTktA_Nhis	Expression vector for transketolase gene of <i>Meiothermus ruber</i> with N-terminal His ₆ Tag	Created in this study
pET28a_gsTpI_nhis	Expression vector for triose phosphate isomerase gene of <i>Geobacillus stearothermophilus</i> with N-terminal His ₆ Tag	Created in this study
pET24a_FLSM3	Expression vector for formolase gene with C-terminal His ₆ Tag	Created in this study
pET24a_FLS_CHIS	Expression vector for formolaseM3 gene with C-terminal His ₆ Tag	Provided by the Chair of Chemistry of Biogenic Resources (¹⁴⁴).
pCBR-NHis-ENO003	Expression vector for enolase gene of <i>Thermotoga maritima</i> with N-terminal His ₆ Tag	Provided by the Chair of Chemistry of Biogenic Resources.
pCBR-NHis-PYK004	Expression vector for pyruvate kinase gene of <i>Thermoplasma acidophilum</i> with N-terminal His ₆ Tag	Provided by the Chair of Chemistry of Biogenic Resources.

Plasmid	Description	Reference
pET28a-BsAlaDH	Expression vector for alanine dehydrogenase gene of <i>Bacillus subtilis</i> with N-terminal His ₆ Tag	Provided by the Chair of Chemistry of Biogenic Resources.
pET28NhisStDHAD1	Expression vector for dihydroxy acid dehydratase gene of <i>Schlegelella thermodepolymerans</i> with N-terminal His ₆ Tag	Provided by the Chair of Chemistry of Biogenic Resources (¹⁴⁵).
pET28a-LlkdcA	Expression vector for Ketoacid decarboxylase gene of <i>Lactococcus lactis</i> with N-terminal His ₆ Tag	Provided by the Chair of Chemistry of Biogenic Resources (¹⁴⁶).
pET28a_KdcA_7M.D	Expression vector for Ketoacid decarboxylase 7M.D gene of <i>Lactococcus lactis</i> with N-terminal His ₆ Tag	Provided by the Chair of Chemistry of Biogenic Resources (¹⁴⁷).
pET28a-NH-yjgB-E.c	Expression vector for alcohol dehydrogenase gene of <i>Escherichia coli</i> with N-terminal His ₆ Tag	Provided by the Chair of Chemistry of Biogenic Resources (¹⁴⁸).
pET28a-NH-yahK-E.c	Expression vector for alcohol dehydrogenase gene of <i>Escherichia coli</i> with N-terminal His ₆ Tag	Provided by the Chair of Chemistry of Biogenic Resources (¹⁴⁸).
pET28a-CH-yqhD-E.c	Expression vector for alcohol dehydrogenase gene of <i>Escherichia coli</i> with N-terminal His ₆ Tag	Provided by the Chair of Chemistry of Biogenic Resources (¹⁴⁸).
pCBR-C-His-AlsS	Expression vector for acetolactate synthase gene of <i>Bacillus subtilis</i> with C-terminal His ₆ Tag	Provided by the Chair of Chemistry of Biogenic Resources (⁷⁵).

Plasmid	Description	Reference
pCBRHisC-ZmPDC	Expression vector for pyruvate decarboxylase gene of <i>Zymomonas mobilis</i> with C-terminal His ₆ Tag	Provided by the Chair of Chemistry of Biogenic Resources (¹⁴⁹).
pet28a-XylA(PS)	Expression vector for xylose isomerase gene of <i>Pseudomonas fluorescens</i> with N-terminal His ₆ Tag	Provided by the Chair of Chemistry of Biogenic Resources.
pET28a_tmTIMfusPGK	Expression vector for triose phosphate isomerase gene of <i>thermotoga Maritima</i> with N-terminal His ₆ Tag	Provided by the Chair of Chemistry of Biogenic Resources

2.2. Methods

2.2.1. DNA manipulation methods

2.2.1.1. Plasmid isolation

Plasmids were isolated from either *Escherichia coli* strain DH5 α or NEB Turbo. The GeneJET Plasmid Miniprep Kit from Thermo Fisher Scientific was used as described in the manufacturer protocol (User Guide: GeneJET Plasmid Miniprep Kit).

2.2.1.2. Genomic DNA isolation

Genomic DNA (gDNA) of *Escherichia coli* strain NEB Turbo was isolated using the DNeasy[®] Ultra Clean[®] Microbial DNA Isolation Kit from Qiagen GmbH. DNA was isolated as described in the manufacturing protocol (DNeasy UltraClean Microbial Kit Handbook).

2.2.1.3. Gene amplification by polymerase chain reaction

Genes of interest were isolated by using polymerase chain reaction (PCR). Thereby genes were either amplified from extracted gDNA or directly from the strain. The procedure was adapted from the NEB protocol (PCR Protocol for Phusion[®] High-Fidelity DNA Polymerase M0530¹⁵⁰): 0.5 μ M of forward and reverse primer were mixed with 50 ng of gDNA, one unit of Phusion[®] High-Fidelity DNA Polymerase, 1x HF-buffer, 1.25 mM DMSO, 200 μ M of dNTP mixture and adjusted to 25 μ L or 50 μ L with Milli-Q water in a 200 μ L PCR cup. Standard parameters for PCR (Table 10) were: 98 °C for 5 min for initial denaturation, followed by a 30x repetitive sequence of a denaturation step of 98 °C for 30 sec, an annealing step for 30 sec with annealing temperature of oligonucleotides calculated via the NEB T_m Calculator web application for Phusion[®] High-Fidelity DNA Polymerase with Phusion[®] High-Fidelity DNA Polymerase buffer (HF-Buffer) and an oligonucleotide concentration of 500 nM (Table 8). The T_m was calculated for the Oligonucleotide sequence without restriction site. An elongation step of 72 °C for a specific time was calculated from the length of the gene of interest (30 sec per kilobase). After the sequence was over, a final elongation step of 10 min at 72 °C was applied to finalize the PCR (Table 11). For amplification directly from the microorganisms, 20 μ L LB-medium or Milli-Q water was inoculated with the microorganism of interest, and 1 μ L of this solution was added to the reaction mixture instead of gDNA. In exceptional cases, a gradient during the annealing step was applied by varying the temperature from 55 °C to 72 °C. Temperature yielding the desired product was subsequently used in a standard PCR.

Table 11: Standard PCR scheme

Step	Temperature [°C]	Time [min]	Cycles
Initial denaturation	98	5	1
Denaturation	98	0.5	
Primer annealing	55 - 72	0.5	30
Elongation	72	0.5 / kb	
Final Elongation	72	10	1
Hold	10		1

2.2.1.4. Colony PCR

Colony PCR was used to control the ligation and transformation procedures. The standard protocol for colony PCR with Taq polymerase was adapted from NEB protocols (PCR Protocol for Taq DNA Polymerase with Standard Taq Buffer M0273¹⁵¹). For this, *Escherichia coli* colonies were picked with a sterile toothpick and transferred to 20 μ L of LB-medium containing a selection antibiotic. 200 μ M dNTP mixture, 0.2 μ M forward Mut_fw-lac_2 and Mut_rev_2 (Table 8), 1.25 mM DMSO and 1x ThermoPol polymerase buffer were mixed and adjusted to 23.875 μ L with Milli-Q water. The reaction was started by adding 1 μ L of cell suspension and 0.6 U (0.125 μ L) Taq DNA Polymerase to the solution. The typical PCR procedure was as follows (Table 12). An initial denaturation cycle for 5 min at 95 °C, followed by a sequence of 30 cycles of denaturation (30 sec at 95 °C), annealing (30 sec at 55 °C) and elongation (1 min/kB at 68 °C). Final elongation was performed at 68 °C for 10 minutes (Table 12). The annealing temperature was increased from 50 °C (calculated via NEB T_m calculator for Taq polymerase and ThermoPol buffer) to 55 °C.

Table 12: Colony PCR scheme

Step	Temperature [°C]	Time [min]	Cycles
Initial denaturation	95	10	1
Denaturation	95	0.5	
Primer annealing	55	0.5	30
Elongation	68	1 / kb	
Final Elongation	68	10	1
Hold	10		1

2.2.1.5. Overlap Extension PCR

Overlap extension PCR was adapted from Williams et al. ¹⁵² and used for site directed mutagenesis. This type of PCR introduced three manipulations leading to the mutations I28L, T90L and N283H to formolase (FLS) to create the variant FLSM3 (Table 13). For this, primers were created carrying the needed base exchanges and the associated flanking primers (Table 8). Four gene sections were amplified (2.2.1.3) and purified as described in section 2.2.1.6. Primer combinations are shown in Table 13. The four sections with base pair (bp) lengths between 144 bp and 944 bp were used in another PCR to create the full-length gene. For this, equal molar ratios of the sections were added with Mut_fw-lac_2 and Mut_rev_2 primer. A PCR was conducted with an annealing temperature of 55 °C for 30 seconds and an elongation temperature of 72 °C for 1 min. The PCR product was purified via gel electrophoresis and cloned into a pJet1.2 vector using the CloneJET PCR-cloning kit. The full-length gene was transferred via restriction ligation cloning (2.2.1.7) to the expression vector pET24a.

Table 13: Primer combinations for overlap extension PCR to create FLSM3.

Gene section	Primer 1	Primer 2	Annealing temperature [°C]
1	Mut_fw-lac_2	Flanking T7mut_RV	65
2	I28L_Formolase	RV_I28L_Overhang_T90L	72
3	T90L_Formolase	RV_T90L_Overhang_N283H	72
4	N283H_Formolase	Mut_rev_2	64

2.2.1.6. DNA separation and purification via gel electrophoresis

Buffers and solutions used for gel electrophoresis are described in Table 14. As marker a 1 kb Plus DNA Ladder (NEB) was used.

Table 14: Buffers and solutions for agarose gel electrophoresis

Buffers and solutions	Preparation	Storage temperature [°C]
50x TAE buffer	2 M Tris base, 50 mM EDTA, 57 mL L ⁻¹ acetic acid	RT
1x TAE buffer	50x TAE buffer diluted with Milli-Q water	RT
1% agarose solution	1% agarose (w v ⁻¹) dissolved in 1x TAE buffer (5 minutes heating in the microwave)	65
5x DNA loading dye	75 mM Tris base, 50 mM EDTA, 50% glycerol (v v ⁻¹), 0.025% bromophenol blue (w v ⁻¹), 0.025% xylene cyanol (w v ⁻¹), pH was adjusted to pH 7.6 with NaOH	-20

For purification and visualization of genes amplified by PCR or restriction methods, DNA was purified by gel extraction. The DNA was diluted with the 5x DNA loading dye, resulting in a 1x DNA loading dye, and loaded onto a 1% agarose gel.

The agarose gel was prepared by mixing 50 - 100 mL of 1% agarose solution 100 μ L of Serva DNA dye and poured into a tray. A special comb was inserted to form wells for loading the DNA samples.

After solidification of the agarose, the tray was placed in a DNA electrophoresis chamber along with the gel. 1x TAE buffer was used to cover the agarose gel. 20 to 50 μ L of the previously prepared DNA samples were added to the gel. 8 μ l of 1 kb plus DNA ladder (NEB) was added to a well to control and confirm DNA size. The chamber was closed and a 110 V to 120 V voltage was applied for 25 to 35 min.

The gel was placed on a transilluminator for visualization with an additional gel extraction step. For visualization without further extraction, DNA bands were visualized using a Gel iX Imager with a camera and UV light using Intas software.

For purification of the DNA bands, DNA was cut out and purified using the NucleoSpin Gel and PCR Clean-up Mini Kit as described in the manufacturer protocol (MACHEREY-NAGEL User manual).

2.2.1.7. Restriction ligation cloning

For restriction ligation cloning, 1000 to 2000 ng of purified plasmid and gene DNA were cut by specific restriction enzymes (Table 7, Table 9) at 37 °C for 2 h in 1x CutSmart buffer (NEB)

in a reaction volume of 40 μL . After 1.5 h, 0.5 μL of Quick CIP (Table 7) was added to the plasmid restriction solution to dephosphorylate the cut plasmid. CIP was inactivated by incubating the solution for 2 min at 80 $^{\circ}\text{C}$. DNA was then separated and purified as described in 2.2.1.6. Ligation of specific plasmid and gene DNA fragments was performed with T4 ligase (Table 7). 50 to 100 ng of plasmid DNA was ligated with gene DNA at a ratio of 1:3 calculated by NEBioCalculator. A standard procedure was established following NEB ligation protocols (Ligation Protocol with T4 DNA Ligase (M0202)): Plasmid DNA and target DNA were mixed in 1x T4 ligase buffer. Milli-Q water was used to adjust the volume to 19 μL in a 200 μL cup. 1 μL of T4 DNA ligase was added to the solution to start the ligation. The solution was incubated at 16 $^{\circ}\text{C}$ for 16 hours. Subsequently, the T4 DNA ligase was inactivated by heating the solution to 65 $^{\circ}\text{C}$ for 20 minutes. After heat treatment, the solution was stored at -20 $^{\circ}\text{C}$ until further use (2.2.1.10).

1.1.1.1. CloneJET PCR Cloning with pJET vector

For pJET cloning, the method described in the CloneJet PCR cloning kit user manual (Thermo Fisher Scientific) was used. 50 ng pJET1.2/blunt cloning vector was mixed with 1 μL of purified gene DNA and 10 μL of 2x reaction buffer (Thermo Fisher Scientific). Milli-Q water was used to adjust the volume to 19 μL and 1 μL T4 ligase (Table 7) was added. The ligation mixture was incubated for 5 to 30 minutes at room temperature and afterward stored at -20 until further usage. DNA sequencing

15 μL of purified plasmid with a concentration of 50 $\mu\text{g } \mu\text{L}^{-1}$ to 100 $\mu\text{g } \mu\text{L}^{-1}$ were sent for sequencing to Eurofins Genomics GmbH, Germany. Sequencing was performed with sequencing primers provided by Eurofins Genomics GmbH Germany, namely T7 and T7 term.

2.2.1.8. Preparation of chemically competent Escherichia coli cells.

The following media, buffers and solutions were used. In the case of SOB-medium, tryptone, yeast extract and NaCl were weight diluted in water and autoclaved together. KCl, MgCl_2 and MgSO_4 were autoclaved separately. Full SOB-Medium was prepared by adding the separately autoclaved components together (Table 15).

Table 15: Buffers and media for the preparation of chemically competent *Escherichia coli* cells

Buffers and solutions	Preparation	Storage temperature [°C]
SOB-medium	0.5% (w v ⁻¹) yeast extract, 2% (w v ⁻¹) tryptone, 10 mM NaCl, 2.5 mM KCl, 10 mM MgCl ₂ , 10 mM MgSO ₄	RT
TB-buffer	10 mM HEPES, 15 mM CaCl ₂ , 250 mM KCl, 55 mM MnCl ₂ , KOH for pH adjusting to pH 6.7	4

The preparation of chemically competent *Escherichia coli* cells procedure was adapted from Inoue et al. ¹⁵³. For this purpose, 250 mL of SOB-medium was inoculated with a freshly prepared pre-culture to an OD₆₀₀ of 0.05 and incubated in a 2-liter flask at 20 °C and 200 rpm to an OD₆₀₀ of 0.6. Cells were then chilled on ice for 10 minutes and centrifuged in a pre-chilled centrifuge at 4 °C and 2500 g for 10 minutes. Cells were resuspended in 80 mL of cold TB-buffer, and DMSO was slowly added to a final concentration of 7%. After incubation on ice for 10 minutes, the cell suspension was divided into 0.1 mL aliquots and immediately frozen in liquid nitrogen. Competent cells were stored at -80 °C until further use.

2.2.1.9. Transformation of chemically competent *Escherichia coli* cells

The following media, buffers and solutions were used. SOC-medium was similarly prepared to SOB-medium (2.2.1.3), whereby 1 M glucose was also separately autoclaved and mixed after autoclaving (Table 16).

For the preparation of LB-agar plates (20 mL LB-agar, 20 µL selection antibiotic), the LB-agar solution was cooled down before the addition of the selection antibiotic and quickly cast after addition.

Table 16: Buffer, media and solutions used in the transformation of chemically competent cells.

Buffers and solutions	Preparation	Storage temperature [°C]
SOC-medium	SOB-Medium (2.2.1.3), 20 mM Glucose	-20
LB-medium	1% Tryptone, 0.5% yeast extract, 1% NaCl	RT
LB-agar	1% Tryptone, 0.5% yeast extract, 1% NaCl, 1.5% agar-agar	65
Selection antibiotic	100 mg mL ⁻¹ kanamycin in Milli-Q water	-20
	100 mg mL ⁻¹ ampicillin in Milli-Q water	

100 μ L of competent *E. coli* cells were thawed on ice for 10 min, split into 50 μ L, and transferred to a sterile Eppendorf tube. Suitable amounts of DNA (50 ng plasmid DNA or 10 μ L ligation mixture) were added to the cells and gently mixed by inverting the tube. Cells were incubated on ice for 30 minutes and afterward, heat shocked by transferring the tube to a pre-warmed water bath at 42 °C for 45 sec. After incubation on ice for 3 minutes, 900 μ L of SOC-Medium was added for cell regeneration and the mixture was incubated at 37 °C for 45 min to 1 h with 150 rpm shaking. Afterward, cells were plated on LB-agar plates containing the appropriate selection antibiotic. For plasmid isolation, a colony from the LB-agar plate was picked and used to inoculate 5 mL LB-medium in a reaction tube containing the appropriate selection antibiotic (diluted 1: 1000). The reaction tube was incubated overnight at 37 °C and 300 rpm. The next day, cells were centrifuged at 1500 g for 10 minutes, and plasmids were isolated using the GeneJET Plasmid Miniprep Kit (Thermo Fisher Scientific) as described in the manufacturer's protocol.

2.2.2. Protein production

2.2.2.1. Gene expression with *Escherichia coli* BL21(DE3)

The following media, buffers and solutions were used. In the auto-induction medium, ZY-medium, 20x NPS solution, 50x5052 solution and MgSO₄ were autoclaved and mixed together afterward. TB-medium and TB 10x phosphate buffer were autoclaved separately and mixed afterward (Table 17, Table 18).

Table 17: Buffers and Media used for protein production

Buffers and solutions	Preparation	Storage temperature [°C]
LB-medium	2.2.1.4	RT
LB-agar	2.2.1.4	65
ZY-Medium	1% Tryptone, 0.5% yeast extract	RT
20x NPS solution	6.6% (NH ₄) ₂ SO ₄ , 13.6% KH ₂ PO ₄ , 14.4% (w v ⁻¹) Na ₂ HPO ₄	RT
50x5052 solution	25% glycerol, 2.5% glucose, 10% α-Lactose	RT
MgSO₄ solution	1 M MgSO ₄ in Milli-Q water	RT
TB-medium	1.4% tryptone, 2.4% yeast extract, 0.4% glycerol	RT
TB 10x phosphate buffer	0.17 M KH ₂ PO ₄ , 0.72 M K ₂ HPO ₄	RT
IPTG solution	1 M IPTG in Milli-Q water	-20
Kanamycin solution	462.2.1.10	-20

Table 18: Preparation of auto-induction medium and TB-medium

Medium	Solutions	mL
	TB-medium	900
TB-medium with TB-buffer	TB 10x phosphate buffer	100
	Kanamycin solution	1
	ZY-Medium	928
	20xNPS	50
Auto-induction medium	50x5052 solution	20
	MgSO ₄ solution	1
	Kanamycin solution	1

E. coli BL21(DE3) was the host of choice for gene expression. The day before performing the protein expression experiments, a freshly transformed *E. coli* BL21(DE3) colony on LB-agar plates with 100 µg mL⁻¹ kanamycin as the selection antibiotic was used to inoculate 20 mL of LB-medium with 100 µg mL⁻¹ kanamycin as a pre-culture. The pre-cultures were incubated overnight at 37 °C and 160 rpm. The next day, the OD₆₀₀ of the pre-culture was determined

using a NanoPhotometer® P-Class (Implen), and one liter auto-induction medium containing $100 \mu\text{g mL}^{-1}$ kanamycin was inoculated in a 5-liter baffled flask to an OD_{600} of 0.05. The flasks were incubated at 37°C and 95 to 140 rpm until an OD_{600} of 0.5 to 0.7 was achieved. The temperature was then lowered to 16 to 25°C , depending on the protein of interest, and incubation continued for a total runtime of 24 hours. Afterward, cells were centrifuged at 3500 g for 30 min. The supernatant was decanted and cells were stored until usage at -20°C . For the FLS and FLSM3 production TB-medium was used instead of autoinduction-medium. Following the protocol from above, the only difference in the procedure was the addition of $100 \mu\text{M}$ IPTG (final concentration) before temperature reduction.

2.2.2.2. Cell lysis

The following buffers and solutions were used. For the preparation of binding buffer, stock solutions of 1 M HEPES, 5 M imidazole, 5 M NaCl were prepared beforehand. These solutions were mixed to prepare the target buffer (Table 19).

Table 19: Buffers for the cell lysis

Buffers and solutions	Preparation	Storage temperature [$^\circ\text{C}$]
DNaseI solution	10% (w v^{-1}) DNaseI, 20 mM Tris-HCl, 50% glycerol, 1 mM MgCl_2	-20
Binding buffer	500 mM NaCl, 20 mM Imidazole, 10% glycerol, 50 mM HEPES pH 7.5 adjusted with NaOH	RT

The cell pellets of expression cultures were resuspended by vortexing in the binding buffer in a 50 mL falcon tube. This way, a solution of a maximum of 20% (w v^{-1}) of the cells were prepared. Lysis was conducted via sonication using the different sonotrodes LS24d10, LS24d3 and VialTweeter (Hielscher Ultrasonics GmbH) with an amplitude of 80% and a cycle length of 0.6-sec puls and 0.4-sec pause for two times eight to ten minutes. For this, the cell suspension in the falcon tube was placed on ice and the sonotrode was dipped into the solution. Cell suspensions in Eppendorf tubes for test lysis via the VialTweeter, were sonicated for 45 sec and afterwards placed on ice for one minute. This procedure was repeated for three times. For the procedure with the falcon, the falcon was turned upside down between the two runs to mix the solution. Afterward, DNaseI solution was supplemented with a final concentration of $10 \mu\text{g mL}^{-1}$ and lysate was incubated for 20 minutes at room temperature to cleave released DNA.

After incubation, the lysate was centrifuged at 40,000 g at 20 °C for 30 minutes (21,000 g for Eppendorf tubes). The supernatant was filtered through a 0.2 µm syringe filter and placed on ice until further use.

2.2.2.3. Protein purification.

For the preparation of binding-, elution- and storage buffer, stock solutions of 1 M HEPES, 5 M imidazole, 5 M NaCl were prepared beforehand. These solutions were mixed to prepare the target buffer. Target buffers were filtered (0.2 µm filter membrane regenerated Celluloseacetat Labsolute®) on the same day before usage on the ÄKTA™ purifier system (Table 20).

Table 20: Buffers for the ÄKTA™ purifier system

Buffers and solutions	Preparation	Storage temperature [°C]
Binding buffer	2.2.2.2	RT
Elution buffer	500 mM NaCl, 500 mM Imidazole, 10% glycerol, 50 mM HEPES pH 7.5 adjusted with NaOH	RT
Storage buffer	50 mM HEPES pH 7.5 adjusted with NaOH	RT

All proteins purified contained a His₆tag and could be purified by immobilized metal ion affinity chromatography (IMAC). For this, an ÄKTA™ purifier system, equipped with a HisTrap™ FF crude column or HisTrap™ FF column was used. Proteins containing a His₆Tag can bind to these columns and be eluted with imidazole. The protein purification process was monitored by UV measurement at 280 nm and conductivity. Samples for quality control were taken from the lysate, flow-through of the washing step, the fraction derived from the imidazole gradient and for the pure pooled protein fraction and analyzed by SDS-PAGE (2.2.2.6). To prepare the column, ten column volumes (CVs) of water were applied with a flow rate of 5 mL min⁻¹. Afterward, the column was equilibrated with 10 CVs of binding buffer. The sample was applied via a sample pump at a flow rate of 5 mL min⁻¹ to bind the protein of interest to the column. After application, the column was washed with 5 to 10 CVs of binding buffer to wash out loosely bound protein. The UV signal was monitored to estimate whether all loosely bound proteins were eluted, and the wash was stopped when it reached near zero. The protein of interest was eluted using a gradient of elution buffer from 0% to 100% in 5 CVs. Fractions of 1.8 mL were collected in a 96-deep well plate and fractions containing protein based on the UV signal were collected. Fractions were pooled based on the UV signal, whereby the first and last

fractions containing an increased UV signal were withdrawn. The HisTrap™ columns were washed after usage with 10 CVs of water and 5 CVs in 20% ethanol. HisTrap™ columns were stored after usage in 20% ethanol at room temperature.

2.2.2.4. *Size exclusion chromatography*

Pooled fractions were then applied to a size exclusion chromatography column (SEC) to remove unwanted imidazole, salts and glycerol using the ÄKTA™ purifier system. In the first step, a HiPrep 26/10 SEC column was washed with 10 CVs of Milli-Q water and afterward equilibrated with 50 mM HEPES-buffer pH 7.5 with a flow rate of 10 mL min⁻¹. A maximum of 15 mL protein solution was loaded onto the column with a flow rate of 5 mL min⁻¹. Afterward, a single protein fraction was eluted by applying 50 mM HEPES-buffer pH 7.5 (storage buffer) with a 5 mL min⁻¹ flow rate. The protein-containing fraction was collected according to the UV signal. To store the HiPrep 26/10 SEC column, the column was washed with Milli-Q water for 10 CVs and 20% ethanol for 5 CVs. Afterward, it was stored in 20% ethanol at room temperature.

2.2.2.5. *Storage of purified protein solutions*

Purified proteins were flash-frozen by adding the solution dropwise to liquid nitrogen and stored at -80 °C as beads.

2.2.2.6. *Protein concentration determination*

Protein concentration was determined using a NanoPhotometer® P-Class (Implen). For this, 2 µL of storage buffer was added and measured as a blank. To measure protein concentration, 2 µL of protein solution was added, and absorption was measured at 280 nm after adding the extinction coefficient and molecular weight of the target enzyme to the system. Extinction coefficient and molecular weight were determined with the ProtParam tool (ExPASy) based on the protein sequence of the target protein. The extinction coefficient is estimated based on the composition of amino acids. Here the molar extinction coefficients of cystine, tyrosine and tryptophan are used to calculate the extinction coefficient of the target protein (Formula 1)¹⁵⁴. With the extinction coefficient of the proteins calculated, the protein concentration can be further calculated by the Lambert-Beer law (Formula 2).

$$\epsilon_{prot(280)} = N_{Tyr} * \epsilon_{Tyr(280)} + N_{Trp} * \epsilon_{Trp(280)} + N_{Cystine} * \epsilon_{Cystine(280)} \quad (1)$$

$\epsilon_{prot(280)}$: Target protein extinction coefficient at 280 nm [$M^{-1} cm^{-1}$]
 $\epsilon_{Tyr(280)}$: Extinction coefficient of tyrosine at 280 nm [$1490 M^{-1} cm^{-1}$]
 $\epsilon_{Trp(280)}$: Extinction coefficient of tryptophan at 280 nm [$5500 M^{-1} cm^{-1}$]
 $\epsilon_{Cystine(280)}$: Extinction coefficient of cystine at 280 nm [$125 M^{-1} cm^{-1}$]
 N_{Tyr} : Number of tyrosine in one protein
 N_{Trp} : Number of tryptophan in one protein
 $N_{Cystine}$: Number of cystine in one protein

$$C_{prot} = \frac{A_{280}}{d * \epsilon_{prot(280)}} * MW_{prot} \quad (2)$$

c_{prot} : Target protein concentration [$mg mL^{-1}$]
 A_{280} : Absorption at 280 nm
 d : layer thickness [cm]
 MW_{prot} : Molecular weight of the target protein [Da]
 $\epsilon_{prot(280)}$: Target protein extinction coefficient at 280 nm [$M^{-1} cm^{-1}$]

1.1.1.2. Sodium dodecyl sulfate polyacrylamide gel electrophoresis

Buffer solutions for sodium dodecyl sulfate polyacrylamide gel electrophoresis (SDS-PAGE) were prepared as follows (Table 21).

Table 21: Buffers and solutions used for SDS-PAGE

Buffers and solutions	Preparation	Storage temperature [°C]
4x lower buffer	1.5 M Tris base, 0.8% (w v ⁻¹) sodium dodecyl sulfate, pH adjustment to pH 8.8 by HCl (37% w w ⁻¹)	RT
4x upper buffer	0.5 M Tris-HCl, 0.8% (w v ⁻¹) sodium dodecyl sulfate, one spar tip bromphenol blue, pH adjustment to pH 6.8 with NaOH (10 M)	RT
10% Ammonium persulfate solution (10% APS)	10% ammonium persulfate in Milli-Q water	-20
Coomassie staining solution	171 mM Coomassie G250, 3 mL concentrated HCl (37% w w ⁻¹)	RT
5x SDS loading dye	25% (v% v ⁻¹) glycerol, 12.5% (v% v ⁻¹) β-mercaptoethanol, 7.5% (w v ⁻¹) sodium dodecyl sulfate, 0.25 M Tris base solution pH 6.8 adjusted with HCl (37% w w ⁻¹), 0.4 mM bromphenol blue	-20
10x SDS running buffer	0.25 M Tris base, 1.92 M glycine, 1% sodium dodecyl sulfate	RT

The purity and molecular weight of proteins purified by Immobilized metal-affinity chromatography (IMAC) and Size exclusion chromatography (SEC) were determined by sodium dodecyl sulfate polyacrylamide gel electrophoresis (SDS-PAGE). An SDS gel consists of a separation and a collection gel, which must be cast before running the SDS-PAGE. For the preparation of these two gel parts, several stock solutions were prepared.

A 4x lower buffer and 4x upper buffer were prepared for the separation gel. Bromophenol blue was added to the upper buffer to have a better resolution of the wells.

SDS gels were set in an SDS-gel chamber using a two-step procedure (Table 22). First, a 12% separation gel was cast. The gel was overlaid with isopropanol before solidification to obtain a clear edge. After the gel was solidified, the isopropanol was discarded and a collection gel (5%) was poured over the separation gel. A comb with 10 or 15 wells was placed in the fresh collection gel before solidifying. Freshly prepared SDS gels were stored at 4 °C in wet tissue.

Table 22: Preparation of SDS-gels

Components	Separation gel [12% acrylamide] for 2 small 1 mm gels	Collection gel [5% acrylamide] for 2 small 1 mm gels
	Volume [μ L]	Volume [μ L]
30% Bis-acrylamide solution	4000	840
water	3290	2770
Lower buffer 4x	2500	
Upper buffer 4x		1250
10% APS	100	50
TEMED	10	5

After the preparation of the gels, further stock solutions were prepared for the SDS-PAGE. 100 mL of 10x running buffer was diluted with 900 mL of Milli-Q water to 1x running buffer. Prior to protein analysis by SDS-PAGE, 16 μ L of protein solution was mixed with 4 μ L of 5x SDS loading dye and incubated at 95 °C for 5 minutes. After heating, the solution was centrifuged for 1 minute. Meanwhile, the SDS gel was placed in a gel electrophoresis chamber and filled with 1x SDS running buffer. The comb was removed and a maximum of 20 μ L of the protein solution was pipetted into the wells. 3 to 10 μ g of the protein samples were loaded onto the gel to achieve good separation and resolution. For determination of the molecular weight of the proteins and quality control, 5 μ L of PageRuler™ unstained protein ladder (Thermo Fisher Scientific) was added to a free well. To perform SDS-PAGE, the gel chamber was closed and connected to a power supply. A constant current with a variable voltage was set at 30 mA per gel for 45 min to 1 h. The gel was then loaded onto the cell. After the running front passed the gel edge, the gel was removed from the glass plates and placed in a staining chamber. Milli-Q water was poured onto the gel and heated in a microwave for 3 min to wash the gel. The water was discarded and a Coomassie staining solution was added. The solution was heated in a microwave for three to five minutes to stain the gel. The staining solution was then removed and Milli-Q water was added again, with a tissue placed on the gel to facilitate removal of the staining solution. After another microwave cycle of three minutes, the Milli-Q water was replaced. The gel was decolorized in a shaker until good contrast was achieved if necessary.

The de-stained gel was transferred to a Gel iX Imager (Intas) with a camera and white light using Intas software for documentation. A white extension was placed onto the bottom of the chamber to receive a better resolution. A picture was taken with the system for analysis.

2.2.3. Enzymatic activity determination via NAD(P)H detection

The specific activity and kinetic characterization of enzymes were determined by measuring the absorbance of NAD(P)H at 340 nm using an Epoch 2 spectrophotometer (Biotek) with 96 well microplates (Greiner polystyrene, F-bottom clear). The target enzyme was either studied directly by catalyzing a reaction involving the reduction of NAD(P)⁺ or the oxidation of NAD(P)H, or it was coupled to a reaction involving NAD(P)H oxidation or NAD(P)⁺ reduction, respectively. The specific activity (U mg⁻¹) were determined by applying Formula 3.

$$v = \frac{a * V_{ges} * Df}{V_{enz} * \epsilon_{NADH} * d * c_{enz}} \quad (3)$$

v: Specific activity [U mg⁻¹]

a: slope

V_{ges}: Assay volume [mL]

Df: dilution factor

V_{enz}: Enzyme volume added [mL]

ϵ_{NADH} : Extinction coefficient NADH at 340 nm [6220 M⁻¹ cm⁻¹]

d: Layer thickness

c_{enz}: Enzyme concentration [mg mL⁻¹]

Further description of the assay for transketolase, dihydroxyacetone kinase, triose phosphate isomerase, glyceraldehyde 3-phosphate dehydrogenase (non-phosphorylative), phosphoglycerate mutase, enolase, pyruvate kinase, alanine dehydrogenase and alcohol dehydrogenase can be found in 3.2 and 3.3 by assaying the enzymes in suitable conditions and the matrix of the associated cascade Example reaction setups are provided in the following.

2.2.3.1. Xylose isomerase

The activity of xylose isomerase of *Pseudomonas fluorescence* (pfXylA) was assayed in a coupled approach with xylulokinase from *Escherichia coli* (ecXylB), pyruvate kinase and lactate dehydrogenase by measuring the oxidation of NADH. Standard reactions contained 100 mM xylose, 1 mM ATP, 0.3 mM NADH, 1 mM PEP, 10 mM MgCl₂, and 50 mM HEPES pH 7.5, 2 μL pyruvate kinase, lactate dehydrogenase mix (rabbit muscle) corresponding to 1.2 – 2 U pyruvate kinase and 1.8 – 2.8 U lactate dehydrogenase and 5 μg ecXylB in 200 μL at 37 °C.

2.2.3.2. *Xylulokinase*

The activity of xylulokinase of *Escherichia coli* (ecXylB) was assayed in a coupled approach with pyruvate kinase and lactate dehydrogenase by measuring the oxidation of NADH. Standard reactions were applied in 200 μ L at 37°C containing 1 mM xylulose, 1 mM ATP, 0.3 mM NADH, 1 mM PEP, 10 mM MgCl₂, and 50 mM HEPES pH 7.5 and 2 μ L pyruvate kinase, lactate dehydrogenase mix (rabbit muscle) corresponding to 1.2 – 2 U pyruvate kinase and 1.8 – 2.8 U lactate dehydrogenase.

2.2.3.3. *Transketolase*

The activity of transketolase of *Escherichia coli* (ecTktA) was assayed in a coupled approach with aldehyde dehydrogenase of *Thermoplasma acidophilum* (taAIDH) variant M42 by measuring the reduction of NAD⁺. Here, 5 mM xylulose, 1mM formaldehyde, 5 mM NAD⁺, 1 mM TPP, 10 mM MgCl₂, 0 – 0.5 mM MnCl₂ and 50 mM HEPES pH 7.5 as well as 25 μ g M42 were applied to the reaction in 200 μ L at 37 °C and the reaction was started with addition of transketolase. Additionally to this approach, ecTktA was assayed in a coupled approach with glyceraldehyde 3-phosphate dehydrogenase (GapDH) (phosphorylating) from rabbit muscle. Here, 1 mM xylulose-5-phosphate and 1 mM formaldehyde were used as substrate and the assay solution contained an additional 1 mM MgSO₄, 1mM MnCl₂, 50 mM potassium phosphate pH 7.5, 1 mM NAD⁺, 0.5 mM TPP and 16 μ g GapDH.

2.2.3.4. *Glyceraldehyde 3-phosphate dehydrogenase*

The activity of glyceraldehyde 3-phosphate dehydrogenase (GapN) of *Clostridium cellulovorans* or *Thermococcus kodakarensis* (ccGapN, tkGapN) was assayed in two ways. A direct assay with glyceraldehyde 3-phosphate is described in 3.3. Due to the expense of glyceraldehyde 3-phosphate, a coupled approach with aldolase with the substrate fructose 1,6-bisphosphate was conducted. Here 20 μ g of aldolase was used to produce glyceraldehyde 3-phosphate from fructose 1,6-bisphosphate, which can then be measured by oxidation to glycerate 3-phosphate with simultaneous reduction of NAD⁺. Reactions were applied in 200 μ L at 25, 30, or 37°C containing 1 mM fructose 1,6-bisphosphate, 0.5 mM TPP, 1 mM NAD(P)⁺, 20 μ g of aldolase and 50 mM HEPES pH 7.5.

2.2.3.5. *Triosephosphate isomerase*

The activity of triosephosphate isomerase of *Geobacillus stearothermophilus* (gsTpI) was assayed with GAPDH and 3-phosphoglycerate kinase by measuring the reduction of NAD⁺.

Reactions containing 5 mM potassium phosphate pH 7.5, 2.5 mM NAD⁺, 1 mM ADP, 1 mM dihydroxyacetone phosphate (DHAP), 50 mM HEPES pH 7.5, 24 µg GapDH (rabbit muscle) and 4.6 U ml⁻¹ 3-phosphoglycerate kinase (yeast). The reaction was started by the addition of gsTpI to the assay mixture.

The activity of triosephosphate isomerase fusion protein with phosphoglycerate kinase of *Thermotoga maritima* (tmTpI) was assayed with GAPDH by measuring the reduction of NAD⁺. Reactions containing 5 mM potassium phosphate pH 7.5, 10 mM MgCl₂, 2.5 mM NAD⁺, 1 mM ADP, 1 mM dihydroxyacetone phosphate (DHAP), 50 mM HEPES pH 7.5 and 10 µg GapDH (rabbit muscle). The reaction was started by adding tmTpI to the assay mixture at 37 °C or 30 °C.

2.2.3.6. Dihydroxyacetone kinase

The activity of dihydroxyacetone Kinase of *Kozakia baliensis* (kbDhaK) was assayed in two ways. A first coupled approach with pyruvate kinase and lactate dehydrogenase and a second coupled approach via triose phosphate isomerase and glyceraldehyde 3-phosphate dehydrogenase (non-phosphorylating). The coupling with triose phosphate isomerase and glyceraldehyde 3-phosphate dehydrogenase (non-phosphorylating) is further described in 3.3 and 2.2.6. An assay setup without all cascade components present is described in the following. Here 1 mM dihydroxyacetone, 1 mM ATP, 0.3 mM NADH, 1 mM PEP, 10 mM of MgCl₂, 50 mM HEPES pH 7.5 and 2 µL pyruvate kinase, lactate dehydrogenase mix (rabbit muscle) corresponding to 1.2 – 2 U pyruvate kinase and 1.8 – 2.8 U lactate dehydrogenase setting the assay matrix. Reactions were carried out at 30 °C or 37 °C and started by adding kbDhaK to the assay solution.

2.2.3.7. Phosphoglycerate mutase

The phosphoglycerate mutase activity of *Geobacillus stearothermophilus* (gsPgM) was assayed in a coupled approach with enolase (tmENO) and PyK/LDH mix. Here, 1 mM 3-phosphoglycerate, 1 mM MnCl₂, 10 mM MgCl₂, 1 mM ADP, 0.3 mM NADH, 50 mM HEPES pH 7.5, 5.6 µg tmENO, and 2 µl pyruvate kinase, lactate dehydrogenase mix (rabbit muscle) corresponding to 1.2 – 2 U pyruvate kinase and 1.8 – 2.8 U lactate dehydrogenase. The reaction was started by adding gsPgM to the reaction mixture at 37 °C or 30 °C.

2.2.3.8. Enolase

The enolase activity of *Thermotoga maritima* (tmENO) was assayed in a coupled approach with PyK/LDH mix by measuring the oxidation of NADH. Here, 2 mM 2-phosphoglycerate, 1 ADP,

0.3 mM NADH, 10 mM MgCl₂, 50 mM HEPES pH 7.5 and 2 µl pyruvate kinase, lactate dehydrogenase mix (rabbit muscle) corresponding to 1.2 – 2 U pyruvate kinase and 1.8 – 2.8 U lactate dehydrogenase were provided. The reaction was started by adding tmENO to the reaction mixture at 37 °C or 30 °C.

2.2.3.9. Pyruvate kinase

The pyruvate kinase activity of *Thermoplasma acidophilum* (taPyK) was assayed in a coupled approach with lactate dehydrogenase mix by measuring the oxidation of NADH. Here, 1 mM PEP, 1 mM ADP, 10 mM MgCl₂, 0.3 mM NADH, 50 mM HEPES pH 7.5 and 9 µg Lactate dehydrogenase from rabbit muscle were provided in the mixture. The reaction was started by adding taPyK to the reaction mixture at 37 °C or 30 °C.

2.2.3.10. Acetolactate synthase

The activity of acetolactate synthase of *Bacillus subtilis* (bsAlsS) was assayed in a coupled system with ketol-acid reductoisomerase from *Geobacillus stearothermophilus* (gsIlvC) by measuring the oxidation of NADPH. Reactions were applied in 200 µL at 37°C containing one mM pyruvate, 1 mM TPP, 0.3 mM NADPH, 10 mM MgCl₂, and 50 mM HEPES pH 7.5 and 0.1 mg gsIlvC.

2.2.3.11. Ketolacid reductoisomerase

The activity of ketol-acid reductoisomerase of *Geobacillus stearothermophilus* (gsIlvC) was assayed in a coupled system with acetolactate synthase from *Bacillus subtilis* (bsAlsS) by measuring the oxidation of NADPH. Reactions were applied in 200 µL at 37°C containing 1 mM pyruvate, 1 mM TPP, 0.3 mM NADPH, 10 mM MgCl₂, and 50 mM HEPES pH 7.5 and 16 µg bsAlsS.

2.2.3.12. Dihydroxy-acid dehydratase

The activity of dihydroxy-acid dehydratase of *Schlegelella thermodepolymerans* (stIlvD) was assayed in a coupled system with alpha-keto-acid decarboxylase from *Lactococcus lactis* (llKDC) and alcohol dehydrogenase of *Escherichia coli* (ecYahK) by measuring the oxidation of NADPH. Reactions were applied in 200 µL at 37°C containing 1 mM 2,3-Dihydroxyisovalerate, 1 mM TPP, 0.3 mM NADPH, 10 mM MgCl₂, and 50 mM HEPES pH 7.5, 23 µg llKDC and 60 µg ecYahK.

2.2.3.13. *Alpha-keto-acid decarboxylase*

The activity of alpha-keto-acid decarboxylase of *Lactococcus lactis* (llKDC) was assayed in a coupled system with alcohol dehydrogenase of *Escherichia coli* (ecYahK) by measuring the oxidation of NADPH. Reactions were applied in 200 μ L at 37°C containing 2.5 mM 2-ketoisovalerate, 1 mM TPP, 0.3 mM NADPH, 10 mM MgCl₂, and 50 mM HEPES pH 7.5 and 60 μ g ecYahK.

2.2.3.14. *Alcohol dehydrogenase*

The activity of alcohol dehydrogenases of *Escherichia coli* (ecYqhD, ecYjgB and ecYahK) was assayed in a direct assay by measuring the oxidation of NADPH. Assays containing 50 mM HEPES pH 7.5, 0.3 mM NADPH and a substrate as 2.5 mM isobutyraldehyde, 2.5 mM formaldehyde, or 5 mM glyceraldehyde. Reactions were started by adding ADH to the reaction mixture at 37 °C.

2.2.3.15. *Aldehyde dehydrogenase*

The activity of aldehyde dehydrogenase of *Thermoplasma acidophilum* (taAIDH) variant M42¹⁵⁵ was assayed by measuring the direct reduction of NAD⁺. Assay mixtures containing 50 mM HEPES pH 7.5, 5 mM NAD⁺ and a substrate as 5 mM glyceraldehyde or 5 mM glycol aldehyde or 5 mM formaldehyde. Reactions were started by adding M42 to the reaction mixture at 30 °C or 37 °C.

2.2.3.16. *Alanine dehydrogenase*

The activity of alanine dehydrogenase of *Bacillus subtilis* (bsAlaDH) was assayed by directly measuring the oxidation of NADH. Reactions containing 50 mM HEPES pH 7.5, 200 mM (NH₄)₂SO₄, 0.3 mM NADH and 1 mM pyruvate. The reaction was started by adding alanine dehydrogenase to the reaction mixture at 30 °C.

2.2.4. Enzyme kinetic measurements

For the enzymes transketolase, dihydroxyacetone kinase, alcohol dehydrogenase, alanine dehydrogenase, Pyruvate kinase, enolase, phosphoglycerate mutase, glyceraldehyde 3-phosphate dehydrogenase (non-phosphorylative) and triosephosphate isomerase enzyme kinetic measurements were conducted. Transketolase (ecTktA) and alcohol dehydrogenase (ecYahK, ecYqhD and ecYjgB) were conducted at 37 °C, whereby the other enzymes were assayed at 30 °C. Dihydroxyacetone kinase (kbDhaK) was assayed at both temperatures and

kinetics for dihydroxyacetone but also for D-glyceraldehyde in a similar assay system with a concentration range of 0.002 to 50 mM was measured. A more detailed description of the kinetic measurements is provided in chapters 3.2 and 3.3. Kinetic parameters were calculated based on the Michaelis Menten- or Hill-fit (Formula 4 and Formula 5) of Origin (2021b)

$$y = \frac{v_{max} * x}{(K_m + x)} \quad (4)$$

y: specific activity [U mg⁻¹]
*v*_{max}: maximum velocity [U mg⁻¹]
*K*_m: Michalis constant [mM]
x: substrate concentration [mM]

$$y = \frac{v_{max} * x^n}{(k^n + x^n)} \quad (5)$$

y: specific activity [U mg⁻¹]
*v*_{max}: maximum velocity [U mg⁻¹]
k: Michaelis constant [mM]
n: cooperative sites
x: substrate concentration [mM]

2.2.5. Enzyme thermostability analysis

The melting point of the cascade enzymes was determined by a thermal shift assay. A gradient was run with a temperature increase from 25 °C to 100 °C or from 5 °C to 100 °C with an increase of 1 °C or 0.5 °C per minute or per five seconds, respectively. A standard reaction was conducted with 2 µL protein (protein concentration 1 mg mL⁻¹, if a poor resolution of 1 mg mL⁻¹ appeared, protein concentrations were raised to 5 mg mL⁻¹), 2 µL SYPRO® orange protein gel stain (1:80 dilution in Milli-Q water of a 5000x concentrated stock solution from Sigma-Aldrich) and additives as described in 3.2 and 3.3 to have a final volume of 25 µL in Hard-Shell® 96-Well PCR Plates (Bio-Rad™). Melt curves and melting point were analyzed as described in the protein thermal shift assay protocol of Bio-Rad™ (Protein Thermal Shift Assays Made Easy with the Bio-Rad™ Family of CFX Real-Time PCR Systems Protocol). CFX Maestro Software was used to set up the thermal shift assay and analyze melting temperatures. In scan mode, the FRET channel was applied and all samples were determined as “unknown.” For the analysis, the derivative of the melting curve is provided in the analysis window of the software and the peak type was set to „Negative.” Afterward, melting temperatures are displayed in the data table.

2.2.5.1. Long-term thermostability analysis

For the enzymes kbDhak, bsAlsS, gsPgM, gsIlvC, lIKDC, ecYjgB, pfXylA, taPyK, tkGapN, tmENO and ccGapN, additional thermostability measurements were conducted whereby the enzymes were incubated over a runtime of 32 h at 37 °C. Additionally, the incubation at 37 °C ccGapN and tkGapN were incubated at 25 °C. For that, enzymes were diluted to concentrations between 0.1 and 2.7 mg mL⁻¹ (Table 23) and incubated in 50 mM HEPES pH 7.5 and 10 mM MgCl₂. The exception to this was gsPgM. Here additionally, 1 mM MnCl₂ was added. For ccGapN no MgCl₂ was added. Time points were taken by diluting the enzymes (Table 23) and adding them to an assay mixture to conduct an enzyme activity assay as described before (2.2.3). Residual activity was calculated by normalizing the activity values to the activity measured at 0 h. Residual activity percentage was plotted vs. incubation time.

Table 23: Concentration of enzymes during incubation and final dilution of enzymes in Assay

Enzyme	Concentration [mg mL ⁻¹]	Final dilution in assay
kbDhaK	1.2	250
taPyK	0.3	250
tmENO	0.1	250
tkGapN	0.1	100
gsIlvC	2.7	500
gsPgM	0.3	250
pfXylA	0.2	200
bsAlsS	0.4	500
llKDC	0.2	500
ecYjgB	0.4	50
ccGapN	0.1	500

2.2.6. Enzyme stability with the addition of formaldehyde and isobutanol

2.2.6.1. Enzyme activity with additional formaldehyde

Enzyme activity in the presence of formaldehyde was determined by measuring the enzyme activity with additional 5- and 10-mM formaldehyde at 30 °C as described in Section 3.3.

2.2.6.2. Formaldehyde stability of kbDhaK with separation experiments

Separation experiments of kbDhaK were conducted by assaying the activity of kbDhaK by using the coupled PyK/LDH assay system as described in 3.3. For kbDhaK, a 400 μ L solution including 1 mM ATP, 5 mM NAD⁺, 50 mM HEPES, 10 mM MgCl₂, 0.5 mM TPP, 0.5 mM G1P, 200 mM (NH₄)₂SO₄, 0.1 mM MnCl₂ similar to the methanol cascade conditions (3.3) was constructed with 1 mg mL⁻¹ kbDhaK and 0 – 10 mM formaldehyde. Incubation at 30 °C and 50 rpm on a nutating shaker (VWR Rocking Platform, VWR, Germany) was started by adding enzyme to the mixture. After an incubation time of 2 h, 200 μ L of the mixture was separated and filtered via a centrifugal filter (modified PES 10 kDa VWR). The filtered enzyme was re-diluted in 200 μ L solution without adding formaldehyde and incubated further. Samples were taken from the solution and 1:100 diluted in 50 mM HEPES pH 7.5. 20 μ L of this dilution was added to the assay mixture (3.3), yielding an additional dilution of 1:10.

2.2.6.3. Formaldehyde stability of *kbDhaK*, *taPyK* and *tmENO*

For the enzymes *kbDhaK*, *taPyK*, and *tmENO*, additional formaldehyde stability measurements were conducted whereby the enzymes were incubated with 1, 5 and 10 mM formaldehyde over a runtime of 24 h at 37 °C in 50 mM HEPES pH 7.5 and 10 mM MgCl₂ (Table 24). As an exception, *kbDhaK* was incubated with 1 mg mL⁻¹ bovine serum albumin and no MgCl₂. Time points were taken by diluting the enzymes and adding them to an assay mixture to conduct an enzyme activity assay using an Epoch 2 spectrophotometer (Biotek) with 96 well microplates (Greiner polystyrene, F-bottom clear at 37 °C. The assay for *kbDhaK* contained 1 mM dihydroxyacetone, 1 mM ATP, 0.3 mM NADH, 1 mM PEP, 1 mM MgCl₂, 50 mM HEPES pH 7.5, and 2 µL pyruvate kinase, lactate dehydrogenase mix (rabbit muscle) corresponding to 1.2 – 2 U pyruvate kinase and 1.8 – 2.8 U lactate dehydrogenase. The assay mixture for *tmENO* contained 2 mM 2PG, 0.3 mM NADH, 1 mM ADP, 50 mM HEPES pH 7.5, 10 mM MgCl₂ and 2 µL pyruvate kinase, lactate dehydrogenase mix (rabbit muscle) corresponding to 1.2 – 2 U pyruvate kinase and 1.8 – 2.8 U lactate dehydrogenase. The assay mixture for *taPyK* contained 1 mM PEP, 1 mM ADP, 0.3 mM NADH, 50 mM HEPES pH 7.5, 10 mM MgCl₂ and 6 U mL⁻¹ LDH (rabbit muscle).

Table 24: Concentration of enzymes during incubation and final dilution of enzymes in Assay

Enzyme	Concentration [mg mL ⁻¹]	Final dilution in assay
kbDhaK	0.7	400
taPyK	0.3	200
tmENO	0.1	200

2.2.6.4. Enzyme activity in the presence of methanol

Enzyme activity in the presence of methanol was determined to be similar to enzyme activity with the presence of formaldehyde (2.2.5.1) by adding 60 or 150 mM methanol to the assay mixture and performing an activity assay at 30 °C described in 3.3.

2.2.6.5. Isobutanol stability

Isobutanol stability analysis was conducted similarly to formaldehyde stability analysis over a runtime of 32 h. 1 or 8% isobutanol was added to an enzyme solution of *kbDhaK*, *bsAlsS*, *gsPgm*, *gsIlvC*, *llKDC*, *ecYjgB*, *pfXylA*, *taPyK*, *tkGapN* or *tmENO* and incubated at 37 °C in 200 µL. Concentrations of enzymes in the assay and during incubations are shown in Table 23.

Time points were taken and enzymes were diluted as described in 2.2.4.1 and added into the enzyme assay solution to perform activity assays as described in 2.2.3.

2.2.7. Enzyme regulation and inhibition measurements

2.2.7.1. *ATP/ADP regulation*

Due to the regulatory effect of the ATP/ADP level, studies were performed to evaluate the effect on taPyK and kbDhaK. As described in 3.3, 0 to 5 mM ATP or ADP was added to the assay mixture to perform the activity assay 3.3. To determine kbDhaK activity with additional ADP concentrations, kbDhaK activity was coupled to a triosephosphate isomerase and glyceraldehyde 3-phosphate dehydrogenase (non-phosphorylating), which reduces NADP⁺.

2.2.7.2. *Inhibitory effect of manganese*

Additional manganese showed an inhibitory or inactivating effect on several enzymes. To investigate this effect, manganese concentrations of 0 to 5 mM were added to the assay systems of kbDhak, taPyK and gsPgM, as described in 3.3.

2.2.7.3. *Phosphoglycerate mutase manganese kinetics*

The activity of the phosphoglycerate mutase of *Geobacillus stearothermophilus* (gsPgM) is strictly dependent on manganese. Because of this, kinetics were conducted to determine the affinity on manganese. For that, an assay solution with 100 mM HEPES pH 7.5, 2 mM ADP, 0.3 mM NADH, 1mM MgCl₂, 4 mM 3-phosphoglycerate, 11 µg enolase (tmENO) and 0.5 µL pyruvate kinase, lactate dehydrogenase mix (rabbit muscle) corresponding to 0.3 – 0.5 U pyruvate kinase and 0.5 – 0.7 U lactate dehydrogenase with 0.002 mg mL⁻¹ gsPgM was setup. The reaction was started with the addition of 0 – 5 mM MnCl₂ and assayed at 30 °C.

2.2.7.4. *Enzyme inhibition kinetics with additional manganese*

In the studies with additional manganese above, taPyK and kbDhaK kinetics were analyzed by adding manganese. For this, kinetic measurements of taPyk were adapted to measure K_m values for MgCl₂ and K_i values for MnCl₂. To do so, phosphoenolpyruvate concentration was set to 5 mM and MgCl₂ and MnCl₂ concentrations were varied from 0 to 10 mM. Measurements were conducted in 200 µL volume and at 30 °C. Similarly, kbDhaK kinetic measurements were adapted. The ATP concentration was fixed to 1 mM and dihydroxyacetone to 5 mM. Together with that, the system was switched to the triosephosphate and glyceraldehyde 3-phosphate dehydrogenase system to have no interference of pyruvate kinase due to MgCl₂ or MnCl₂. Final

reactions were conducted in 200 μL at 30 $^{\circ}\text{C}$ with 1 mM NADP⁺, 50 mM HEPES pH 7.5, 0 to 10 mM MgCl₂ and MnCl₂ 45 μg gsTpi and 72 μg ccGapN. The data fitted to exponential decay (Formula 6). The derived values were used to calculate the IC₅₀ (Formula 7).

$$y = A1 * \exp\left(\frac{-x}{t1}\right) + y0 \quad (6)$$

y: specific activity [U mg^{-1}] or [%]

x: inhibitor concentration [mM]

A1: amplitude

t1⁻¹: decay constant

y0: offset

$$\text{IC50} = \text{LN}\left(\frac{50-y0}{A1}\right) * t1 \quad (7)$$

IC50: Half maximal inhibitory concentration

2.2.8. Thermodynamics pathway analysis using eQuilibrator

The thermodynamic driving force of the cascade was analyzed using max-min driving force (MDF) calculations as described in 3.3. To create estimates of the change in Gibbs energy, the eQuilibrator (3.0) pathway analysis web tool ¹⁴² (Table 3) was used with default settings (Metabolite concentrations: 1 μM to 10 mM, a pH of 7.5, an ionic strength of 0.25 M, and a $-\log[\text{Mg}^{2+}]$ (pMg) of 3). First, a SBtab pathway model file was created based on a pathway definition file (Table 28). The derived SBtab file was next used in the MDF framework of the eQuilibrator (3.0) pathway analysis web tool to perform the pathway analysis.

2.2.9. Cascade reactions

The enzymatic cascades provided in this study were conducted in a volume range from 50 μL to 500 μL . In brief, a master mix was created containing salts, cofactors, buffers and additives. Purified enzymes were concentrated using centrifugal filters (modified PES 10 kDa VWR) and brought to the concentration needed for usage in the cascade. Reactions were started by adding the enzymes to the master mix. Time points were taken by using centrifugal filters (modified PES 10 kDa VWR) to remove the enzymes. More detailed descriptions are provided in 3.2 and 3.3.

2.2.10. Quantification via gas chromatography

A headspace GC-FID-based method was used to quantify volatile compounds such as methanol, ethanol, isobutanol, acetaldehyde and isobutyraldehyde. GC-FID had a Headspace Tri Plus

autosampler and a Stabilwax column (length: 30m, ID: 0.25 mm film thickness: 0.25 μm , Restek, Bellefonte, USA). Helium was used as carrier gas. For analysis, 200 μL of the diluted sample was added to a 5 or 10-mL headspace vial and incubated for 15 min at 40 $^{\circ}\text{C}$. The injection was performed in split mode with a flow of 10 mL min^{-1} and an injection volume of 700 μL in headspace mode. For signal analysis and quantification, Xcalibur™ (Thermo Fisher Scientific) software was used. Methanol standard curve was determined in a range of 40 mM to 0.2 mM, isobutanol standard curve was determined in a range of 0.05 mM to 10 mM. The ethanol standard curve was determined from 0.2 mM to 10.4 mM. Acetaldehyde standard curve was determined in a range of 0.1 mM to 10 mM. Isobutyraldehyde standard curve was determined in a range of 0.1 mM to 10 mM (3.2 and 3.3).

2.2.11. Quantification via HPLC

2.2.11.1. L-alanine quantification via derivatization

The following buffers and solutions were prepared before running the HPLC (Table 25)

Table 25: Buffers used for quantification of metabolites via HPLC

Buffers and solutions	Preparation
Borate buffer	1 M boric acid adjusted with NaOH to pH 10.7
Phosphate buffer	1.6 g L^{-1} $\text{NaH}_2\text{PO}_4 \cdot \text{H}_2\text{O}$, 2.1 g L^{-1} Na_2HPO_4 adjusted with NaOH to pH 7.2
Buffer A	48.5% phosphate buffer, 48.5% Milli-Q water, 3% acetonitrile
Buffer B	50% phosphate buffer, 50% acetonitrile
Storage buffer	50% Milli-Q water, 50% acetonitrile
OPA reagent	OPA (Dr. Maisch) diluted 1:10 with borate buffer

L-alanine was quantified via an HPLC (Ultimate300 HPLC-system, Dionex Softron GmbH, Germaring, Germany) system equipped with a UV detector. L-alanine quantification was conducted via derivatization with an OPA/3-MPA reagent. Separated using a GromSil OPA-3, 3 μM , 125 mm \times 4.0 mm column (Dr. Maisch GmbH Ammerbuch-Entringen, Germany). Samples were diluted 1:10 and 1:20 in Milli-Q water and filtered with centrifugal filters modified PES 10 kDa (VWR). After filtration, 36 μM L-norvaline and 167 mM borate buffer were added to the samples, which were further diluted 1:30. Samples were derivatized by the addition of 6 μL OPA reagent to 14 μL of the sample by mixing 12x using online derivatization

and injected to the HPLC. A gradient run was set with a 100% buffer A starting setting. From 0 min to 8 min, the run was isocratic with 100% A. From 8 minutes to 15 minutes, a gradient was set from 0% buffer B to 20% buffer B and from 15 minutes to 18 minutes, from 20% buffer B to 55% buffer B. The method finished from 18 to 20 minutes with 0% buffer B. An L-alanine standard curve was prepared similar to the samples in 1 to 25 mM. L-alanine was quantified via Chromeleon version 6.8 software (Thermo Fisher Scientific). In the L-alanine quantification, the L-alanine amount was determined using the internal standard L-norvaline.

2.2.11.2. Quantification of other metabolites via HPLC

The following buffers and solutions were prepared before running the HPLC (Table 26)

Table 26: Buffers used for quantification of metabolites via HPLC

Buffers and solutions	Column	Preparation
Buffer A	Triart-Diol HILIC	0.1% (v v ⁻¹) formic acid pH 4.5 adjusted with ammonium (32%)
Buffer B		0.1% (v v ⁻¹) formic acid in acetonitrile
H₂SO₄ solution	Rezex™ ROA-Organic Acid H ⁺	2.5 mM H ₂ SO ₄ in Milli-Q water

Xylose, xylulose, glyceraldehyde, dihydroxyacetone, and pyruvate were analyzed and quantified by an HPLC Ultimate300 HPLC-system (Dionex Softron GmbH, Gernaring, Germany) equipped with a UV and RI detector. Xylose, xylulose, glyceraldehyde, dihydroxyacetone and pyruvate were diluted 1:10 to 1:30 in a concentration range of 5 mM to 0.5 mM in 2.5 mM H₂SO₄ and separated with a Rezex™ ROA-Organic Acid H⁺ (8%) 300 x 7.8 mm LC Column (Phenomenex, Germany) in an isocratic run with 2.5 mM H₂SO₄ at 70 °C for 42 min. Standard curves for xylose, xylulose, glyceraldehyde dihydroxyacetone, and pyruvate were generated in a similar range with a maximum concentration of 5 mM (for pyruvate, 2.5 mM). Quantification of metabolites was performed using Chromeleon version 6.8 software (Thermo Fisher Scientific). The amount was determined by calibration with standard curves (3.2).

HEPES was detected using an HPLC system (Ultimate300 HPLC system, Dionex Softron GmbH, Gernaring, Germany) coupled to an ELSD detector (30°C evaporation temperature, 50°C nebulizer temperature, 1.2 slm carrier flow) and equipped with a Triart-Diol HILIC

column (100 x 2.0 mm, 1.9 μm , YMC). Separation was performed at 7 °C with a flow rate of 0.4 mL min⁻¹ using gradient elution. Starting conditions were 15% buffer A and 85% buffer B. After an isocratic run of 2 minutes, a gradient was applied from 2 to 5 minutes from 15% buffer A to 30% buffer A and from 85% buffer B to 70% buffer B. These conditions were held for 4 minutes. Starting conditions were again applied from 9 minutes to 16 minutes. A HEPES standard with a maximal concentration of 3 mM was applied. Samples were diluted in 70% acetonitrile with a maximal concentration of 1.5 mM HEPES. Quantification of metabolites was performed using Chromeleon version 6.8 software (Thermo Fisher Scientific). The amount was determined by calibration with standard curves (3.3).

2.2.12. Quantification via chemical assays

2.2.12.1. Formaldehyde quantification

Formaldehyde was quantified by the acetylacetone method. Nash reagent (0.1 M acetic acid, 0.2% (v v⁻¹) acetylacetone, 3.89 M ammonium acetate) was added to a 1:200 diluted cascade sample in a 1 to-1 ratio. Incubation at 37 °C was carried out for 30 minutes. After incubation, formaldehyde concentration was determined by measuring absorbance at 412 nm via an Epoch 2 spectrophotometer (Biotek). Quantification of the amount of formaldehyde was determined using a formaldehyde standard curve prepared in the cascade matrix in a range of 0.01 mM to 1 mM (3.3).

2.2.12.2. Dihydroxyacetone quantification

The diphenylamine assay was used to quantify dihydroxyacetone present in cascade samples. Diphenylamine (60 μM), H₂SO₄ (10% (v v⁻¹)), and acetic acid (90% (v v⁻¹)) were mixed and added to a 1:5 or 1:10 diluted cascade sample. Incubation of mixed samples was conducted at 105 °C for 30 minutes. Afterward, samples were cooled down to room temperature. Dihydroxyacetone concentration was determined by measuring the absorbance at 615 nm at 25 °C via an Epoch 2 spectrophotometer (Biotek). Quantification of the amount of dihydroxyacetone was determined using a dihydroxyacetone standard curve prepared in the cascade matrix in a range of 0.01 mM to 3.0 mM (3.2 and 3.3).

2.2.12.3. L-alanine quantification

The following buffers and solutions were prepared before (Table 27)

Table 27: Buffers for L-alanine quantification via fluorescamine

Buffers and solutions	Preparation
Borate buffer	1 M boric acid adjusted with NaOH to pH 10.0
Fluorescamine solution	0.1% fluorescamine in dry acetonitrile

Samples were diluted 1:100 in Milli-Q water to quantify L-alanine via fluorescence-based assay. 5 μL of the sample was added to 8 μL of borate buffer pH, 45 μL fluorescamine solution, and 100 μL of Milli-Q water. The fluorescence (λ_{em} : 486 nm, λ_{ex} : 396 nm) was measured using a Varioscan spectral scanning multimode reader (Thermo electron Corporation). Quantification of the amount of L-alanine was determined using an L-alanine standard curve prepared in the cascade matrix in a range of 1 mM to 50 mM (3.3).

3. Results

3.1. Cell-free enzyme cascades — application and transition from development to industrial implementation

Today, biocatalysis is an important part of the chemical industry and is used in various industrial applications. However, only a few examples of *in vitro* systems for the production of bulk and commodity chemicals have been successfully implemented on a large technical scale. Nevertheless, more and more cell-free *in vitro* enzymatic cascades are being realized for a variety of different chemicals from cheap substrates, waste materials or even greenhouse gases such as CO₂. The challenge for these "proof-of-concept" cascades is now to take them through a transition phase to the final industrial scale.

In the following review, the latest achievements in the realization of new cell-free enzymatic *in vitro* systems for the production of different chemicals based on renewable substrates or waste streams are presented.

An initial discussion of the key elements of cell-free enzymatic *in vitro* systems provides an insight into key aspects of *in vitro* biocatalysis and relates them to *in vitro* systems and metabolic engineering approaches.

The following part focuses on the valorization of C1-chemicals such as CO₂, methanol or formaldehyde by the latest proof-of-principle *in vitro* systems gives insides of their achievements and discusses occurring problems that need to be solved for bringing these systems to the level of upscaling.

Based on several examples, the five key features parameter screening, flux balance, scalability, product recovery, and enzyme engineering are elaborated and discussed.

Together with this, the last part of the review deals with a new concept that synergizes the strengths of *in vitro* and *in vivo* systems. Using the iPROBE as an example, this system is described and discussed, and the workflows of separate *in vitro* and *in vivo* systems are compared to the synergistic approach. The review concludes with an outlook on how cell-free enzymatic systems can be of great value to conventional chemical production and how a synergy of *in vitro* and *in vivo* could lead these conventional chemical productions to a greener and more sustainable future.

This publication was conceived by Mariko Teshima, Vivian Pascal Willers, and Volker Sieber. The visualization was done by Mariko Teshima and Vivian Pascal Willers. The original draft was written by Mariko Teshima and Vivian Pascal Willers, and the publication was edited by Mariko Teshima, Vivian Pascal Willers, and Volker Sieber. Mariko Teshima and Vivian Pascal Willers contributed equally to this publication.

3.2. Integrating Carbohydrate and C1 Utilization for Chemicals Production

The conversion of biogenic resources into various platform chemicals as an alternative to existing petroleum-based synthetic processes is of general interest. This publication focuses on a new concept in which cell-free enzymatic cascades can be used to utilize the second most abundant sugar in nature, xylose, as well as highly interesting C1-chemicals (formaldehyde and methanol) that can be directly derived from CO₂, for the synthesis of isobutanol and ethanol.

To implement this so-called sugar-guided CO₂ fixation pathway, the general concept of the enzymatic cascade was first established based on naturally existing pathways (xylulose monophosphate pathway, glycolysis, and valine and ethanol pathways). The result is a modular enzymatic cascade with up to 13 enzymes.

Once the cascade concept was established, the key enzymes, transketolase, dihydroxyacetone kinase, and alcohol dehydrogenase, were screened for activity and substrate or product specificity.

For further characterization of all enzymes present in the cascade, a fast and efficient thermofluor-based screening was set up to analyze the variations of melting temperature with respect to different buffers and pH. Tris pH 7.5 was found to be the most suitable buffer. Further validation the cascade was based on the products yield of the cascades, isobutanol or ethanol. Under the best conditions, 85% theoretical yield of isobutanol or 75% theoretical yield of ethanol could be produced from 10 mM formaldehyde and 10 mM xylose. However, the yield decreased with increasing substrate concentration and no conversion was observed at 50 mM substrate concentration.

To optimize the cascade, formaldehyde was replaced by the inactivating compound methanol and the cascade was extended by the addition of alcohol oxidase and catalase. With this modification, 27 mM isobutanol or 66 mM ethanol could be produced from 50 mM methanol and 50 mM xylose.

This publication was conceived by Vivian Pascal Willers and Volker Sieber. The experimental methodology and investigations were performed by Vivian Pascal Willers. The visualization was done by Vivian Pascal Willers. The original draft was written by Vivian Pascal Willers, and the publication was edited and reviewed by Volker Sieber. The project was supervised by Barbara Beer and Volker Sieber.

3.3. Cell-free enzymatic L-alanine synthesis from green methanol

Methanol is used as an environmentally friendly energy carrier for storing electricity generated from renewable sources or as a transportation fuel. However, it can also be used for the synthesis of more complex molecules. This publication deals with the use of methanol to produce the amino acid L-alanine via a cell-free enzymatic one-pot cascade.

The methanol to L-alanine pathway (MAP) consists of a C1-fixation module where dihydroxyacetone (DHA) is formed from methanol via two enzymes. DHA is then converted by a glycolysis-based module to pyruvate by six enzymes. Pyruvate is then converted to the amino acid L-alanine by alanine dehydrogenase.

After defining the concept of the cascade and the initial low conversion of methanol to L-alanine, one focus was to investigate the kinetics of all cascade enzymes and their interplay to optimize the L-alanine yield. All enzymes were characterized in terms of k_{cat} and K_m value. Furthermore, variations in manganese and ATP/ADP ratios resulted in strong differences in the activity of dihydroxyacetone kinase and pyruvate kinase. By adjusting the concentrations, higher L-alanine titers could be achieved.

Further optimization of the cascade was achieved by characterizing all the enzymes for their stability in formaldehyde and methanol. By adjusting the enzyme concentrations, a theoretical yield of 75% L-alanine was observed from 60 mM methanol.

By switching the enzyme formolase (FLS), which is able to produce dihydroxyacetone from formaldehyde, to a previously engineered variant FLSM3, 18 mM L-alanine could be synthesized from 60 mM methanol. Further adjustment of the oxygen supply resulted in the conversion of 150 mM methanol to 44 mM L-alanine with a theoretical yield of 88%.

This publication was conceived by Vivian Pascal Willers and Volker Sieber. The experimental methodology and investigations were performed by Vivian Pascal Willers. A part of the enzymatic characterization was performed by Manuel Döring. The visualization was done by Vivian Pascal Willers. The original draft was written by Vivian Pascal Willers, and the publication was edited and reviewed by Volker Sieber. The project was supervised by Barbara Beer and Volker Sieber.

4. Discussion and Outlook

4.1. Cell-free enzymatic cascades for the production of amino acids and biofuels from C1-chemicals: From proof of concept to industrial application

New concepts for the direct use of CO₂ or CO₂-derived C1-compounds are the focus of research. With the ever-improving ability to produce methanol from CO₂, with pilot plants already established that are approaching the production of methanol from CO₂ via hydrogen and renewable energy, CO₂ can be used as an energy source, transportation fuel, and also as a building block.

Recently, the conversion of CO₂-derived C1-compounds to chemicals has been facilitated by fermentation using natural or synthetic methylotrophs and cell-free enzyme cascades.

Especially the flexibility of enzyme cascades and their biological origin make them a promising target for switching the production of basic chemicals from fossil substrates to renewable resources. Removing enzymes from cells and using purified enzymes has the great advantage of creating pathways that do not depend on or interfere with the overall metabolism of an organism¹⁵⁶.

In addition, the artificial and highly controlled environment allows manipulation and adaptation to the needs of the desired process. With the decreasing price of gene synthesis and the emergence of enzyme engineering platforms and machine learning optimization tools, cell-free enzyme cascades have a chance to be realized in industrial processes as an alternative to chemical production and whole-cell fermentation. However, parameters such as enzyme production, enzyme purification and enzyme stability are critical and must be cost effective to compete with existing production methods.

Various concepts are being developed for the use of methanol as a substrate in cell-free enzyme cascades, such as the production of starch or the plastic alternative PHB from CO₂-derived methanol. In addition, the research presented in this study aims at upgrading methanol to various chemicals as biofuel in the form of ethanol or isobutanol, or as food and feed additive such as L-alanine. However, as described in Section 3.1, all these new concepts need to be taken from proof of principle to the industrial phase.

4.1.1. Optimizing the efficiency of enzymatic proof of concept cascades

After the initial design of the cascades and early optimization, L-alanine as well as biofuels could be produced on a small scale in this study. High efficiencies between 90% and 88% were achieved for the production of L-alanine from 60- and 150 mM methanol, respectively. For the

production of isobutanol, a high efficiency of 85% could be achieved with 10 mM formaldehyde and 10 mM xylose, but no isobutanol formation could be detected when using 50 mM formaldehyde and 50 mM xylose as starting concentration. Switching from 50 mM formaldehyde to 50 mM methanol yielded isobutanol, with 54% yield. For bulk chemicals such as isobutanol or L-alanine, high conversion efficiencies with more than 95% yield are required for profitable industrial production¹⁵⁷. For L-alanine, high efficiency and yield has already been achieved and only fine tuning is needed to reach the 95% target. Here, reaction engineering could be applied by iteratively changing either the enzyme concentrations or the concentrations of the cascade compounds, to further increase the yield. The next step for isobutanol production is to increase the efficiency of the process using 50 mM methanol. As shown by the simultaneous utilization of methanol and xylose and the formation of isobutanol, the system does not interfere with by-product formation or substrate conversion without product formation. However, after 5 hours, simultaneous substrate conversion is hindered and more xylose is consumed rather than methanol. This imbalance in substrate conversion could indicate a decrease in activity of the methanol-oxidizing alcohol oxidase and with that no formaldehyde to be used by the transketolase. Because of that, the latter could catalyze side reactions without formaldehyde. Since transketolases can use a variety of aldehyde substrates, missing formaldehyde as co substrate could lead to more rapid conversion of xylose than methanol^{158, 159}. To validate this assumption, by-products possibly formed by transketolase could be analyzed and, if found, the substrate specificity of transketolase could be targeted. To find out if the methanol oxidase lead to the imbalance, methanol oxidase could be spiked into the system to see if methanol consumption is accelerated again. If methanol consumption is accelerated, the alcohol oxidase may be unstable, and optimizing the stability of the alcohol oxidase must be the future task. Stability could be engineered using computational tools such as FIREPROT or ancestral sequence reconstruction^{160, 161} and provide a rational or semi-rational design approach to solve this problem. In addition, alcohol oxidase could be stabilized by immobilization. This could not only make the alcohol oxidase more stable to have a higher turnover number, but could also be used to recycle the alcohol oxidase and reuse it for multiple runs^{162, 163}. Because alcohol oxidase is present in both (L-alanine and biofuel) systems, optimizing this enzyme would be beneficial for both cascades.

4.1.2. Optimizing the yield of enzymatic proof of concept cascades

In contrast to the high efficiency of the systems, the product titers of both systems are relatively low. With 2 g L⁻¹ isobutanol and 4 g L⁻¹ L-alanine, the titers are far from industrial-relevant titers of >200 g L⁻¹⁸⁷. To reach these high numbers, the first step would be an acceleration of

the space-time yield of the two processes, because a run time over several days, might cause stability problems of certain enzymes. Stability tests of pfXylA, llKDC and ecYjgB at 37°C revealed a loss of activity of more than 40-60% within 30 hours (*Figure 12* and *Figure 13*).

Isobutanol is initially produced with a space-time-yield of $0.7 \text{ g L}^{-1} \text{ h}^{-1}$, but declines rapidly. L-alanine is produced at $0.3 \text{ g L}^{-1} \text{ h}^{-1}$ and, in contrast to isobutanol, the space-time yield remains constant for 6.5 h and then declines. The difference between these two space-time-yields may occur either due to the instable pfXylA or due to instability of enzymes in the valine pathway, because the lower glycolysis module is similar. One key enzyme here could be the alcohol dehydrogenase, which has low activity coupled with a low melting point indicating thermal instability and with that a rapid activity loss at 37 °C. Long term temperature stability tests could be performed to test the activity loss of the alcohol dehydrogenase at 37 °C. A further limiting factor which leads to a decrease in space-time-yield, could occur due to oxygen limitations¹⁶⁴ and with that a strong decrease in activity of the alcohol oxidase. To test this limitation, the headspace to liquid ratio could be increased and the reaction solution could be gassed with oxygen. In addition, the oxygen concentration could be increased if oxygen is bubbled through the liquid during the reaction¹⁶⁵.

In contrast to that, enzymes from lower glycolysis are not oxygen dependent and have mostly moderate specific activities and reach relevant activities of 20 U mg^{-1} . Due to that, only minor optimization is required. The key enzymes formolase, glyceraldehyde-3-phosphate dehydrogenase and alcohol dehydrogenase, however, need to be optimized up to 100-fold to reach 20 U mg^{-1} . A calculation for the L-alanine cascade suggests, when each enzyme was engineered for a reasonable activity of 20 U mg^{-1} and a stability that would lead to a total turnover number (TTN) of 10^6 ⁹², as commonly seen in industrial biotransformation's, productivity up to 650 g (l*h)^{-1} could be achieved with 6 g of enzyme per kg L-alanine produced.

4.2. Enzymatic cascade design and optimization for the production of commodity chemicals

Besides improving the activity of the key enzymes, the development of a cell-free enzyme cascade is also about optimizing the process itself. The question of how to design these systems is often related to several parts associated with the cascade. Does the cascade originate from a metabolic pathway that allows for a blueprint? Does this pathway have its own system for regenerating cofactors, how many enzymes are involved, are all reactions natural, or are some of the required reactivity's artificial, and do the enzymes or intermediates interfere with each other?

In the production of basic chemicals, these general parameters must be adapted to the fact that the overall process must be as inexpensive as possible, since product prices for bulk chemicals such as isobutanol or L-alanine are low. Considering the enzymes used, a significant cost factor in systems with purified enzymes is the purification process itself¹⁶⁶. However, to address this issue, various aspects are discussed, such as the use of lysates without further purification¹⁶⁷, the immobilization of enzymes to increase reusability¹⁶⁸ or the use of thermophilic enzymes, allowing a simplified purification by heat treatment^{169, 170}. In general, the thermostability of the enzymes is an important factor that determines the run time of the entire process, as stable enzymes can extend the run time of the process and provide process stability. Furthermore, thermostable enzymes tend to be more tolerant to toxic compounds or solvents^{171 172}.

4.2.1. Enzymatic stability in enzyme cascades

In the systems developed in this study, a mixture of enzymes derived from thermophilic and mesophilic organisms was used to generate higher process stability in the presence of toxic intermediates such as formaldehyde, substrates as methanol and products such as isobutanol or ethanol, with having a moderate activity at low temperature. Additional data on formaldehyde- (Appendix: Figure 12) and isobutanol tolerance (Appendix: Figure 13 and Figure 14) of cascade enzymes confirm a correlation between formaldehyde stability and thermostability, as well as isobutanol stability and thermostability (Figure 6). Over 24 hours, the stability of dihydroxyacetone kinase (kbDhaK) from mesophilic *Kozakia baliensis* decreased by 100% in the presence of 5- and 10-mM formaldehyde, whereas the addition of 1 mM formaldehyde reduced activity by only 60% after 24 hours. Similar trends were observed with the addition of isobutanol. Here, the activity in 1% isobutanol decreased by 40% after 31 hours, while no activity was detected in 8% isobutanol. In contrast, the activity of enolase (tmENO), derived from a thermophilic organism, remained at about 80% after 24 hours in 1 mM formaldehyde

and is still active in 10 mM formaldehyde with about 80% activity loss after 24 hours. Isobutanol does not have a substantial effect on the activity of tmENO, and the activity remains at 70% after 31 hours of incubation in 8% isobutanol. Similar to the properties of tmENO, the pyruvate kinase derived from a thermophilic organism (taPyK) remained at 20% activity in 10 mM formaldehyde. However, this time activity in 8% isobutanol drops after 3h and no activity could be detected afterward. Still, the enzyme activity remains 87% in 1% isobutanol after 31 h of incubation. Looking at the trends of the relationship between melting temperature and stability, there is a tendency that enzymes with higher melting points are also more stable towards toxic components.

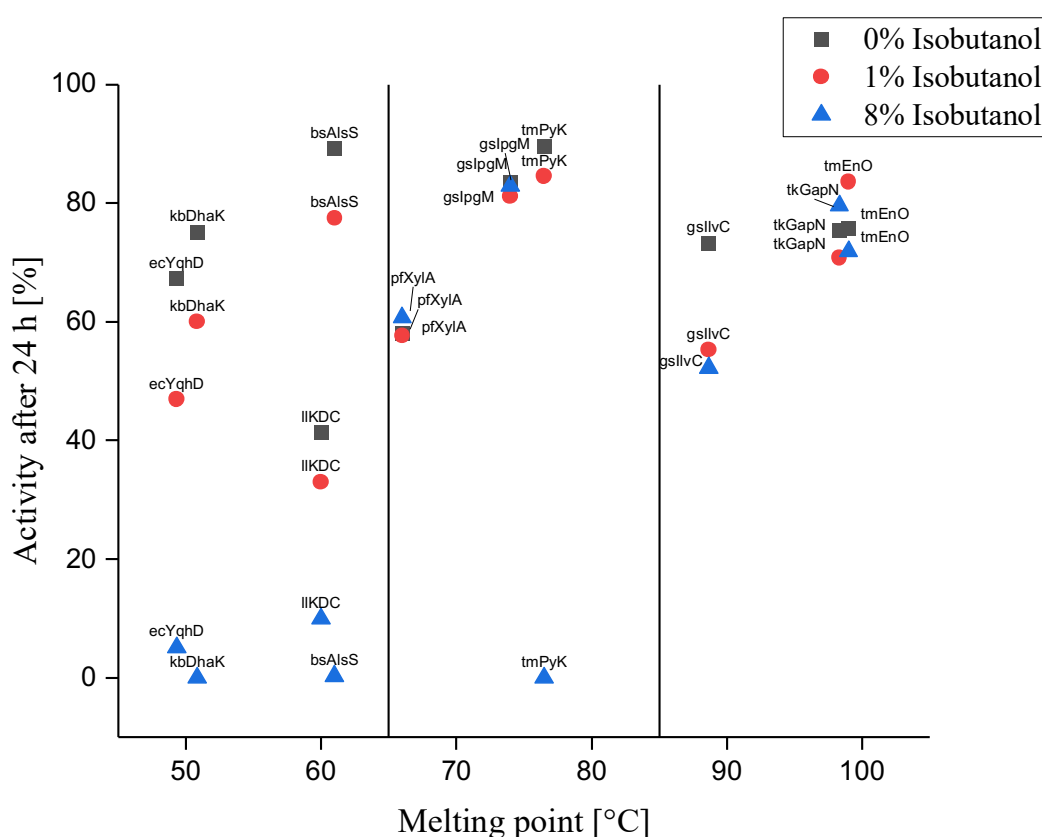


Figure 6 Correlation between melting point (T_m) and isobutanol tolerance of different cascade enzymes represented as activity of the enzymes after 24 h incubation in isobutanol at 37 °C. Activity after 24 h was normalized to activity at 0 h without the addition of isobutanol.

This tendency could also be shown by Hanatani et al. In their study, a cascade design containing only thermophilic enzymes produced L-cysteine from glucose. An important criterion here was the stability in the presence of toxic sodium hydrosulfide and stability at elevated temperature¹⁷³. Similarly, Sherkhonov et al. were able to massively improve isobutanol titers to 3 M

isobutanol from glucose by replacing isobutanol-intolerant enzymes with thermophilic variants¹³¹. By replacing the remaining mesophilic enzymes in our systems, the cost of purification could be further reduced. In addition, process stability and runtime could be extended due to the higher stability of the thermophilic enzymes and thus, higher turnover could be achieved. However, due to the need for specific enzymes and their high activity and specificity, such as dihydroxyacetone kinase, no promising alternative could be found until now, and a compromise between stability and activity was chosen as the right way for efficient production in these cascades.

4.2.2. Cofactor regeneration systems in enzymatic cascades

A further important cost-determining factor in cell-free enzymatic cascades is the use and regeneration of cofactors. The designed cascades have an intrinsic ATP and NAD(P)⁺ regeneration system due to the combination of primary and secondary metabolic routes. In contrast to cascades without an intrinsic regeneration system, low amounts of both cofactors can be applied and keep the system running. However, reducing cofactors can reduce the costs of the overall system. To recycle NAD(P)⁺, an intrinsic recycling system based on tkGapN and either bsAlaDH or gsIlvC/ecYqhD was built. However, using tkGapN for NAD(P)H recycling is not ideal because it has low activity at low temperatures. More active variants must be found to reduce the amount of the enzyme. However, many of the characterized GapN enzymes originate from hyperthermophilic organisms and are inactive at low temperatures^{174, 175}. Our study identified a GapN from the mesophilic bacterium *Clostridium cellulovorans* (ccGapN) via genome mining. However, it shows a strong preference for NADP⁺ rather than NAD⁺ and is rather unstable at 37 °C (Appendix: Figure 9 and Figure 10). To accelerate the activity of tkGapN, activity engineering could be a valuable tool to further optimize the system. While the L-alanine dehydrogenase has a low K_m for NADH in the low μM range¹⁷⁶, K_m for NAD⁺ of tkGapN is in the high mM range¹⁷⁷. The cofactor preference of tkGapN is still on NADP⁺ with a K_m in the low μM range. To improve cofactor usage, a cofactor switch engineering could reduce the overall amount of NAD⁺ in the system¹⁷⁸.

Further improvement of the system could be achieved by switching the system from ATP-dependent to ATP-free. While both systems use the lower glycolysis as the backbone, replacing this part would be necessary to develop an ATP-free cascade. Guterl et al. developed a minimized reaction cascade for producing isobutanol and ethanol via pyruvate from glucose⁷⁵. While the overall system initially relies on the non-phosphorylative branch of the Entner-Doudoroff pathway, D-glyceraldehyde recycling shows a fast and efficient way to produce pyruvate from D-glyceraldehyde. As a possible target in the system, the lower glycolysis

containing six enzymes could be reduced to a minimum of three enzymes. For this, D-glyceraldehyde generated by transketolase could be directly converted to pyruvate via aldehyde dehydrogenase and dihydroxy-acid dehydratase in two steps. The generated dihydroxyacetone, first needs to be isomerized to glyceraldehyde and could then be utilized via the same pathway. However, the isomerization of dihydroxyacetone to D-glyceraldehyde (Figure 7) is a difficult reaction ($K'_{eq} = 2.2 \cdot 10^{-3}$). Still, the feasibility of catalyzing the reaction was demonstrated by Toteva et al. with a xylose isomerase ¹⁷⁹.

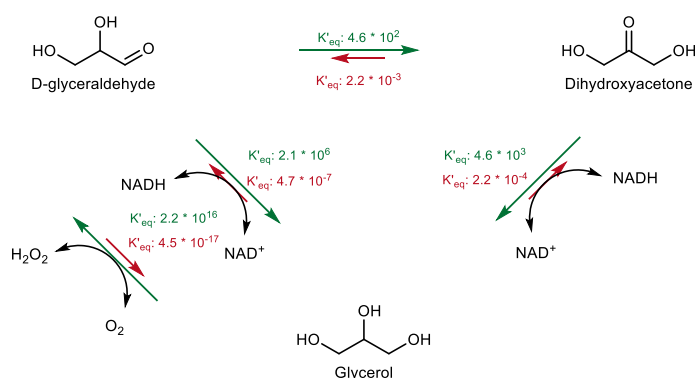


Figure 7: Schematic representations of equilibria between dihydroxyacetone, glycerol and D-glyceraldehyde adapted from Walgode et al. ¹⁸⁰ Equilibrium constants were calculated via the Equilibrator web tool (eEquilibrator 3.0 with a pH of 7.5, a PMG of 3.0 and an ionic strength of 0.25 ¹⁴²).

Another approach for the production of D-glyceraldehyde from dihydroxyacetone, could be the use of two glycerol dehydrogenases with different specificities for dihydroxyacetone and D-glyceraldehyde (Figure 7). A first glycerol dehydrogenase could perform the conversion of dihydroxyacetone to glycerol. A second glycerol dehydrogenase with a D-glyceraldehyde specificity could then be used to oxidize glycerol back to D-glyceraldehyde ¹⁸¹. However, also here, the oxidation of glycerol with NAD(P)^+ is challenging, because the thermodynamic equilibrium relies on the substrate instead of the product ($K'_{eq} = 4.7 \cdot 10^{-7}$). To generate D-glyceraldehyde from glycerol, the oxidation of glycerol needs to be coupled with a reaction which has a strong flux from D-glyceraldehyde to a product based on it. In contrast to the oxidation of glycerol with NAD(P)^+ , the oxidation with oxygen is more favorable ($K'_{eq} = 2.2 \cdot 10^{16}$) and might be performed via glycerol oxidase ¹⁸². However, this reaction is likely to be limited by the low solubility of oxygen in water at 25 °C ¹⁸³. Furthermore, an enzyme has to be found which specifically produces D-glyceraldehyde.

4.2.3. Cross-talk between components in enzyme cascades

One criterion for the success of an already established system and its improvement from proof-of-principle to industrially relevant scale is, in addition to activity and cofactor usage, the fine-tuning of the system to bring out the optimum of the process. The interplay between enzymes, cascade components, and intermediates is crucial. Intermediates within the system can inhibit the activity of enzymes in the system or lead to by-products through side activities of enzymes. In our systems' case, various adaptations were made to efficiently convert the substrates to the final products. Besides the toxic effect of formaldehyde, discussed in the following (Section 4.3), the primary metabolism is regarded as highly controlled¹⁸⁴. Therefore, it was expectable that, e.g., cofactor level might have an influence or a regulatory effect on cascade enzymes. In our case, the ATP/ADP levels influenced the activity of the kinases used. To bypass this, starting concentrations of ATP were varied and the concentration of pyruvate kinase producing ATP was increased, leading to rapid conversion of ADP to ATP. Furthermore, the metal cofactor dependency was a problem. Most enzymes in the system are magnesium-dependent. However, phosphoglycerate mutase is strictly manganese dependent. Adjustment of manganese concentrations reduced the inhibitory effect but at the expense of phosphogluconate mutase (gsPgm) activity. Metal-dependent inhibition was also present in the system of Enoki et al.; here, a three-enzyme cascade was designed to produce γ -oxy functionalized α -amino acids. In addition to a different pH and temperature optimum, different metal cofactor preferences were also present¹⁰⁹. Here, a similar approach was used to optimize the amount of metal ions by determining the concentration of metal ions at which the highest substrate-to-product conversion could be achieved. These examples show how a proof-of-principle system with low product yield can be optimized by reaction optimization. However, the examples also show that the process is very laborious and requires time and resources to screen the parameters. To optimize multi-enzyme cascades such as the systems presented here in the future, a statistical model could be created for further optimization. Using machine learning and scaling down the system to a few μ l, many parameters could be varied as described by Pandi et al.¹¹⁴ and the optimal cascade composition could be found for future upscaling to industrially relevant scales.

4.3. Methanol assimilation through formaldehyde condensing enzymes

Building complexity is a prerequisite for using CO₂-derived C1-molecules for further use in platforms and standard chemicals. As an essential building block, formaldehyde is the key in converting C1-molecules into higher molecular structures¹⁸⁵. In nature, formaldehyde fixation usually occurs in a cyclic system, such as the xylulose monophosphate (XuMP) or ribulose monophosphate pathway (RuMP). Key enzymes in these pathways are a dihydroxyacetone synthase in the XuMP pathway and a D-hexulose-6-phosphate synthase in the RuMP pathway^{186 187}. Furthermore, formaldehyde is fixed in the serine cycle via a first conversion to methylene tetrahydrofolate enzymatically or spontaneously and a subsequent condensation with glycine to serine by serine hydroxymethyltransferase¹⁸⁸. Together with the natural fixation routes, artificial pathways were created to shorten sugar-independent fixation of formaldehyde. The two major enzymes for this direct fixation are formolase (FLS) and glycolaldehyde synthase (GALS)^{46, 189}. These two enzymes were artificially designed for the condensation of formaldehyde to the C3 molecule dihydroxyacetone by catalyzing a formose reaction or to the C2 molecule glycolaldehyde. A similar route for the production of glycolaldehyde could be shown by the use of a glyoxylate carboligase¹⁹⁰. This enzyme has a higher affinity for formaldehyde than the glycolaldehyde synthase mentioned above, but its catalytic efficiency is lower. Together with these specifically designed enzymes for converting formaldehyde, engineered aldolases such as fructose-6-phosphate aldolase (FSA) can utilize a broad range of aldehydes. Recently also, the utilization of formaldehyde was shown by an FSA variant. Here the C3 molecule glyceraldehyde could be synthesized by adding formaldehyde to glycolaldehyde¹⁹¹.

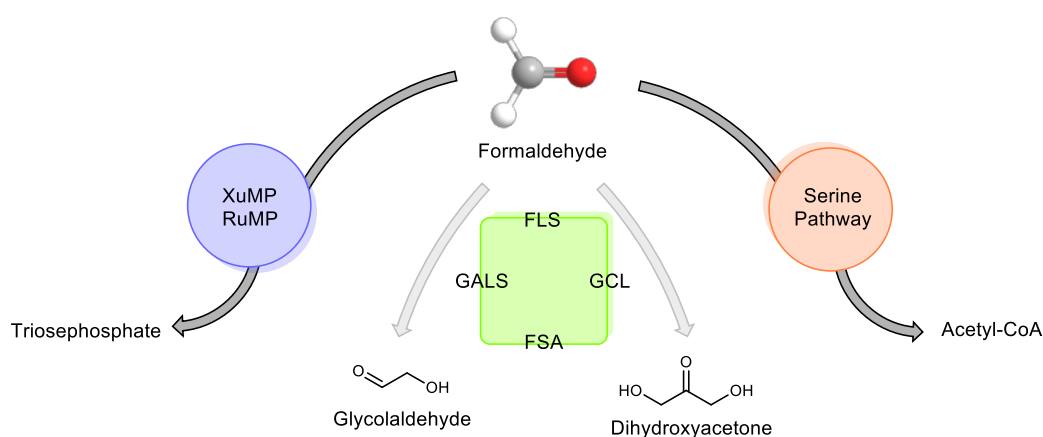


Figure 8: Formaldehyde conversion via cyclic xylulose monophosphate pathway (XuMP), ribulose monophosphate pathway (RuMP) and serine pathway together with linear formaldehyde assimilation pathways via formolase (FLS), glycolaldehyde synthase (GALS), glyoxylate carboligase (GCL) and fructose-6-phosphate aldolase (FSA).

However, in this case, FSA is also capable of condensing two glycolaldehyde molecules or performing a double addition of two glycolaldehyde molecules and one formaldehyde molecule, resulting in a wide variety of products rather than a specific end product. To facilitate the ability of those enzymes to put formaldehyde in use, we were interested in how natural and artificial enzymes for formaldehyde fixation may work in a complex cascade system and how well those enzymes are tunable to generate high yields and efficiencies without the production of byproducts.

4.3.1. Natural- and synthetic formaldehyde fixation in enzyme cascades

To evaluate the different routes for formaldehyde fixation, one cascade deals with the valorization of methanol via a sugar-guided formaldehyde fixation similar to the XuMP pathway.

However, due to the instability and complex purification of dihydroxyacetone synthase¹⁹², we used a transketolase capable of catalyzing a similar reaction¹⁹³. In comparison with the dihydroxyacetone synthase from *Candida boidinii* (*cbDHAS*), the best transketolase from *Escherichia coli* (*ecTktA*) showed two times higher v_{\max} values of 8.2 U mg⁻¹ (v_{\max} *cbDHAS*: 4.9 U mg⁻¹) even with the unphosphorylated donor substrate xylulose and formaldehyde yielding glyceraldehyde and dihydroxyacetone. Still, the K_m value for formaldehyde increased 5-fold to 2.1 mM. In comparison with the artificial formaldehyde fixation by FLS via the formose reaction, the affinity in terms of transketolase for formaldehyde is 11 times higher than the affinity of FLSM3 for formaldehyde and the k_{cat} of transketolase for 5 mM formaldehyde and xylulose is 50 times higher¹¹⁰.

Due to formaldehyde's high toxicity and reactivity, demonstrated in our transketolase system, formaldehyde fixation must occur rapidly in enzyme cascade reactions to convert formaldehyde to a less harmful intermediate. Therefore, high activity and affinity are required. Considering the formaldehyde concentrations during the cascade runtime, it is noticeable that, although the kinetic properties of FLSM3 are not optimal for this purpose, only negligible amounts of formaldehyde could be detected with FLSM3 as a formaldehyde fixation enzyme. However, in this case, this low concentration of formaldehyde could only be achieved by using a massive amount of FLSM3 with up to 13 mg mL⁻¹ enzyme to obtain a comparable unit amount to alcohol oxidase, which produces formaldehyde. In contrast, only one-tenth (1.5 mg mL⁻¹) of transketolase was required to produce isobutanol and ethanol from methanol and xylose in reasonable amounts, demonstrating the strength of formaldehyde conversion by transketolase. However, in the case of the isobutanol cascade, it cannot be ruled out that formaldehyde brought production to a halt, since, in tests with mechanical formaldehyde addition, the formaldehyde

concentration in the system increased over time and low yields of product were obtained. To test if formaldehyde occur in the methanol system and brought the conversion to a halt, higher amounts of transketolase could promote formaldehyde conversion and further increase final yields.

An option for reducing the amount of enzyme with a concomitant increase in formaldehyde titer is to decouple the formaldehyde-converting reaction from the residual cascade in two separate pots or in a system where enzymes are added stepwise. With the stepwise addition, recently, the amount of FLSM3 could be reduced to 5 mg mL⁻¹ to convert 100 mM methanol to 22.5 mM dihydroxyacetone. Furthermore a set up with GLAS could produce 8 mM glycolaldehyde from 20 mM methanol^{110 194 195}. By the stepwise addition of enzymes, formaldehyde concentrations only influence the formaldehyde fixing enzyme. Variants of formolase or glycolaldehyde synthase were created, which can resist up to 1 M formaldehyde¹⁹⁶. Together with that, transketolase activity was shown with up to 0.4 M formaldehyde¹⁹⁷. Due to this high stability of transketolase and formolase, high dihydroxyacetone titers and high-end product titers might be achievable.

When comparing the driving force of formaldehyde fixation, it is noticeable that the intrinsic drive of the formose reaction to dihydroxyacetone with the default eQuilibrator set up (eQuilibrator 3.0, pH 7.5, pMg 3.0 and ionic strength 0.25 M) ($K'_{eq3FALD \rightarrow DHA}$: $1.4 \cdot 10^{14}$, $K'_{eq2FALD \rightarrow GA}$: $1.1 \cdot 10^8$, $K'_{eqFALD+GA \rightarrow DHA}$: $1.3 \cdot 10^6$) is highly favorable for the production of dihydroxyacetone with nearly no back flux. Due to this, a two-pot process would be a reasonable option for further scale-up. The reaction catalyzed by transketolase also has a drive to dihydroxyacetone, although, unlike the formose reaction, the drive is not as strong (K'_{eq} : $3.9 \cdot 10^5$). Since the initial isomerization of xylose to xylulose is reversible, the drive is even less when starting from xylose (K'_{eq} : $6.9 \cdot 10^4$). However, since the reaction catalyzed by transketolase also produces glyceraldehyde, which is also a reactive and toxic aldehyde, this procedure may not be suitable for transketolase.

While the amount of formolase, and transketolase used in these cascades is still an enormous amount of enzymes for a low-cost product¹⁵⁷, the activities of both enzymes need to be raised to reach high titers in a reasonable amount of time. Nevertheless, the two cascades designed in this study, offer excellent potential for increasing product yield, productivity, and efficiency.

While the formolase reaction already has a high efficiency without the accumulation of formaldehyde, separating the formaldehyde to dihydroxyacetone conversion from the residual cascade could significantly raise the total product yield. In the case of transketolase, splitting formaldehyde fixation and residual cascade would not be effective for producing high product titers due to the accumulation of glyceraldehyde and a higher back flux to xylose. However, industrially relevant activities⁹² could be achieved faster due to the favorable kinetic properties

of the transketolase instead of formolase. To improve the fixation of C1-compounds, AI and deep-learning-directed *de novo* enzyme constructions may be a future vision in addition to the methods discussed above¹⁹⁸. By applying these techniques to the formose reaction, enzymes that have more favorable kinetic properties than formolase or glycolaldehyde synthase could be constructed.

4.4. *In vitro* vs *In vivo* C1-valorization to various chemicals

Since the systems described above are still in the proof-of-concept phase and need further development to reach industrial relevant levels, the question is whether the future of C1-valorization is an *in vitro*, *in vivo* or in a combined approach. Microorganisms can utilize C1-chemicals such as methanol or formate, but can also be used in gas fermentations to directly utilize H₂, CO₂ or CO gases. In particular, gas fermentation with H₂/CO mixtures for producing various platform chemicals such as ethanol, isopropanol, or acetone has recently come into focus and caused attention due to its commercialization and test phases in pilot plants¹⁹⁹⁻²⁰². However, the low solubility of gaseous substrates, the low energy status of acetogens, and the thermodynamic limitations of acetogenesis complicates a further broadening of the range of accessible products²⁰²⁻²⁰⁴.

Due to the ease of using liquid substrates instead of gases in bioprocesses²⁰⁵, methylotrophic organisms that convert CO₂-derived methanol or formate are essential hosts for the valorization of C1-chemicals. To expand the range of products that can be derived from methanol using natural methylotrophs and to increase and improve titers toward industrially applicable titers, engineering approaches are being pursued, *e.g.*, to introduce specific metabolic pathways for targeted chemical production. Methanol is converted to formaldehyde via methanol dehydrogenases or alcohol oxidases, which is converted via natural assimilation pathways such as the XuMP, RuMP, and serine pathways²⁰⁶⁻²⁰⁸. However, the use of native methylotrophs has several disadvantages, such as low carbon yield and insufficient accumulation of metabolic intermediates for the production of secondary metabolites, strict gene regulation of methanol-utilizing enzymes with suppression in the presence of other carbon sources, or insufficient energy production from methanol alone^{47, 209, 210}. By using *Protomonas extorquens*, Sirirote et al. produced L-serine efficiently from glycine and methanol with up to 54.5 g L⁻¹. However, glycine was used as a carbon source with around 39.3%. In contrast, methanol incorporation only has 8.3% (Production of L-serine from methanol and glycine by resting cells of a methylotroph under automatically controlled conditions). Since there are still drawbacks to genetically modifying native methylotrophs despite some developmental successes, earlier pathway prototyping using *in vitro* systems could be a way to expand the range of products made from these organisms.

However, due to the capabilities of *in vitro* systems, the production of chemicals from methanol and formate may also have a future in industrial applications, bypassing the use of methylotrophic organisms. In our study, we utilized xylose to increase the production of biofuels and platform chemicals from methanol and to build molecules from methanol faster than from methanol alone. By applying a combined approach like this, it has to be sure that all

carbon from methanol and the sugar is converted to the same product. As an example: The production of one product from various substrates could be efficiently shown by Sutiono et al.³⁵. Here two different sugars could be converted into one product via an intelligent enzyme selection. In the case of the transketolase system of this study, the incorporation could be efficiently controlled and corrected by adjusting enzyme concentrations, whereby methanol and xylose consumption keeps similar during the runtime of the system. This lead to a one to one conversion of methanol and xylose to the final products.

4.4.1. Integration of new to nature and natural methanol utilizing pathway to create synthetic methylotrophs vs *in vitro* applications

Besides natural methylotrophs, the focus is on already established microbial hosts as *Escherichia coli* to create synthetic methylotrophs. This is because, despite some developmental successes in the genetic modification of native methylotrophs, there are still drawbacks and lower yields. For the integration of C1-utilization, different pathways were introduced into common microbial host systems such as *Escherichia coli*, *Corynebacterium glutamicum*, or *Saccharomyces cerevisiae*²¹¹. Thereby natural and non-natural methanol utilization pathways were integrated. Wang et al. integrated a formolase pathway with methanol dehydrogenase and FLS for methanol utilization. After expression in a formaldehyde dehydrogenase-deficient *Escherichia coli* strain and subsequent adaptive laboratory evolution, methanol assimilation into biomass was demonstrated²¹². Furthermore, the SACA pathway for acetyl-CoA production was integrated into *Escherichia coli* with a methanol dehydrogenase to keep the formaldehyde concentration low. The strain grew successfully on methanol via the SACA pathway, although the contribution of methanol to biomass was only 3%¹⁸⁹. Apart from these linear methanol assimilation pathways, also natural cyclic pathways were integrated *in vivo*. To improve the properties of methanol utilization in *Escherichia coli*, De Simone et al. attempted to integrate parts of the XuMP pathway into *Escherichia coli*. After integrating a methanol dehydrogenase and a dihydroxyacetone synthase, methanol was successfully integrated into central metabolites, with higher methanol assimilation than the parent strain²¹³. An adaptive laboratory evolution approach performed by Espinosa et al. has uncovered and enhanced natural methanol assimilation in *Saccharomyces cerevisiae* that may be attributable to a type of XuMP pathway²¹⁴.

As an example of synthetic autonomous methylotrophy, Chen et al. successfully integrated parts of the RuMP pathway into *Escherichia coli*. By applying metabolic robustness criteria and a laboratory evolution approach, they could demonstrate its growth on methanol alone²¹⁵.

Furthermore, a recent study by Zhang et al. could show an engineering of a *Saccharomyces cerevisiae* strain to use methanol as the sole carbon source and targeted the production of the polyketide flaviolin²¹⁶. These experiments show that methylotrophy can be integrated into conventional host organisms. Biomass can be accumulated, and important metabolites show the incorporation of methanol. However, only the minority of approaches are able to producing specific chemicals with these synthetic organisms.

A major problem besides the difficulty of reprogramming an entire organism is the high toxicity of formaldehyde, which has a dramatic effect on cell viability. Regardless of whether the host is a native or a synthetic methylotrophic organism, low concentrations of formaldehyde, ranging from 0.3 mM to 5 mM, inhibit the growth of important hosts like *Yarrowia lipolytica*, *Saccharomyces cerevisiae*, or *Pichia pastoris*⁴⁷. Because of this, a problem in integrating the newly developed linear assimilation pathways is the high K_m value for formaldehyde and the low activity of the formolase or glycolaldehyde synthases developed so far. The use of these enzymes *in vivo* could trigger the accumulation of toxic formaldehyde, leading to viability issues of the hosts.

As a smart reaction concept, to prevent high formaldehyde concentrations, Jo et al.²¹⁷ demonstrated the use of paraformaldehyde as less toxic precursor to formaldehyde. In their study they produced glycolic acid via the use of paraformaldehyde, which slowly converts to formaldehyde.

In contrast to that, the implementation of these systems *in vitro* already shows more significant success in the production of chemicals. Compared with the *in vivo* implemented SACA pathway, the SACA pathway could be efficiently integrated into the *in vitro* production of PHB from CO₂-derived methanol¹⁹⁴. Similar to the SACA pathway, the formolase pathway could be used *in vitro* to produce various chemicals. As described in Section 4.3, the tolerance of purified enzymes can be drastically higher. For example, in our system, we could show that 10 and even 20 mM formaldehyde could still be efficiently converted into isobutanol with 85% and 72% yield, respectively. Another advantage to circumvent the accumulation of formaldehyde *in vitro* is the possibility of adapting the concentration of enzymes quickly. In the L-alanine cascade, an increase in formolase concentration could compensate the low activity and yield with no formaldehyde accumulation over the whole runtime of the system. Furthermore, as shown with paraformaldehyde, smart substrate engineering, or the gradual addition of formaldehyde via pumps, as shown in our isobutanol setup, might help bypass formaldehyde's toxicity and can be easily applied *in vitro*.

As the production of chemicals from CO₂ will need to increase in the coming years, exciting concepts are already showing the impact that biocatalysis can have on the production of various chemicals from C1. However, both *in vivo* and *in vitro* systems are still in the early proof-of-

principle phase and high industrial titers are rare. A commercialized example is the production of ethanol from synthesis gas at LanzaTech²⁰¹. Still, it is challenging to expand the chemical scope produced by acetogenic bacteria. To broaden the scope and commercialize routes *in vitro* and *in vivo*, the biocatalysis systems need to evolve and could work together as in the iPROBE approach⁶⁶. Here, the cell-free systems act as a versatile screening platform, e.g. to find optimal enzyme ratios by using different ratios of cell lysates. In this way, not only can the optimal enzyme ratio be found, but the cell environment can also be mimicked. The optimal enzyme ratios can then be used in the context of *in vivo* systems, where the adjusted enzyme ratio is transferred to a specific promoter that promotes high or low expression. Further, the engineered synthetic pathways are much simpler than the natural ones, but the key enzymes still lack relevant specificity and activity.

4.5. Sustainable chemical production from renewable resources by the use of enzymatic cascades

In order to develop concepts for the *in vitro* production of cheap chemical feedstocks, food additives or biofuels, research has recently focused heavily on the design and development of enzyme cascades for the valorization of CO₂ or biomass. The utilization of sugars and compounds that can be obtained from nature or waste streams using multi-enzyme cascades has recently become increasingly popular and has already been demonstrated for the production of Myo-inositol from starch on an industrial scale ²¹⁸.

In addition, the range of products that can be derived from sugars is significantly broadened by the use of enzyme cascades. While industrially relevant titers have already been achieved for the use of glucose, the production of xylose and other sugars from biomass, e.g. for the production of biofuels ¹³¹ is also gaining momentum. Recently, Sutiono et al. was able to optimize an enzymatic cascade for the production of butanetriol from xylose such that butanetriol could be produced close to industrially relevant titers ²¹⁹. The main task for the future, however, will be to upscale these systems to a relevant size to compete with existing processes and to be attractive for investments in new process equipment ²²⁰. Together with that, a challenge will be the combination of various cascades and linking the use of different sources, as well as closing the entire cycle from biomass use to the end product and not just starting from individual refined sugars.

The described concept of utilizing xylose and formaldehyde directly adds to this idea of combining various waste streams into one specific product ^{221, 222}. Moreover, formaldehyde is found, for example, in furniture wood waste or aqueous solutions, e.g., in fish farms and causes a stir due to its harmful health properties ^{223, 224}. However, the toxic C1-compound formaldehyde is complicated to handle, and detoxification using cells is still challenging due to its cytotoxicity ⁴³. In addition, formaldehyde is derivable from CO₂ and can thus contribute to the utilization of CO₂ and the reduction of this greenhouse gas.

Since CO₂ as a resource is the new megatrend in enzymatic cascade development, many concepts are focused on its utilization and on finding suitable ways to get it into useful biological precursor molecules, from two-carbon molecules like ethylene glycol, glycolic acid or acetyl-CoA. To three-carbon molecules such as glycerate and already useful high-molecular-weight products such as the C4 sugar erythrose or even polymeric products such as starch ^{110, 144, 225, 226}. The synthetic routes of these mostly small carbon unit-based target molecules described in our review are still in the early stages and are presented only as proofs of concept. However, due to the possibilities offered by these systems, new routes based on them are rapidly being developed to produce a wider variety of compounds. In this context, the development of

pathways to produce amino acids from CO₂ represents a new chapter that would perfectly complement the pathways presented so far. Amino acids are the building blocks of proteins and are therefore essential for nutrition, health care and as dietary supplements for animals. The production of amino acids from CO₂ could target the goal of nutrient supply and in the future, even enable the production of protein from CO₂. In our developed L-alanine synthesis, we integrate methanol and dihydroxyacetone into the cascade. This links it directly to the metabolic pathways described above and combines oxidative methanol oxidation with the formolase-formose pathway used in synthetic starch synthesis. However, in contrast to starch synthesis, catabolic lower glycolysis forms the second module of the system rather than anabolic upper glycolysis. Due to the intrinsic drive to pyruvate via lower glycolysis, and the centrality of pyruvate, the methanol assimilation pathway, as well as the sugar-guided methanol assimilation pathway, could be the blueprint for further production of a variety of chemicals and amino acids. To further broaden the spectrum of amino acids produced from CO₂ and methanol and to reach the ultimate goal of producing proteins from CO₂ and thus food, new concepts have to be developed on how carbon extension could be realized. The key here is not only to generate C₃ or C₂ amino acids but also to expand the scope to C₄ to C₆ amino acids or even to higher molecular weight amino acids. A possible next step could be extending the L-alanine system to produce the amino acid L-valine, which is already a C₅ amino acid and an essential amino acid.

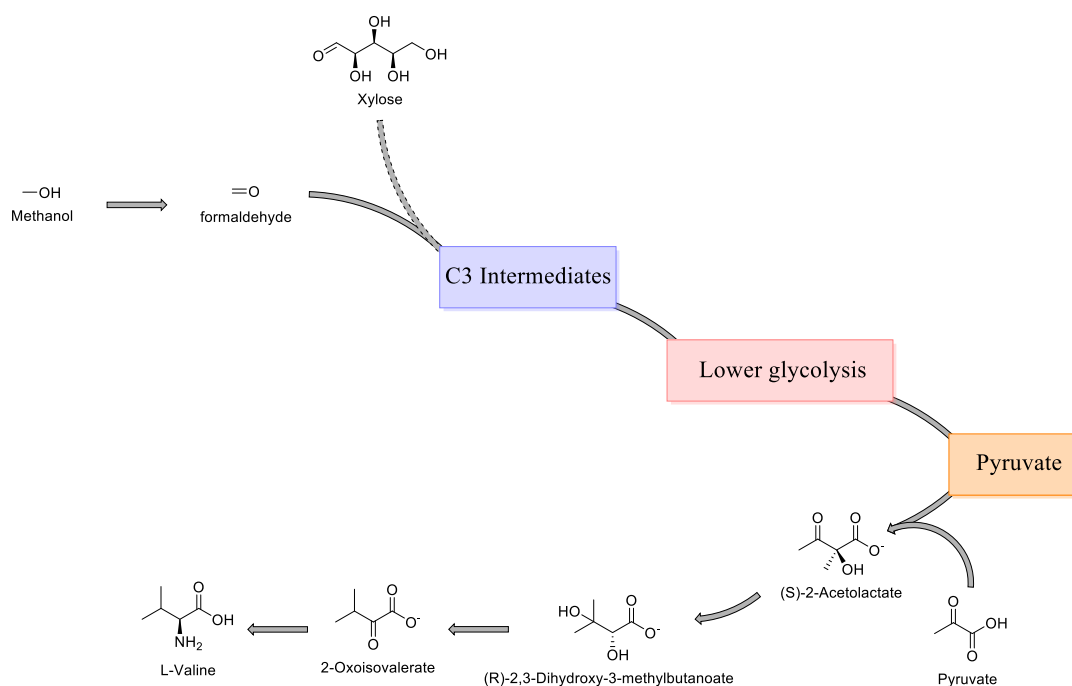


Figure 9: Proposed valine pathway from methanol alone or in combination with xylose

By combining the isobutanol pathway with the L-alanine pathway, the blueprint for L-valine could be established since the isobutanol pathway is based on the natural L-valine pathway. With some adjustment of the combination of these two systems, L-valine production from methanol could be achieved.

5. References

1. Lin, D., Wambersie, L. & Wackernagel, M. Estimating the Date of Earth Overshoot Day 2023. *Nowcasting the World's Footprint & Biocapacity for 1-8* (2023).
2. Footprint Data Foundation, York University Ecological Footprint Initiative and Global Footprint Network., Vol. 2023 (2023).
3. Footprint Data Foundation, York University Ecological Footprint Initiative, and Global Footprint Network: National Footprint and Biocapacity Accounts, 2023 edition. Downloaded [21.04.2023] from <https://data.footprintnetwork.org>
4. Eric Miller, F.G., Apeksha, Kendra Lee, Ahmed Abdul Aziz data.footprintnetwork.org (Global Footprint Network; 2022).
5. York University Ecological Footprint Initiative & Global Footprint Network. National Footprint and Biocapacity Accounts, 2022 edition. Produced for the Footprint Data Foundation and distributed by Global Footprint Network. Available online at: <https://data.footprintnetwork.org>.
6. Isikgor, F.H. & Becer, C.R. Lignocellulosic biomass: a sustainable platform for the production of bio-based chemicals and polymers. *Polymer Chemistry* **6**, 4497-4559 (2015).
7. Zoghalmi, A. & Paës, G. Lignocellulosic Biomass: Understanding Recalcitrance and Predicting Hydrolysis. *Frontiers in Chemistry* **7** (2019).
8. Binder, J.B. & Raines, R.T. Fermentable sugars by chemical hydrolysis of biomass. *Proceedings of the National Academy of Sciences* **107**, 4516-4521 (2010).
9. Tayyab, M. et al. Bioethanol production from lignocellulosic biomass by environment-friendly pretreatment methods: A review. *Appl. Ecol. Environ. Res* **16**, 225-249 (2018).
10. Zhao, Z., Xian, M., Liu, M. & Zhao, G. Biochemical routes for uptake and conversion of xylose by microorganisms. *Biotechnology for biofuels* **13**, 21 (2020).
11. Amin, F.R. et al. Pretreatment methods of lignocellulosic biomass for anaerobic digestion. *AMB Express* **7**, 72 (2017).
12. Periyasamy, S. et al. Chemical, physical and biological methods to convert lignocellulosic waste into value-added products. A review. *Environ. Chem. Lett.* **20**, 1129-1152 (2022).
13. Yu, Y., Long, Y. & Wu, H. Near-Complete Recovery of Sugar Monomers from Cellulose and Lignocellulosic Biomass via a Two-Step Process Combining Mechanochemical Hydrolysis and Dilute Acid Hydrolysis. *Energy Fuels* **30**, 1571-1578 (2016).
14. Demirbas, A. Biofuels sources, biofuel policy, biofuel economy and global biofuel projections. *Energy Convers. Manage.* **49**, 2106-2116 (2008).
15. Okolie, J.A., Mukherjee, A., Nanda, S., Dalai, A.K. & Kozinski, J.A. Next-generation biofuels and platform biochemicals from lignocellulosic biomass. *IJER* **45**, 14145-14169 (2021).
16. Fu, C. et al. Recent advances on bio-based isobutanol separation. *Energy Conversion and Management: X* **10**, 100059 (2021).
17. Su, Y., Zhang, W., Zhang, A. & Shao, W. Biorefinery: The Production of Isobutanol from Biomass Feedstocks. *Applied Sciences* **10**, 8222 (2020).
18. Lakshmi, N.M., Binod, P., Sindhu, R., Awasthi, M.K. & Pandey, A. Microbial engineering for the production of isobutanol: current status and future directions. *Bioengineered* **12**, 12308-12321 (2021).
19. Hussain, A. et al. Advances in microbial metabolic engineering for the production of butanol isomers (isobutanol and 1-butanol) from a various biomass. *BioEnergy Research*, **15**, 1854-1871 (2022).

20. Narisetty, V. et al. Valorisation of xylose to renewable fuels and chemicals, an essential step in augmenting the commercial viability of lignocellulosic biorefineries. *Sustainable Energy & Fuels* **6**, 29-65 (2022).
21. Amaniampong, P.N. et al. in Valorization of Biomass to Value-Added Commodities: Current Trends, Challenges, and Future Prospects. (eds. M.O. Daramola & A.O. Ayeni) 193-220 (Springer International Publishing, Cham; 2020).
22. Saha, B.C. Hemicellulose bioconversion. *Journal of Industrial Microbiology and Biotechnology* **30**, 279-291 (2003).
23. Hahn-Hägerdal, B., Jeppsson, H., Skoog, K. & Prior, B.A. Biochemistry and physiology of xylose fermentation by yeasts. *Enzyme and Microbial Technology* **16**, 933-943 (1994).
24. Robak, K. & Balcerek, M. Current state-of-the-art in ethanol production from lignocellulosic feedstocks. *Microbiol. Res.* **240**, 126534 (2020).
25. Moysés, D.N., Reis, V.C.B., Almeida, J.R.M.d., Moraes, L.M.P.d. & Torres, F.A.G. Xylose fermentation by *Saccharomyces cerevisiae*: challenges and prospects. *Int. J. Mol. Sci.* **17**, 207 (2016).
26. Wilbanks, B. & Trinh, C.T. Comprehensive characterization of toxicity of fermentative metabolites on microbial growth. *Biotechnology for biofuels* **10**, 262 (2017).
27. De Rosa, M. et al. Glucose metabolism in the extreme thermoacidophilic archaeobacterium *Sulfolobus solfataricus*. *Biochemical Journal* **224**, 407-414 (1984).
28. Watanabe, S. et al. Novel non-phosphorylative pathway of pentose metabolism from bacteria. *Sci. Rep.* **9**, 155 (2019).
29. Li, X., Chen, Y. & Nielsen, J. Harnessing xylose pathways for biofuels production. *Curr. Opin. Biotechnol.* **57**, 56-65 (2019).
30. Martín del Campo, J.S. et al. High-yield production of dihydrogen from xylose by using a synthetic enzyme cascade in a cell-free system. *Angew. Chem. Int. Ed.* **52**, 4587-4590 (2013).
31. Cheng, K., Zheng, W., Chen, H. & Zhang, Y.-H.P.J. Upgrade of wood sugar d-xylose to a value-added nutraceutical by in vitro metabolic engineering. *Metab. Eng.* **52**, 1-8 (2019).
32. Boer, H., Andberg, M., Pylkkänen, R., Maaheimo, H. & Koivula, A. In vitro reconstitution and characterisation of the oxidative d-xylose pathway for production of organic acids and alcohols. *AMB Express* **9**, 48 (2019).
33. Jia, X., Kelly, R.M. & Han, Y. Simultaneous biosynthesis of (R)-acetoin and ethylene glycol from D-xylose through in vitro metabolic engineering. *Metabolic engineering communications* **7**, e00074 (2018).
34. Gao, Q. et al. High-yield production of D-1, 2, 4-butanetriol from lignocellulose-derived xylose by using a synthetic enzyme cascade in a cell-free system. *J. Biotechnol.* **292**, 76-83 (2019).
35. Sutiono, S., Pick, A. & Sieber, V. Converging conversion—using promiscuous biocatalysts for the cell-free synthesis of chemicals from heterogeneous biomass. *Green Chem.* **23**, 3656-3663 (2021).
36. IEA Global Energy Review: CO₂ Emissions in 2021. *IEA, Paris* <https://www.iea.org/reports/global-energy-review-co2-emissions-in-2021-2> (2022).
37. M D Hatch, a. & Slack, C.R. Photosynthetic CO₂-Fixation Pathways. *Annual Review of Plant Physiology* **21**, 141-162 (1970).
38. Evans, M.C., Buchanan, B.B. & Arnon, D.I. A new ferredoxin-dependent carbon reduction cycle in a photosynthetic bacterium. *Proceedings of the National Academy of Sciences* **55**, 928-934 (1966).
39. STRAUSS, G. & FUCHS, G. Enzymes of a novel autotrophic CO₂ fixation pathway in the phototrophic bacterium *Chloroflexus aurantiacus*, the 3-hydroxypropionate cycle. *European Journal of Biochemistry* **215**, 633-643 (1993).

40. Garritano, A.N., Song, W. & Thomas, T. Carbon fixation pathways across the bacterial and archaeal tree of life. *PNAS Nexus* **1**, pgac226 (2022).
41. Klein, V.J., Irla, M., Gil López, M., Brautaset, T. & Fernandes Brito, L. Unravelling Formaldehyde Metabolism in Bacteria: Road towards Synthetic Methylophony. *Microorganisms* **10**, 220 (2022).
42. Crowther, G.J., Kosály, G. & Lidstrom, M.E. Formate as the main branch point for methylotrophic metabolism in *Methylobacterium extorquens* AM1. *J. Bacteriol.* **190**, 5057-5062 (2008).
43. Yurimoto, H., Kato, N. & Sakai, Y. Assimilation, dissimilation, and detoxification of formaldehyde, a central metabolic intermediate of methylotrophic metabolism. *The Chemical Record* **5**, 367-375 (2005).
44. He, H., Höper, R., Dodenhöft, M., Marlière, P. & Bar-Even, A. An optimized methanol assimilation pathway relying on promiscuous formaldehyde-condensing aldolases in *E. coli*. *Metab. Eng.* **60**, 1-13 (2020).
45. Bogorad, I.W. et al. Building carbon-carbon bonds using a biocatalytic methanol condensation cycle. *Proceedings of the National Academy of Sciences* **111**, 15928-15933 (2014).
46. Siegel, J.B. et al. Computational protein design enables a novel one-carbon assimilation pathway. *Proceedings of the National Academy of Sciences* **112**, 3704-3709 (2015).
47. Zhan, C. et al. Strategies and challenges with the microbial conversion of methanol to high-value chemicals. *Biotechnology and Bioengineering* **118**, 3655-3668 (2021).
48. IEA Putting CO₂ to Use. IEA, Paris <https://www.iea.org/reports/putting-co2-to-use> (2019).
49. Zhang, W. et al. Current advance in bioconversion of methanol to chemicals. *Biotechnology for biofuels* **11**, 260 (2018).
50. Navarro-Jaén, S. et al. Highlights and challenges in the selective reduction of carbon dioxide to methanol. *Nature Reviews Chemistry* **5**, 564-579 (2021).
51. Singh, R.K. et al. Insights into cell-free conversion of CO₂ to chemicals by a multienzyme cascade reaction. *ACS Catalysis* **8**, 11085-11093 (2018).
52. Cazelles, R. et al. Reduction of CO₂ to methanol by a polyenzymatic system encapsulated in phospholipids-silica nanocapsules. *New Journal of Chemistry* **37**, 3721-3730 (2013).
53. Marpani, F., Pinelo, M. & Meyer, A.S. Enzymatic conversion of CO₂ to CH₃OH via reverse dehydrogenase cascade biocatalysis: Quantitative comparison of efficiencies of immobilized enzyme systems. *Biochem. Eng. J.* **127**, 217-228 (2017).
54. García, A.C., Moral-Vico, J., Abo Markeb, A. & Sánchez, A. Conversion of Carbon Dioxide into Methanol Using Cu-Zn Nanostructured Materials as Catalysts. *Nanomaterials* **12**, 999 (2022).
55. Ruland, H. et al. CO₂ Hydrogenation with Cu/ZnO/Al₂O₃: A Benchmark Study. *ChemCatChem* **12**, 3216-3222 (2020).
56. Lu, B., Yan, X. & Liu, Q. Enhanced solar hydrogen generation with the direct coupling of photo and thermal energy – An experimental and mechanism study. *ApEn* **331**, 120468 (2023).
57. Guil-López, R. et al. Methanol synthesis from CO₂: a review of the latest developments in heterogeneous catalysis. *Materials* **12**, 3902 (2019).
58. Albo, J., Alvarez-Guerra, M., Castaño, P. & Irabien, A. Towards the electrochemical conversion of carbon dioxide into methanol. *Green Chem.* **17**, 2304-2324 (2015).
59. Wu, J., Huang, Y., Ye, W. & Li, Y. CO₂ Reduction: From the Electrochemical to Photochemical Approach. *Adv Sci (Weinh)* **4**, 1700194 (2017).
60. Byrne, G. et al. Biologicalisation: Biological transformation in manufacturing. *CIRP Journal of Manufacturing Science and Technology* **21**, 1-32 (2018).

61. Miehe, R. et al. The biological transformation of industrial manufacturing – Technologies, status and scenarios for a sustainable future of the German manufacturing industry. *Journal of Manufacturing Systems* **54**, 50-61 (2020).
62. Miehe, R. et al. The biological transformation of the manufacturing industry – envisioning biointelligent value adding. *Procedia CIRP* **72**, 739-743 (2018).
63. Miehe, R. et al. The Biological Transformation of Industrial Manufacturing-Future Fields of Action in Bioinspired and Bio-based Production Technologies and Organization. *Procedia Manufacturing* **39**, 737-744 (2019).
64. Sheldon, R.A. & Brady, D. Green Chemistry, Biocatalysis, and the Chemical Industry of the Future. *ChemSusChem* **15**, e202102628 (2022).
65. Woodley, J.M. Biocatalysis for future sustainable manufacturing. *Biochem (Lond)* **44**, 6-8 (2022).
66. Karim, A.S. et al. In vitro prototyping and rapid optimization of biosynthetic enzymes for cell design. *Nat. Chem. Biol.* **16**, 912-919 (2020).
67. Francois, J.M., Alkim, C. & Morin, N. Engineering microbial pathways for production of bio-based chemicals from lignocellulosic sugars: current status and perspectives. *Biotechnology for Biofuels* **13**, 118 (2020).
68. Pickens, L.B., Tang, Y. & Chooi, Y.H. Metabolic engineering for the production of natural products. *Annu Rev Chem Biomol Eng* **2**, 211-236 (2011).
69. Claassens, N.J., Burgener, S., Vögeli, B., Erb, T.J. & Bar-Even, A. A critical comparison of cellular and cell-free bioproduction systems. *Curr. Opin. Biotechnol.* **60**, 221-229 (2019).
70. Lin, B. & Tao, Y. Whole-cell biocatalysts by design. *Microbial Cell Factories* **16**, 106 (2017).
71. Bowie, J.U. et al. Synthetic Biochemistry: The Bio-inspired Cell-Free Approach to Commodity Chemical Production. *Trends Biotechnol.* **38**, 766-778 (2020).
72. Gong, Z., Nielsen, J. & Zhou, Y.J. Engineering Robustness of Microbial Cell Factories. *Biotechnol. J.* **12**, 1700014 (2017).
73. Guo, Q. et al. Methanol-Dependent Carbon Fixation for Irreversible Synthesis of d-Allulose from d-Xylose by Engineered Escherichia coli. *Journal of Agricultural and Food Chemistry* **70**, 14255-14263 (2022).
74. Rollin, J.A., Tam, T.K. & Zhang, Y.H.P. New biotechnology paradigm: cell-free biosystems for biomanufacturing. *Green Chem.* **15**, 1708-1719 (2013).
75. Guterl, J.K. et al. Cell-free metabolic engineering: production of chemicals by minimized reaction cascades. *ChemSusChem* **5**, 2165-2172 (2012).
76. Xie, L. et al. Conversion of D-glucose to L-lactate via pyruvate by an optimized cell-free enzymatic biosystem containing minimized reactions. *Synthetic and systems biotechnology* **3**, 204-210 (2018).
77. Siedentop, R., Claaßen, C., Rother, D., Lütz, S. & Rosenthal, K. Getting the Most Out of Enzyme Cascades: Strategies to Optimize In Vitro Multi-Enzymatic Reactions. *Catalysts* **11**, 1183 (2021).
78. Peters, C. & Buller, R. Linear enzyme cascade for the production of (–)-iso-isopulegol. *Zeitschrift für Naturforschung C* **74**, 63-70 (2019).
79. Siedentop, R., Dziennus, M., Lütz, S. & Rosenthal, K. Debottlenecking of an In Vitro Enzyme Cascade Using a Combined Model- and Experiment-Based Approach *Chem. Ing. Tech.* **95**, 543-548 (2023).
80. Korman, T.P., Opgenorth, P.H. & Bowie, J.U. A synthetic biochemistry platform for cell free production of monoterpenes from glucose. *Nature communications* **8**, 15526 (2017).
81. Česnik, M. et al. Cascade enzymatic synthesis of l-homoserine – mathematical modelling as a tool for process optimisation and design. *Reaction Chemistry & Engineering* **5**, 747-759 (2020).

82. Dudley, Q.M., Karim, A.S. & Jewett, M.C. Cell-free metabolic engineering: biomufacturing beyond the cell. *Biotechnol. J.* **10**, 69-82 (2015).
83. Zhang, X., Wu, H., Huang, B., Li, Z. & Ye, Q. One-pot synthesis of glutathione by a two-enzyme cascade using a thermophilic ATP regeneration system. *J. Biotechnol.* **241**, 163-169 (2017).
84. Su, H.-H. et al. Efficient Bioconversion of Sucrose to High-Value-Added Glucaric Acid by In Vitro Metabolic Engineering. *ChemSusChem* **12**, 2278-2285 (2019).
85. Ghaffari-Moghaddam, M., Eslahi, H., Omay, D. & Zakipour-Rahimabadi, E. Industrial applications of enzymes. *Review Journal of Chemistry* **4**, 341-361 (2014).
86. Woodley, J.M. Ensuring the Sustainability of Biocatalysis. *ChemSusChem* **15**, e202102683 (2022).
87. Sheldon, R.A. & Brady, D. Streamlining Design, Engineering, and Applications of Enzymes for Sustainable Biocatalysis. *ACS Sustainable Chemistry & Engineering* **9**, 8032-8052 (2021).
88. Bernal, C., Rodríguez, K. & Martínez, R. Integrating enzyme immobilization and protein engineering: An alternative path for the development of novel and improved industrial biocatalysts. *Biotechnol. Adv.* **36**, 1470-1480 (2018).
89. Doukyu, N. & Ogino, H. Organic solvent-tolerant enzymes. *Biochem. Eng. J.* **48**, 270-282 (2010).
90. Rogers, T.A. & Bommarius, A.S. Utilizing simple biochemical measurements to predict lifetime output of biocatalysts in continuous isothermal processes. *Chemical engineering science* **65**, 2118-2124 (2010).
91. Nazor, J., Liu, J. & Huisman, G. Enzyme evolution for industrial biocatalytic cascades. *Curr. Opin. Biotechnol.* **69**, 182-190 (2021).
92. Wu, S., Snajdrova, R., Moore, J.C., Baldenius, K. & Bornscheuer, U.T. Biocatalysis: enzymatic synthesis for industrial applications. *Angew. Chem. Int. Ed.* **60**, 88-119 (2021).
93. Benítez-Mateos, A.I., Roura Padrosa, D. & Paradisi, F. Multistep enzyme cascades as a route towards green and sustainable pharmaceutical syntheses. *Nat. Chem.* **14**, 489-499 (2022).
94. Ellis, G.A. et al. Artificial Multienzyme Scaffolds: Pursuing in Vitro Substrate Channeling with an Overview of Current Progress. *ACS Catalysis* **9**, 10812-10869 (2019).
95. Schmidt, S., Schallmey, A. & Kourist, R. in *Enzyme Cascade Design and Modelling*. (eds. S. Kara & F. Rudroff) 31-48 (Springer International Publishing, Cham; 2021).
96. Abu, R. & Woodley, J.M. Application of Enzyme Coupling Reactions to Shift Thermodynamically Limited Biocatalytic Reactions. *ChemCatChem* **7**, 3094-3105 (2015).
97. García-Junceda, E., Lavandera, I., Rother, D. & Schrittwieser, J.H. (Chemo)enzymatic cascades—Nature's synthetic strategy transferred to the laboratory. *J. Mol. Catal. B: Enzym.* **114**, 1-6 (2015).
98. Ricca, E., Brucher, B. & Schrittwieser, J.H. Multi-Enzymatic Cascade Reactions: Overview and Perspectives. *Adv. Synth. Catal.* **353**, 2239-2262 (2011).
99. Kara, S., Schrittwieser, J.H., Hollmann, F. & Ansorge-Schumacher, M.B. Recent trends and novel concepts in cofactor-dependent biotransformations. *Applied Microbiology and Biotechnology* **98**, 1517-1529 (2014).
100. Cutlan, R., De Rose, S., Isupov, M.N., Littlechild, J.A. & Harmer, N.J. Using enzyme cascades in biocatalysis: Highlight on transaminases and carboxylic acid reductases. *Biochim. Biophys. Acta* **1868**, 140322 (2020).
101. Peng, T. et al. Multienzyme Redox System with Cofactor Regeneration for Cyclic Deracemization of Sulfoxides. *Angew. Chem. Int. Ed.* **61**, e202209272 (2022).

102. Lichman, B.R. et al. One-pot triangular chemoenzymatic cascades for the syntheses of chiral alkaloids from dopamine. *Green Chem.* **17**, 852-855 (2015).
103. Losada-Garcia, N. et al. Recent advances in enzymatic and chemoenzymatic cascade processes. *Catalysts* **10**, 1258 (2020).
104. Welch, P. & Scopes, R.K. Studies on cell-free metabolism: Ethanol production by a yeast glycolytic system reconstituted from purified enzymes. *J. Biotechnol.* **2**, 257-273 (1985).
105. Finnigan, W., Hepworth, L.J., Flitsch, S.L. & Turner, N.J. RetroBioCat as a computer-aided synthesis planning tool for biocatalytic reactions and cascades. *Nature Catalysis* **4**, 98-104 (2021).
106. Liu, Z. et al. In Vitro Reconstitution and Optimization of the Entire Pathway to Convert Glucose into Fatty Acid. *ACS Synthetic Biology* **6**, 701-709 (2017).
107. Li, Z. et al. Production of value-added chemicals from glycerol using in vitro enzymatic cascades. *Communications Chemistry* **1**, 71 (2018).
108. Diehl, C., Gerlinger, P.D., Paczia, N. & Erb, T.J. Synthetic anaplerotic modules for the direct synthesis of complex molecules from CO₂. *Nat. Chem. Biol.* **19**, 168-175 (2023).
109. Enoki, J., Meisborn, J., Müller, A.-C. & Kourist, R. A Multi-Enzymatic Cascade Reaction for the Stereoselective Production of γ -Oxyfunctionalized Amino Acids. *Front. Microbiol.* **7** (2016).
110. Cai, T. et al. Cell-free chemoenzymatic starch synthesis from carbon dioxide. *Science* **373**, 1523-1527 (2021).
111. Paschalidis, L., Beer, B., Sutiono, S., Sieber, V. & Burger, J. Design of enzymatic cascade reactors through multi-objective dynamic optimization. *Biochem. Eng. J.* **181**, 108384 (2022).
112. Xue, R. & Woodley, J.M. Process technology for multi-enzymatic reaction systems. *Bioresour. Technol.* **115**, 183-195 (2012).
113. Zhou, C. et al. Design of an in vitro multienzyme cascade system for the biosynthesis of nicotinamide mononucleotide. *Catalysis Science & Technology* **12**, 1080-1091 (2022).
114. Pandi, A. et al. A versatile active learning workflow for optimization of genetic and metabolic networks. *Nature communications* **13**, 3876 (2022).
115. Siedentop, R. et al. Bayesian Optimization for an ATP-Regenerating In Vitro Enzyme Cascade. *Catalysts* **13**, 468 (2023).
116. Finnigan, W. et al. Engineering a Seven Enzyme Biotransformation using Mathematical Modelling and Characterized Enzyme Parts. *ChemCatChem* **11**, 3474-3489 (2019).
117. Han, L. & Liang, B. New approaches to NAD(P)H regeneration in the biosynthesis systems. *World J. Microbiol. Biotechnol.* **34**, 141 (2018).
118. Murata, K., Uchida, T., Kato, J. & Chibata, I. Polyphosphate Kinase: Distribution, Some Properties and Its Application as an ATP Regeneration System. *Agricultural and Biological Chemistry* **52**, 1471-1477 (1988).
119. Iwai, N., Kitahara, Y. & Kitazume, T. One-pot three-step continuous enzymatic synthesis of 5-fluoro-5-deoxy-d-ribose. *J. Mol. Catal. B: Enzym.* **73**, 1-4 (2011).
120. Jossek, R. & Steinbüchel, A. In vitro synthesis of poly(3-hydroxybutyric acid) by using an enzymatic coenzyme A recycling system. *FEMS Microbiol. Lett.* **168**, 319-324 (1998).
121. Weckbecker, A. & Hummel, W. Glucose Dehydrogenase for the Regeneration of NADPH and NADH in Microbial Enzymes and Biotransformations. (ed. J.L. Barredo) Humana Press **17**, 225-238 (2005).
122. Abdel-Hady, G.N. et al. Engineering Cofactor Specificity of a Thermostable Phosphite Dehydrogenase for a Highly Efficient and Robust NADPH Regeneration System. *Frontiers in Bioengineering and Biotechnology* **9** (2021).
123. Al-Shameri, A., Siebert, D.L., Sutiono, S., Lauterbach, L. & Sieber, V. Hydrogenase-based oxidative biocatalysis without oxygen. *Nature Communications* **14**, 2693 (2023).

124. Beer, B., Pick, A. & Sieber, V. In vitro metabolic engineering for the production of α -ketoglutarate. *Metab. Eng.* **40**, 5-13 (2017).
125. Shaked, Z.e. & Whitesides, G.M. Enzyme-catalyzed organic synthesis: NADH regeneration by using formate dehydrogenase. *Journal of the American Chemical Society* **102**, 7104-7105 (1980).
126. Andexer, J.N. & Richter, M. Emerging Enzymes for ATP Regeneration in Biocatalytic Processes. *ChemBioChem* **16**, 380-386 (2015).
127. Mordhorst, S. & Andexer, J.N. Round, round we go—strategies for enzymatic cofactor regeneration. *Nat. Prod. Rep.* **37**, 1316-1333 (2020).
128. Drepper, T. et al. Novel biocatalysts for white biotechnology. *Biotechnol. J.* **1**, 777-786 (2006).
129. Arora, B., Mukherjee, J. & Gupta, M.N. Enzyme promiscuity: using the dark side of enzyme specificity in white biotechnology. *Sustainable Chemical Processes* **2**, 25 (2014).
130. Hult, K. & Berglund, P. Enzyme promiscuity: mechanism and applications. *Trends Biotechnol.* **25**, 231-238 (2007).
131. Sherkhanov, S. et al. Isobutanol production freed from biological limits using synthetic biochemistry. *Nature Communications* **11**, 4292 (2020).
132. Karau, A. & Grayson, I. in *Biotechnology of Food and Feed Additives*. (eds. H. Zorn & P. Czermak) 189-228 (Springer Berlin Heidelberg, Berlin, Heidelberg; 2014).
133. Williams, M. Dietary supplements and sports performance: amino acids. *J. Int. Soc. Sports Nutr.* **2**:2, 63 (2005).
134. Gmelch, T.J., Sperl, J.M. & Sieber, V. Optimization of a reduced enzymatic reaction cascade for the production of L-alanine. *Sci. Rep.* **9**, 11754 (2019).
135. Consortium, T.U. UniProt: the Universal Protein Knowledgebase in 2023. *Nucleic Acids Research* **51**, D523-D531 (2022).
136. Chang, A. et al. BRENDA, the ELIXIR core data resource in 2021: new developments and updates. *Nucleic Acids Research* **49**, D498-D508 (2020).
137. Sayers, E.W. et al. Database resources of the national center for biotechnology information. *Nucleic Acids Res.* **50**, D20-d26 (2022).
138. Altschul, S.F., Gish, W., Miller, W., Myers, E.W. & Lipman, D.J. Basic local alignment search tool. *J. Mol. Biol.* **215**, 403-410 (1990).
139. Gasteiger, E. et al. ExpASY: The proteomics server for in-depth protein knowledge and analysis. *Nucleic Acids Res.* **31**, 3784-3788 (2003).
140. Gasteiger, E. et al. in *The Proteomics Protocols Handbook*. (ed. J.M. Walker) 571-607 (Humana Press, Totowa, NJ; 2005).
141. Corpet, F. Multiple sequence alignment with hierarchical clustering. *Nucleic Acids Res.* **16**, 10881-10890 (1988).
142. Beber, M.E. et al. eQuilibrator 3.0: a database solution for thermodynamic constant estimation. *Nucleic Acids Research* **50**, D603-D609 (2021).
143. Noor, E. et al. Pathway thermodynamics highlights kinetic obstacles in central metabolism. *PLoS computational biology* **10**, e1003483 (2014).
144. Güner, S., Wegat, V., Pick, A. & Sieber, V. Design of a synthetic enzyme cascade for the in vitro fixation of a C 1 carbon source to a functional C 4 sugar. *Green Chem.* **23**, 6583-6590 (2021).
145. Sutiono, S., Teshima, M., Beer, B., Schenk, G. & Sieber, V. Enabling the direct enzymatic dehydration of D-glycerate to pyruvate as the key step in synthetic enzyme cascades used in the cell-free production of fine chemicals. *ACS Catalysis* **10**, 3110-3118 (2020).
146. Gocke, D. et al. Branched-Chain Keto Acid Decarboxylase from *Lactococcus lactis* (KdcA), a Valuable Thiamine Diphosphate-Dependent Enzyme for Asymmetric C-C Bond Formation. *Adv. Synth. Catal.* **349**, 1425-1435 (2007).

147. Sutiono, S., Carsten, J. & Sieber, V. Structure-Guided Engineering of α -Keto Acid Decarboxylase for the Production of Higher Alcohols at Elevated Temperature. *ChemSusChem* **11**, 3335-3344 (2018).
148. Pick, A., Rühmann, B., Schmid, J. & Sieber, V. Novel CAD-like enzymes from *Escherichia coli* K-12 as additional tools in chemical production. *Applied microbiology and biotechnology* **97**, 5815-5824 (2013).
149. Sutiono, S., Satzinger, K., Pick, A., Carsten, J. & Sieber, V. To beat the heat – engineering of the most thermostable pyruvate decarboxylase to date. *RSC Advances* **9**, 29743-29746 (2019).
150. Chester, N. & Marshak, D.R. Dimethyl sulfoxide-mediated primer T_m reduction: a method for analyzing the role of renaturation temperature in the polymerase chain reaction. *Analytical biochemistry* **209**, 284-290 (1993).
151. Saiki, R.K. et al. Enzymatic Amplification of β -Globin Genomic Sequences and Restriction Site Analysis for Diagnosis of Sickle Cell Anemia. *Science* **230**, 1350-1354 (1985).
152. Williams, E.M., Copp, J.N. & Ackerley, D.F. in *Directed Evolution Library Creation* 83-101 (Springer, 2014).
153. Inoue, H., Nojima, H. & Okayama, H. High efficiency transformation of *Escherichia coli* with plasmids. *Gene* **96**, 23-28 (1990).
154. Gill, S.C. & von Hippel, P.H. Calculation of protein extinction coefficients from amino acid sequence data. *Analytical Biochemistry* **182**, 319-326 (1989).
155. Gmelch, T.J., Sperl, J.M. & Sieber, V. Molecular dynamics analysis of a rationally designed aldehyde dehydrogenase gives insights into improved activity for the non-native cofactor NAD⁺. *ACS Synthetic Biology* **9**, 920-929 (2020).
156. France, S.P., Hepworth, L.J., Turner, N.J. & Flitsch, S.L. Constructing Biocatalytic Cascades: In Vitro and in Vivo Approaches to de Novo Multi-Enzyme Pathways. *ACS Catalysis* **7**, 710-724 (2017).
157. Lima-Ramos, J., Tufvesson, P. & Woodley, J.M. Application of environmental and economic metrics to guide the development of biocatalytic processes. *Green Processing and Synthesis* **3**, 195-213 (2014).
158. Sprenger, G.A., Schörken, U., Sprenger, G. & Sahn, H. Transketolase A of *Escherichia coli* K12: purification and properties of the enzyme from recombinant strains. *European journal of biochemistry* **230**, 525-532 (1995).
159. Wohlgemuth, R. C2-Ketol elongation by transketolase-catalyzed asymmetric synthesis. *J. Mol. Catal. B: Enzym.* **61**, 23-29 (2009).
160. Musil, M. et al. FireProt: web server for automated design of thermostable proteins. *Nucleic Acids Research* **45**, W393-W399 (2017).
161. Spence, M.A., Kaczmarek, J.A., Saunders, J.W. & Jackson, C.J. Ancestral sequence reconstruction for protein engineers. *Curr. Opin. Struct. Biol.* **69**, 131-141 (2021).
162. Lopez-Gallego, F. et al. Stabilization of different alcohol oxidases via immobilization and post immobilization techniques. *Enzyme and Microbial Technology* **40**, 278-284 (2007).
163. Mangkorn, N. et al. Synthesis and characterization of *Ogataea thermomethanolica* alcohol oxidase immobilized on barium ferrite magnetic microparticles. *Journal of Bioscience and Bioengineering* **127**, 265-272 (2019).
164. Wahart, A.J.C., Staniland, J., Miller, G.J. & Cosgrove, S.C. Oxidase enzymes as sustainable oxidation catalysts. *Royal Society Open Science* **9**, 211572 (2022).
165. Srinivasamurthy, V.S.T., Böttcher, D. & Bornscheuer, U.T. A multi-enzyme cascade reaction for the production of 6-hydroxyhexanoic acid. *Zeitschrift für Naturforschung C* **74**, 71-76 (2019).
166. You, C. & Percival Zhang, Y.H. Biomanufacturing by in vitro biosystems containing complex enzyme mixtures. *Process Biochem.* **52**, 106-114 (2017).

167. Spöring, J.-D., Graf von Westarp, W., Kipp, C.R., Jupke, A. & Rother, D. Enzymatic Cascade in a Simultaneous, One-Pot Approach with In Situ Product Separation for the Asymmetric Production of (4S,5S)-Octanediol. *Organic Process Research & Development* **26**, 2038-2045 (2022).
168. Han, P., Zhou, X. & You, C. Efficient Multi-Enzymes Immobilized on Porous Microspheres for Producing Inositol From Starch. *Frontiers in Bioengineering and Biotechnology* **8** (2020).
169. Falcicchio, P., Levisson, M., Kengen, S.W.M., Koutsopoulos, S., van der Oost, J. (Hyper)thermophilic Enzymes: Production and Purification. In: Labrou, N. (eds) Protein Downstream Processing. Methods in Molecular Biology Humana Press, Totowa, NJ. **1129**. 487-496 (2014).
170. Sun, F., Zhang, X.-Z., Myung, S. & Zhang, Y.-H.P. Thermophilic *Thermotoga maritima* ribose-5-phosphate isomerase RpiB: optimized heat treatment purification and basic characterization. *Protein expression and purification* **82**, 302-307 (2012).
171. Saravanan, T. et al. Engineering a thermostable transketolase for arylated substrates. *Green Chem.* **19**, 481-489 (2017).
172. Atalah, J., Cáceres-Moreno, P., Espina, G. & Blamey, J.M. Thermophiles and the applications of their enzymes as new biocatalysts. *Bioresour. Technol.* **280**, 478-488 (2019).
173. Hanatani, Y. et al. In vitro production of cysteine from glucose. *Applied microbiology and biotechnology* **103**, 8009-8019 (2019).
174. Ettema, T.J.G., Ahmed, H., Geerling, A.C.M., van der Oost, J. & Siebers, B. The non-phosphorylating glyceraldehyde-3-phosphate dehydrogenase (GAPN) of *Sulfolobus solfataricus*: a key-enzyme of the semi-phosphorylative branch of the Entner–Doudoroff pathway. *Extremophiles* **12**, 75-88 (2008).
175. Brunner, N.A., Siebers, B. & Hensel, R. Role of two different glyceraldehyde-3-phosphate dehydrogenases in controlling the reversible Embden–Meyerhof–Parnas pathway in *Thermoproteus tenax*: regulation on protein and transcript level. *Extremophiles* **5**, 101-109 (2001).
176. Lerchner, A., Jarasch, A. & Skerra, A. Engineering of alanine dehydrogenase from *Bacillus subtilis* for novel cofactor specificity. *Biotechnology and Applied Biochemistry* **63**, 616-624 (2016).
177. Matsubara, K., Yokooji, Y., Atomi, H. & Imanaka, T. Biochemical and genetic characterization of the three metabolic routes in *Thermococcus kodakarensis* linking glyceraldehyde 3-phosphate and 3-phosphoglycerate. *Mol. Microbiol.* **81**, 1300-1312 (2011).
178. Cahn, J.K.B. et al. A General Tool for Engineering the NAD/NADP Cofactor Preference of Oxidoreductases. *ACS Synthetic Biology* **6**, 326-333 (2017).
179. Toteva, M.M., Silvaggi, N.R., Allen, K.N. & Richard, J.P. Binding Energy and Catalysis by d-Xylose Isomerase: Kinetic, Product, and X-ray Crystallographic Analysis of Enzyme-Catalyzed Isomerization of (R)-Glyceraldehyde. *Biochemistry* **50**, 10170-10181 (2011).
180. M. Walgode, P., D. Coelho, L.C., V. Faria, R.P. & E. Rodrigues, A. Dihydroxyacetone Production: From Glycerol Catalytic Oxidation with Commercial Catalysts to Chromatographic Separation. *Ind. Eng. Chem. Res.* **60**, 10551-10565 (2021).
181. Liepins, J., Kuorelahti, S., Penttilä, M. & Richard, P. Enzymes for the NADPH-dependent reduction of dihydroxyacetone and D-glyceraldehyde and L-glyceraldehyde in the mould *Hypocrea jecorina*. *The FEBS Journal* **273**, 4229-4235 (2006).
182. Uwajima, T., Shimizu, Y. & Terada, O. Glycerol oxidase, a novel copper hemoprotein from *Aspergillus japonicus*. Molecular and catalytic properties of the enzyme and its application to the analysis of serum triglycerides. *J. Biol. Chem.* **259**, 2748-2753 (1984).

183. Truesdale, G.A., Downing, A.L. & Lowden, G.F. The solubility of oxygen in pure water and sea-water. *Journal of Applied Chemistry* **5**, 53-62 (1955).
184. Sanchez, S. & Demain, A.L. Metabolic regulation and overproduction of primary metabolites. *Microb. Biotechnol.* **1**, 283-319 (2008).
185. Desmons, S., Fauré, R.g. & Bontemps, S. Formaldehyde as a promising C1 source: The instrumental role of biocatalysis for stereocontrolled reactions. *ACS Catalysis* **9**, 9575-9588 (2019).
186. Nobuo, K. et al. Purification and properties of a transketolase responsible for formaldehyde fixation in a methanol-utilizing yeast, *Candida boidinii* (Kloeckera sp.) No. 2201. *Biochimica et Biophysica Acta (BBA) - General Subjects* **715**, 143-150 (1982).
187. Orita, I. et al. The ribulose monophosphate pathway substitutes for the missing pentose phosphate pathway in the archaeon *Thermococcus kodakaraensis*. *J. Bacteriol.* **188**, 4698-4704 (2006).
188. Yu, H. & Liao, J.C. A modified serine cycle in *Escherichia coli* converts methanol and CO₂ to two-carbon compounds. *Nature Communications* **9**, 3992 (2018).
189. Lu, X. et al. Constructing a synthetic pathway for acetyl-coenzyme A from one-carbon through enzyme design. *Nature communications* **10**, 1378 (2019).
190. Jo, H.-J. et al. Glyoxylate carboligase-based whole-cell biotransformation of formaldehyde into ethylene glycol via glycolaldehyde. *Green Chem.* **24**, 218-226 (2022).
191. Szekrenyi, A. et al. Asymmetric assembly of aldose carbohydrates from formaldehyde and glycolaldehyde by tandem biocatalytic aldol reactions. *Nat. Chem.* **7**, 724-729 (2015).
192. Waites, M.J. & Quayle, J.R. The Interrelation between Transketolase and Dihydroxyacetone Synthase Activities in the Methylophilic Yeast *Candida boidinii*. *Microbiology* **124**, 309-316 (1981).
193. Dickens, F. & Williamson, D. Formaldehyde as an acceptor aldehyde for transketolase, and the biosynthesis of triose. *Nature* **181**, 1790-1790 (1958).
194. Zhang, J. et al. Hybrid synthesis of polyhydroxybutyrate bioplastics from carbon dioxide. *Green Chem.* **25**, 3247-3255 (2023).
195. Yang, J. et al. Transformation of formaldehyde into functional sugars via multi-enzyme stepwise cascade catalysis. *Catalysis Science & Technology* **7**, 3459-3463 (2017).
196. Li, T. et al. One-pot chemoenzymatic synthesis of glycolic acid from formaldehyde. *Green Chem.* **24**, 5064-5069 (2022).
197. Guérard-Hélaine, C. et al. Transketolase–Aldolase Symbiosis for the Stereoselective Preparation of Aldoses and Ketoses of Biological Interest. *Adv. Synth. Catal.* **359**, 2061-2065 (2017).
198. Yeh, A.H.-W. et al. De novo design of luciferases using deep learning. *Nature* **614**, 774-780 (2023).
199. Köpke, M., Mihalcea, C., Bromley, J.C. & Simpson, S.D. Fermentative production of ethanol from carbon monoxide. *Curr. Opin. Biotechnol.* **22**, 320-325 (2011).
200. Liew, F.E. et al. Carbon-negative production of acetone and isopropanol by gas fermentation at industrial pilot scale. *Nat. Biotechnol.* **40**, 335-344 (2022).
201. Heffernan, J.K. et al. Enhancing CO₂-Valorization Using *Clostridium autoethanogenum* for Sustainable Fuel and Chemicals Production. *Frontiers in Bioengineering and Biotechnology* **8** (2020).
202. Lee, H., Bae, J., Jin, S., Kang, S. & Cho, B.K. Engineering Acetogenic Bacteria for Efficient One-Carbon Utilization. *Front. Microbiol.* **13**, 865168 (2022).
203. Katsyv, A. & Müller, V. Overcoming Energetic Barriers in Acetogenic C1 Conversion. *Frontiers in Bioengineering and Biotechnology* **8** (2020).

204. Takors, R. et al. Using gas mixtures of CO, CO₂ and H₂ as microbial substrates: the do's and don'ts of successful technology transfer from laboratory to production scale. *Microb. Biotechnol.* **11**, 606-625 (2018).
205. Cotton, C.A.R., Claassens, N.J., Benito-Vaquerizo, S. & Bar-Even, A. Renewable methanol and formate as microbial feedstocks. *Curr. Opin. Biotechnol.* **62**, 168-180 (2020).
206. Gao, J., Li, Y., Yu, W. & Zhou, Y.J. Rescuing yeast from cell death enables overproduction of fatty acids from sole methanol. *Nature Metabolism* **4**, 932-943 (2022).
207. Drejer, E.B. et al. Methanol-based acetoin production by genetically engineered *Bacillus methanolicus*. *Green Chem.* **22**, 788-802 (2020).
208. Zhu, W.-L. et al. Bioconversion of methanol to value-added mevalonate by engineered *Methylobacterium extorquens* AM1 containing an optimized mevalonate pathway. *Applied Microbiology and Biotechnology* **100**, 2171-2182 (2016).
209. Zhang, P. et al. Catabolite repression of Aox in *Pichia pastoris* is dependent on hexose transporter PpHxt1 and pexophagy. *Appl Environ Microbiol* **76**, 6108-6118 (2010).
210. Zhan, C. et al. Transcription factor Mxr1 promotes the expression of Aox1 by repressing glycerol transporter 1 in *Pichia pastoris*. *FEMS Yeast Res.* **17**, fox015 (2017).
211. Cho, J.S., Kim, G.B., Eun, H., Moon, C.W. & Lee, S.Y. Designing Microbial Cell Factories for the Production of Chemicals. *JACS Au* **2**, 1781-1799 (2022).
212. Wang, X. et al. Biological conversion of methanol by evolved *Escherichia coli* carrying a linear methanol assimilation pathway. *Bioresources and Bioprocessing* **4**, 41 (2017).
213. De Simone, A. et al. Mixing and matching methylotrophic enzymes to design a novel methanol utilization pathway in *E. coli*. *Metab. Eng.* **61**, 315-325 (2020).
214. Espinosa, M.I. et al. Adaptive laboratory evolution of native methanol assimilation in *Saccharomyces cerevisiae*. *Nature Communications* **11**, 5564 (2020).
215. Chen, F.Y.H., Jung, H.-W., Tsuei, C.-Y. & Liao, J.C. Converting *Escherichia coli* to a Synthetic Methylotroph Growing Solely on Methanol. *Cell* **182**, 933-946.e914 (2020).
216. Zhan, C. et al. Reprogramming methanol utilization pathways to convert *Saccharomyces cerevisiae* to a synthetic methylotroph. *Nature Catalysis* **6**, 435-450 (2023).
217. Jo, H.-J. et al. Multilayer Engineering of an *Escherichia coli*-Based Biotransformation System to Exclusively Produce Glycolic Acid from Formaldehyde. *ACS Sustainable Chemistry & Engineering* **11**, 1078-1086 (2023).
218. You, C. et al. An in vitro synthetic biology platform for the industrial biomanufacturing of myo-inositol from starch. *Biotechnology and Bioengineering* **114**, 1855-1864 (2017).
219. Sutiono, S. et al. Biocatalytic Production of 1,2,4-Butanetriol beyond a Titer of 100 g/L: Boosting by Intermediates. *ACS Sustainable Chemistry & Engineering* **11**, 6592-6599 (2023).
220. Woodley, J.M. Towards the sustainable production of bulk-chemicals using biotechnology. *N. Biotechnol.* **59**, 59-64 (2020).
221. Gonzalez-Gil, G., Kleerebezem, R. & Lettinga, G. Conversion and toxicity characteristics of formaldehyde in acetoclastic methanogenic sludge. *Biotechnology and Bioengineering* **79**, 314-322 (2002).
222. Geng, W. et al. Techno-economic analysis of hemicellulose extraction from different types of lignocellulosic feedstocks and strategies for cost optimization. *Biofuels, Bioproducts and Biorefining* **14**, 225-241 (2020).
223. Gibier, M., Sadeghisadeghabad, M., Girods, P., Zoulalian, A. & Rogaume, Y. Furniture wood waste depollution through hydrolysis under pressurized water steam: Experimental work and kinetic modelization. *J. Hazard. Mater.* **436**, 129126 (2022).
224. Masters, A.L. A Review of Methods for Detoxification and Neutralization of Formalin in Water. *N. Am. J. Aquacult.* **66**, 325-333 (2004).

225. Zhou, J. et al. Three multi-enzyme cascade pathways for conversion of C1 to C2/C4 compounds. *Chem Catalysis* **2**, P2675-2690 (2022).
226. Nattermann, M. et al. Engineering a Highly Efficient Carboligase for Synthetic One-Carbon Metabolism. *ACS Catalysis* **11**, 5396-5404 (2021).

6. Appendices

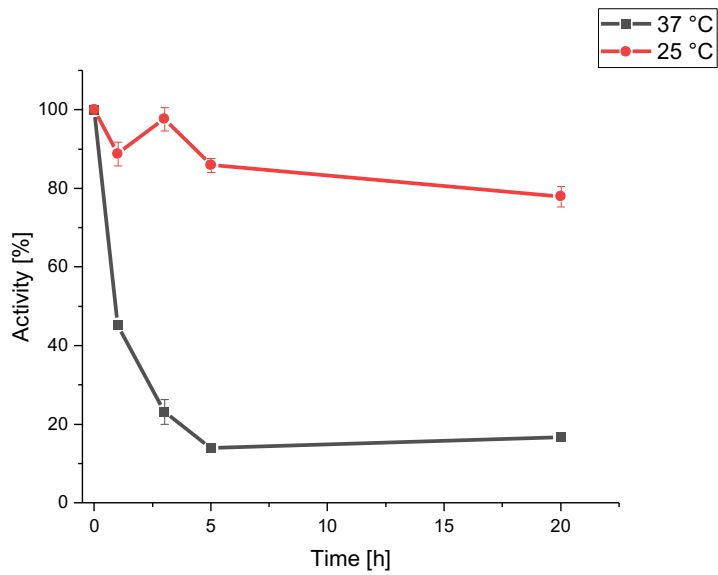


Figure 10: Activity of *ccGapN* on glyceraldehyde 3-phosphatase from fructose 1,6-bisphosphate in a coupled assay system with aldolase over a time period of 20 h. The assay was conducted as described in Section 2.2.3 and 2.2.4.

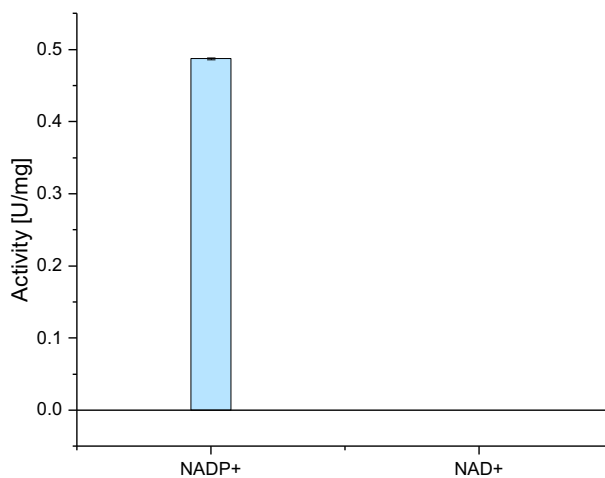


Figure 11: Activity of *ccGapN* on glyceraldehyde 3-phosphatase from fructose 1,6-bisphosphate in a coupled assay system with aldolase with addition of either NADP^+ or NAD^+ as cofactor.. The assay was conducted as described in Section 2.2.3 and 2.2.4.

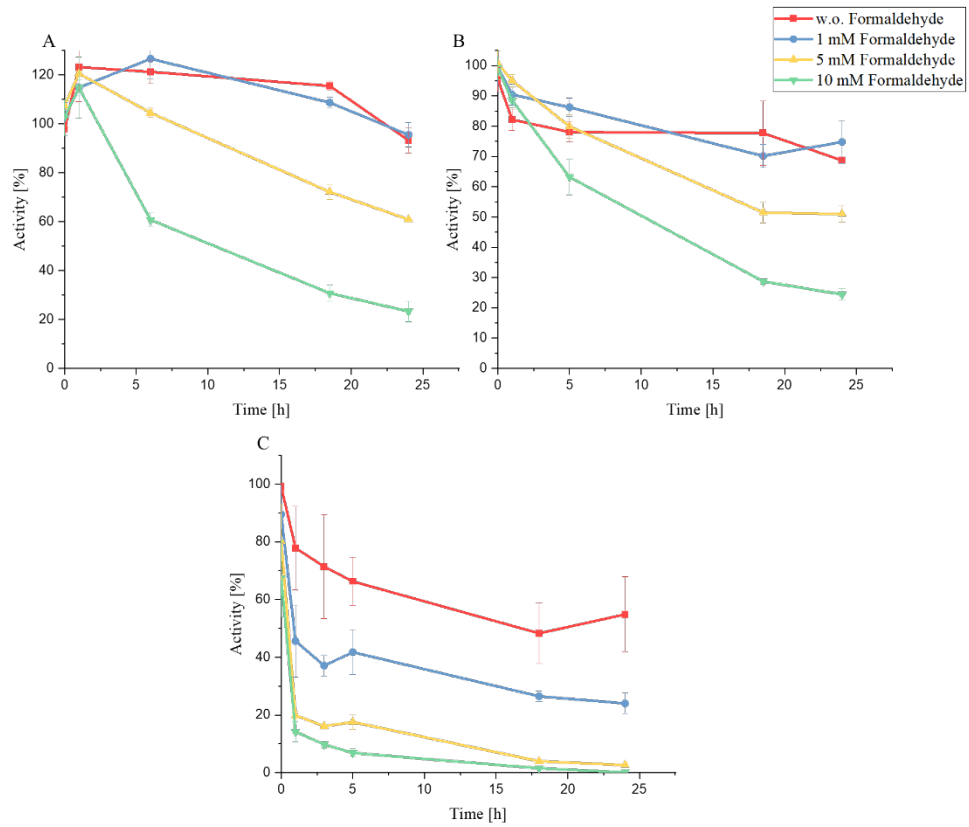


Figure 12: Formaldehyde tolerance (Section 2.2.6.3) over a time period of 24 h at 37 °C of A: *taPyK*, B: *tmENO*, C: *kbDhaK*. Activity was measure as described in Section 2.2.3.

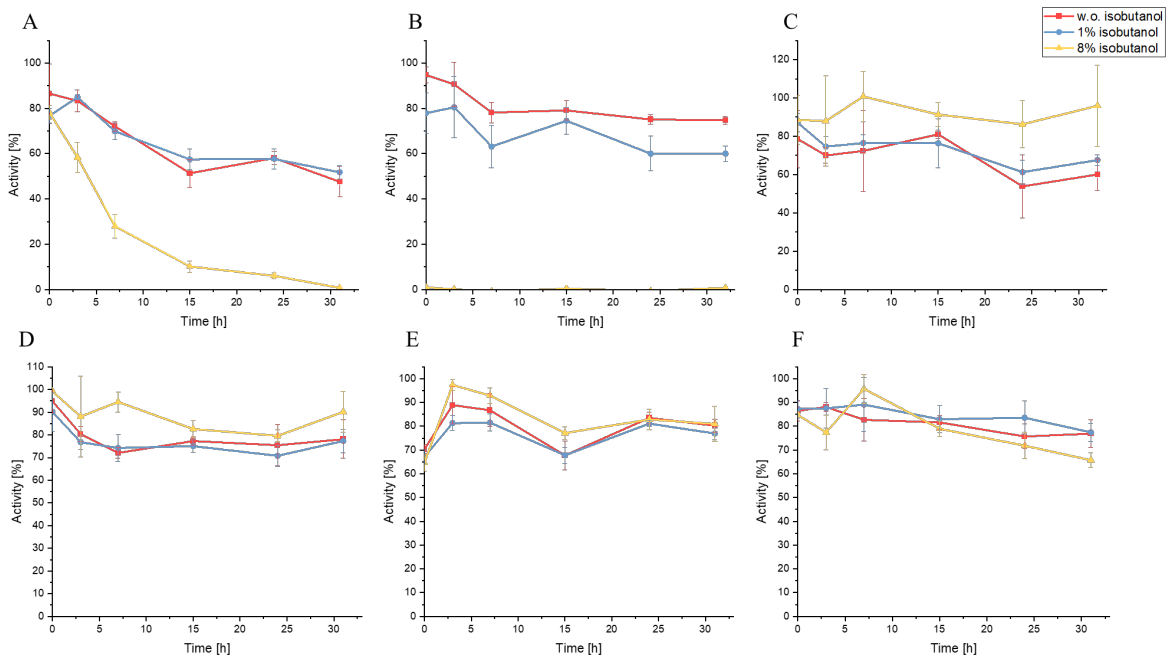


Figure 13: Isobutanol tolerance (Section 2.2.6.5) over a time period of 32 h at 37 °C of A: *pfXylA*, B: *kbDhaK*, C: *tmTpi_fusPgK*, D: *tkGapN*, E: *gsPgM*, F: *tmENO*. Activity was measure as described in Section 2.2.3.

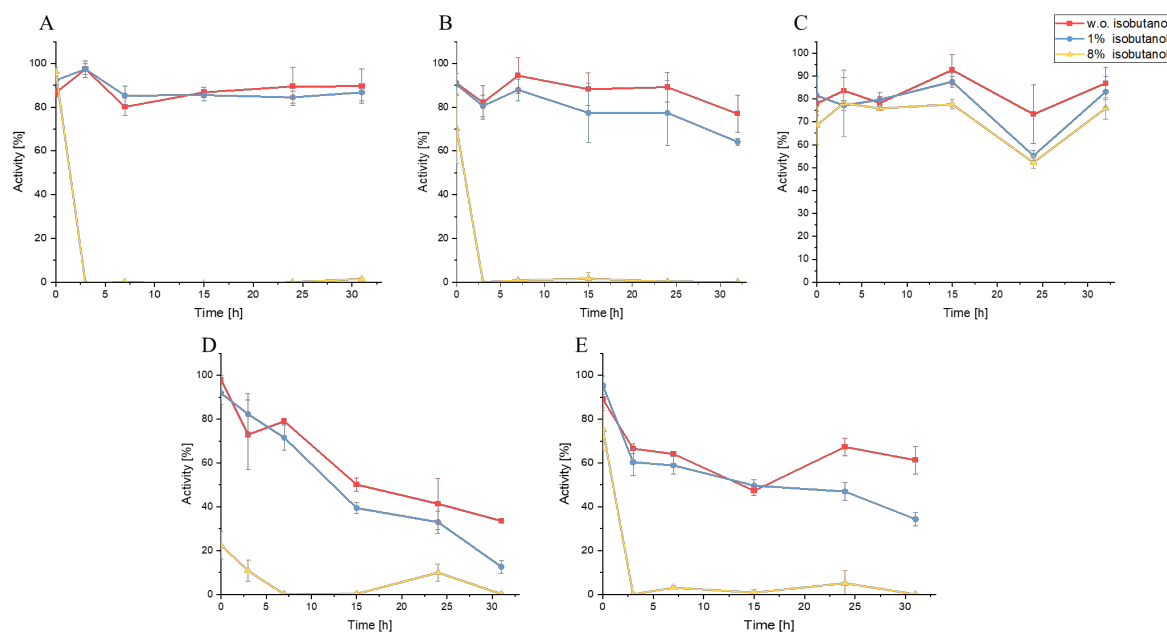


Figure 14: Isobutanol tolerance (2.2.6.5) over a time period of 32 h at 37 °C of A: *taPyK*, B: *bsAlsS*, C: *gsIlvC* D: *llKDC*, E: *ecYjgB*. Activity was measure as described in 2.2.3.

Table 28: SBtab file for the MDF analysis of the methanol to L-alanine pathway

!!!SBtab DocumentName='Pathway Model' SBtabVersion='1.0'	
!!SBtab TableName='Reaction' TableID='Reaction' TableType='Reaction'	
!ReactionFormula	!RelativeFlux
Methanol + O2 <=> H2O2 + Methanal	3
3 H2O2 <=> 1.5 O2 + 3 H2O	1
3 Methanal <=> Glycerone	1
Glycerone + ATP <=> Glycerone phosphate + ADP	1
Glycerone phosphate <=> D-Glyceraldehyde 3-phosphate	1
NAD+ + D-Glyceraldehyde 3-phosphate + H2O <=> NADH + D-Glycerate-3-phosphate	1
D-Glycerate-3-phosphate <=> D-Glycerate-2-phosphate	1
D-Glycerate-2-phosphate <=> Phosphoenolpyruvate + H2O	1
ADP + Phosphoenolpyruvate <=> Pyruvate + ATP	1
Pyruvate + NH3 + NADH <=> L-Alanine + NAD+ + H2O	1

* License National Footprint and Biocapacity Accounts 2022 Edition: This Data Package provided by Global Footprint Network is licensed under a Creative Commons Attribution-ShareAlike 4.0 International License (CC-BY-SA 4.0).

Cell-free enzyme cascades — application and transition from development to industrial implementation

Mariko Teshima, Vivian Pascal Willers, Volker Sieber

Current Opinion in Biotechnology
Volume 79, February 2023, 102868

DOI: <https://doi.org/10.1016/j.copbio.2022.102868>

© 2022 Elsevier Ltd. All rights reserved.

Journal Author Rights

Please note that, as the author of this Elsevier article, you retain the right to include it in a thesis or dissertation, provided it is not published commercially. Permission is not required, but please ensure that you reference the journal as the original source. For more information on this and on your other retained rights, please visit: <https://www.elsevier.com/about/our-business/policies/copyright#Author-right>



ELSEVIER

Cell-free enzyme cascades – application and transition from development to industrial implementation

Mariko Teshima^{1,*}, Vivian Pascal Willers^{1,*} and Volker Sieber^{1,2,3}

In the vision to realize a circular economy aiming for net carbon neutrality or even negativity, cell-free bioconversion of sustainable and renewable resources emerged as a promising strategy. The potential of *in vitro* systems is enormous, delivering technological, ecological, and ethical added values. Innovative concepts arose in cell-free enzymatic conversions to reduce process waste production and preserve fossil resources, as well as to redirect and assimilate released industrial pollutions back into the production cycle again. However, the great challenge in the near future will be the jump from a concept to an industrial application. The transition process in industrial implementation also requires economic aspects such as productivity, scalability, and cost-effectiveness. Here, we briefly review the latest proof-of-concept cascades using carbon dioxide and other C1 or lignocellulose-derived chemicals as blueprints to efficiently recycle greenhouse gases, as well as cutting-edge technologies to mature these concepts to industrial pilot plants.

Addresses

¹ Technical University of Munich, Campus Straubing, 94315 Straubing, Germany

² SynBioFoundry@TUM, Technical University of Munich, 94315 Straubing, Germany

³ School of Chemistry and Molecular Biosciences, The University of Queensland, St. Lucia 4072, Australia

Corresponding author: Sieber, Volker (Sieber@tum.de)

* These authors contributed equally.

Current Opinion in Biotechnology 2023, 79:102868

This review comes from a themed issue on **Chemical Biotechnology**

Edited by **Bernd Nidetzky** and **Byung-Gee Kim**

Available online xxxx

<https://doi.org/10.1016/j.copbio.2022.102868>

0958–1669/© 2022 Elsevier Ltd. All rights reserved.

Introduction

Humans have generated 1.7 trillion tons of carbon dioxide (CO₂) pollution, with a 49% CO₂ increase to 417 ppm from the pre-industrial era [1,2]. The convenience-oriented supply and fast-and-abundant motto

of industrial production have led to the accumulation of undegradable wastes and greenhouse gases, driving climate change. Furthermore, we are situated in global social uncertainty caused by rising energy costs due to the unstable political situation. These problems challenge us to globally rethink our behaviors.

Being aware of these threats, politics and industry work in close cooperation to approach a shift toward a sustainable circular bioeconomy, with a significant focus on biotransformations and biocatalysis, especially for the production of chemicals and energy from renewables. The driving force of this motivation is the exploitation of the power of natural biological systems, which are generally characterized by nontoxic and highly selective reactions under physiological conditions [3]. The moderate reaction temperatures reduce energy inputs, and minimum side-product generation facilitates downstream processing.

From the 2000s global energy crisis, microbial alcohol production from plant-originated sugars was extensively investigated for use as supplements to fossil-based fuels [4,5]. In this context, metabolic engineering flourished as a promising approach for adjusting microorganisms' biosynthetic pathways to efficiently produce more complex products, such as isobutanol or longer-chain biodiesels [4,6].

However, these living cell systems have recently been increasingly supported, improved, or even replaced by cell-free multienzymatic cascades. The complexity of *in vitro* transformations has increased to such an extent that they replace not only one or two challenging reactions but also enable the total synthesis of a wide range of value-added chemicals such as replacements of fossil-based polymers and plastics or food additives and active pharmaceutical ingredients [7,8].

Moreover, *in vitro* systems benefit from their simplicity of directly implementing state-of-the-art technologies from an expanded enzyme toolbox, including new-to-nature reactions and enzyme engineering [9,10]. They also circumvent challenges of whole-cell systems through liberation from living cell burdens and offer higher variability, flexibility, and controllability [11].

Herein, we will present the latest developments in cell-free synthetic biochemistry, with a focus on producing

commodity chemicals and low-cost precursor molecules, thereby evaluating the scalability and industrial implementation of such processes. As a highlight of this review, we will showcase a synergistic concept where cell-free systems were used to accelerate metabolic engineering for final *in vivo* chemical production, which succeeded in upscaling to a pilot plant scale [12].

Cell-free biosynthesis

Cell-free artificial enzyme cascades take bottom-up approaches demonstrating a counterpart of metabolic engineering applied for whole-cell biomanufacturing. This latter top-down strategy demands considerable efforts to delete/downregulate the competing metabolic pathways naturally required for cell viability. Conversely, enzymatic activities that lead to desired product formation must be introduced/upregulated.

Contrary to this, cell-free artificial enzyme cascades start with the reconstruction or *de novo* construction of biosynthetic pathways using minimal components: first, the search for robust biocatalysts for the whole pathway from the substrate to the final product is performed considering the longevity of future reactor runs [13•,14]. Inactivation and degradation of enzymes by mechanical stress, higher process temperature, or toxicity of solvents and chemical components such as intermediates or products are the issues for consideration. Second, the system has to be supplemented with enough cofactors such as NAD(P)H and ATP [15]. If purified enzymes are the matter of choice, a self-sustaining and continuously operating system with cofactor regeneration/recycling, occasionally including sacrificial substrates, is required [16]. Keeping the expensive cofactor feed at a minimum [17] and achieving a high cofactor turnover [18,19] are essential issues, as shown in the artificial cofactor development and engineering of enzymes accepting cofactor analogs [20–23]. Furthermore, cofactor-immobilizing technologies coupled with regeneration emerged to allow for the variability of *in vitro* cascade processes [24,25]. On the other hand, the use of cell lysates with overexpressed biocatalysts ensures sufficient cofactor sources [16,26,27]. The third component is the environment surrounding the active enzymes with substrates/intermediates/products; generally physiological, mild conditions with a high buffer capacity. Advantageously, *in vitro* systems can select not only cell-like but also artificial environments with spatial compartmentalization, sequential temporal adjustment of environmental parameters [28], or two-phase systems with an organic solvent [29,30].

In techno-economic considerations, all these factors must meet the demands regarding costs, sustainability,

and process scalability, especially in the case of high-volume commodity chemicals.

Proof-of-concept enzyme cascades

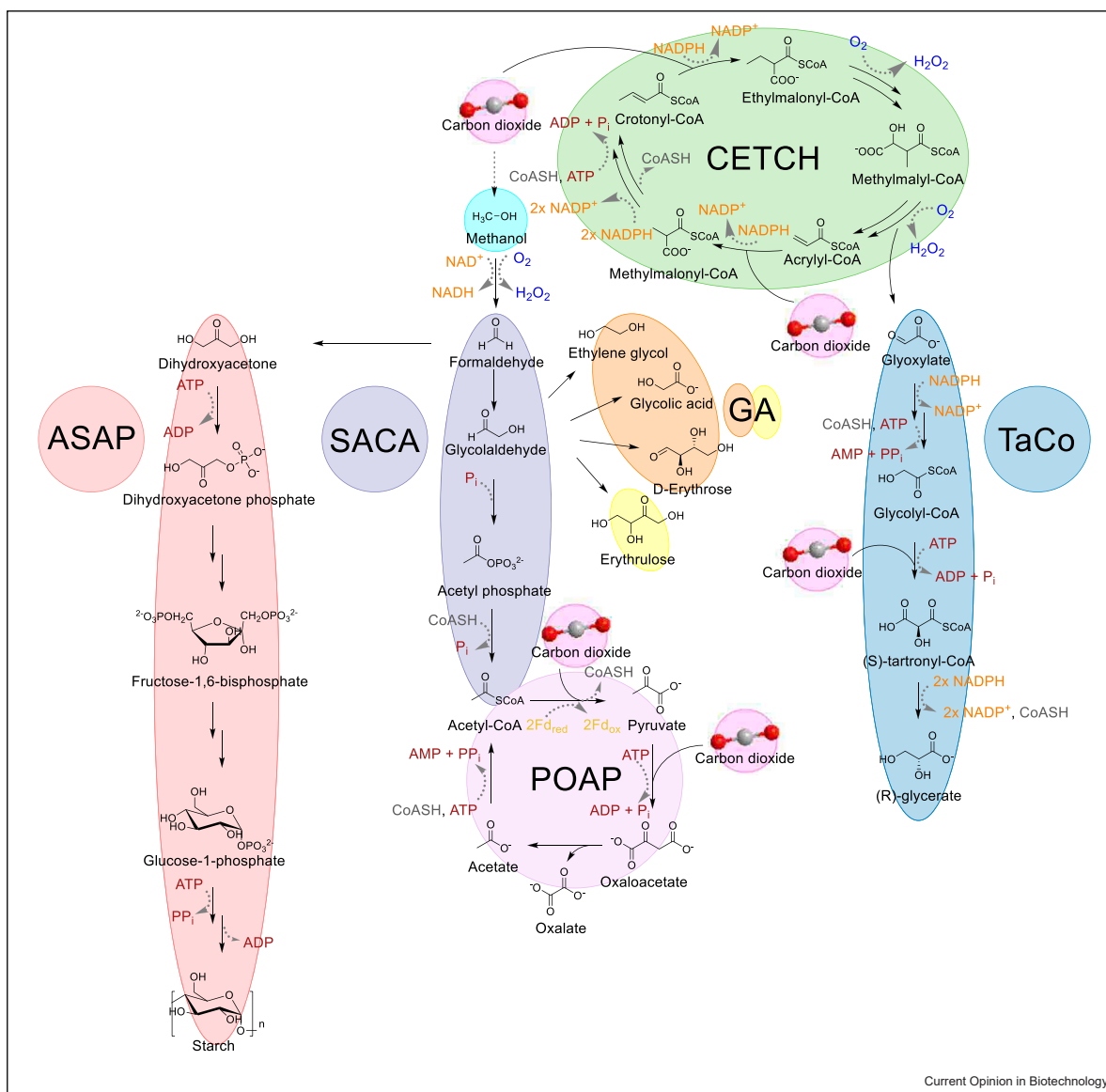
Owing to the urgent need for anthropogenic CO₂ recycling, several prototypes of *in vitro* enzyme cascades were presented in the last years to assimilate C1 compounds (Figure 1). CETCH cycle (*crotonyl-CoA/ethylmalonyl-CoA/hydroxybutyryl-CoA cycle*) presented by Erb and coworkers in 2016 was a milestone publication aimed at higher efficiency of CO₂ fixation than in nature by exploiting enoyl-CoA-dependent carboxylases/reductase [31••]. This designer CO₂ fixation pathway emphasizes the significant power of cell-free artificial cascades by using 17 enzymes from all three domains of life.

Recently, Scheffen et al. [32•] further expanded the CETCH cycle by tartronyl-CoA (TaCo) module to assimilate one additional CO₂ molecule to glyoxylate. The obtained C3 glycerate can easily be directed to central carbon metabolism by phosphorylation. The key to realizing the hypothetical TaCo pathway was the extensive development of glycol-CoA carboxylase as a new-to-nature enzyme. As showcased here, many reactions and pathways based on direct CO₂ fixation by carboxylases from dissolved bicarbonate have been published in recent years, for example, the POAP (pyruvate carboxylase, oxaloacetate acetylhydrolase, acetate-CoA ligase, and pyruvate synthase) cycle [29,33,34].

Similarly, Cai and coworkers [35••] drafted the *artificial starch anabolic pathway* (ASAP) with just 11 core reactions instead of the 60 steps known in plants. The key steps were the conversion of ‘green’ methanol (chemically generated from CO₂) to formaldehyde by alcohol oxidase and, subsequently, three equivalents of formaldehyde to one molecule of dihydroxyacetone by an artificial formolase (FLS). Interestingly, the whole cascade was computationally outlined using databases (MetaCyc and ATLAS) and applying combinatorial algorithms and flux balance analysis. Experimental evaluations supported the process of modular assembling and enzyme engineering optimized the cascade flux for starch synthesis. However, the high enzyme load of 5 g L⁻¹ FLS (> 50% of the core enzymes) is an apparent limiting factor that seemingly hampers the upscaling.

Nevertheless, C1 chemistry using FLS is an emerging topic, and improving its activity by enzyme engineering is the first step to upscale reaction cascades with FLS. To expand the potential of FLS for a broader reaction spectrum, Güner et al. [36•] subjected FLS to high-throughput screening to shift its activity from C3 generation to C4 erythrulose

Figure 1



Recently developed and validated *in vitro* cascades for the assimilation of C1 compounds. Energy supply and redox balances within the enzyme cascades are highlighted in red letters for phosphate transfer cofactor, orange letters for redox cofactors NAD(P)⁺/NAD(P)H, yellow letters for iron-sulfur protein ferredoxin Fd_{red}/Fd_{ox}, gray letters for coenzyme A (CoASH), and in blue letters for molecular oxygen as electron acceptor. CO₂ can be chemically, enzymatically, or electrically converted into the C1 compound methanol. Methanol can be used in *in vitro* enzymatic systems to produce various products. The ASAP uses chemically derived methanol from CO₂ to produce starch. The SACA uses formaldehyde for the production of acetyl-CoA. In addition, there are smaller pathways that use GA derived from formaldehyde to produce ethylene glycol, glycolic acid, D-erythrose, and erythrulose. In this process, erythrulose is produced by FLS and the other chemicals by GA synthase. Alternatively, CO₂ can be fixed directly into bicarbonate. Here, the crotonyl-coenzyme A (CoA)/ethylmalonyl-CoA/hydroxybutyryl-CoA cycle binds two CO₂ molecules per cycle and generates glyoxylate. Glyoxylate is one of the initial substrates for the TaCo pathway. Here, one CO₂ molecule is bound for the formation of glycerate. The POAP cycle includes pyruvate carboxylase, oxaloacetate acetylhydrolase, acetate-CoA ligase, and pyruvate synthase, and builds oxalate by binding two CO₂ molecules.

synthesis in an atom-economic way. Alternatively, C–C bond formation from formaldehyde using glycolaldehyde (GA) synthase also finds applications in a *Synthetic acetyl-CoA* (SACA) pathway [37] or C2-/C4-obtaining cascades [38].

Guiding proof of concept to upscaling

Synthetic CO₂ fixation and valorization into bulk chemical products through *in vitro* systems is gaining momentum. One major reason is the high potential to realize net negative carbon footprints despite the

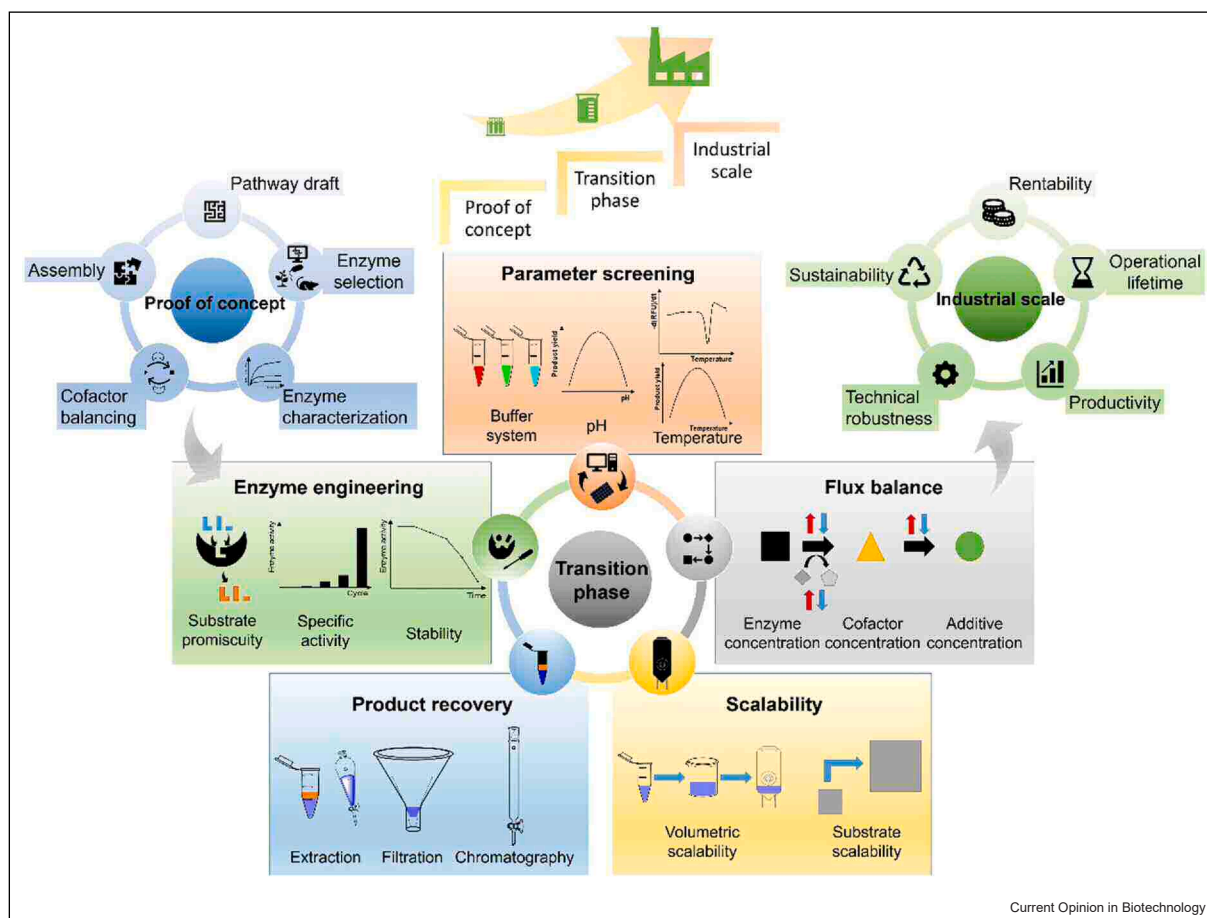
energy-consuming production process [39]. However, in contrast to microorganisms utilizing C1 gases with the expectation of competitive economic performance in future industrialization, cell-free systems in the proof-of-concept phase are facing the challenges of upscaling [40]. For the first transition step, the once-confirmed systems are dissected for perfection and fine-tuning to reduce enzyme load and further optimize productivity (Figure 2). However, examining all variables (enzyme ratios, concentrations of additives, cofactors, etc.) in a multienzymatic system while maintaining the fluxes of the cascade is laborious and time-consuming [17].

To tackle this issue, Pandi and coworkers [41•] developed METIS, a versatile machine learning workflow for optimizing complex cell-free systems. Applying this workflow to the CETCH cycle, an example of a complex cell-free system that includes enzymes, cofactors, and additives, 10^{25} different conditions could be analyzed by performing only 1000 experiments. Furthermore, with

this limited number of experiments, a 10-fold improvement in productivity and a nearly sixfold improvement in efficiency were achieved.

Besides the CO₂ assimilation in enzymatic cascades as an innovative newcomer for green commodity chemical production, the valorization of renewable biomass wastes (annual output of 40 million tons) is building another strategic branch to realize a circular bioeconomy [42]. However, the efficient conversion of pentoses (D-xylose and L-arabinose) is still a big challenge [43]. In contrast to the machine learning approach, Shen et al. [44•] addressed this obstacle by constructing a quantitative mathematical model for the D-xylose-utilizing oxidative Weinberg pathway in an iterative multistep process between model and experiment using a time-resolved NMR analysis. Paschalidis et al. [45] used a related pathway to apply multiobjective optimization to design enzymatic cascade reactors. Their experimentally validated complete kinetic model of the five-enzyme

Figure 2



Key features of the three steps that an *in vitro* enzyme cascade passes through in the process of an industrial implementation: the proof of concept (blue cycle), transition phase (multicolor cycle), and the final industrial scale (green cycle). Highlighted here is the transition phase with key parameters for optimizing cell-free enzymatic cascades to achieve the properties required for the industrial phase.

cascade for converting glucuronic acid to 2-ketoglutarate helps to visualize and address trade-offs between space–time yield, enzyme consumption, and cofactor consumption. In addition to that, open-source platforms such as COPASI offer a user-friendly alternative for simulating the dynamics of multienzymatic cascades [46]. It will be a reasonable option for cascade optimization if an interdisciplinary interface between wet-lab biochemists and bioinformaticians is missing. In any case, kinetics-based mathematical modeling will play a pivotal role in implementing a cost-effective transition phase for process optimization/intensification regarding scale-up and simulating complex industrial plants [30,47].

For couitilization of D-xylose and L-arabinose, Sutiono and coworkers [48•] presented a unique converging conversion approach, that is, stereoconvergent synthesis of one single product from two diastereomers as starting substrates. Exploiting enzyme promiscuity enabled the reduction of the enzyme set used for the multienzymatic cascades, one of the most critical features in reducing process costs. In addition, as a remarkable advantage of cell-free systems, this work demonstrated the plug-and-play strategy, the easy adaptability of the system by replacing a few enzymes to get different products at high yields.

Sherkhanov and coworkers [13•] succeeded in their study to overcome the first technical hurdles for industrially relevant upscaling for producing isobutanol from D-glucose. Sixteen enzymes were stabilized by genome mining and enzyme engineering to improve the operational production lifetime. The ATP rheostat system from their previous work was employed to maintain a high ATP concentration against hydrolysis [49]. To overcome the equilibration and product toxicity issues, phenetol was used as an organic overlay, from which the product was continuously removed *in situ*. In this way, the transition from a 200- μ L analytical scale to a 15-mL bioreactor led to the final titer of 275 g L⁻¹ (95% yield) in 4.5 days, supported by additional supplementation of two less stable enzymes. However, the upscaling to the liter or even larger scale has yet to be seen. This study represents a counterpart of the minimal cascade concept proposed by Guterl et al. some years ago [50], considering the industrial competitiveness of cell-free biofuel production. The complex pyruvate synthetic module was consolidated into the single-cofactor four-enzyme pathway for process cost minimization, employing archaeal glycolysis and engineering of enzyme promiscuity.

2,5-Furandicarboxylic acid (FDCA), the main component of poly(ethylene 2,5-furandicarboxylate), is a highly desired value-added chemical for replacement of fossil-based poly(ethylene terephthalate) (PET)/poly(butylene terephthalate) (PBT) with sustainable origin

[51,52]. Despite the current exclusively chemical process, multistep biotransformation holds significant potential as an energy-friendly alternative for the future [51,53].

Birmingham and coworkers [54••] evolved O₂-dependent galactose oxidase, one of the prominent enzymes used for benzylic primary alcohol oxidation, by screening in a glove box with ~0.2% (v/v) O₂, considering the limited oxygen diffusion in large reactors. In iterative and interactive "coordinated reaction and enzyme engineering" inclusive of extensive screening of organic cosolvents, they finally demonstrated an upscaling of the one-reaction process of 5-hydroxymethylfurfural (HMF) to 2,5-diformylfuran (DFF) (capable of being further converted to FDCA) to a 1.44-L biphasic system in a bioreactor. This resulted in a specific yield of 570 g_{DFF}/g_{purified biocatalyst} with a 92% isolated yield.

Synergy between *in vitro* and *in vivo* for upscaling

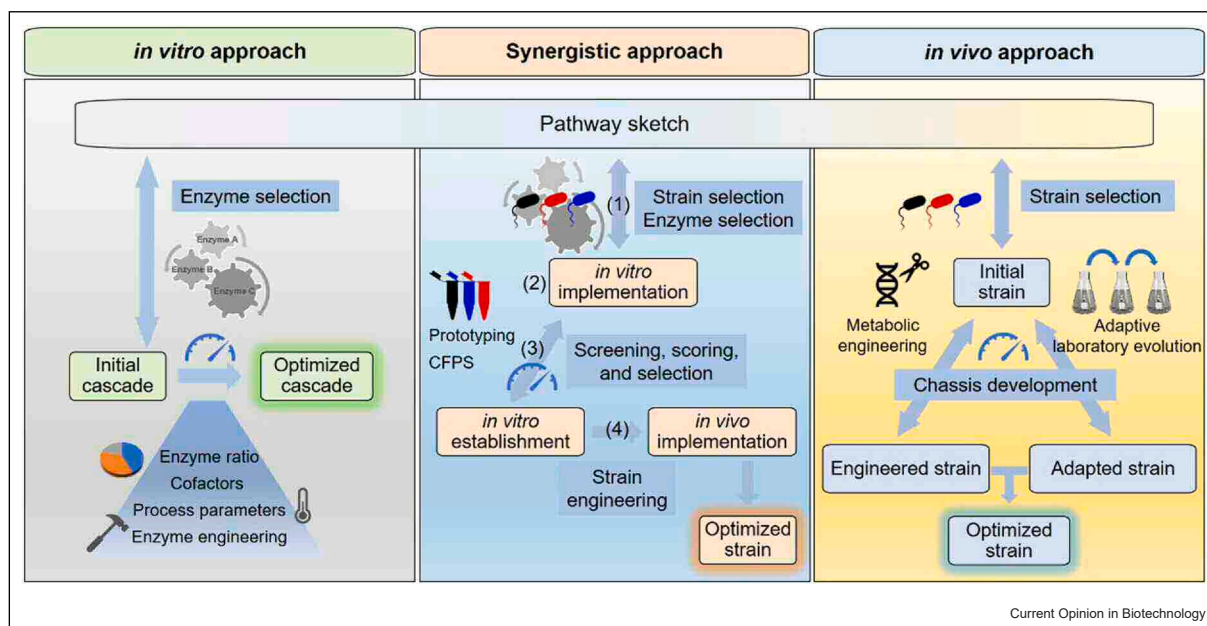
Even though stand-alone complex multienzymatic systems *in vitro* for bulk chemical production are not yet widely used in industry, there are attractive concepts harnessing the strengths of cell-free systems in developing microbial chemical production [55]. For this purpose, Karim and coworkers [56••] demonstrated the so-called iPROBE approach (*in vitro* prototyping and rapid optimization of biosynthetic enzymes) for efficient optimization of *in vivo* biosynthetic pathways for an industrial scale-up (Figure 3).

The iPROBE process can be divided into four steps: (1) the design, where the metabolic pathway and target enzymes are defined, (2) the construction step, where these enzymes are expressed (heterologously in *E. coli* or in systems of cell-free protein synthesis), mixed in lysates, and tested, (3) the testing step, where the results are evaluated using the TREE score, (4) and the application step, where the best combinations are selected and implemented in the strain of choice. Using this approach, the production of approximately 15 g L⁻¹ of 3-hydroxybutyrate in *Clostridium* was achieved, with a close correlation of $r = 79$ between the *in vitro* prototyping and the *in vivo* upscaling approach.

The iPROBE workflow was then further applied by Vögeli and coworkers [57] to implement reverse β -oxidation pathways in bacteria. Here, the focus was on product specificity. After several rounds of optimization with different *E. coli* background lysates (from *E. coli* strains with different knockouts), high selectivity for C6 or C4 acids and alcohols was achieved.

Liew and coworkers [58•] used the workflow to produce acetone and isopropanol from syngas with *Clostridium*.

Figure 3



Comparison of workflows to optimize a cell-free enzymatic cascade (left), *in vivo* biosynthesis (right), and a synergistic approach harnessing the technical feasibility of *in vitro* prototyping for the development of a robust *in vivo* pathway (middle). The synergistic approach applies the technical simplicity of the *in vitro* system for multiplexed analysis/screening of enzymatic setups for optimizing the cascade flow. This *in vitro* prototyping is performed by mixing a lysate from the selected strain and the additional lysates with separately expressed enzymes. Alternatively, the technology of cell-free protein synthesis (CFPS) is used. After selecting the best setups according to the TREE scoring, the pathways are reconstructed in the *in vivo* system. The numbers indicate the critical steps described in the text. The speedometers represent the key optimization steps in the workflows.

To direct the flux to the desired products, iPROBE was used to identify knockouts that reduce the formation of by-products and to increase the titer by selecting enzymes with desired properties. In the end, industrially relevant productivity of $3 \text{ g L}^{-1} \text{ h}^{-1}$ was achieved in a 120-L pilot plant. Together with omics approaches, kinetic modeling, and systems biology analysis, this study demonstrates the power of the interplay between *in vitro* and *in vivo* methods and describes the entire pathway from μL -scale prototyping to 120-L-scale fermentation in an industrial pilot plant.

Outlook

In the post-growth era of consumer society, we have become aware of the looming ecological threats, prompting us to seek solutions for the coexistence of further economic development and the prosperity of our life activity and habitats. Accordingly, we endeavor to shift to sustainable chemical production and the depletion of accumulated industrial waste.

In this process, cell-free enzymatic systems have attracted substantial attention. With their high flexibility and adaptability, but also with high efficiency and minimal by-product formation at the same time, they set a considerable added value to conventional industrial chemical production. Nowadays, many *in vitro* concepts

for producing various chemicals from low-cost and sustainable resources are known. However, the biggest challenge in this field is the transition of these concepts to practical applications. It means additional parameters such as cost minimization while maintaining longevity, high space-time yield, and product titer play a significant role in realizing a vision of stand-alone cell-free enzymatic systems in the industry. Nevertheless, only a few models for multienzymatic cell-free cascades on an industrial scale are established to date and, if known, mainly in the sector of high-value products.

Moving away from the black-and-white decision of *in vivo* or *in vitro* systems, cell-free systems can offer a powerful complement to already-established *in vivo* systems and enhance each benefit in a synergistic way. Concepts such as cell-free prototyping to reduce laborious and costly work will be the near future of cell-free enzymatic systems. In this way, the innovative combination of *in vivo* and *in vitro* systems will boost greener chemical production from renewable resources, and we hope to step forward in a sustainable circular economy with technological development by retaining the earth's viability.

Author contributions

Mariko Teshima: Conceptualization, Visualization, Writing – original draft, Writing – review & editing.

Vivian Pascal Willers: Conceptualization, Visualization, Writing – original draft, Writing – review & editing.
Volker Sieber: Conceptualization, Writing – review & editing. These authors contributed equally: Mariko Teshima, Vivian Pascal Willers.

Conflict of interest statement

The authors declare that they have no known competing financial interests or personal relationships that could have appeared to influence the work reported in this paper.

Data Availability

No data were used for the research described in the article.

Acknowledgements

We thank Bundesministerium für Bildung und Forschung (BMBF), Germany, Förderkennzeichen: 031B0351C and International Graduate School of Science and Engineering (IGSSE) of Technical University of Munich, Germany (13th cohort — 13.08 E-Cas, GSC 81), supported by Deutsche Forschungsgemeinschaft (DFG), for financial support.

References and recommended reading

Papers of particular interest, published within the period of review, have been highlighted as:

- of special interest
- of outstanding interest

1. U.S. Department of Commerce NNOAA, Earth System Research Laboratories, Global Monitoring Laboratory: **Trends in Atmospheric Carbon Dioxide, Global Monthly Mean CO₂**; 2 Oct. 2022.
 2. Our World In Data GCDL: **Cumulative CO₂ Emissions by World Region**; 2 Oct. 2022.
 3. Benítez-Mateos AI, Roura Padrosa D, Paradisi F: **Multistep enzyme cascades as a route towards green and sustainable pharmaceutical syntheses**. *Nat Chem* 2022, **14**:489-499.
 4. Rude MA, Schirmer A: **New microbial fuels: a biotech perspective**. *Curr Opin Microbiol* 2009, **12**:274-281.
 5. Dahman Y, Syed K, Begum S, Roy P, Mohtasebi B: **14-Biofuels: Their characteristics and analysis, Biomass, Biopolymer-Based Materials and Bioenergy**. *Woodhead Publishing* 2019, 277-325.
 6. Atsumi S, Hanai T, Liao JC: **Non-fermentative pathways for synthesis of branched-chain higher alcohols as biofuels**. *Nature* 2008, **451**:86-89.
 7. Bergquist PL, Siddiqui S, Sunna A: **Cell-free biocatalysis for the production of platform chemicals**. *Front Energy Res* 2020, **8**:193.
 8. Pyser JB, Chakrabarty S, Romero EO, Narayan AR: **State-of-the-art biocatalysis**. *ACS Cent Sci* 2021, **7**:1105-1116.
 9. Özgen FF, Runda ME, Schmidt S: **Photo-biocatalytic cascades: combining chemical and enzymatic transformations fueled by light**. *ChemBioChem* 2021, **22**:790-806.
 10. Liang AD, Serrano-Plana J, Peterson RL, Ward TR: **Artificial metalloenzymes based on the biotin-streptavidin technology: enzymatic cascades and directed evolution**. *Acc Chem Res* 2019, **52**:585-595.
 11. Rasor BJ, Vögeli B, Landwehr GM, Bogart JW, Karim AS, Jewett MC: **Toward sustainable, cell-free biomanufacturing**. *Curr Opin Biotechnol* 2021, **69**:136-144.
 12. Liew FE, Nogle R, Abdalla T, Rasor BJ, Canter C, Jensen RO, Wang L, Strutz J, Chirania P, De Tissera S: **Carbon-negative production of acetone and isopropanol by gas fermentation at industrial pilot scale**. *Nat Biotechnol* 2022, **40**:335-344.
 13. Sherkhonov S, Korman TP, Chan S, Faham S, Liu H, Sawaya MR, Hsu WT, Vikram E, Cheng T, Bowie JU: **Isobutanol production freed from biological limits using synthetic biochemistry**. *Nat Commun* 2020, **11**:4292.
- A multienzymatic cascade for isobutanol production with the highest product titer so far. Experiments for upscaling and extension of the operational lifetime by enzyme stabilization and *in situ* product removal.
14. Siedentop R, Claaßen C, Rother D, Lütz S, Rosenthal K: **Getting the most out of enzyme cascades: strategies to optimize *in vitro* multi-enzymatic reactions**. *Catalysts* 2021, **11**:1183.
 15. Mordhorst S, Andexer JN: **Round, round we go—strategies for enzymatic cofactor regeneration**. *Nat Prod Rep* 2020, **37**:1316-1333.
 16. Bowie JU, Sherkhonov S, Korman TP, Valliere MA, Opgenorth PH, Liu H: **Synthetic biochemistry: the bio-inspired cell-free approach to commodity chemical production**. *Trends Biotechnol* 2020, **38**:766-778.
 17. Gmelch TJ, Sperl JM, Sieber V: **Optimization of a reduced enzymatic reaction cascade for the production of L-alanine**. *Sci Rep* 2019, **9**:11754.
 18. Dudley QM, Karim AS, Jewett MC: **Cell-free metabolic engineering: biomanufacturing beyond the cell**. *Biotechnol J* 2015, **10**:69-82.
 19. Al-Shameri A, Petrich MC, Junge Puring K, Apfel UP, Nestl BM, Lauterbach L: **Powering artificial enzymatic cascades with electrical energy**. *Angew Chem Int Ed* 2020, **59**:10929-10933.
 20. Zachos I, Doring M, Tafertshofer G, Simon RC, Sieber V: **Carba nicotinamide adenine dinucleotide phosphate: robust cofactor for redox biocatalysis**. *Angew Chem Int Ed Engl* 2021, **60**:14701-14706.
 21. Zachos I, Genth R, Sutiono S, Marczyński M, Lieleg O, Sieber V: **Hot flows: evolving an archaeal glucose dehydrogenase for ultrastable Carba-NADP* using microfluidics at elevated temperatures**. *ACS Catal* 2022, **12**:1841-1846.
 22. Zachos I, Güner S, Essert A, Lommes P, Sieber V: **Boosting artificial nicotinamide cofactor systems**. *Chem Commun* 2022, **58**:11945-11948.
 23. Black WB, Zhang L, Mak WS, Maxel S, Cui Y, King E, Fong B, Sanchez Martinez A, Siegel JB, Li H: **Engineering a nicotinamide mononucleotide redox cofactor system for biocatalysis**. *Nat Chem Biol* 2020, **16**:87-94.
 24. Kim S, Kwon K, Tae G, Kwon I: **Nano-entrapping multiple oxidoreductases and cofactor for all-in-one nanoreactors**. *ACS Sustain Chem Eng* 2021, **9**:6741-6747.
 25. Hartley CJ, Williams CC, Scoble JA, Churches QI, North A, French NG, Nebl T, Coia G, Warden AC, Simpson G: **Engineered enzymes that retain and regenerate their cofactors enable continuous-flow biocatalysis**. *Nat Catal* 2019, **2**:1006-1015.
 26. Alissandratos A: ***In vitro* multi-enzymatic cascades using recombinant lysates of E. coli: an emerging biocatalysis platform**. *Biophys Rev* 2020, **12**:175-182.
 27. Lim HJ, Kim D-M: **Cell-free synthesis of industrial chemicals and biofuels from carbon feedstocks**. *Curr Opin Biotechnol* 2022, **73**:158-163.
 28. Li Z, Shen S, Li Z: **Towards the conversion of CO₂ into optically pure N-carbamoyl-L-aspartate and orotate by an *in vitro* multi-enzyme cascade**. *Green Chem* 2020, **22**:5798-5805.
 29. Milić M, Byström E, Domínguez de María P, Kara S: **Enzymatic cascade for the synthesis of 2, 5-furandicarboxylic acid in biphasic and microaqueous conditions: 'Media-Agnostic' biocatalysts for biorefineries**. *ChemSusChem* 2022, **15**:e202102704.
 30. Johannsen J, Meyer F, Engelmann C, Liese A, Fieg G, Bubenheim P, Waluga T: **Multi-enzyme cascade reaction in a miniplant two-**

- phase-system: model validation and mathematical optimization.** *AIChE J* 2021, **67**:e17158.
31. Schwander T, Schada von Borzyskowski L, Burgener S, Cortina • NS, Erb TJ: **A synthetic pathway for the fixation of carbon dioxide *in vitro*.** *Science* 2016, **354**:900-904.
A benchmark publication for the synthetic CO₂ fixation.
 32. Scheffen M, Marchal DG, Beneyton T, Schuller SK, Klose M, Diehl • C, Lehmann J, Pfister P, Carrillo M, He H: **A new-to-nature carboxylation module to improve natural and synthetic CO₂ fixation.** *Nat Catal* 2021, **4**:105-115.
A modular cascade with central new-to-nature carbon fixation enzyme.
 33. Aleku GA, Roberts GW, Titchiner GR, Leys D: **Synthetic enzyme-catalyzed CO₂ fixation reactions.** *ChemSusChem* 2021, **14**:1781-1804.
 34. Xiao L, Liu G, Gong F, Zhu H, Zhang Y, Cai Z, Li Y: **A minimized synthetic carbon fixation cycle.** *ACS Catal* 2021, **12**:799-808.
 35. Cai T, Sun H, Qiao J, Zhu L, Zhang F, Zhang J, Tang Z, Wei X, Yang • J, Yuan Q: **Cell-free chemoenzymatic starch synthesis from carbon dioxide.** *Science* 2021, **373**:1523-1527.
The *in vitro* starch synthesis pathway using green methanol as substrate. The computational assembly of the minimized cascade supported by experimental validations.
 36. Güner S, Wegat V, Pick A, Sieber V: **Design of a synthetic enzyme cascade for the *in vitro* fixation of a C1 carbon source to a functional C4 sugar.** *Green Chem* 2021, **23**:6583-6590.
 37. Lu X, Liu Y, Yang Y, Wang S, Wang Q, Wang X, Yan Z, Cheng J, Liu C, Yang X: **Constructing a synthetic pathway for acetyl-coenzyme A from one-carbon through enzyme design.** *Nat Commun* 2019, **10**:1378.
 38. Zhou J, Tian X, Yang Q, Zhang Z, Chen C, Cui Z, Ji Y, Schwaneberg U, Chen B, Tan T: **Three multi-enzyme cascade pathways for conversion of C1 to C2/C4 compounds.** *Chem Catal* 2022, **2**:2675-2690.
 39. Scown CD, Keasling JD: **Sustainable manufacturing with synthetic biology.** *Nat Biotechnol* 2022, **40**:304-307.
 40. Liang B, Fu R, Ma Y, Hu L, Fei Q, Xing X-H: **Turning C1-gases to isobutanol towards great environmental and economic sustainability via innovative biological routes: two birds with one stone.** *Biotechnol Biofuels Bioprod* 2022, **15**:107.
 41. Pandi A, Diehl C, Yazdizadeh Kharrazi A, Scholz SA, Bobkova E, • Faure L, Nattermann M, Adam D, Chapin N, Foroughijabbari Y: **A versatile active learning workflow for optimization of genetic and metabolic networks.** *Nat Commun* 2022, **13**:3876.
A machine learning-guided pathway optimization with application on CETCH cycle.
 42. Sanderson K: **Lignocellulose: a chewy problem.** *Nature* 2011, **474**:S12-S14.
 43. Kuschmierz L, Shen L, Bräsen C, Snoep J, Siebers B: **Workflows for optimization of enzyme cascades and whole cell catalysis based on enzyme kinetic characterization and pathway modelling.** *Curr Opin Biotechnol* 2022, **74**:55-60.
 44. Shen L, Kohlhaas M, Enoki J, Meier R, Schönenberger B, • Wohlgemuth R, Kourist R, Niemeyer F, van Niekerk D, Bräsen C: **A combined experimental and modelling approach for the Weimberg pathway optimisation.** *Nat Commun* 2020, **11**:1098.
The construction of a computational model for precise simulation and prediction of the Weimberg pathway by a combined approach of mathematical modeling and experimental validations.
 45. Paschalidis L, Beer B, Sutiono S, Sieber V, Burger J: **Design of enzymatic cascade reactors through multi-objective dynamic optimization.** *Biochem Eng J* 2022, **181**:108384.
 46. Bergmann FT, Hoops S, Klahn B, Kummer U, Mendes P, Pahle J, Sahle S: **COPASI and its applications in biotechnology.** *J Biotechnol* 2017, **261**:215-220.
 47. Česnik M, Sudar M, Hernández K, Charnock S, Vasić-Rački Đ, Clapés P, Findrik Blažević Z: **Cascade enzymatic synthesis of l-homoserine – mathematical modelling as a tool for process optimisation and design.** *React Chem Eng* 2020, **5**:747-759.
 48. Sutiono S, Pick A, Sieber V: **Converging conversion—using promiscuous biocatalysts for the cell-free synthesis of chemicals from heterogeneous biomass.** *Green Chem* 2021, **23**:3656-3663.
The concept of exploiting the enzyme promiscuity for converting mixed substrates to one single product.
 49. Opgenorth PH, Korman TP, Iancu L, Bowie JU: **A molecular rheostat maintains ATP levels to drive a synthetic biochemistry system.** *Nat Chem Biol* 2017, **13**:938-942.
 50. Guterl JK, Garbe D, Carsten J, Steffler F, Sommer B, Reisse S, Philipp A, Haack M, Ruhmann B, Koltermann A, et al.: **Cell-free metabolic engineering: production of chemicals by minimized reaction cascades.** *ChemSusChem* 2012, **5**:2165-2172.
 51. Totaro G, Sisti L, Marchese P, Colonna M, Romano A, Gioia C, Vannini M, Celli A: **Current advances in the sustainable conversion of 5-hydroxymethylfurfural into 2, 5-furandicarboxylic acid.** *ChemSusChem* 2022, **15**:e202200501.
 52. Energy Efficiency and Renewable Energy USDoe: **Top Value Added Chemicals from Biomass Volume I—Results of Screening for Potential Candidates from Sugars and Synthesis Gas**; 2004.
 53. Lalanne L, Nyanhongo GS, Guebitz GM, Pellis A: **Biotechnological production and high potential of furan-based renewable monomers and polymers.** *Biotechnol Adv* 2021, **48**:107707.
 54. Birmingham WR, Toftgaard Pedersen A, Dias Gomes M, Boje • Madsen M, Breuer M, Woodley JM, Turner NJ: **Toward scalable biocatalytic conversion of 5-hydroxymethylfurfural by galactose oxidase using coordinated reaction and enzyme engineering.** *Nat Commun* 2021, **12**:4946.
Interactive enzyme and reaction engineering to optimize galactose oxidase activity at low oxygen concentration considering the future large-scale production process.
 55. Zhang J, Yang X, Dong R, Gao L, Li J, Li X, Huang S, Zhang C, Chang H: **Cascade biocatalysis for regio- and stereoselective aminohydroxylation of styrenyl olefins to enantiopure arylglycinols.** *ACS Sustain Chem Eng* 2020, **8**:18277-18285.
 56. Karim AS, Dudley QM, Juminaga A, Yuan Y, Crowe SA, Heggstad • JT, Garg S, Abdalla T, Grubbe WS, Rasor BJ: ***In vitro* prototyping and rapid optimization of biosynthetic enzymes for cell design.** *Nat Chem Biol* 2020, **16**:912-919.
An innovative synergistic concept for prototyping *in vivo* pathways exploiting the simplicity and practicability of *in vitro* systems.
 57. Vögeli B, Schulz L, Garg S, Tarasava K, Clomburg JM, Lee SH, Gonnot A, Mouly EH, Kimmel BR, Tran L: **Cell-free prototyping enables implementation of optimized reverse β-oxidation pathways in heterotrophic and autotrophic bacteria.** *Nat Commun* 2022, **13**:3058.
 58. Liew FE, Nogle R, Abdalla T, Rasor BJ, Canter C, Jensen RO, Wang • L, Strutz J, Chirania P, De Tissera S: **Carbon-negative production of acetone and isopropanol by gas fermentation at industrial pilot scale.** *Nat Biotechnol* 2022, **40**:335-344.
Showcasing an application of *in vitro* prototyping for *in vivo* microbial production of acetone and isopropanol by gas fermentation in an industrial pilot plant-scale.

Integrating Carbohydrate and C1 Utilization for Chemicals Production

Vivian Pascal Willers, Barbara Beer, Volker Sieber

ChemSusChem

Volume 16, 2023, e202202122

DOI: <https://doi.org/10.1002/cssc.202202122>

This article is licensed under a Creative Commons Attribution 4.0 International License
(CC BY 4.0)

Integrating Carbohydrate and C1 Utilization for Chemicals Production

Vivian Pascal Willers,^[a] Barbara Beer,^[a, b] and Volker Sieber^{*[a, c, d]}

In the face of increasing mobility and energy demand, as well as the mitigation of climate change, the development of sustainable and environmentally friendly alternatives to fossil fuels will be one of the most important tasks facing humankind in the coming years. In order to initiate the transition from a petroleum-based economy to a new, greener future, biofuels and synthetic fuels have great potential as they can be adapted to already common processes. Thereby, especially synthetic fuels from CO₂ and renewable energies are seen as the next big step for a sustainable and ecological life. In our study, we directly address the sustainable production of the most common biofuel, ethanol, and the highly interesting next-

generation biofuel, isobutanol, from methanol and xylose, which are directly derivable from CO₂ and lignocellulosic waste streams, respectively, such as integrating synthetic fuel and biofuel production. After enzyme and reaction optimization, we succeeded in producing either 3 g L⁻¹ ethanol or 2 g L⁻¹ isobutanol from 7.5 g L⁻¹ xylose and 1.6 g L⁻¹ methanol. In our cell-free enzyme system, C1-compounds are efficiently combined and fixed by the key enzyme transketolase and converted to the intermediate pyruvate. This opens the way for a hybrid production of biofuels, platform chemicals and fine chemicals from CO₂ and lignocellulosic waste streams as alternative to conventional routes depending solely either on CO₂ or sugars.

Introduction

In the face of climate change, depletion of fossil resources, and increasing energy demand, alternative, sustainable energy sources are in demand to replace traditional energy production methods while reducing waste and greenhouse gases such as carbon dioxide (CO₂). One major step will be the replacement of fossil fuels by green electricity, hydrogen or renewable and sustainable biofuels. Here biocatalysis comes into play, which is considered as a green and sustainable technology.^[1] Traditional, first-generation biofuel production relies on production from edible crops,^[2] but due to food versus fuel debates, this approach needs alternative solutions.^[3] Lignocellulosic biomass has high potential as feedstock for the production of biofuels and platform chemicals. It is cheap, economically friendly and

ethically acceptable because it is not competing with the food supply.^[4] Moreover, in the year 2018 lignocellulosic biomass has been the most abundantly available bio resource with a global yield of up to 1.3 billion tons per year.^[5]

However, efficient utilization of residual biomass with an advantageous solution for biofuel production includes the perspective of efficiently converting most of the sugars it contains to the same product.^[6] In addition to glucose, xylose with a share of up to 30 to 40% of carbohydrate content in lignocellulose must also be taken into account and used for the production of biofuels.^[7] One major drawback in biofuel production using xylose as substrate is that it's not readily utilized by microorganisms.^[8] For the two most studied microorganisms *Saccharomyces cerevisiae* and *Escherichia coli*, growth on xylose is limited^[9] and biofuel production based on xylose is only possible by non-conventional or engineered strains. However, titers are not comparable to glucose derived titers. In addition, the production comes with low efficiency and high production cost.^[8a] Besides, one major drawback which comes up for the utilization of glucose and xylose using microorganisms is catabolite repression, i.e., glucose actively represses the expression of genes for xylose transporters and xylose conversion making a co-fermentation of glucose and xylose difficult.^[10]

Ethanol as one of the most common and widely used biofuels by now,^[11] is naturally produced by many organisms like yeast or bacteria, by conversion of the central metabolite pyruvate.^[12] Bioethanol production is mostly based on sugarcane production by fermentation of glucose with established hosts such as *Saccharomyces cerevisiae*, which use their natural utilization pathways for ethanol production.^[13] In addition, potential waste streams such as crude glycerol expand the possibilities for ethanol production.^[14] To produce ethanol from xylose, xylose is first metabolized via xylose isomerase, xylose

[a] V. P. Willers, Dr. B. Beer, Prof. Dr. V. Sieber
Chair of Chemistry of Biogenic Resources
Technical University of Munich
Campus Straubing, 94315 Straubing (Germany)
E-mail: Sieber@tum.de

[b] Dr. B. Beer
Current address:
CASCAT GmbH
94315 Straubing (Germany)

[c] Prof. Dr. V. Sieber
Technical University of Munich
94315 Straubing (Germany)

[d] Prof. Dr. V. Sieber
School of Chemistry and Molecular Biosciences
The University of Queensland
St. Lucia 4072 (Australia)

Supporting information for this article is available on the WWW under <https://doi.org/10.1002/cssc.202202122>

© 2022 The Authors. ChemSusChem published by Wiley-VCH GmbH. This is an open access article under the terms of the Creative Commons Attribution License, which permits use, distribution and reproduction in any medium, provided the original work is properly cited.

reductase, xylose dehydrogenase or the Dahms pathway, which leads to the pentose phosphate pathway, or directly to pyruvate.^[15] In this process, a maximum of 1.66 molecules of ethanol are formed from one molecule of xylose.^[16] Whereas the production of ethanol from xylose is implemented in different microorganisms like *Zymomonas mobilis* or *Saccharomyces cerevisiae* with titers of 43.1 g L⁻¹ (0.45 g g⁻¹ xylose) and 16.4 g L⁻¹ (0.41 g g⁻¹ xylose) respectively,^[8a] isobutanol production from xylose is rare.

Isobutanol is considered as next-generation biofuel, as well as commodity chemical and has great advantages considering energy density and physicochemical properties compared to ethanol.^[17] Isobutanol can also be produced from pyruvate in five steps via acetolactate synthase (AlsS), ketol-acid reductoisomerase (IlvC), dihydroxy-acid dehydratase (IlvD), alpha-keto-acid decarboxylase (KDC) and alcohol dehydrogenase (ADH).^[18] If only xylose is used for the production of isobutanol, one molecule of xylose yields at maximum 0.83 molecules of isobutanol.^[19]

Glucose, the most abundant sugar in lignocellulose, is efficiently transformed to isobutanol with yields up to 22 g L⁻¹ (86% theoretical yield between 40 h and 112 h) in a time range of 112 h, using *E. coli*^[20] or with different cell free system with yields up to 275 g L⁻¹.^[18,21] In contrast, the conversion of xylose suffers from low product titers, with 92.9 mg L⁻¹.^[22] The highest titer of isobutanol so far was reached by Zhang et al. using xylose and *S. cerevisiae* strain Yzy197 in a fed batch approach to produce 3.1 g L⁻¹ in 192 h (maximum daily theoretical yield of 9.4%) in a mixed approach for the production of branched-chain higher alcohols.^[23] This demonstrates that there is room for improvement and need for it as the long fermentation time and low efficiency prohibitive. Accordingly, in order to produce biofuels sustainably and economically from lignocellulosic biomass and as basic requirement to replace chemical synthesis for isobutanol involving high temperatures and pressures,^[24] rapid and efficient utilization of xylose is necessary.^[15]

Whereas xylose assimilation pathways mostly rely on cleavage of xylose to a C3 and a C2 precursor molecule, which is either rearranged for example in the pentose phosphate pathway or directly used for the production of various chemicals like ethylene glycol, acetoin or glycolic acid.^[25] C1 assimilation pathways can link the cleavage of a sugar to the fixation of a CO₂ based C1-compound.^[26] One example of this pathway is the naturally occurring xylulose monophosphate pathway found in methylotrophic yeast.^[27] Here xylulose 5-phosphate is cleaved together with formaldehyde into glyceraldehyde 3-phosphate and dihydroxyacetone by dihydroxyacetone synthase. These C3 precursors are then rearranged and every cycle of fixation produces 0.33 molecules of pyruvate from one C1-compound.^[28] By combining the pyruvate generated from xylose and CO₂, one molecule of isobutanol or two molecules of ethanol can be produced from one molecule of xylose and CO₂. The strategy of using methanol as the C1-compound and a second carbon compound as xylose or gluconate was shown recently.^[29] Here for example, methanol-auxotrophic *E. coli* strains were developed as proof-of-concept, in which ethanol or a mixture of ethanol and 1-butanol were

obtained from the redesigned ribulose-5-phosphate pathway. However, only 43% of the produced ethanol and 71% of 1-butanol contained carbon derived from methanol.^[29a]

In addition to whole-cell systems, *in vitro* systems have recently become increasingly important because they are becoming more complex and offer the possibility of producing various compounds from cheap substrates with high efficiency. Furthermore, these synthetic cascades based on purified enzymes have many advantages. They have high controllability, adaptability, manipulatable reaction conditions, easy product recovery, and higher tolerance to toxic substances.^[30] Moreover, the suppression of carbon catabolism mentioned above does not occur, and the separation of products such as isobutanol can be easily performed by using approaches with a two-phase system.^[21]

The immersive potential to integrate C1-compounds in enzymatic cascades was shown by Cai et al., who set up a multi-enzymatic cascade for the production of starch from CO₂-based methanol.^[31] Isobutanol production based on CO₂ was shown *in vivo* as proof of concept by Atsumi et al. with a final titer of 0.45 g L⁻¹ by using cyanobacteria.^[32] The highest titer of isobutanol from CO₂ was reached by Miao et al. producing 0.9 g L⁻¹ in a time span of 40 days.^[33] However, no *in vitro* pathway using CO₂ for the production of isobutanol was shown before. Guo et al. proposed a pathway from CO₂ to isobutyraldehyde by combining the carbon-carbon bond forming modules from Cai et al. with a glycolysis module to form pyruvate and from pyruvate a third module to isobutyraldehyde, but lacked experimental proof.^[34] In this way, isobutanol could be produced exclusively from C1-chemicals, but the key enzyme formolase, which produces dihydroxyacetone from formaldehyde, lacks high activity and specificity for formaldehyde. Large amounts of expensive protein would be required to produce isobutyraldehyde or isobutanol.

Inspired by the intriguing possibilities of using green C1-chemicals, that are derived directly from CO₂ using green energy/hydrogen, as building blocks for the production of sustainable carbon compounds, coupled with the challenging use of the C5 sugar xylose from lignocellulosic biomass waste, we developed an artificial enzymatic xylose-based C1 fixation and utilization pathway (XFUP). This pathway allows the efficient use of CO₂-derived C1-compounds using xylose to produce ethanol and isobutanol. With the need for new pathways to produce biofuels and commodity chemicals with lower environmental burden, the optimized XFUP enables highly efficient production of isobutanol in a minimum time span at low temperatures, and with non-toxic solvents. In a proof of concept 8.5 mM isobutanol could be obtained from 10 mM xylose and formaldehyde corresponding to 85% theoretical yield in 12 h. Furthermore, adaptation of the system to methanol leads to a final titer of either 3 g L⁻¹ ethanol or 2 g L⁻¹ isobutanol in 24 h.

Results and Discussion

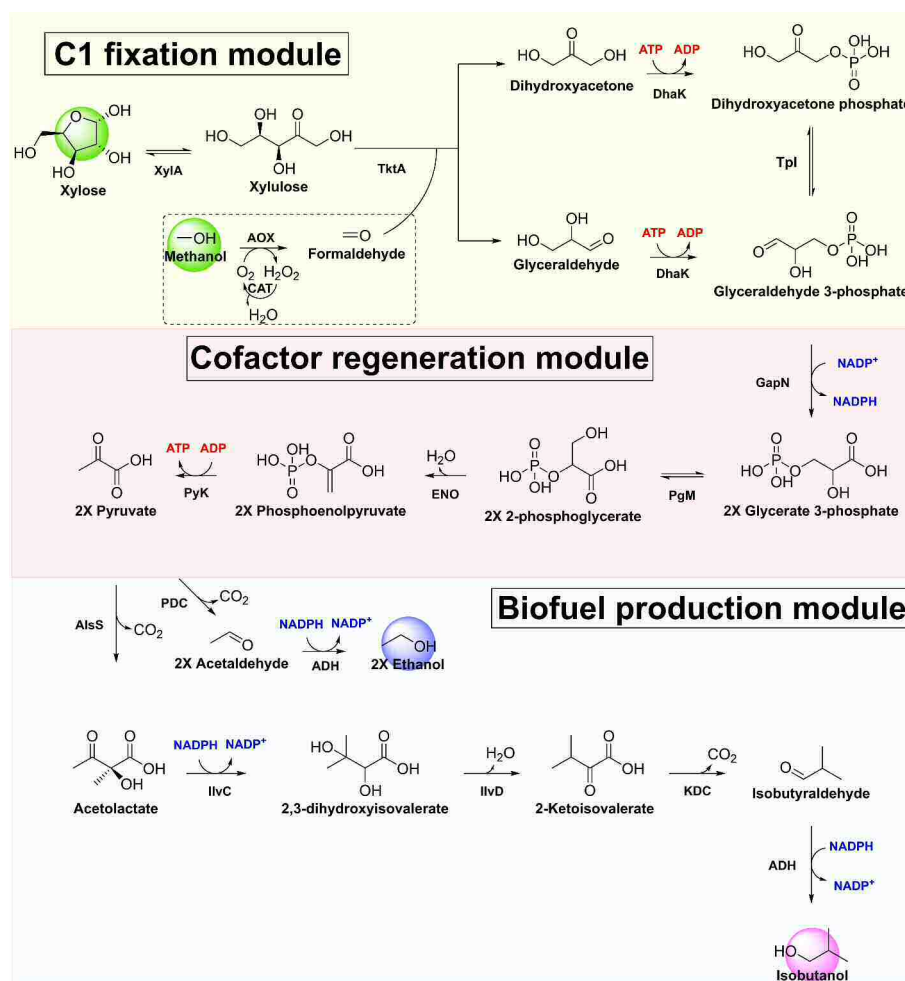
Implementation of a sugar-guided CO₂ fixation pathway to biofuels

For the production of ethanol and isobutanol from C1-precursors with xylose, we built up a modular cascade, consisting of a C1 fixation module, a cofactor regeneration module as well as a biofuel production module, which is adaptable, to produce either ethanol or isobutanol (Scheme 1).

The C1 fixation module is based on the xylulose monophosphate pathway consuming xylose and formaldehyde with the key enzyme transketolase (TktA). Here, xylose is isomerized by xylose isomerase (XylA) and directly utilized by transketolase with the fixation of formaldehyde to produce glyceraldehyde and dihydroxyacetone. Dihydroxyacetone and glyceraldehyde are then phosphorylated by a dual active dihydroxyacetone kinase (DhaK) by producing two molecules of ADP. Naturally, xylulose is phosphorylated first by xylulokinase and its product xylulose-5-phosphate is utilized by dihydroxyacetone synthase to produce dihydroxyacetone and glyceraldehyde-3-phosphate

by assimilation of formaldehyde. However, the ability of transketolase to utilize xylulose directly together with the dual active dihydroxyacetone kinase circumvents a possible negative interaction between xylulokinase and dihydroxyacetone kinase due to an imbalanced ATP/ADP concentration and reduces the number of enzymes of the module.

The sugar guided fixation of CO₂ via C1 metabolites provides an efficient alternative to the newly developed formolase based fixation pathway,^[35] where three formaldehyde molecules can build up one molecule of pyruvate. The key enzyme in this pathway, formolase, represents the bridge between C1 metabolism and C3 precursor molecules present in glycolysis by coupling three formaldehyde molecules to one dihydroxyacetone. Besides the ingenuity of this reaction, it is also the biggest bottleneck of the pathway, due to the unfavorable kinetic properties of the until now best formolase variant fls-M3 to formaldehyde with a k_{cat} of 0.2 s⁻¹ and a K_m of 23.6 mM.^[31] To avoid the accumulation of high toxic concentrations of formaldehyde, which inactivate enzymes and inhibit the growth of microorganisms, high concentrations of formolase are required, which is not economically feasible in up-



Scheme 1. Schematic representation of modular cascade with ATP (blue) and NADP⁺ (red) regeneration system including enzymes, substrates, intermediates and final products. Yellow highlighted alternative methanol entry point to the cascade.

scaling approaches. In contrast, the class of transketolases and dihydroxyacetone synthases that occur naturally in sugar-directed formaldehyde fixation pathways could provide an alternative due to their advantageous kinetic properties (e.g., K_m of DhaS of *Candida Boindii* on formaldehyde 1.0 mM and v_{max} of 4.9 $U\ mg^{-1}$ in a reaction with xylulose 5-phosphate).^[36]

The cofactor regeneration module is based on the lower glycolysis and provides pyruvate as precursor and platform intermediate for the production of ethanol and isobutanol as well as the regeneration of NADPH and ATP. Key enzymes here are pyruvate kinase (PyK), which regenerates ATP by producing pyruvate and a non-phosphorylating NADP⁺ dependent glyceraldehyde 3-phosphate dehydrogenase (GapN) to balance ATP consumption as well as NADPH recycling.^[37]

Finally, the cascade finishes with a biofuel production module that either is based on the natural valine pathway for the production of isobutanol by pyruvate or on the natural ethanol pathway for the production of ethanol from pyruvate. For ethanol production pyruvate is decarboxylated by pyruvate decarboxylase (PDC) and emerging acetaldehyde is further reduced by an NADPH dependent ADH. For the production of isobutanol AlsS combines two pyruvates to acetolactate. Acetolactate is further processed via the natural valine pathway enzymes to 2-ketoisovalerate by producing one molecule of NADP⁺. 2-Ketoisovalerate is then decarboxylated by KDC and reduced by the NADPH dependent ADH from the ethanol pathway. To drive the reaction, both, the cofactor regeneration module as well as the biofuel production module start with a nearly irreversible reaction (aldehyde dehydrogenase and keto-acid decarboxylase, resp.).

Characterization of key enzymes of XFUP

Transketolase

With the xylose guided fixation and valorization of C1-compounds as the major advantage of the cascade, we first characterized three transketolases (TktA) from the microorganisms *Escherichia coli* (ecTktA), *Variovorax paradoxus* (vpTktA) and *Meiothermus ruber* (mrTktA) for their activity on formaldehyde and xylulose (Figure S2). By comparing the kinetic properties of these with a fixed formaldehyde concentration of 5 mM (Table 1) a range of values of catalytic efficiency from 0.3 to 0.6 [$s^{-1}\ mM^{-1}$] was observed. The highest activity was observed for ecTktA with 8 $U\ mg^{-1}$. However, affinity of ecTktA for xylulose was low (K_m : 15.9 mM). In contrast to that, activity of mrTktA was the lowest with 1.3 $U\ mg^{-1}$, nevertheless it had the highest

Table 1. Kinetic parameters of different transketolases with xylulose (0–100 mM) at a fixed formaldehyde concentration of 5 mM ($n = 3$).

Transketolase	K_m [mM]	v_{max} [$U\ mg^{-1}$]	k_{cat} [s^{-1}]	Efficiency [$s^{-1}\ mM^{-1}$]
ecTktA	15.9 ± 0.3	8.2 ± 0.1	10.0 ± 0.2	0.6
vpTktA	9.2 ± 0.3	3.1 ± 0.1	4.0 ± 0.1	0.4
mrTktA	6.4 ± 0.1	1.3 ± 0.0	1.6 ± 0.0	0.3

affinity for xylulose with 6.4 mM. For the best transketolase ecTktA kinetics were also measured with a fixed concentration of 50 mM xylulose. Here a high affinity was observed with a K_m of 2.1 mM to formaldehyde (Figure S2). However, when different concentrations of formaldehyde were applied on the other transketolases, inhibition occurred at formaldehyde concentrations above 10 mM whereby the strongest inhibition was observed for mrTktA with a 50% reduced activity with 20 mM formaldehyde (Figure S3). When transketolase and formolase are compared, it is noticeable that the catalytic efficiency of all tested transketolases in the presence of 5 mM formaldehyde is at least one order of magnitude higher, and in the case of ecTktA more than 1.5 orders of magnitude higher than the catalytic efficiency of the formolase-formose reaction. Due to its low catalytic efficiency, future applications of formolase with high substrate loading are not yet possible. Transketolases, with their high activity even at low formaldehyde concentrations, could be an interesting alternative for the use and utilization of CO₂-derived formaldehyde. In conjunction, it could serve as a better starting point for an engineering campaign to become industrially attractive.

Dihydroxyacetone kinase

Because the reaction of transketolase with xylulose and formaldehyde yields glyceraldehyde and dihydroxyacetone, phosphorylation of both intermediates is essential to connect the artificial xylulose monophosphate pathway with the lower glycolysis (Figure S4 and Table S2). Dihydroxyacetone kinase from *Kozakia baliensis* (kbDhaK) has a very high affinity for dihydroxyacetone (K_m : 86 ± 30 μM), making it the perfect target for phosphorylation of dihydroxyacetone in the cascade. Surprisingly, we observed activity on glyceraldehyde as substrate in a similar range, with a lower affinity than dihydroxyacetone (K_m : 364.9 ± 32.0 μM). Nevertheless, the affinity is in the μM range and with this dual activity of kbDhaK it is possible to ensure a rapid transfer from the C1 fixation module to lower glycolysis.

Alcohol dehydrogenase

In addition to the unnatural reaction of ecTktA and kbDhaK, the promiscuity of ADH plays a key role in the composition of the cascade. Therefore, a major goal in the selection of alcohol-producing ADH is to minimize its ability to convert formaldehyde in the cascade. As a consequence, we screened three ADHs of *Escherichia coli*^[38] on isobutyraldehyde and formaldehyde conversion (Figure S5 and Table S3). ADH ecYahK commonly used in isobutanol production^[37,39] due to its high affinity (K_m of 0.2 ± 0.0 mM) and moderate activity of 2.2 ± 0.3 $U\ mg^{-1}$ is also able to reduce formaldehyde to methanol with a K_m of 6.1 ± 1.4 mM to formaldehyde and an activity of 1.9 ± 0.2 $U\ mg^{-1}$ in a similar range as for isobutyraldehyde. ADH ecYqhD has a high affinity for isobutyraldehyde (K_m : 2.3 ± 0.3 mM) but a very low affinity for formaldehyde (K_m : 53.4 ±

8.6 mM). However, the activity on both substrates is similarly low with $0.2 \pm 0.0 \text{ U mg}^{-1}$. ADH ecYjgB has a very low affinity for isobutyraldehyde (K_m : $> 100 \text{ mM}$) and formaldehyde (K_m : $> 100 \text{ mM}$). Because of that ecYjgB was not considered further for application in the cascade.

By comparing ecYqhD and ecYahK, ecYahK seems promising as its catalytic efficiency for isobutyraldehyde is more than 50 times higher than for formaldehyde. In contrast to that ecYqhD catalytic efficiency for isobutyraldehyde is only 26 times as high as for formaldehyde (Table S3). However, when we investigated the activity of ADHs on glyceraldehyde, which is also an intermediate in the cascade, ecYahK exhibited 24-fold higher activity than ecYqhD (Figure S6). Due to this site activity and the fact that the formaldehyde concentration in the cascade is kept low, the low activity of ecYqhD on formaldehyde and the low activity on glyceraldehyde were decisive to use ecYqhD as ADH for the cascade. Nevertheless, the low activity of ecYqhD with isobutyraldehyde could cause a bottleneck in the cascade and affect the overall flux, since ADH is part of the NADP^+ /NADPH regeneration system. Therefore, ecYqhD could be a target for a future engineering approach to strengthen the selectivity and activity of the enzyme.

XFUP assembly and first optimization

Defining the overall cascade set up

Because the cascade assembles 13 enzymes, a quick but efficient thermofluor based stability assay was set up. With this assay the effect of different buffer systems in a pH range of 7.0 to 8.0 on the melting temperature of the cascade enzymes was analyzed (Figure 1a). We speculated that a reduced thermal stability shows a negative influence of the buffer on XFUP and contrary a raised thermal stability a beneficial influence on XFUP.

The highest difference in melting temperature caused by the buffer system showed the GapN of *Thermococcus kodakar-*

ensis (tkGapN) with a decrease in melting temperature of around 10°C from $> 99^\circ\text{C}$ in tris(hydroxymethyl)aminomethan (TRIS) buffer and 4-(2-hydroxyethyl)-1-piperazineethanesulfonic acid (HEPES) buffer to 90°C in potassium phosphate (KPi) buffer. Another example for a decrease in melting temperature due to the buffer system is ecYqhD. Similar to tkGapN, ecYqhD melting temperature decreases from 50°C in HEPES and TRIS buffer to 42°C in KPi buffer. In contrast, the melting temperature of triosephosphate isomerase of *Geobacillus stearothermophilus* (gsTpi) increases from 74°C in HEPES and TRIS buffer to 78°C in KPi buffer. By comparing HEPES and TRIS buffer we detected smaller changes in melting temperature. While dihydroxy-acid dehydratase of *Schlegelella thermodepolymerans* (stIIVD) has a melting temperature of 70°C in HEPES pH 8.0, this melting temperature drops to 66°C in TRIS pH 8.0. Contrary, a thermostable variant of *Lactococcus lactis* KDC (lKDC_7 M.D),^[40] has a melting temperature of 75°C in HEPES pH 7.0 but a melting temperature of 76°C in TRIS pH 7.0.

The pH of the buffer also changes the melting temperature of the different enzymes. While *Bacillus subtilis* AlsS (bsAlsS) and lKDC_7 M.D show a melting temperature of 62°C and 75°C in HEPES at pH 7.0, respectively, those two enzymes have a decreased melting temperature of 60°C and 69°C in HEPES, at pH 8.0. These findings are in accordance with the analysis of the pH range for lKDC of Wei et al., which reported an optimal pH of 6.0 to 7.0.^[41] Also a decrease in melting temperature of bsAlsS at high pH is in accordance with the pH profile of bsAlsS recorded by Sommer et al., which show that bsAlsS has a pH optimum at pH 6.0.^[42] Vice versa, xylose isomerase of *Pseudomonas fluorescens* (pfXylA) and *Geobacillus stearothermophilus* ketol-acid reductoisomerase (gsIIVC) melting temperatures increase from 63°C and 85°C in HEPES pH 7.0 to 68°C and 89°C in HEPES pH 8.0, respectively.

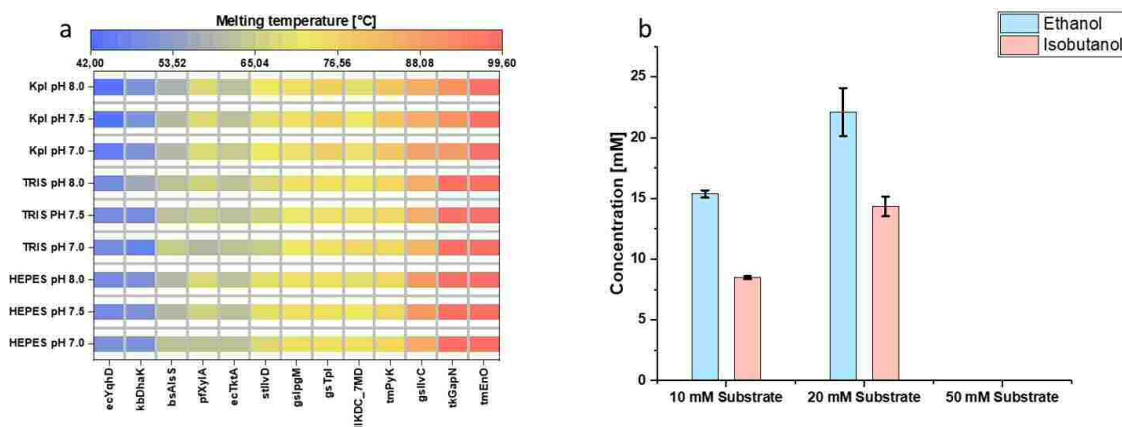


Figure 1. Cascade optimization and initial biofuel production. (a) Thermofluor screening with melting temperature of isobutanol cascade enzymes in three different buffer systems with pH 7.5. (b) Resulting isobutanol and ethanol concentrations after buffer optimization in TRIS pH 7.5 after 12 h of incubation for isobutanol and 16 h incubation for ethanol ($n=3$).

Cascade assembly and biofuel production

Summarizing the thermofluor results, a more acidic pH of 7.0 and a more basic pH of 8.0 lead to stronger changes in the melting temperature of the enzymes to higher but also to lower values than a neutral pH of 7.5. To not imbalance the cascade by providing a pH which might aid one enzyme but harms others, we chose a pH of 7.5 for initial experiments. By analyzing the buffer systems at pH 7.5 we could also see strong differences between the different enzymes. We speculated that HEPES buffer might be the most constant one because all enzymes showed an intermediate melting temperature. However, to verify how changes in thermal stability observed by thermofluor analysis due to the buffer system can be adapted to the performance of the cascade, we conducted three cascades with different buffer systems (HEPES, TRIS, KPi) at pH 7.5 and 37 °C for the production of isobutanol with 10 mM xylose and formaldehyde as starting substrates (Figure S7).

To ensure rapid conversion of formaldehyde, we chose high concentrations of enzymes from the first module resulting in a similar unit amount of 150 mU (Table S4 and Table S5), measured with low substrate concentrations (Table S2). To further drive the transketolase reaction and provide rapid ATP regeneration, enzyme units from module two were increased by more than three times the units of transketolase. The final enzyme units of module three were similar to those of module one, while KDC and ADH had half the units of module one. Here a lower amount of units were chosen due to a possible site activity of ADH on formaldehyde and glyceraldehyde. As control, we conducted the cascade without transketolase.

By applying these conditions, the cascade with potassium phosphate as buffer system shows the lowest performance. After 12 h, 5.0 ± 0.2 mM isobutanol was formed corresponding to a theoretical yield of 50%. Similarly, in the system with HEPES buffer. Here, 5.6 ± 0.5 mM isobutanol corresponding to 56% theoretical yield was produced in 12 h. The best performance was obtained using a system with TRIS buffer. After 12 h, 8.5 ± 0.1 mM isobutanol (Figure 1b) was built up corresponding to 85% theoretical yield. No isobutanol was built without the addition of transketolase.

To investigate the effect of the toxic formaldehyde together with the buffer system, we doubled the xylose and formaldehyde concentrations to 20 mM (Figure S7). This time the buffer effect increased, with the system with TRIS producing 14.3 ± 0.8 mM isobutanol after 12 h (Figure 1b). The system buffered with potassium phosphate produced only 5.5 ± 0.5 mM isobutanol and the system buffered with HEPES produced 9.2 ± 0.3 mM isobutanol. When the substrate concentration was further increased to 50 mM xylose and formaldehyde, isobutanol could no longer be detected and the enzymes precipitated.

To show the flexibility of the cascade, we used the optimized buffer conditions (TRIS pH 7.5) to produce ethanol as an alternative biofuel (Figure 1b). Therefore, the core of the cascade was not changed and only bsAlsS, gslIvC, stllvD and IIKDC_7.M.D were switched to PDC of *Zymomonas mobilis* (zmPDC).^[18] At 10 mM, 20 mM, and 50 mM xylose and

formaldehyde, 75%, 55%, and 0% theoretical yield ethanol could be produced, respectively (Figure 1b).

With these initial experiments, a foundation was laid and three statements could be made to address these findings. First, the cascade design performed well and the adaptability of the cascade for the production of isobutanol or ethanol could be efficiently realized. Second, the results of the thermofluor analysis were consistent with the output of the cascade, however not HEPES but TRIS pH 7.5 was the most suitable buffer system. Third, the upscaling of the substrates xylose and formaldehyde from 10 mM to 20 mM could increase the total yield of isobutanol and ethanol significantly from 8.5 mM isobutanol to 14.3 mM isobutanol and from 15 mM ethanol to 22 mM ethanol. Nevertheless, the efficiency of the cascade in production was reduced. In addition to that, an increase from 20 mM to 50 mM xylose and formaldehyde completely inactivates the cascade, whereby no isobutanol or ethanol could be detected. However, these concentrations are already well above the tolerance of *Escherichia coli* to formaldehyde, with even a low concentration of 1.5 mM severely impairing cell growth.^[43]

Since formaldehyde is a highly reactive and toxic compound, these results highlight the dramatic effects of high formaldehyde concentrations on enzymatic cascades. We suggest that the lower efficiency of the cascade at 20 mM substrate already indicates formaldehyde inactivation, which is exacerbated by even higher concentrations. To overcome this obstacle and realize larger scale *in vitro* systems with integrated C1 fixation up to a future vision of industrial scale, enzymes need to be stabilized either by protein engineering or enzyme immobilization to tolerate higher formaldehyde concentrations.

Optimizing the cascade performance in presence of formaldehyde

As an alternative solution to the problem of high concentrations of toxic formaldehyde, we decided to titrate formaldehyde into the system.

As first option, we used micro syringe pumps to slowly add formaldehyde to the cascade. For this, formaldehyde had a concentration of 100 mM and the flow rate was adjusted to $20 \mu\text{L h}^{-1}$ and $10 \mu\text{L h}^{-1}$ respectively. We applied 50 mM xylose as starting substrate. With this rate, we expected to have equimolar concentrations of xylose and formaldehyde after five hours (ten hours). After five hours (ten hours), we stopped formaldehyde supply and let the cascade run further to see whether it converts the residual formaldehyde and xylose into isobutanol over time (Figure S8). In this setup, formaldehyde solution was pumped into the system via syringes. A major disadvantage of this setup was that the additional formaldehyde diluted the preparation. In addition, it could not be ruled out that the pump pulses were not completely accurate and uniform and thus partial high formaldehyde concentrations could occur during runtime.

In the setting with a formaldehyde supply of $20 \mu\text{L h}^{-1}$, isobutanol was rapidly produced with an initial rate of 5.2 mM h^{-1} . However, this rate also rapidly declined after two

hours and nearly no isobutanol was produced afterwards. After seven hours a maximum of 10.5 ± 1.2 mM isobutanol was produced. In contrast to that, isobutanol production in the setting with $10 \mu\text{L h}^{-1}$ formaldehyde supply was slower with an initial rate of 1.7 mM h^{-1} . This time, however, the rate remained constant for four hours, and only then, it decreased rapidly. A total of 7.3 ± 1.7 mM isobutanol was produced after ten hours. The microsyringe approach achieved an initial conversion of xylose and formaldehyde, in contrast to the direct application of 50 mM formaldehyde. However, this approach was not very efficient and isobutanol production quickly came to a halt. By measuring the formaldehyde concentration formaldehyde strongly increased after six hours ($10 \mu\text{L h}^{-1}$ approach) and after three hours respectively ($20 \mu\text{L h}^{-1}$ approach). This strong increase with simultaneous stagnation of isobutanol production could give a hint for enzyme inactivation at this point. In addition, the formaldehyde concentration increased faster than expected, which could be a result of inaccuracy of the microsyringe pumps. Nevertheless, the slower titration of formaldehyde prolonged the production of isobutanol, but again, isobutanol production ends after four hours, and titers are comparable to those of the higher rate titration.

As a more promising alternative to direct formaldehyde titration, we next used methanol as an alternative starting substrate. For this, we added alcohol oxidase and catalase to the system and re-run the cascade with methanol, a less denaturing but similarly important C1-compound that can be obtained directly from CO_2 .^[44,45] Under the same conditions as before, we were able to generate 26.6 ± 1.8 mM isobutanol from 50 mM xylose and methanol after 24 h of incubation (Figure 2a). A control without the addition of transketolase and methanol oxidase lead to no isobutanol production (Figure S9).

Again, the adaptability of the cell-free system was demonstrated. By adding zmPDC instead of the enzymes for the artificial valine pathway, we switched the system to produce ethanol from xylose and methanol. Using 50 mM xylose and methanol, we were able to produce 66.0 ± 4.5 mM ethanol after six hours (Figure 2b).

These results show that effective prevention of high formaldehyde concentration is the crucial step to operate the

system and achieve scalable production of the final products ethanol and isobutanol. However, when looking at the consumption rates of methanol and xylose, there is a sharp decrease directly after the first 30 minutes of runtime. This sharp decrease clearly indicates oxygen limitation in the system. As oxygen has a low solubility in aqueous solutions^[46] and the K_m for oxygen of alcohol oxidase of *Pichia pastoris* (ppAOX) is between 0.4 and 1 mM in presence of methanol,^[47] reaction rates quickly decline if not actively forcing oxygen into the system. However, this oxygen limitation could also be a reason why the cascade works more efficiently with methanol than when formaldehyde is added with a syringe pump. The slower rate gives the transketolase more time to consume formaldehyde which does not lead to partially high concentrations.

Apart from this, stability of ppAOX could be a reason for the diminished methanol consumption, due to quick loss in activity at elevated temperatures.^[47] Because of that future application needs to first address the oxygen affinity by enzyme engineering approaches to keep the oxygen consumption rate high over a certain time span and process engineering to introduce oxygen in an efficient manner without compromising enzyme stability.^[48] In addition, oxidase stability could also be a key issue to address, either by lower temperature or more stable oxidases. The final issue that would be needed for scale-up is an engineering of ADH. The ADH still suffers from a low activity towards isobutyraldehyde and to get enough velocity in the cascade, the converting ADH has to be highly active and specific for isobutyraldehyde.

Conclusion

The efficient use of CO_2 -based C1-compounds will be one of the greatest opportunities for biocatalysis in the coming years. There are more and more concepts for new enzymes that are able to convert methanol, formaldehyde or formate directly into molecules with higher carbon chain length. However, these pathways pass through the highly reactive and toxic compound formaldehyde, which can deactivate and crosslink enzymes.

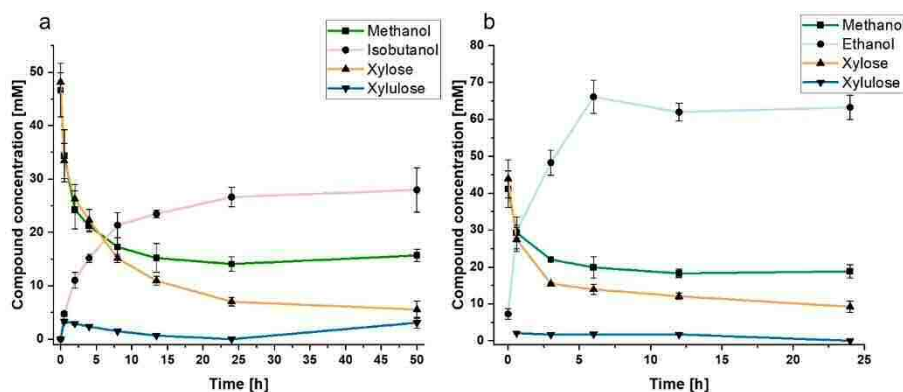


Figure 2. Time course of substrate, product and intermediates of the final cascade. (a) Isobutanol set up with methanol and xylose as substrates. (b) Ethanol set up with methanol and xylose as substrates ($n = 3$).

Therefore, control over formaldehyde concentration is essential to create sustainable and scalable pathways for industrial application. By exploiting the adaptability of *in vitro* systems, we were able to prevent high formaldehyde concentrations and inactivation of pathway enzymes by the in-situ production of formaldehyde via methanol. In combination with sugar-directed utilization of formaldehyde via transketolase, accumulating formaldehyde is directly converted into key intermediates of glycolysis, which can then be further utilized via pyruvate to generate isobutanol, ethanol or other chemicals.

Using xylose, the second most abundant sugar in nature and after glucose the main carbohydrate of lignocellulosic biomass, and methanol, a C1-compound derivable from CO₂, we have developed a cell-free system for sustainable and efficient production of the most common biofuel ethanol and the highly interesting next-generation biofuel isobutanol with titers of 3 g L⁻¹ ethanol and 2 g L⁻¹ isobutanol from 7.5 g L⁻¹ xylose and 1.6 g L⁻¹ methanol, respectively. As an alternative to C1-only pathways, xylose-based C1 fixation and utilization pathway (XFUP) fixes formaldehyde using xylose with an active transketolase, preventing interference of high partial formaldehyde concentrations. In addition, the modular design of the cascade allows rapid addition or modification of modules. Thus, in future research and application, a combination of xylose valorization with the already known glucose-isobutanol pathway is possible and both sugars can be converted simultaneously without the problem of catabolite repression. Thus, sugar-guided C1 fixation efficiently combines two waste streams and opens the way for environmentally and economically friendly production of biofuels and chemical feedstocks from waste materials.

Experimental Section

Chemicals and strains

All chemicals were purchased from Sigma-Aldrich, Roth, Alfa Aesar, Merck, Cayman chemical, Carbosynth, Serva, Fisher scientific and VWR unless otherwise noted.

Escherichia coli (E. coli) NEB® Turbo cells (New England Biolabs® inc.) were used as cloning strain. *E. coli* BL21(DE3) F⁻ ompT gal dcm lon hsdSB(rB- mB-) λ(DE3 [lacI lacUV5-T7 gene 1 ind1 sam7 nin5]) (Novagen) were used for heterologous gene expression.

Pyruvate kinase/Lactate dehydrogenase mix (PK/LDH) from rabbit muscle, alcohol oxidase (AOX) of *Pichia pastoris*, catalase (CAT) of *Corynebacterium glutamicum*, glyceraldehyde 3-phosphate dehydrogenase (GAPDH) from rabbit muscle and aldolase from rabbit muscle were purchased from Sigma-Aldrich. Lactate dehydrogenase (LDH) from rabbit muscle was purchased from Roth.

Molecular cloning and plasmid construction

Plasmid pET28a was provided by Novagen. pCBRH_{isN}, pCBRH_{isC} were constructed on the basis of pET28a and prepared as published by Guterl et al.^[18] Phusion High-Fidelity DNA Polymerase (NEB) was used for gene amplification from genomic DNA. Restriction enzymes and T4 ligase (NEB) were used for restriction ligation cloning of plasmids and genes (Table S1).

Protein expression

E. coli BL21(DE3) was used as host strain for heterologous gene expression. Expression was carried out in two steps. First 20 mL of lysogeny broth (LBmedium containing 100 μg mL⁻¹ kanamycin were inoculated with a colony from the LB agar plate and incubated for 16 h at 37 °C and 150 rpm. Main cultures were cultivated in shaking flasks containing 20% (v v⁻¹) ZYP-5052 auto induction medium^[49] including 100 μg mL⁻¹ kanamycin. The main culture was inoculated to an OD₆₀₀ of 0.05 and incubated at 37 °C and 90 rpm until an OD₆₀₀ of 0.6–0.8. Temperature was reduced to 25 °C for enzymes derived from thermophilic organisms and to 16 °C for enzymes derived from mesophilic organisms and incubated for 20 h. Cells were harvested by centrifugation (20 °C, 3500 g, 30 min), the supernatant was discarded and the cell pellet was stored at –20 °C.

Protein purification

Cell lysates were prepared on ice using ultra sonication (Ultraschallprozessor UIS250 V Hielscher Ultrasonic GmbH) and centrifuged afterwards (20 °C, 18000 g, 30 min). For enzymes originated from thermophilic organisms an additional heat treatment was applied before centrifugation (65 °C, 45 min).

Proteins containing a His₆-tag were purified using an AEKTA Pure system equipped with a 5 mL HiTrapFF Crude column. First, the column was equilibrated with binding buffer (50 mM HEPES pH 8.0, 20 mM imidazole, 500 mM NaCl). Then the supernatant was applied. A washing step with binding buffer was used to remove unbound proteins. To elute the His₆-tagged proteins from the column, the imidazole concentration was raised from 20 mM to 500 mM. The eluate was fractionated and protein-containing fractions were collected. The buffer was exchanged via HiPrep 26/10 desalting column to 50 mM HEPES pH 7.5. Purified protein solutions were frozen in liquid nitrogen and stored at –80 °C.

Protein concentration determination

Protein concentration was determined using a NanoPhotometer® P-Class (IMPLEN). Absorption was measured at 280 nm after adding extinction coefficient and molecular weight of the target enzyme to the system (Table S1).

Enzyme activity assay

Enzyme activity measurements were conducted in 200 μL reactions with HEPES pH 7.5 and 10 mM MgCl₂ at 37 °C. Conditions were tailored according to the analyzed enzymes and coupling enzymes. Reactions were started by addition of the target enzyme and measured by Biotek epoch-2 microplate spectrophotometer (Biorad) (Table S2).

ATP depended reactions were coupled to pyruvate kinase and lactate dehydrogenase with the use of phosphoenolpyruvate as co-substrate. Activity was measured by following the absorbance of NADH at 340 nm.

NAD(P)⁺/NAD(P)H depended reactions were directly measured by following the absorbance of NAD(P)H at 340 nm.

All other reactions were coupled to ATP depended reactions and monitored as described for ATP dependent reactions or coupled to NAD(P)⁺ or NAD(P)H consuming reactions by following the absorbance of NAD(P)H at 340 nm

Enzyme kinetic measures

Transketolase

Transketolase (TktA) kinetics (Figure S2) were measured in a coupled approach with glyceraldehyde specific aldehyde dehydrogenase taAldH (M42)^[50] by measuring reduction of NAD⁺. To test whether M42 activity is reduced by formaldehyde, activity of M42 was tested on glyceraldehyde by measuring the reduction of NAD⁺ in presence of 0 to 20 mM formaldehyde (Figure S3). Due to formaldehyde inactivation, M42 concentration was raised four times in kinetic measurements to counteract reduced activity in high formaldehyde concentrations.

Xylulose kinetics were conducted with a concentration range of 0 to 100 mM of xylulose and a fixed concentration of 5 mM formaldehyde. Reaction was started by addition of xylulose to the reaction mixture. Formaldehyde kinetics were conducted with a concentration range of 0 to 20 mM of formaldehyde and a fixed concentration of 50 mM xylulose. Reaction was started by addition of formaldehyde to the reaction mixture.

Formaldehyde inhibition of vpTktA and mrTktA (Figure S3) was measured similar to the kinetics with formaldehyde. Here, a fixed concentration of 5 mM xylulose was applied. However, to counteract the inhibition of the coupling enzyme, M42 concentration was increased fourfold. Reaction was started by addition of formaldehyde to the reaction mixture.

Dihydroxyacetone kinase

Dihydroxyacetone kinase (DhaK) kinetics (Figure S4) were measured in a coupled approach with pyruvate kinase and lactate dehydrogenase by measuring oxidation of NADH^[51] in 382 μ L. Standard reactions contained additional 1.25 mM PEP, 0.3 mM NADH, 2 mM ADP, 5 to 0.005 mM dihydroxyacetone and 3.8 μ L Pyk/LDH mix. Reactions were started by addition of dihydroxyacetone to the reaction mixture.

Alcohol dehydrogenase

Alcohol dehydrogenase (ADH) kinetics (Figure S5) were measured by directly measuring the oxidation of NADPH.^[38] Standard reaction contained additional 0.3 mM NADPH and 0 to 50 mM isobutyraldehyde or 0 to 250 mM formaldehyde. Reaction was started by addition of the substrate to the reaction mixture.

Melting point analysis

Melting point analysis was performed in 25 μ L reaction volume with 2 μ L SYPROTM Orange (1:80 dilution) 2 μ L of protein (concentration), and 100 mM TRIS pH 7.5, HEPES pH 7.5 or Kpl pH 7.5 in the cascade matrix. Measurements were performed with a CFX96 Touch Real-Time PCR detection system (Biorad). The temperature was increased in increments of 1 °C from 25 °C to 100 °C with one minute per kelvin increase. The melting curves were prepared as described in the manufacturer's instructions (Biorad). Melting point data were derived from the minimum of the negative derivative of the fluorescence curve versus temperature (Biorad).

Enzymatic cascade

Enzymatic cascades for the production of ethanol and isobutanol were conducted as follows. The enzymes were concentrated and

desalted with a buffer changed to the cascade buffer using modified PES 10 kDa (VWR) centrifugal filters.

Initial cascade with buffer test and formaldehyde as substrate

The first cascades were run in three different buffer systems (TRIS-HCl, Kpl, HEPES) with a pH of 7.5 and a concentration of 100 mM in a volume of 50 μ L in a 1.5-mL tube at 700 rpm ThermoMixer C, Eppendorf, Germany) and 37 °C. Cascade mixtures containing cofactors, buffer and substrates were prepared in the tube and then the enzyme mixture was added. Samples were taken directly after enzyme addition and at the indicated time points. They were diluted 1 to 10 or 1 to 20 in 2.5 mM H₂SO₄ and filtered using modified PES 10 kDa (VWR) centrifugal filters.

Formaldehyde addition via micro syringe pumps

Cascades with formaldehyde titration were conducted similarly in a volume of 200 μ L in a 2 mL tube applying 700 rpm (ThermoMixer C, Eppendorf, Germany) at 37 °C. Substrates (except formaldehyde), buffers and cofactors were presented in the tube and then the enzyme mixture was added. The reaction tubes were perforated and the cascade solution was connected to the formaldehyde solution through a tubing. 100 mM formaldehyde stock solution was applied directly through the tubing with a gas tight syringe (SGE) and microsyringe pump (Flowstart EVO, Future Chemistry, The Netherlands) after addition of the enzymes. The flow rate of formaldehyde was set to either 20 μ L h⁻¹ or 10 μ L h⁻¹ and the tube was sealed with parafilm. The flow rate of formaldehyde was set to 0 μ L h⁻¹ after five (20 μ L h⁻¹) and ten hours (10 μ L h⁻¹) of application. Samples over a period of 26 h (20 μ L h⁻¹) or 18 h (10 μ L h⁻¹) were taken and handled as described before.

Final cascade with methanol

Cascades with methanol as substrate instead of formaldehyde were conducted in a volume of 200 μ L in a 2 mL tube applying 700 rpm (ThermoMixer C, Eppendorf, Germany) at 37 °C. Substrates, buffers and cofactors were presented in the tube and then the enzyme mixture was added (Table S3). In contrast to the cascades before catalase and methanol oxidase were added to the reaction mixtures. Samples over a period of 46 h (isobutanol) and 24 h (ethanol) were taken as described before.

Cascade control experiments

Control experiments were conducted similarly to the cascade experiments without the addition of methanol oxidase and transketolase (Figure S7).

Quantification of cascade substrates, intermediates and products

Quantification of methanol, acetaldehyde, isobutyraldehyde ethanol and isobutanol

Methanol, acetaldehyde, isobutyraldehyde, ethanol and isobutanol were quantified by headspace GC-FID [Thermo Scientific Trace GC Ultra, equipped with a flame ionization detector (FID) and a Headspace Tri Plus autosampler] equipped with a Stabilwax column [30 m, 0.25 mm internal diameter, 0.25 μ m film thickness (Restek, Bellefonte, USA)] with helium as carrier gas similar to Guterl et al.^[18] The oven temperature was held at 50 °C for 2 min and raised with

10 °C min⁻¹ to 80 °C held for 1 min. 200 µL of the samples were added to a 10 mL headspace vial for analysis. Prior to injection samples were incubated at 40 °C for 15 min. Injection was carried out via split mode with 10 mL min⁻¹ flow, with an injection volume of 700 µL using headspace mode.

Quantification of xylose, xylulose, glyceraldehyde, dihydroxyacetone and pyruvate

Xylose, xylulose, glyceraldehyde, dihydroxyacetone and pyruvate were analyzed and quantified using an HPLC (Ultimate300 HPLC-system, Dionex Softron GmbH, Germering, Germany) system coupled to an UV-detector at 210 nm and an RI detector, equipped with a Rezex™ ROA-Organic Acid H+ (8%) 300 x 7.8 mm LC Column (Phenomenex, Germany). Separation was conducted in an isocratic run with 2.5 mM H₂SO₄ at 70 °C for 42 min.^[14a] Signal analysis and amount calculation was conducted by using Chromeleon Software (ThermoFisher Scientific).

Quantification of formaldehyde

Formaldehyde was quantified using the acetylacetone method.^[52] Therefore formaldehyde standards (1 mM, 0.8 mM, 0.4 mM, 0.2 mM, 0.1 mM, 0.05 mM, 0.01 mM and 0 mM) were prepared in the cascade mix (Table S5). 50 µL of diluted cascade samples or standards were mixed with 50 µL Nash reagent [0.2% (v v⁻¹) acetylacetone, 0.1 M acetic acid and 3.89 M ammonium acetate] in a 96 well plate and incubated for 30 min at 37 °C. Absorbance was measured at 412 nm with a Biotek epoch-2 microplate spectrophotometer (Biorad).

Acknowledgements

The work was supported by Bundesministerium für Bildung und Forschung (BMBF), Förderkennzeichen:031B0351C Deutsche Forschungsgemeinschaft (DFG) through TUM International Graduate School of Science and Engineering (IGSSE), GSC 81

We thank S. Sutiono for advice on revising the manuscript. We thank B. Rühmann, P. Lommes, and A. Schmidt for advice and assistance with the analytics. We thank M. Teshima, A. Al-Shameri, E. Hupfeld, and A. Pick for fruitful discussion. Open Access funding enabled and organized by Projekt DEAL.

Conflict of Interest

All authors declare that they have no competing interests.

Data Availability Statement

The authors declare that the data supporting the findings of this study are available within the paper and its supplementary information.

Keywords: biofuels · enzyme cascade · lignocellulosic biomass · methanol · xylose

- [1] R. A. Sheldon, J. M. Woodley, *Chem. Rev.* **2018**, *118*, 801–838.
- [2] Y. Su, W. Zhang, A. Zhang, W. Shao, *Appl. Sci.* **2020**, *10*, 8222.
- [3] S. Fatma, A. Hameed, M. Noman, T. Ahmed, M. Shahid, M. Tariq, I. Sohail, R. Tabassum, *Protein Pept. Lett.* **2018**, *25*, 148–163.
- [4] S. Kwak, Y.-S. Jin, *Microb. Cell Fact.* **2017**, *16*, 82.
- [5] J. Baruah, B. K. Nath, R. Sharma, S. Kumar, R. C. Deka, D. C. Baruah, E. Kalita, *Front. Energy Res.* **2018**, *6*, 141.
- [6] a) A. D. Chintagunta, G. Zuccaro, M. Kumar, S. J. Kumar, V. K. Garlapati, P. D. Postemsky, N. S. Kumar, A. K. Chandel, J. Simal-Gandara, *Front. Microbiol.* **2021**, *12*, 658284; b) A. Lachke, *Reson* **2002**, *7*, 50–58.
- [7] K. Cheng, W. Zheng, H. Chen, Y.-H. P. J. Zhang, *Metab. Eng.* **2019**, *52*, 1–8.
- [8] a) Z. Zhao, M. Xian, M. Liu, G. Zhao, *Biotechnol. Biofuels* **2020**, *13*, 21; b) T. W. Jeffries, *Adv Biochem Eng Biotechnol.* **1983**, *27*, 1–32.
- [9] a) E. M. Ammar, X. Wang, C. V. Rao, *Sci. Rep.* **2018**, *8*, 609; b) C. Van Zyl, B. A. Prior, S. G. Kilian, J. L. Kock, *Microbiology* **1989**, *135*, 2791–2798.
- [10] W. Yin, Y. Cao, M. Jin, M. Xian, W. Liu, *ACS Synth. Biol.* **2021**, *10*, 2266–2275.
- [11] S. G. Karp, J. D. Medina, L. A. Letti, A. L. Woiciechowski, J. C. de Carvalho, C. C. Schmitt, R. de Oliveira Penha, G. S. Kumlehn, C. R. Soccol, *Biofuels Bioprod. Biorefin.* **2021**, *15*, 899–912.
- [12] S. Malakar, S. K. Paul, K. R. Jolvis Pou, in *Biotechnological Progress and Beverage Consumption* (Eds.: A. M. Grumezescu, A. M. Holban), Academic Press, **2020**, 1–37.
- [13] L. Canilha, A. Kumar Chandel, T. S. dos Santos Milessi, F. A. Fernandes Antunes, W. L. da Costa Freitas, M. das Graças Almeida Felipe, S. S. da Silva, *J. Biomed. Biotechnol.* **2012**, *2012*, 989572.
- [14] a) S. Sutiono, M. Teshima, B. Beer, G. Schenk, V. Sieber, *ACS Catal.* **2020**, *10*, 3110–3118; b) F. Yang, M. A. Hanna, R. Sun, *Biotechnol. Biofuels* **2012**, *5*, 13.
- [15] X. Li, Y. Chen, J. Nielsen, *Curr. Opin. Biotechnol.* **2019**, *57*, 56–65.
- [16] Y. Cam, C. Alkim, D. Trichez, V. Trebosc, A. Vax, F. Bartolo, P. Besse, J. M. François, T. Walther, *ACS Synth. Biol.* **2016**, *5*, 607–618.
- [17] T. C. Ezeji, N. Qureshi, V. Ujor, in *Bioenergy Res.: Adv. Appl.* (Eds.: V. K. Gupta, M. G. Tuohy, C. P. Kubicek, J. Saddler, F. Xu), Elsevier, Amsterdam, **2014**, 109–118.
- [18] J. K. Guterl, D. Garbe, J. Carsten, F. Steffler, B. Sommer, S. Reiß, A. Philipp, M. Haack, B. Rühmann, A. Koltermann, *ChemSusChem* **2012**, *5*, 2165–2172.
- [19] a) D. Dugar, G. Stephanopoulos, *Nat. Biotechnol.* **2011**, *29*, 1074–1078; b) N. Maleki, M. Safari, M. A. Eiteman, *Eng. Life Sci.* **2018**, *18*, 40–47.
- [20] S. Atsumi, T. Hanai, J. C. Liao, *Nature* **2008**, *451*, 86–89.
- [21] S. Sherkhanov, T. P. Korman, S. Chan, S. Faham, H. Liu, M. R. Sawaya, W.-T. Hsu, E. Vikram, T. Cheng, J. U. Bowie, *Nat. Commun.* **2020**, *11*, 4292.
- [22] P. Promdonkoy, W. Mhuantong, V. Champreda, S. Tanapongpipat, W. Runguphan, *J. Ind. Microbiol. Biotechnol.* **2020**, *47*, 497–510.
- [23] a) P. Promdonkoy, W. Siripong, J. J. Downes, S. Tanapongpipat, W. Runguphan, *AMB Expr.* **2019**, *9*, 160; b) J. M. Clomburg, R. Gonzalez, *Appl. Microbiol. Biotechnol.* **2010**, *86*, 419–434; c) Y. Zhang, S. Lane, J.-M. Chen, S. K. Hammer, J. Luttinger, L. Yang, Y.-S. Jin, J. L. Avalos, *Biotechnol. Biofuels* **2019**, *12*, 223.
- [24] C. Fu, Z. Li, C. Jia, W. Zhang, Y. Zhang, C. Yi, S. Xie, *Energy Convers. Manage. X* **2021**, *10*, 100059.
- [25] a) X. Jia, R. M. Kelly, Y. Han, *Metab. Eng. Commun.* **2018**, *7*, e00074; b) H. Boer, M. Andberg, R. Pylkkänen, H. Maaheimo, A. Koivu, *AMB Expr.* **2019**, *9*, 48.
- [26] H. Yurimoto, N. Kato, Y. Sakai, *Chem. Rec.* **2005**, *5*, 367–375.
- [27] H. Yurimoto, M. Oku, Y. Sakai, *Int. J. Microbiol.* **2011**, *2011*, 101298.
- [28] W. Zhang, T. Zhang, S. Wu, M. Wu, F. Xin, W. Dong, J. Ma, M. Zhang, M. Jiang, *RSC Adv.* **2017**, *7*, 4083–4091.
- [29] a) C.-T. Chen, F. Y.-H. Chen, I. W. Bogorad, T.-Y. Wu, R. Zhang, A. S. Lee, J. C. Liao, *Metab. Eng.* **2018**, *49*, 257–266; b) F. Meyer, P. Keller, J. Hartl, O. G. Gröninger, P. Kiefer, J. A. Vorholt, *Nat. Commun.* **2018**, *9*, 1508.
- [30] a) P. L. Bergquist, S. Siddiqui, A. Sunna, *Front. Energy Res.* **2020**, *8*, 193; b) H. J. Lim, D.-M. Kim, *Curr. Opin. Biotechnol.* **2022**, *73*, 158–163; c) N. Losada-García, Z. Cabrera, P. Urrutia, C. García-Sanz, A. Andreu, J. M. Palomo, *Catalysts* **2020**, *10*, 1258.
- [31] T. Cai, H. Sun, J. Qiao, L. Zhu, F. Zhang, J. Zhang, Z. Tang, X. Wei, J. Yang, Q. Yuan, W. Wang, X. Yang, H. Chu, Q. Wang, C. You, H. Ma, Y. Sun, Y. Li, C. Li, H. Jiang, Q. Wang, Y. Ma, *Science* **2021**, *373*, 1523–1527.
- [32] S. Atsumi, W. Higashide, J. C. Liao, *Nat. Biotechnol.* **2009**, *27*, 1177–1180.
- [33] R. Miao, H. Xie, P. Lindblad, *Biotechnol. Biofuels* **2018**, *11*, 267.
- [34] L. Guo, L. Sun, Y.-X. Huo, *Biotechnol. Biofuels Bioprod.* **2022**, *15*, 80.

- [35] J. B. Siegel, A. L. Smith, S. Poust, A. J. Wargacki, A. Bar-Even, C. Louw, B. W. Shen, C. B. Eiben, H. M. Tran, E. Noor, *Proc. Nat. Acad. Sci.* **2015**, *112*, 3704–3709.
- [36] a) K. Nobuo, H. Toshio, S. Chikahiro, N. Tsutomu, T. Yoshiki, Y. Hideaki, *Biochim. Biophys. Acta* **1982**, *715*, 143–150; b) Y. T. Ro, C. Y. Eom, T. Song, J. W. Cho, Y. M. Kim, *J. Bacteriol.* **1997**, *179*, 6041–6047; c) G. A. Sprenger, U. Schörken, G. Sprenger, H. Sahn, *Eur. J. Biochem.* **1995**, *230*, 525–532.
- [37] P. H. Opgenorth, T. P. Korman, L. Iancu, J. U. Bowie, *Nat. Chem. Biol.* **2017**, *13*, 938–942.
- [38] A. Pick, B. Rühmann, J. Schmid, V. Sieber, *Appl. Microbiol. Biotechnol.* **2013**, *97*, 5815–5824.
- [39] G. M. Rodriguez, S. Atsumi, *Metab. Eng.* **2014**, *25*, 227–237.
- [40] S. Sutiono, J. Carsten, V. Sieber, *ChemSusChem* **2018**, *11*, 3335–3344.
- [41] J. Wei, J. G. Timler, C. M. Knutson, B. M. Barney, *FEMS Microbiol. Lett.* **2013**, *346*, 105–112.
- [42] B. Sommer, H. von Moeller, M. Haack, F. Qoura, C. Langner, G. Bourenkov, D. Garbe, B. Loll, T. Brück, *ChemBioChem* **2015**, *16*, 110–118.
- [43] R. K. Bennett, G. J. Gregory, J. E. Gonzalez, J. R. G. Har, M. R. Antoniewicz, E. T. Papoutsakis, *Front. Microbiol.* **2021**, *12*, 638426.
- [44] S. Navarro-Jaén, M. Virginie, J. Bonin, M. Robert, R. Wojcieszak, A. Y. Khodakov, *Nat. Chem. Rev.* **2021**, *5*, 564–579.
- [45] a) S. Chakraborty, J. Nayak, B. Ruj, P. Pal, R. Kumar, S. Banerjee, M. Sardar, P. Chakraborty, *J. Environ. Chem. Eng.* **2020**, *8*, 103935; b) H. Guzmán, F. Salomone, E. Batuecas, T. Tommasi, N. Russo, S. Bensaid, S. Hernández, *Chem. Eng. J.* **2021**, *417*, 127973.
- [46] W. R. Birmingham, A. Toftgaard Pedersen, M. Dias Gomes, M. Bøje Madsen, M. Breuer, J. M. Woodley, N. J. Turner, *Nat. Commun.* **2021**, *12*, 4946.
- [47] R. Couderc, J. Baratti, *Agric. Biol. Chem.* **1980**, *44*, 2279–2289.
- [48] M. Dias Gomes, B. R. Bommarius, S. R. Anderson, B. D. Feske, J. M. Woodley, A. S. Bommarius, *Adv. Synth. Catal.* **2019**, *361*, 2574–2581.
- [49] F. W. Studier, *Protein Expression Purif.* **2005**, *41*, 207–234.
- [50] T. J. Gmelch, J. M. Sperl, V. Sieber, *ACS Synth. Biol.* **2020**, *9*, 920–929.
- [51] D. Gauss, I. Sánchez-Moreno, I. Oroz-Guinea, E. García-Junceda, R. Wohlgemuth, *Eur. J. Org. Chem.* **2018**, 2892–2895.
- [52] H.-J. Jo, J.-H. Kim, Y.-N. Kim, P.-W. Seo, C.-Y. Kim, J.-W. Kim, H.-n. Yu, H. Cheon, E. Y. Lee, J.-S. Kim, *Green Chem.* **2022**, *24*, 218–226.

Manuscript received: November 14, 2022
Revised manuscript received: December 14, 2022
Accepted manuscript online: December 15, 2022

ChemSusChem

Supporting Information

Integrating Carbohydrate and C1 Utilization for Chemicals Production

Vivian Pascal Willers, Barbara Beer, and Volker Sieber*© 2022 The Authors. ChemSusChem published by Wiley-VCH GmbH. This is an open access article under the terms of the Creative Commons Attribution License, which permits use, distribution and reproduction in any medium, provided the original work is properly cited.

Supplemental tables and figures

Supplemental tables

Table S1: Enzyme list including source organism, molecular weight, extinction coefficient accession number and restriction enzymes used for cloning or source, if applicable.

Enzyme	Name	Source organism	Molecular-weight [Da]	Extinction coefficient [M ⁻¹ cm ⁻¹]	UniProt accession number	Source/ cloning
ppAOX	Alcohol oxidase	<i>Pichia pastoris</i>				Sigma
cgCAT	Catalase	<i>Corynebacterium glutamicum</i>				Sigma
pfXylA	Xylose isomerase	<i>Pseudomonas fluorescens</i>	51457	62340	C3K8E3	NdeI, Hind III
ecTktA	Transketolase	<i>Escherichia coli</i>	73164	94770	P27302	NdeI, XhoI
vpTktA	Transketolase	<i>Variovorax paradoxus</i>	77605	92820	A0A679IMI8	NdeI, XhoI
mrTktA	Transketolase	<i>Meiothermus ruber</i>	72808	91790	D3PT03	NdeI, XhoI
kbDhaK	Dihydroxyacetone kinase	<i>Kozakia baliensis</i>	55488	47330	A0A1D8UUV1	NdeI, XhoI
gsTpi	Triose phosphate isomerase	<i>Geobacillus stearothermophilus</i>	29345	16960	P00943	NdeI, SacI
tkGapN	Non phosphorylating glyceraldehyde 3-phosphate dehydrogenase	<i>Thermokokus kodakarensis</i>	71585	40910	Q5JG59	NdeI, XhoI
gsPgm	Phosphoglycerate isomerase	<i>Geobacillus stearothermophilus</i>	59166	43780	Q9X519	NdeI, SacI
tmENO	Enolase	<i>Thermotoga maritima</i>	49033	27850	P42848	pCBRHisN ^[1]
taPyK	Pyruvate kinase	<i>Thermoplasma acidophilum</i>	61310	20860	P32044	pCBRHisN ^[1]

bsAlsS	Acetolactate synthase	<i>Bacillus subtilis</i>	625884	52830	Q04789	pCBRHisC ^[1]
gsIlvC	Ketol-acid reductoisomerase	<i>Geobacillus stearothermophilus</i>	37348	35870	Q8RL86	NheI, Hind III
stIlvD	Dihydroxy-acid dehydratase	<i>Schlegelella thermodepolymerans</i>	59180	46870	A0A2S5T1G9	Sutiono and Coworkers ^[2]
IlKDC	Keto-isovalerate decarboxylase	<i>Lactococcus lactis</i>	60884	52830	Q6QBS4	Gocke and coworkers ^[3]
IlKDC_7M.D	Keto-isovalerate decarboxylase	<i>Lactococcus lactis</i>	60884	52830		Sutiono and Coworkers ^[4]
ecYqhD	Alcohol dehydrogenase	<i>Escherichia coli</i>	42097	42400	Q46856	Pick and coworkers ^[5]
ecYjgB	Alcohol dehydrogenase	<i>Escherichia coli</i>	38665	40910	P27250	Pick and coworkers ^[5]
ecYahK	Alcohol dehydrogenase	<i>Escherichia coli</i>	40431	27390	P75691	Pick and coworkers ^[5]
ecXylB	Xylulokinase	<i>Escherichia coli</i>	54781	82390	P09099	NdeI, XhoI

Table S2: Kinetic properties of kbDhaK on dihydroxyacetone (DHA) and glyceraldehyde (GLA) (n = 3).

Enzyme	K_{mDHA} [mM]	K_{mGLA} [mM]	V_{maxDHA} [U/mg]	V_{maxGLA} [U/mg]	k_{catDHA} [s ⁻¹]	k_{catGLA} [s ⁻¹]	$k_{catDHA}K_{mDHA}$ [s ⁻¹ M ⁻¹]	$k_{catGLA}K_{mGLA}$ [s ⁻¹ M ⁻¹]
kbDhaK	0.1 ± 0.0	0.4 ± 0.0	10.1 ± 0.8	3.3 ± 0.1	9.9 ± 0.7	3.2 ± 0.1	115116	8000

Table S3: Kinetic properties of three ADHs with isobutyraldehyde (Iso) and formaldehyde (FALD) (n = 3).

Enzyme	K_{miso} [mM]	K_{mFALD} [mM]	V_{maxiso} [U/mg]	$V_{maxFALD}$ [U/mg]	k_{catiso} [s ⁻¹]	$k_{catFALD}$ [s ⁻¹]	$k_{catiso}K_{miso}$ [s ⁻¹ M ⁻¹]	$k_{catFALD}K_{mFALD}$ [s ⁻¹ M ⁻¹]
ecYqhD	2.3 ± 0.3	53.4 ± 8.6	0.2 ± 0.0	0.2 ± 0.0	0.2 ± 0.0	0.1 ± 0.0	79	3
ecYahK	0.2 ± 0.0	6.1 ± 1.4	3.0 ± 0.1	1.9 ± 0.2	2.0 ± 0.1	1.3 ± 0.1	12415	216
ecYjgB	335.5 ± 137.4	191.4 ± 69.7	117.7 ± 42.9	26.7 ± 8.2	75.8 ± 27.7	18.0 ± 5.5	226	94

Table S4: Cascade enzymes activity on cascade metabolites with coupling enzymes and cofactors (n = 3). Activities were measured by following the reduction/oxidation of NAD(P)⁺/NAD(P)H with a Biotek epoch-2 microplate spectrophotometer (Biorad).

Enzyme	Activity [U/mg]	Metabolites	Coupling enzymes	Cofactors
pfXylA	3.2 ± 0.5	100 mM Xylose	ecXylB, PK/LDH	1 mM ATP, 0.3 mM NADH, 1 mM PEP
ecTktA	1.4 ± 0.0	5 mM Xylulose 1 mM Formaldehyde	M42 (taAldH)	5 mM NAD ⁺ , 1 mM TPP
kbDhaK	10.0 ± 0.1	1 mM Dihydroxyacetone	PK/LDH	1 mM ATP, 0.3 mM NADH, 1 mM PEP
gsTpi	25.2 ± 2.8	1 mM Dihydroxyacetone-phosphate	GAPDH	5 mM NAD ⁺ , 5 mM KPO ₄ ,
tkGapN	2.0 ± 0.1	1 mM Fructose-1,6-bisphosphate	Aldolase	2.5 mM NADP ⁺ , 0.5 mM glucose 1-phosphate, 0.5 mM TPP
gspgM	22.8 ± 1.9	1 mM 3-Phosphoglycerate	ENO, PK/LDH	0.3 mM NADH, 1 mM ADP, 1 mM MnCl ₂
tmENO	39.5 ± 1.6	1 mM 2-Phosphoglycerate	PK/LDH	1 mM ADP, 0.3 mM NADH
taPyK	7.2 ± 0.1	1 mM Phosphoenolpyruvate (PEP)	LDH	1 mM ADP, 0.3 mM NADH
bsALsS	1.7 ± 0.0	1 mM Pyruvate	gsIivC	0.3 mM NADPH, 1 mM TPP
gsIivC	0.6 ± 0.0	1 mM Pyruvate	bsALsS	0.3 mM NADPH, 1 mM TPP
stIivD	0.9 ± 0.1	1 mM 2,3 Dihydroxyisovalerate ⁺	IiKDC, ecYahK	0.3 mM NADPH, 1 mM TPP
IiKDC	22.1 ± 0.4	2.5 mM 2 Ketoisovalerate	ecYahK	0.3 mM NADPH 1 mM TPP
ecYqhD	0.1 ± 0.0	2.5 mM Isobutanol		0.3 mM NADPH

Table S5: Final cascade conditions with enzyme load as well as buffer, cofactor and substrate load.

Enzyme	µg/mL	mU	Compound	Concentration [mM]
ppAOX	25	60	ATP	4
cgCAT		500	NADP+	2
pfXylA	375	150	MgCl ₂	10
ecTktA	1500	150	MnCl ₂	0.5
tkGAPN	1324	450	TPP	0.5
kbDHAK	300	300	G1P	0.5
gsTpl	570	3420	Xylose	50
gspgM	750	450	MeOH	50
tmEnolase	45	450	TRIS-HCl pH 7.5	100
taPyruvateKinase	1324	450		
bsALS	300	120		
gsIivC	2500	300		
stIivD	1500	300		
IiKDC_7M.D	150	75		
ecYqhD	2250	67,5		

Supplemental figures

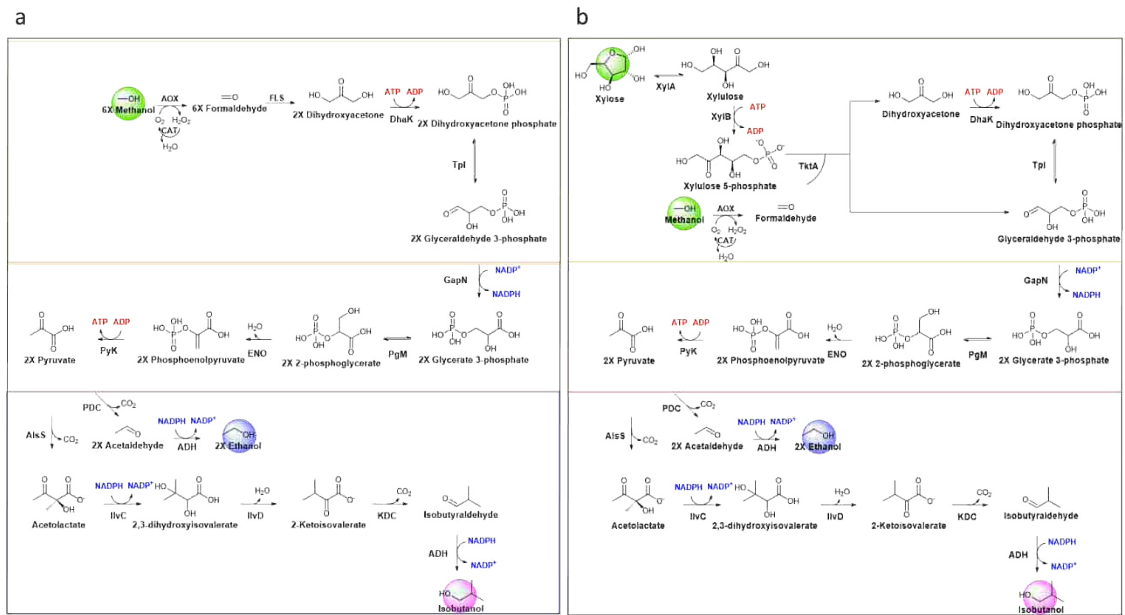


Figure S1: Alternative cascade schemes for ethanol/isobutanol production based on methanol. *a*: Proposed pathway from methanol to ethanol/isobutanol without sugar-based C1 fixation using formolase. *b*: Proposed pathway from xylose and methanol to ethanol/isobutanol with sugar-based C1 fixation with additional xylulokinase.

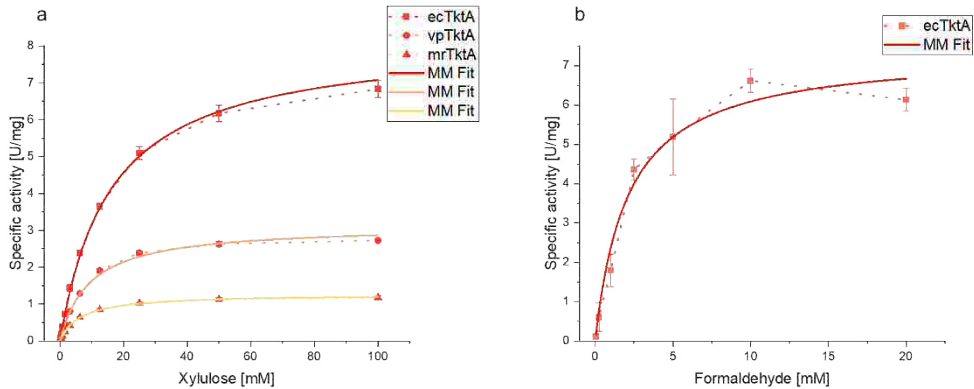


Figure S2: Kinetics of transketolases with xylulose and formaldehyde with Michaelis Menten fit (MM FIT). *a*: Kinetics of three different transketolases with a fixed formaldehyde concentration of 5 mM. *b*: Kinetic of ecTktA with a fixed xylulose concentration of 50 mM ($n = 3$).

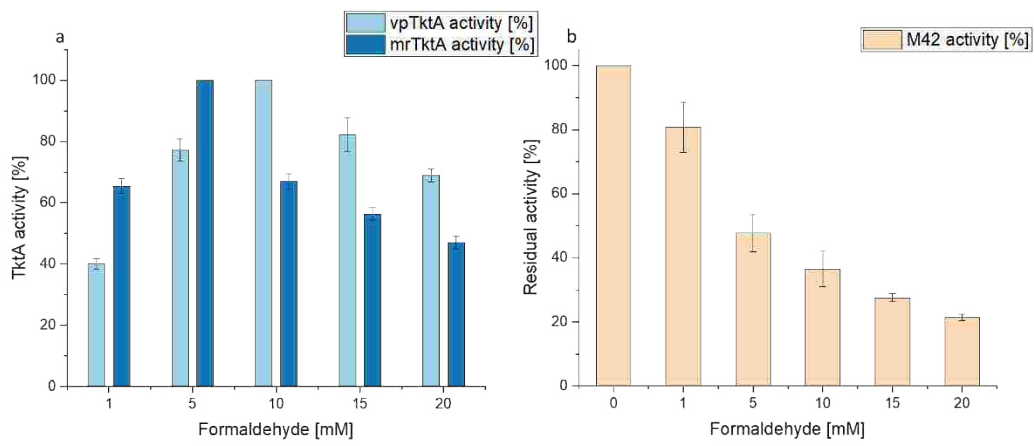


Figure S3: a: Activity of vpTktA and mrTktA with a fixed concentration of 5 mM xylulose and 1 to 20 mM formaldehyde. b: Activity of M42 (coupling enzyme of transketolase) on 1 mM glyceraldehyde with increasing amounts of formaldehyde ($n = 3$).

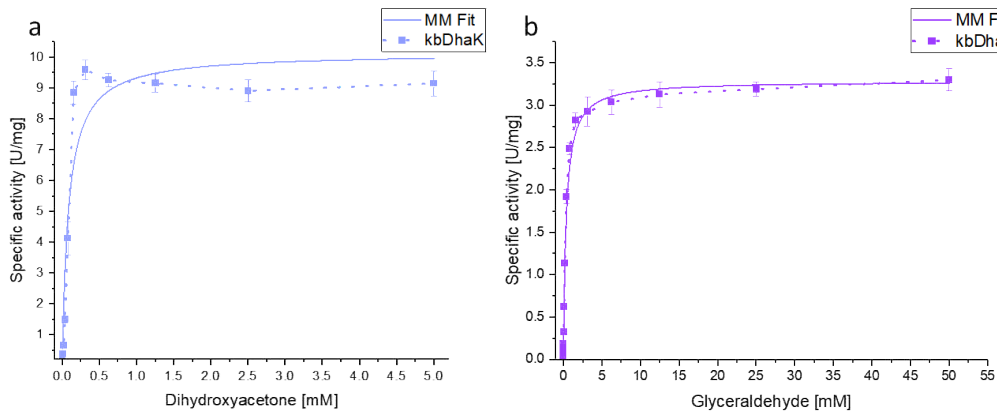


Figure S4: Kinetic of kbDhaK on dihydroxyacetone (a) and glyceraldehyde (b) ($n = 3$).

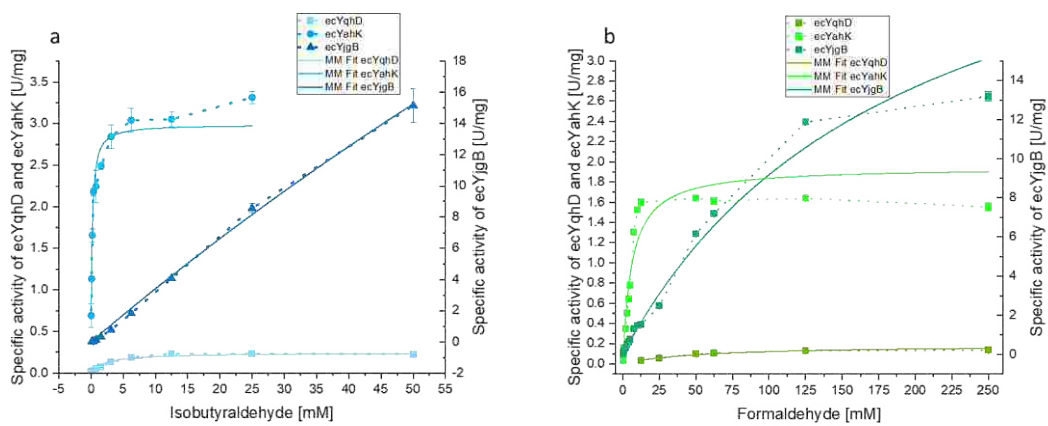


Figure S5: Kinetics of three different ADHs on isobutyraldehyde and formaldehyde including Michaelis Menten (MM) fit. a: Kinetics with isobutyraldehyde. b: Kinetics with formaldehyde ($n = 3$).

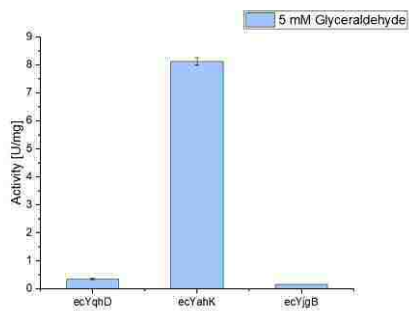


Figure S6: Activity of *ecYqhD*, *ecYahK* and *ecYjgB* on glyceraldehyde ($n = 2$).

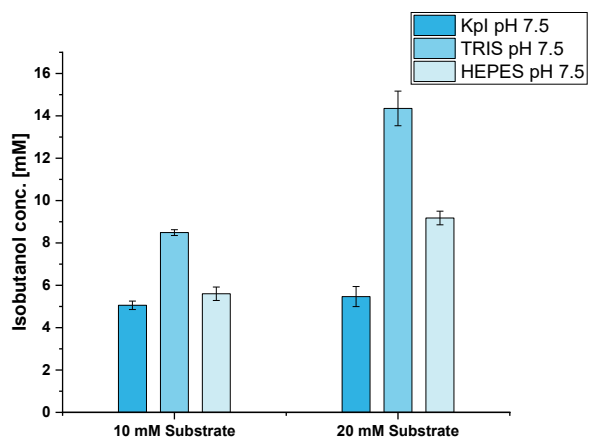


Figure S7: Isobutanol production in various buffer systems at pH 7.5, 37°C. Samples were taken after 12 h of incubation ($n = 3$).

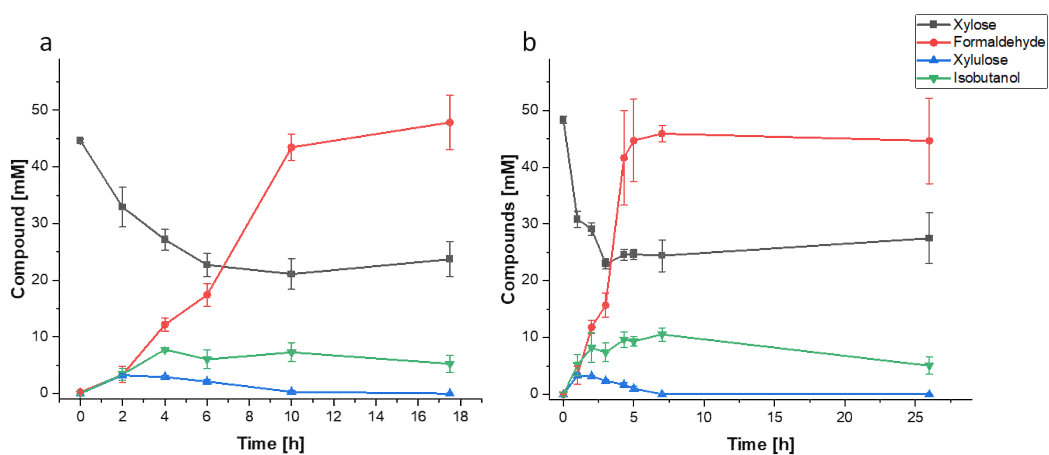


Figure S8: Time curves of isobutanol production via mechanical formaldehyde supply using micro syringe pumps. Concentrations were adjusted to the increasing volume ($n = 3$). a: Application of 10 $\mu\text{l/h}$ of formaldehyde (100 mM), with stop of application of formaldehyde after 10 h. b: Application of 20 $\mu\text{l/h}$ of formaldehyde (100 mM), with stop of application of formaldehyde after 5 h.

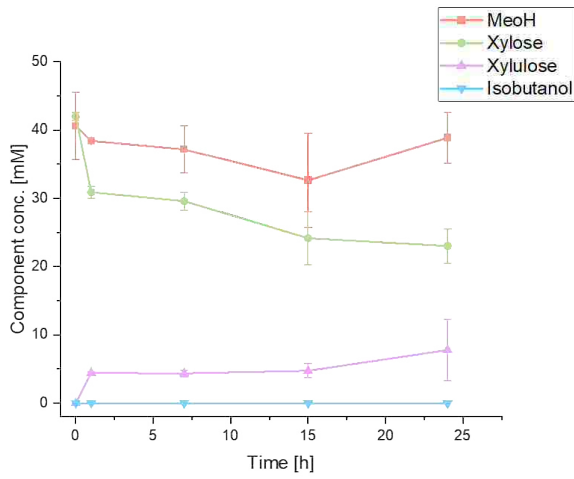


Figure S9: Final isobutanol cascade control experiment without alcohol oxidase and transketolase (n = 3).

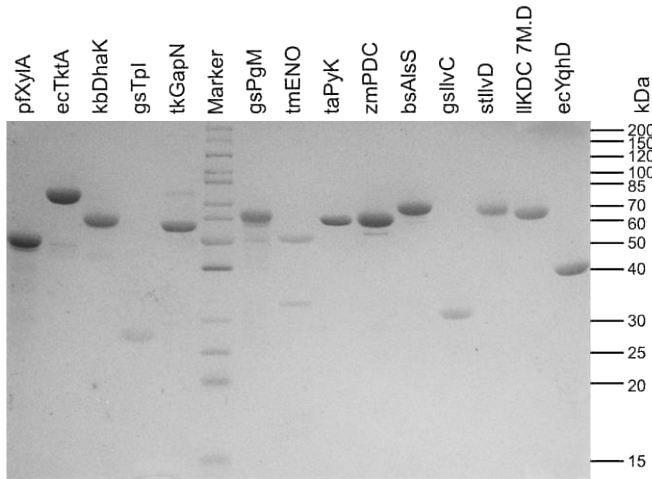


Figure S10: SDS-gel of purified cascade enzymes. PageRuler™ unstained protein ladder (ThermoFisher Scientific) was used as marker.

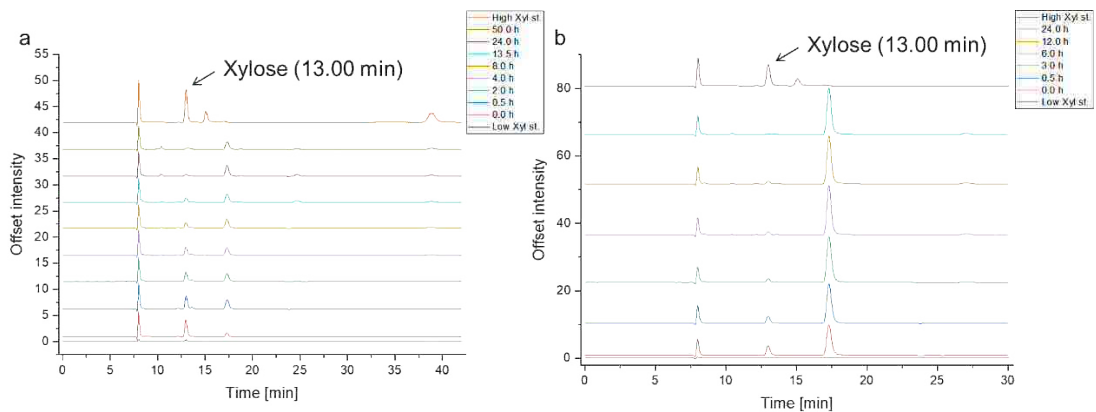


Figure S11: HPLC chromatograms of the final enzyme cascade with time points and high and low standards for xylose. a: Xylose degradation in isobutanol cascade. b: Xylose degradation in ethanol cascade.

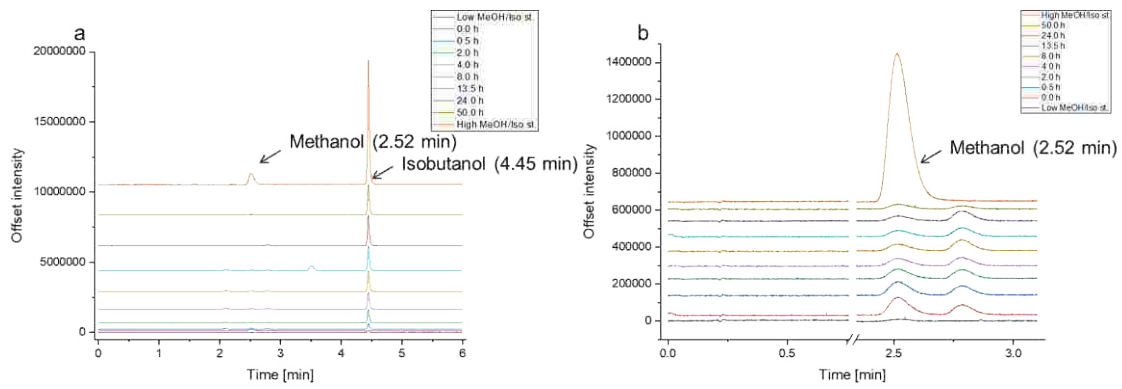


Figure S12: GC-FID chromatograms of the final enzyme isobutanol cascade with time points and high and low standards for methanol and isobutanol. a: Methanol degradation and isobutanol production. b: Zoom on methanol degradation.

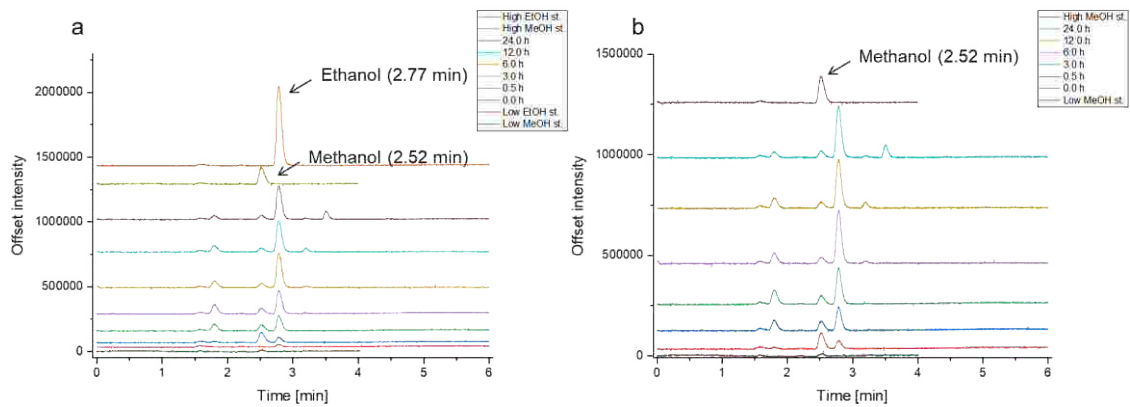


Figure S13: GC-FID chromatograms of the final enzyme ethanol cascade with time points and high and low standards for methanol and ethanol. a: Methanol degradation and ethanol production. b: Zoom on methanol degradation.

Supplemental references and notes

- [1] J. K. Guterl, D. Garbe, J. Carsten, F. Steffler, B. Sommer, S. Reißer, A. Philipp, M. Haack, B. Rühmann, A. Koltermann, *ChemSusChem* **2012**, 5, 2165-2172.
- [2] S. Sutiono, M. Teshima, B. Beer, G. Schenk, V. Sieber, *ACS Catal.* **2020**, 10, 3110-3118.
- [3] D. Gocke, C. L. Nguyen, M. Pohl, T. Stillger, L. Walter, M. Müller, *Adv. Synth. Catal.* **2007**, 349, 1425-1435.
- [4] S. Sutiono, J. Carsten, V. Sieber, *ChemSusChem* **2018**, 11, 3335-3344.
- [5] A. Pick, B. Rühmann, J. Schmid, V. Sieber, *Appl. Microbiol. Biotechnol.* **2013**, 97, 5815-5824.

Cell-free enzymatic L-alanine synthesis from green methanol

Vivian Pascal Willers, Manuel Döring, Barbara Beer, Volker Sieber

Chem Catalysis

Volume 3, March 2023, 100502

DOI: <https://doi.org/10.1016/j.checat.2022.100502>

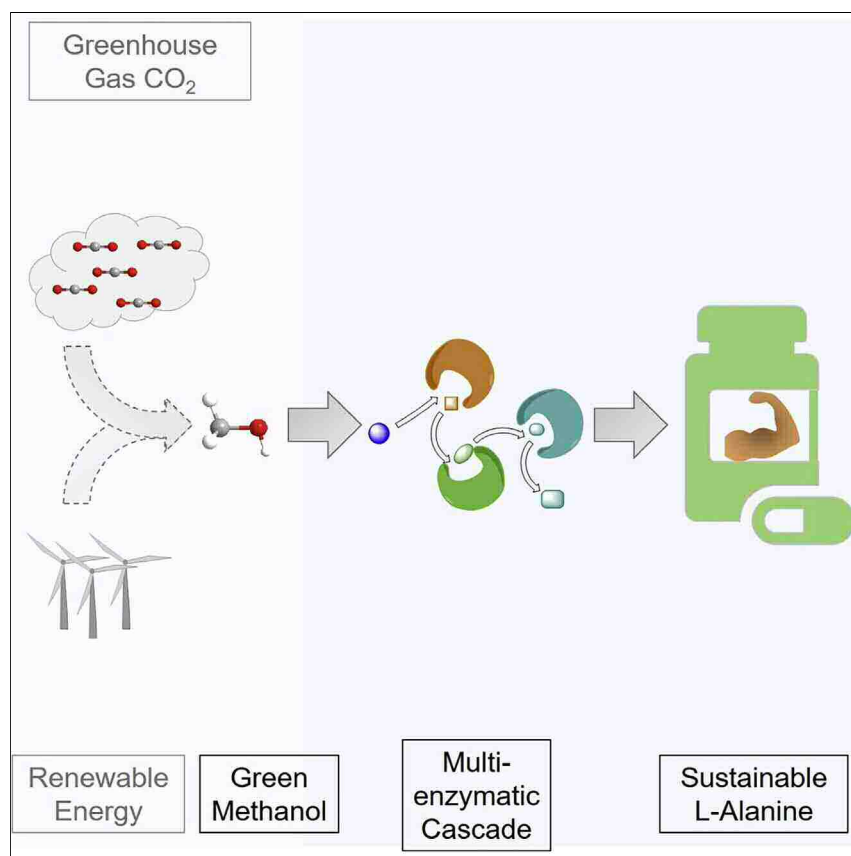
© 2023 Elsevier Inc.

Journal Author Rights

Please note that, as the author of this Elsevier article, you retain the right to include it in a thesis or dissertation, provided it is not published commercially. Permission is not required, but please ensure that you reference the journal as the original source. For more information on this and on your other retained rights, please visit: <https://www.elsevier.com/about/our-business/policies/copyright#Author-rights>

Article

Cell-free enzymatic L-alanine synthesis from green methanol



Vivian Pascal Willers, Manuel Döring, Barbara Beer, Volker Sieber

sieber@tum.de

Highlights

Cofactor-neutral pathway from methanol to L-alanine

Efficient L-alanine production with 90% conversion of methanol to L-alanine

High titer of 3.9 g L^{-1} L-alanine from 4.8 g L^{-1} methanol

Characterization of cascade enzymes in terms of kinetics and inactivation

Willers and coworkers successfully constructed a cofactor-neutral, cell-free enzymatic pathway for the production of the amino acid L-alanine via 9 steps. To gain control of the cascade, enzymes were characterized according to their kinetics and behavior by the addition of harmful formaldehyde and methanol. After generating a balanced interplay between all enzymes, highly efficient methanol conversion to L-alanine with 90% yield could be achieved. After a final reaction optimization 3.9 g L^{-1} L-alanine could be produced from 4.8 g L^{-1} methanol.



Willers et al., Chem Catalysis 3, 100502
 February 16, 2023 © 2023 Elsevier Inc.
<https://doi.org/10.1016/j.cheecat.2022.100502>



Article

Cell-free enzymatic L-alanine synthesis from green methanol

Vivian Pascal Willers,¹ Manuel Döring,¹ Barbara Beer,^{1,4} and Volker Sieber^{1,2,3,5,*}

SUMMARY

Amino acid production today is by far mostly done for feeding livestock for animal protein production or as a direct food additive. Nowadays, amino acid production relies mostly on fermentation of sugars, and the amino acid market for 2022 is estimated to reach ten million tons with over \$13 billion USD market value. However, to make amino acid production more sustainable and ecologically viable, alternative resources and waste streams have to be considered. To contribute to a sustainable future vision, here we show a synthetic methanol alanine pathway (MAP) as a cell-free enzymatic cascade. The pathway consists of nine enzymes with an intrinsic cofactor recycling system and produces L-alanine from methanol with a maximum of 90% theoretical yield. Due to the increasing possibilities of sustainably producing methanol from CO₂, this study paves the way to C1 building-block-based amino acid synthesis at reduced environmental burden.

INTRODUCTION

In recent years, the shortage of fossil raw materials and climate change and global warming have led to a rethink of how we generate energy and treat our environment.¹ An important goal for the next decades is to drastically reduce emissions in order to achieve climate targets and prevent global warming.² However, with energy demand on the rise, we need to develop smart, environmentally friendly alternatives and sustainable recycling systems to keep pace with this consumption.³

CO₂ emissions are one of the main causes of the greenhouse effect and are produced, for example, by the combustion of various carbon-containing materials such as coal, diesel, gasoline, natural gas, wood, or liquefied petroleum gas.⁴ Since 1990, the global-energy-related CO₂ emission has increased by 1.6 times, and in 2021, it reached 33 Gt.⁵

To develop pathways for CO₂ reduction and assimilation, various research groups have proposed electrochemical, photocatalytic, or thermochemical approaches to ensure the conversion of CO₂ into useful chemicals.^{6–8} In addition to the applications mentioned above, biological pathways are also coming into focus.^{9–12} In particular, artificial enzyme cascades with mild, environmentally friendly experimental conditions are attracting attention to reduce CO₂ to hydrocarbons, like methanol (MeOH), formaldehyde (FALD), or format.^{13–15} Furthest developed is the production of MeOH from CO₂ and renewable hydrogen using heterogeneous catalysis,^{16,17} with several industrial plants having been constructed over the last year, offering MeOH as an easy option to store and transport raw material and feedstock.¹⁸

THE BIGGER PICTURE

Mitigating climate change is rightly regarded as one of humankind's most important challenges of our time. Therefore, CO₂ capture and usage as a source for the production of energy, chemicals, and fuels will be prominent in the future. With power-to-X technologies, converting CO₂ to methanol using green energy takes the sustainable value of CO₂-derived methanol and availability to a new level. For the valorization of methanol, we established a multi-enzymatic cascade using ten enzymes to produce the amino acid L-alanine. Fueled by the increasing world population, rising meat consumption, and utilization of agricultural products, in the shadow of global warming, a second dramatic event is taking place: the immense and, in its speed, further accelerating loss of biodiversity and mass extinction of species. By simultaneously reducing CO₂ and producing L-alanine via the key intermediate pyruvate, this case study could lead to and contribute to the synthesis of various amino acids from CO₂.



Table 1. Comparison of MAP with other synthetic C1-utilization pathways

Pathway	C1-condensing enzyme	Substrate	Product	Titer (g L ⁻¹)	Reaction steps	Source
MAP 2.0	FLSM3	methanol	L-alanine	3.9	9	this study
ASAP 3.1	FLSM3	CO ₂	amylopectin	1.3	11	Cai ²³
	FLS_A3	formaldehyde	erythrose	24.6	2	Güner ²⁴
	GALS	methanol	ethylene glycol, glycolic acid, D-erythrose	0.90, 0.33, 0.05	4	Zhou ²⁵
CETCH 5.4	ECRs	NaHCO ₃	glyoxylate	0.040	13	Schwander ²⁶

In recent years, highly challenging C1 chemistry in *in vivo* and *in vitro* biocatalysis is becoming increasingly important for the production of building blocks, drugs, and other higher-molecular-weight products.^{19–21} To take advantage of these C1 compounds produced from CO₂, enzymes that are able to combine these molecules selectively are of high interest. Siegel and coworkers designed an artificial enzyme based on benzaldehyde lyase called formolase, which is capable of catalyzing a carbonylation from FALD to dihydroxyacetone (DHA).²² Despite others, these carbon-ligating enzymes pave the way for building complex molecules from C1 compounds (Table 1).

In a benchmark publication recently, Cai and coworkers²³ succeeded in producing starch from CO₂-derived MeOH via FALD as an intermediate based on the formolase (FLS) reaction. We were wondering whether the direct production of not only starch, as one of the major macronutrients, but also of amino acids from MeOH was possible.

Along with the challenges to tackle climate change mentioned above, another issue of the future will be the growing population and the concomitant question of how we can provide sufficient amounts of protein in line with a reduction of greenhouse gases.²⁷ Estimations show that the demand for animal protein will increase by almost 50% in 2050. However, animal foods produce more greenhouse gases, so alternative sources have to take their place.²⁸

In this work, we would like to envision the power of C1-based production of amino acids as an alternative artificial protein source with L-alanine as a case study. We have designed an enzymatic one-pot cascade for the direct conversion of MeOH to L-alanine (Scheme 1). In our proof of concept, we first addressed the interplay between enzymes and applied conditions. After gaining sufficient flux through the cascade, we could produce 18 mM L-alanine with a theoretical yield of 90% from 60 mM MeOH. A further upscaling with 150 mM MeOH resulted in a final titer of 3.9 g L⁻¹ L-alanine corresponding to 88% theoretical yield.

The MeOH to alanine pathway (MAP) builds on the enormous potential of the FLS reaction and FALD as an intermediate combined with an artificial lower glycolysis. Despite the uniqueness of the FLS reaction, this study also highlights aspects of the enzyme that need to be improved and addressed in the future for further upscaling.

RESULTS AND DISCUSSION

For the development of the MAP, we first considered the steps that are necessary to create a pathway from MeOH to L-alanine. To build the required C3 scaffold, we synthesize DHA from MeOH via alcohol oxidase of *Pichia pastoris* (ppAOX) and FLS.²³ DHA is then directly converted to L-alanine by seven additional steps with intrinsic

¹Chair of Chemistry of Biogenic Resources, Technical University of Munich; Campus Straubing, 94315 Straubing, Germany

²SynBioFoundry@TUM, Technical University of Munich, 94315 Straubing, Germany

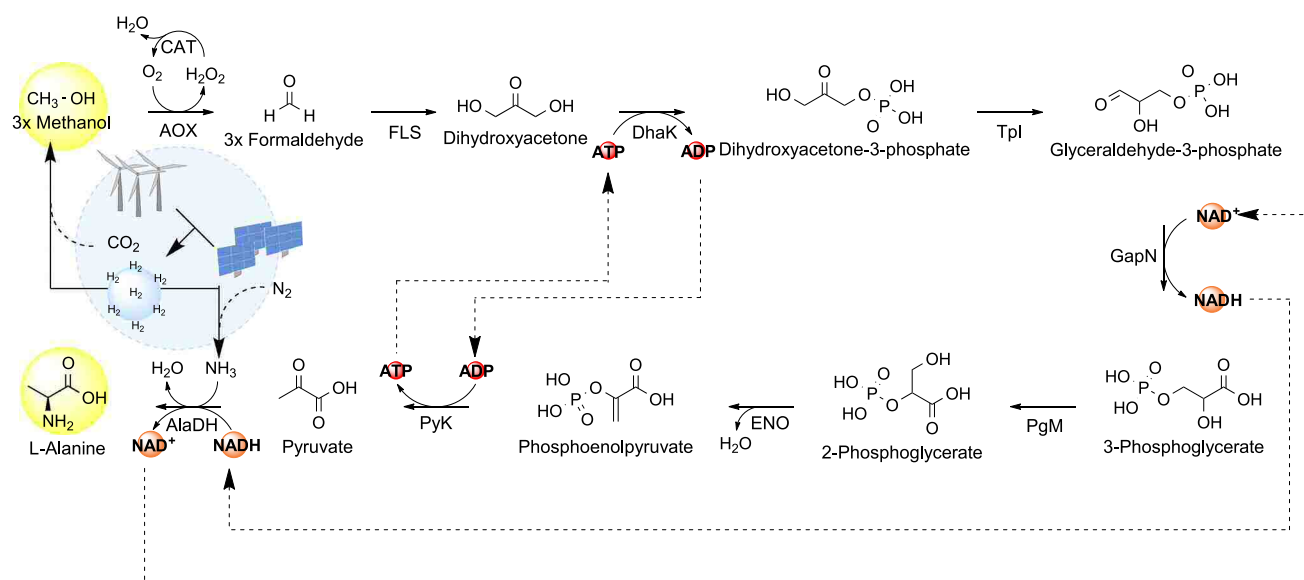
³School of Chemistry and Molecular Biosciences, The University of Queensland, St. Lucia, QLD 4072, Australia

⁴Present address: CASCAT GmbH, 94315 Straubing, Germany

⁵Lead contact

*Correspondence: sieber@tum.de

<https://doi.org/10.1016/j.checat.2022.100502>



Scheme 1. Methanol to alanine pathway (MAP)

ATP and NAD^+ regeneration system based on the interaction between dihydroxyacetone kinase (DhaK) and pyruvate kinase (PyK) as well as glyceraldehyde-3-phosphate dehydrogenase (GapN) and alanine dehydrogenase (AlaDH) with visions for the production of methanol and ammonia with hydrogen using green, sustainable energy.

ATP and NAD^+ regeneration by combining an artificial lower glycolysis with an alanine dehydrogenase.^{29,30} Thereby, we took care to couple reactions involving the reflux of intermediates away from the target product L-alanine with strong pulling reactions to ensure flux from MeOH to L-alanine. Due to the cascade design with FALD formation and L-alanine production using ammonia, we have to consider that undesired side reactions between FALD, ammonia, and DHA or L-alanine may occur.³¹ Together with that, enzymes have to tolerate MeOH, a highly denaturing solvent, as well as FALD, a highly reactive reagent.^{32,33} Because of these challenges, we used a mixture of enzymes derived from thermophilic and mesophilic organisms in order to find a compromise between a high level of stability and activity (Figure S1; Table S1). Enzymes from thermophilic organisms have often been seen to tolerate such denaturants to a higher extent due to their naturally higher thermodynamic stability.³⁴ On the other hand, enzymes have to possess sufficient activity at lower temperatures, which is often not found in those of thermophilic origin.³⁵ In addition, factors such as activity at a neutral pH and identical cofactor specificity have to be considered. Based on these factors, we selected enzymes that have been previously characterized and shown to have activity at lower temperatures and neutral pH.^{29,36–39} To not imbalance the ATP/ADP ratio, we used a non-phosphorylating glyceraldehyde-3-phosphate dehydrogenase (GapN). This previously described⁴⁰ GapN is able to convert glyceraldehyde-3-phosphate to 3-phosphoglycerate by reduction of NAD^+ to be compatible with the alanine dehydrogenase, which is restricted to NADH as a cofactor.

Cascade design and initial assembly

For the initial design of the cascade and to point out thermodynamically unfavorable reactions, we used the eEquilibrator pathway analysis tool.⁴¹ This allowed us to simulate the thermodynamic profile of the cascade (Figure S2; Table S2) and to assess whether the metabolic pathway is thermodynamically feasible. Here, the max-min driving force (MDF) is a measure of the thermodynamic differences in a system

with optimized metabolite concentrations and can be considered for comparing different pathways in terms of their driving force.^{41,42} Subjecting the MAP pathway to the MDF analysis resulted in a total MDF of 11 kJ mol⁻¹, which is similar to the naturally modified Embden-Meyerhof pathway with an MDF also around 11 kJ mol⁻¹.⁴² This high MDF corresponds to a flux efficiency of >95%, implying a high net reaction rate and almost no backward flux in the pathway.⁴² In addition, the similar MDF shows that starting from MeOH is similarly effective as starting from glucose without any loss in its flux.

With the knowledge that the compensation of thermodynamically unfavorable reactions with favorable reactions results in a strong thermodynamic drive to L-alanine, we next focused on the interplay of the selected enzymes with key cascade compounds, intermediates, and cofactors. Therefore, we first determined the kinetics of the cascade enzymes and activity on low substrate concentrations (Tables S4 and S5) to get a picture of kinetic properties and possible bottleneck reactions.

By measuring the kinetics, we found a high fluctuation of the turnover number from 0.15 s⁻¹ for FLS²³ to 154.1 s⁻¹ for gsTpi. The affinities for the substrates are generally high, with “K_m” values in the low mM or even μM range (from 3.6 mM for gsTpi to 30 μM for kbDhaK). The exception to this is FLS with a K_m of 34.14 mM toward FALD. With the knowledge of the forward kinetics of all cascade enzymes, we balanced the activity and adjusted it to the low activity of FLS. To gain a sufficient turnover rate, the FLS concentration was extensively increased. In contrast, the ppAOX concentration was minimized to avoid generating high amounts of toxic FALD. All other enzymes were adjusted to the FLS concentration to ensure a constant flux through the cascade.

However, on the first try, we only detected 2 mM L-alanine from 20 mM MeOH after 20 h. Nevertheless, production was significant, as we did not detect any L-alanine in control experiments without AOX.

The interplay between enzymes in cascade conditions

Due to the low theoretical yield on the first try, we took one step back and focused more closely on the enzymes of the lower glycolysis part. Here, we noticed that the activities of most of the enzymes depend on magnesium (Mg²⁺). However, phosphoglycerate mutase from *Geobacillus stearothermophilus* (gsPgM) is dependent on manganese (Mn²⁺).⁴³ We tested the effects of Mn²⁺ ions on the activity of other cascade enzymes and found a strong reduction in kbDhaK and taPyK activities with a raising Mn²⁺ concentration (Figure S3). We found that half-maximal inhibition occurs at Mn²⁺ concentrations of 0.2 mM for kbDhaK and 1.2 mM for taPyK. In contrast, 0.1 mM Mn²⁺ is required to generate half-maximal activity of gsPgM. Because of the different effects of Mn²⁺ on the cascade enzymes, we decided to find a compromise between Mn²⁺-induced inhibition of taPyK and kbDhaK and activation of gsPgM.

By setting the Mn²⁺ concentration to 0.1 mM, we were able to produce a theoretical yield of 75% L-alanine based on 20 mM DHA.

Because ATP/ADP are regulatory cofactors, we tested whether different ATP/ADP concentrations have a negative influence on the kinases present in the cascade (Figure S3). Indeed, both kinases showed reduced activity at relevant concentrations. The half-maximal inhibition of kbDhaK occurs at 1.6 mM ATP. In contrast, taPyK activity was reduced by only 10% at 1 mM ATP. Because ADP has a stronger effect on kbDhaK than ATP on taPyK at relevant concentrations of 1 mM, we decided to

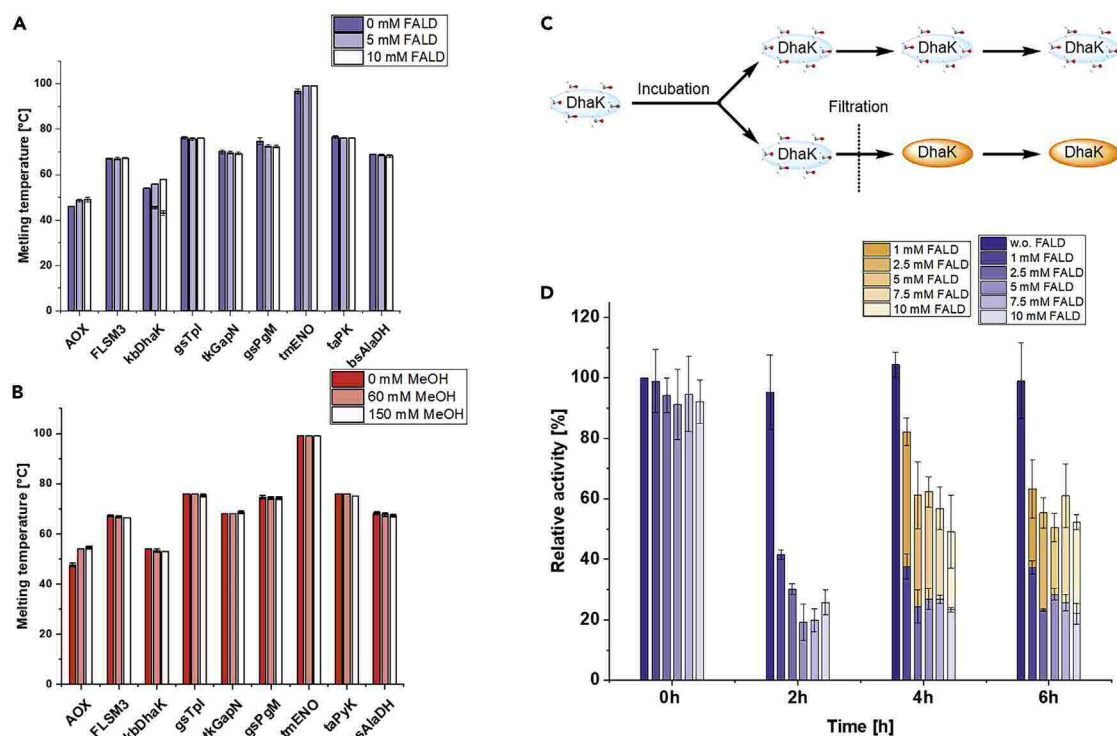


Figure 1. Thermal stability analysis of cascade enzymes with additional formaldehyde and methanol and long-term stability analysis of DhaK (kbDhaK)

(A) Melting-point analysis of cascade enzymes incubated at various formaldehyde concentrations using thermofluor. The additional lower bars superposed on the others indicate second melting temperatures with 5 and 10 mM formaldehyde (kbDhaK). Reactions were performed in triplicate ($n = 3$). Error bars represent SD.

(B) Melting-point analyses of cascade enzymes using thermofluor. Enzymes were incubated at various methanol concentrations mirroring substrate concentrations in the cascade. Reactions were performed in triplicate ($n = 3$). Error bars represent SD.

(C) Scheme of kinetic stability analysis of kbDhaK with formaldehyde incubation and with filtration of the enzyme to remove formaldehyde.

(D) Relative activity of kbDhaK after incubation with different concentrations of formaldehyde (0–10 mM) in blue. Orange bars indicate the relative activity of kbDhaK after filtration of the enzyme and removal of formaldehyde. After filtration, kbDhaK was rediluted in buffer without formaldehyde. Reactions were performed in triplicate ($n = 3$) and analyzed as described in the supplemental experimental procedures. Error bars represent SD.

change the concentrations of kbDhaK and taPyK to have a dominant taPyK that rapidly converts emerging ADP to ATP to keep kbDhaK active. By adjusting the concentrations of kbDhaK and taPyK to fulfill the previously proposed theory (Table S3), we achieved >90% conversion of DHA to L-alanine (Table 1; Figure S4).

After gaining control over the artificial lower glycolysis, we moved on to the full cascade from MeOH to L-alanine. Here, our focus first relied on the major influence of MeOH and FALD on all cascade enzymes. Toxic compounds such as FALD and MeOH might have a strong effect on the stability of the enzymes present, which could cause retardation of the cascade when accumulated.^{31,44} We matched the concentrations of ppAOX and FLS to avoid high transient FALD concentrations in the system. However, we were able to produce only 7 mM L-alanine based on 60 mM MeOH, corresponding to a theoretical yield of 35% (Figure S4).

Effects of MeOH and FALD on cascade enzymes

To determine the effect of different MeOH and FALD concentrations on the stability of the enzymes, we performed a thermofluor analysis to determine the melting point as a measure of the thermal stability of the enzymes (Figure 1). To simulate the conditions of the cascade as closely as possible, we used an environment similar to the

cascade with different MeOH and FALD concentrations. We expected these concentrations based on the high K_m difference of ppAOX and FLS in the cascade (K_m of 1.4 mM of AOX for MeOH,⁴⁵ K_m of FLS for FALD of 34.14 mM).²³

Fortunately, we could not observe a strong shift in the melting temperature of the enzymes incubated with MeOH (Figure S5). Upon incubation with FALD, most enzymes also were unaffected; however, the melting temperature of kbDhaK showed abnormal behavior. We observed a splitting of the signals at 5 mM FALD into a strong one at around 46°C and a weaker one at around 56°C. With 10 mM FALD (Figure S6), this splitting increased even further. To test if this behavior has an influence on the activity, we incubated kbDhaK with and without FALD over a period of 6 h and determined the residual activity. Here, we observed that already low concentrations of FALD severely decrease enzyme activity. With a concentration of 1 mM FALD, activity decreased to ~45% after 2 h. With 10 mM FALD, this effect is even stronger, and the enzyme lost nearly 75% activity after 2 h of incubation (Figure 1). However, comparing this FALD-induced inactivation with the DHA kinase used by Cai and coworkers,²³ kbDhaK appears to be less sensitive, as ppDhaK immediately loses 60% activity in the presence of 10 mM FALD, whereas kbDhaK loses only 10% activity. In addition, the strength of kbDhaK became apparent when FALD was removed from the solution. After a short incubation, kbDhaK restored 60% of the activity, attenuating the strong inactivation. Because the removal of FALD restored parts of the activity of kbDhaK, we speculated that FALD has not only a toxicity effect on kbDhaK but also acts as a reversible inhibitor. This effect of FALD is rather rare, and normally, the property of FALD to crosslink enzymes and have irreversible effects are more in focus. However, Wait and coworkers observed a similar effect of formal FALD dehyde while investigating hydrogenases and stated that FALD binds to highly conserved lysine and cysteine residues, involved in the catalytic process, as a removable Schiff base or thioacetal, respectively.⁴⁶ By altering the catalytic site by exchanging potential attacking points of FALD, we could possibly lower the inhibition of FALD to kbDhaK. This would lead to an improved flux in the cascade by strengthening the connection between primary C1 utilization and lower glycolysis. However, further studies have to be done, involving the elucidation of the structure of kbDhaK, to verify a similar behavior of FALD to kbDhaK as to hydrogenases. Nevertheless, we could not restore the full activity of kbDhaK, confirming the irreversible toxic effect of FALD.

Together with kbDhaK, we tested the effect of different FALD and MeOH concentrations (Figure S7) on the activity of all other enzymes to compare the temperature stability with the activity. Here, most of the enzymes were rather unaffected by MeOH concentrations of 60 and 150 mM. However, FALD concentrations of 5 and 10 mM have a negative effect on the activity of several enzymes, reducing their activity by 5%–10%. Nevertheless, this loss of activity is small compared with kbDhaK. Surprisingly, tkGapN lost around 50% activity with the addition of 10 mM FALD. This loss in activity seems not to be related to thermal stability because the melting temperature is unaffected by FALD.

Based on the stability and activity data, we started to rebuild the cascade using various concentrations of the most affected enzymes kbDhaK and tkGapN. After increasing kbDhaK concentration (Table S3), we converted 60 mM MeOH into 15 mM L-alanine after 24 h (theoretical yield of 75%) (Figure S4).

With this high theoretical yield, we kept our enzymes constant and increased the amount of MeOH from 60 to 90 and 150 mM to see how far we could go in this setup.

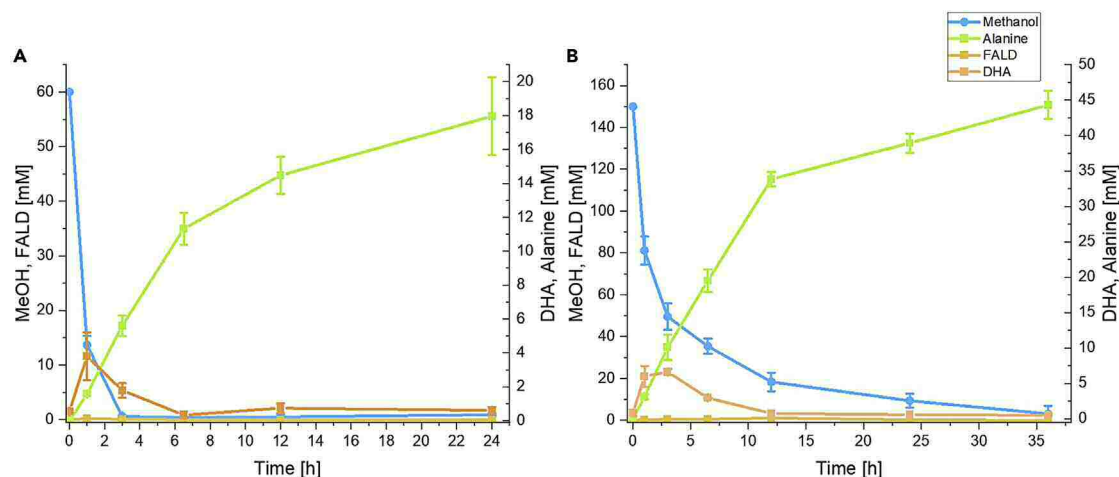


Figure 2. MAP 2.0 with optimized enzyme load and conditions

(A) Time course of L-alanine production with 60 mM methanol as substrate concentration. Reactions were performed in triplicate ($n = 3$) and analyzed as described in the methods. Concentrations of all compounds were corrected for evaporation. Therefore, all concentrations were adjusted to variations of the HEPES buffer (Figure S9). Error bars represent SD.

(B) Time course of L-alanine production with 150 mM substrate concentrations. The 0 h sample represents the initial weighed concentration of the preparation. Reactions were performed in triplicate ($n = 3$) and analyzed as described in the methods. Concentrations of all compounds were corrected for evaporation. Therefore, all concentrations were adjusted to variations of the HEPES buffer (Figure S9). Error bars represent SD.

Initially, all three specimens behaved similarly with L-alanine production rates of around 2.7 mM h^{-1} , and only the sample with 150 mM MeOH had a lower rate of 2.3 mM h^{-1} in the first 4 h. Still, we detected 21 and 25 mM L-alanine from 90 to 150 mM MeOH (Figure S8).

Further optimization and final cascade

To further optimize the yield of the cascade, we used FLSM3 reported by Cai and coworkers, which has a reduced K_m for FALD (23.59 mM) and an optimized DHA-to-glycolaldehyde ratio.²³ In addition, we observed a strong shift in melting temperature of 11°C from 56°C of FLS to 67°C of FLSM3. This higher melting temperature leads not only to increased thermostability but also possibly to a longer half-life under the reaction conditions.

By applying adjusted FLSM3 and the artificial lower glycolysis enzymes to the cascade (Table S3), we were surprisingly able to detect amounts of L-alanine that corresponded to a theoretical yield of over 100%. We noted, though, that the reaction volume was lower than expected, suggesting evaporation. To gain insight into the extent of evaporation during the cascade run and to correct the determined titers and yields, we measured compounds, whose concentrations should stay constant during the cascade run time. We decided to measure the HEPES buffer of the samples and corrected the titers of all measured cascade compounds accordingly to counteract overestimation (Figure S9). After correction, we found that after 24 h of incubation, 18 mM L-alanine from 60 mM MeOH corresponding to 90% theoretical yield was produced (Figure 2). With this success, we again tackled the conversion of 150 mM MeOH, but this time, we additionally improved the oxygen supply by incubating the reaction vessel with oxygen before adding the enzymes and substrate solution.

Using this setup, we were able to produce 44 mM L-alanine from 150 mM MeOH. This corresponds to a theoretical yield of 88% after 36 h (Figure 2). Initially, we

converted MeOH at a high rate of 46 mM h^{-1} at a 60 mM initial concentration and 69 mM h^{-1} at a 150 mM initial concentration. We could observe a similar trend by L-alanine formation with initial rates of 1.6 and 3.1 mM h^{-1} (Figure S8), respectively. We were surprised to find that MeOH conversion is faster at higher MeOH concentrations, even though both concentrations are well above the actual K_m of ppAOX for MeOH. We assumed that this might be due to a beneficial effect of incubation with oxygen before initiation counteracting the oxygen-induced increased K_m of ppAOX relative to oxygen. Still, the L-alanine production rate was lower than the MeOH consumption rate, indicating partial accumulation of intermediates. Since all intermediates except FALD and DHA are restricted by ATP and NAD^+ concentrations, we focused on these two intermediates and monitored FALD and DHA titers. Indeed, we observed an accumulation of DHA in both cascades. With 60 mM MeOH, 4 mM DHA was observed after 1 h. For the 150 mM batch, a maximum of 7 mM DHA was detected after 3 h. However, FALD titers were kept low in both cases. These results indicated a partial imbalance in the flux of the cascade. However, with a declining MeOH consumption rate, the accumulation was dissolved. In addition, we observed a yellowish coloration of the samples during the first 6 h of the cascade, possibly due to the interaction of FALD with ammonium or DHA. Surprisingly, this coloration fades after 6 h again.

Overall, after 24 h, we were able to generate 18 mM L-alanine from 60 mM MeOH with a carbon balance of 94%. After upscaling, we were able to generate 44 mM L-alanine from 150 mM MeOH with a carbon balance of 92%. We assume that this slight decrease in carbon balance is partly due to the evaporation of MeOH because the system is not entirely gas tight. By measuring MeOH in a control experiment without the addition of ppAOX and FLS, the MeOH concentration decreased over time, pointing out evaporation (Figure S10).

However, possible interactions of the FALD with, e.g., DHA or ammonium may also account for the loss. In addition, due to the limitation of ATP and NAD^+ , 4% of the carbon could still be present as an intermediate of lower glycolysis.

After the successful proof of concept, we started to think about the scope of L-alanine synthesis and its extension to other amino acids or platform chemicals. As pyruvate is a central metabolite, a variety of platform chemicals such as ethanol, lactate 2,3-butanediol, or isobutanol,^{47–49} but also essential amino acids such as valine,⁵⁰ could be produced in a cofactor-neutral manner. When considering the intermediate steps of the cascade, other amino acids such as serine or glycine could also be produced in a cofactor-neutral manner. However, it remains to be seen to what extent the additional enzymes influence the equilibrium in the cascade and whether they are compatible with the cascade in terms of side reactions and inhibition.

In order to further advance L-alanine production, several issues need to be addressed to achieve higher titers, scale, and economic feasibility. One of the major bottlenecks is certainly the low activity of some enzymes, especially FLS. However, FLS does not appear to be the rate-limiting enzyme in this cascade due to the accumulation of DHA. Nevertheless, the amount of enzyme used to generate this flux to DHA is not feasible in further upscaling approaches. Enzyme engineering has proven to be a powerful tool for stabilizing enzymes and increasing their activity. While the FLSM3 variant developed by Cai and coworkers offered an advantage of 31% lower K_m and 40% higher k_{cat} , as well as an optimized intermediate ratio of DHA to glycolaldehyde, additional improvements are needed to further raise affinity and

activity. Likewise, tkGapN, the non-phosphorylating GapN, which still prefers NADP⁺ instead of NAD⁺ as a cofactor, can be engineered for a changed cofactor dependence.²⁹

Nevertheless, despite these bottlenecks, the cell-free enzymatic L-alanine synthesis from MeOH holds several advantages to traditional and described L-alanine synthesis routes.

Today, L-alanine synthesis is mainly based on the synthesis of environmentally harmful petroleum-based L-aspartic acid or on the fermentation of glucose. Although high titers of up to 121 g L⁻¹ can be obtained from the fermentation of glucose with 0.88 g L-alanine/g glucose, one problem is that various by-products are formed due to pyruvate as an intermediate. In addition, L-alanine can also inhibit cell growth, which leads to problems during upscaling.⁵¹ In addition to fermentation, cell-free enzymatic pathways also tackle the production of L-alanine from glucose. Despite the promising concept of a minimized reaction cascade with lower cofactor requirements, the final titer of L-alanine and its efficiency is rather low with 29 mM L-alanine from 25 mM glucose.³⁰ A key fact is that apart from the production of L-alanine from L-aspartic acid, its production is mainly based on glucose. However, alternative carbon sources derived from different waste streams need to be also taken into account to avoid food versus chemicals issues. As an alternative to L-alanine derived from glucose, the production of L-alanine from MeOH may be of great interest. Our cascade not only efficiently converts an alternative carbon source into L-alanine but can also help reduce a climate-damaging waste stream, as MeOH can be derived from CO₂.

The cell-free character also has advantages such as lower cytotoxicity effects, no membrane-limited mass transport, and high controllability in contrast to fermentation. Since the cascade is constructed as a one-pot system, there is no need to isolate intermediates, no toxic or non-toxic by-products are generated, and intermediates are controlled by cofactors. Together with that, a direct conversion from the substrate to the product is achieved.

Conclusion

With the advent of multi-enzyme cascades, there is an ongoing debate about their benefits compared with fermentative approaches. In the special case of C1 utilization via MeOH and FALD, the advantage of the former becomes clear as both molecules are highly toxic. Modifying living cells to withstand higher concentrations of FALD is much more difficult than tuning enzymes for a cell-free system. By simply increasing the concentration of C1-utilizing enzymes, toxic intermediates can be suppressed. In addition, the replacement of the target enzymes, either with more stable homologs or with engineered enzyme variants, provides a rapid and adaptable process for overcoming toxicity caused by substrates and intermediates.

To slow down the ongoing loss of biodiversity due to the increasing exploitation of terrestrial and marine habitats, and to stop it in the future, we need alternative ways to provide the basic essential classes of macronutrients. One possible approach is based on the idea of synthetic nutrition, where all essential nutrients can be produced artificially, efficiently, and with a small footprint. This principle of efficient food delivery is already being applied in astronaut nutrition, where foods with the lowest energy and space requirements and the longest shelf life are needed. Since one of the most important nutrients is amino acids, we wanted to demonstrate in a

case study that amino acids can be built from the smallest molecular building blocks. We developed a one-pot enzymatic cascade to efficiently produce the amino acid L-alanine from MeOH with a yield of 88% alanine from 150 mM (3.9 g L^{-1}) MeOH. Cai and coworkers reported that their chemo-enzymatic starch synthesis from CO_2 is 3.5 times that of the solar-to-starch efficiency for plants. When not considering the energy for ammonia synthesis (as this is commonly supplied as fertilizer), the solar-to-alanine efficiency of our cascade is even higher, as no extra energy in the form of ATP has to be supplied.

Due to the central metabolic role of the intermediate pyruvate, the system can be adapted to produce different types of MeOH-based platform chemicals and amino acids. With all substrates, i.e., MeOH and ammonia, being available from “green” electricity requiring only CO_2 and N_2 , one can imagine a carbon-neutral cascade, which can be the starting point for a sustainable and environmentally friendly amino acid synthesis and further extend the supply of protein.

EXPERIMENTAL PROCEDURES

Resource availability

Lead contact

Further information and requests for resources should be directed to and will be fulfilled by the lead contact, Volker Sieber (sieber@tum.de).

Materials availability

This study did not generate new materials.

Data and code availability

The authors declare that the data supporting the findings of this study as well as methods and experimental procedures are available within the paper and its [supplemental information](#).

SUPPLEMENTAL INFORMATION

Supplemental information can be found online at <https://doi.org/10.1016/j.checat.2022.100502>.

ACKNOWLEDGMENTS

The work was supported by Bundesministerium für Bildung und Forschung (BMBF), Förderkennzeichen: 031B0351C, and Deutsche Forschungsgemeinschaft (DFG) through TUM International Graduate School of Science and Engineering (IGSSE), GSC 81. We thank Dr. A. Roth and F. Vogelgsang (Fraunhofer-Institut für Grenzflächen- und Bioverfahrenstechnik IGB Bio-, Elektro- und Chemokatalyse BioCat, Institutsteil Straubing) for kindly provision of “green methanol.” We thank M. Teshima for advice on manuscript revision. We thank A. Al-Shameri, E. Hupfeld, A. Pick, S. Güner, and S. Sutiono for fruitful discussion.

AUTHOR CONTRIBUTIONS

Conceptualization, V.P.W. and V.S.; methodology, V.P.W. and M.D.; investigation, V.P.W.; visualization, V.P.W.; funding acquisition, V.S.; project administration, V.S.; supervision, B.B. and V.S.; writing – original draft, V.P.W. and V.S.; writing – review & editing, B.B. and V.S.; lead author, V.S.

DECLARATION OF INTERESTS

All authors declare that they have no competing interests.

Received: October 7, 2022

Revised: November 30, 2022

Accepted: December 28, 2022

Published: January 23, 2023

REFERENCES

- Owusu, P.A., and Asumadu-Sarkodie, S. (2016). A review of renewable energy sources, sustainability issues and climate change mitigation. *Cogent Engineering* 3, 1167990. <https://doi.org/10.1080/23311916.2016.1167990>.
- Intasian, P., Prakinee, K., Phintha, A., Trisrivirat, D., Weeranoppanant, N., Wongnate, T., and Chaiyen, P. (2021). Enzymes, in vivo biocatalysis, and metabolic engineering for enabling a circular economy and sustainability. *Chem. Rev.* 121, 10367–10451. <https://doi.org/10.1021/acs.chemrev.1c00121>.
- IEA (2019). World Energy Outlook 2019 (IEA). <https://www.iea.org/reports/world-energy-outlook-2019>.
- Guo, S., Asset, T., and Atanassov, P. (2021). Catalytic Hybrid electrocatalytic/biocatalytic cascades for carbon dioxide reduction and valorization. *ACS Catal.* 11, 5172–5188. <https://doi.org/10.1021/acscatal.0c04862>.
- IEA (2021). Global Energy Review 2021 (IEA). <https://www.iea.org/reports/global-energy-review-2021>.
- Al-Rowaili, F.N., Jamal, A., Ba Shammakh, M.S., and Rana, A. (2018). A review on recent advances for electrochemical reduction of carbon dioxide to methanol using metal-organic framework (MOF) and non-MOF catalysts: challenges and future prospects. *ACS Sustainable Chem. Eng.* 6, 15895–15914. <https://doi.org/10.1021/acssuschemeng.8b03843>.
- Chen, G., Waterhouse, G.I.N., Shi, R., Zhao, J., Li, Z., Wu, L.Z., Tung, C.H., and Zhang, T. (2019). From solar energy to fuels: recent advances in light-driven C1 chemistry. *Angew. Chem., Int. Ed. Engl.* 58, 17528–17551. <https://doi.org/10.1002/anie.201814313>.
- Parvez, A.M., Afzal, M.T., Victor Hebb, T.G., and Schmid, M. (2020). Utilization of CO₂ in thermochemical conversion of biomass for enhanced product properties: a review. *J. CO₂ Util.* 40, 101217. <https://doi.org/10.1016/j.jcou.2020.101217>.
- Shi, J., Jiang, Y., Jiang, Z., Wang, X., Wang, X., Zhang, S., Han, P., and Yang, C. (2015). Enzymatic conversion of carbon dioxide. *Chem. Soc. Rev.* 44, 5981–6000. <https://doi.org/10.1039/C5CS00182J>.
- Sultana, S., Chandra Sahoo, P., Martha, S., and Parida, K. (2016). A review of harvesting clean fuels from enzymatic CO₂ reduction. *RSC Adv.* 6, 44170–44194. <https://doi.org/10.1039/C6RA05472B>.
- Navarro-Jaén, S., Virginie, M., Bonin, J., Robert, M., Wojcieszak, R., and Khodakov, A.Y. (2021). Highlights and challenges in the selective reduction of carbon dioxide to methanol. *Nat. Rev. Chem* 5, 564–579. <https://doi.org/10.1038/s41570-021-00289-y>.
- Bhatia, S.K., Bhatia, R.K., Jeon, J.-M., Kumar, G., and Yang, Y.-H. (2019). Carbon dioxide capture and bioenergy production using biological system—A review. *Renew. Sustain. Energy Rev.* 110, 143–158. <https://doi.org/10.1016/j.rser.2019.04.070>.
- Singh, R.K., Singh, R., Sivakumar, D., Kondaveeti, S., Kim, T., Li, J., Sung, B.H., Cho, B.-K., Kim, D.R., Kim, S.C., et al. (2018). Insights into cell-free conversion of CO₂ to chemicals by a multi-enzyme cascade reaction. *ACS Catal.* 8, 11085–11093. <https://doi.org/10.1021/acscatal.8b02646>.
- Calzadiaz-Ramirez, L., and Meyer, A.S. (2022). Formate dehydrogenases for CO₂ utilization. *Curr. Opin. Biotechnol.* 73, 95–100. <https://doi.org/10.1016/j.copbio.2021.07.011>.
- Marpani, F., Pinelo, M., and Meyer, A.S. (2017). Enzymatic conversion of CO₂ to CH₃OH via reverse dehydrogenase cascade biocatalysis: Quantitative comparison of efficiencies of immobilized enzyme systems. *Biochem. Eng. J.* 127, 217–228. <https://doi.org/10.1016/j.bej.2017.08.011>.
- Zhong, J., Yang, X., Wu, Z., Liang, B., Huang, Y., and Zhang, T. (2020). State of the art and perspectives in heterogeneous catalysis of CO₂ hydrogenation to methanol. *Chem. Soc. Rev.* 49, 1385–1413. <https://doi.org/10.1039/C9CS00614A>.
- Ren, M., Zhang, Y., Wang, X., and Qiu, H. (2022). Catalytic hydrogenation of CO₂ to methanol: a review. *Catalysts* 12, 403. <https://doi.org/10.3390/catal12040403>.
- Bertau, M., Offermanns, H., Plass, L., Schmidt, F., and Wernicke, H.-J. (2014). Methanol: The Basic Chemical and Energy Feedstock of the Future (Springer). https://doi.org/10.1007/978-3-642-39709-7_1.
- Sahoo, K.K., Goswami, G., and Das, D. (2021). Biotransformation of methane and carbon dioxide into high-value products by methanotrophs: current state of art and future prospects. *Front. Microbiol.* 12, 636486. <https://doi.org/10.3389/fmicb.2021.636486>.
- Li, Z., Shen, S., and Li, Z. (2020). Towards the conversion of CO₂ into optically pure N-carbamoyl-L-aspartate and orotate by an in vitro multi-enzyme cascade. *Green Chem.* 22, 5798–5805. <https://doi.org/10.1039/DO9C02268C>.
- Desmons, S., Fauré, R., and Bontemps, S. (2019). Formaldehyde as a promising C1 source: the instrumental role of biocatalysis for stereocontrolled reactions. *ACS Catal.* 9, 9575–9588. <https://doi.org/10.1021/acscatal.9b03128>.
- Siegel, J.B., Smith, A.L., Poust, S., Wargacki, A.J., Bar-Even, A., Louw, C., Shen, B.W., Eiben, C.B., Tran, H.M., Noor, E., et al. (2015). Computational protein design enables a novel one-carbon assimilation pathway. *Proc. Natl. Acad. Sci. USA* 112, 3704–3709. <https://doi.org/10.1073/pnas.1500545112>.
- Cai, T., Sun, H., Qiao, J., Zhu, L., Zhang, F., Zhang, J., Tang, Z., Wei, X., Yang, J., Yuan, Q., et al. (2021). Cell-free chemoenzymatic starch synthesis from carbon dioxide. *Science* 373, 1523–1527. <https://doi.org/10.1126/science.abh4049>.
- Güner, S., Wegat, V., Pick, A., and Sieber, V. (2021). Design of a synthetic enzyme cascade for the in vitro fixation of a C1 carbon source to a functional C4 sugar. *Green Chem.* 23, 6583–6590. <https://doi.org/10.1039/D1GC02226A>.
- Zhou, J., Tian, X., Yang, Q., Zhang, Z., Chen, C., Cui, Z., Ji, Y., Schwaneberg, U., Chen, B., and Tan, T. (2022). Three multi-enzyme cascade pathways for conversion of C1 to C2/C4 compounds. *Chem Catalysis* 2, 2675–2690. <https://doi.org/10.1016/j.checcat.2022.07.011>.
- Schwander, T., Schada von Borzyskowski, L., Burgener, S., Cortina, N.S., and Erb, T.J. (2016). A synthetic pathway for the fixation of carbon dioxide in vitro. *Science* 354, 900–904. <https://doi.org/10.1126/science.aah5237>.
- Ranganathan, J., Waite, R., Searchinger, T., and Hanson, C. (2018). How to Sustainably Feed 10 Billion People by 2050, in 21 Charts, 8 (World Res. Inst.), Available online: <https://www.wri.org/blog/2018/12/how-sustainably-feed-10-billion-people-2050-21-charts>.
- Henchion, M., Hayes, M., Mullen, A.M., Fenelon, M., and Tiwari, B. (2017). Future protein supply and demand: strategies and factors influencing a sustainable equilibrium. *Foods* 6, 53. <https://doi.org/10.3390/foods6070053>.
- Sherkhanov, S., Korman, T.P., Chan, S., Faham, S., Liu, H., Sawaya, M.R., et al. (2020). Isobutanol production freed from biological limits using synthetic biochemistry. *Nat. Commun.* 11, 4292. <https://doi.org/10.1038/s41467-020-18124-1>.
- Gmelch, T.J., Sperl, J.M., and Sieber, V. (2019). Optimization of a reduced enzymatic reaction cascade for the production of L-alanine. *Sci*

- Rep. 9, 11754. <https://doi.org/10.1038/s41598-019-48151-y>.
31. Kamps, J.J.A.G., Hopkinson, R.J., Schofield, C.J., et al. (2019). How formaldehyde reacts with amino acids. *Commun Chem* 2, 126. <https://doi.org/10.1038/s42004-019-0224-2>.
32. Doukyu, N., and Ogino, H. (2010). Organic solvent-tolerant enzymes. *Biochem. Eng. J.* 48, 270–282. <https://doi.org/10.1016/j.bej.2009.09.009>.
33. Desmons, S., Faure, R.g., and Bontemps, S. (2019). Formaldehyde as a promising C1 source: The instrumental role of biocatalysis for stereocontrolled reactions. *ACS Catalysis* 9, 9575–9588. <https://doi.org/10.1021/acscatal.9b03128>.
34. Turner, P., Mamo, G., and Karlsson, E.N. (2007). Potential and utilization of thermophiles and thermostable enzymes in biorefining. *Microb Cell Fact* 6, 9. <https://doi.org/10.1186/1475-2859-6-9>.
35. Shoichet, B.K., Baase, W.A., and Kuroki, R. (1995). A relationship between protein stability and protein function. *Proc. Natl. Acad. Sci. U. S. A.* 92, 452–456. <https://doi.org/10.1073/pnas.92.2.452>.
36. Schurig, H., Rutkat, K., Jaenicke, R., and Rachel, R. (1995). Octameric enolase from the hyperthermophilic bacterium *Thermotoga maritima*: purification, characterization, and image processing. *Protein Science* 4, 228–236. <https://doi.org/10.1002/pro.5560040209>.
37. Fahey, R., Kolb, E., and Harris, J. (1971). Triose phosphate isomerase from *Bacillus stearothermophilus*. *Biochem. J.* 124 (5), 77P. <https://doi.org/10.1042/bj1240077p>.
38. Potter, S., and Fothergill-Gilmore, L.A. (1992). Purification and properties of pyruvate kinase from *Thermoplasma acidophilum*. *FEMS Microbiol. Lett.* 94 (3), 235–239. <https://doi.org/10.1111/j.1574-6968.1992.tb05324.x>.
39. Grimshaw, C., and Cleland, W. (1981). Kinetic mechanism of *Bacillus subtilis* L-alanine dehydrogenase. *Biochemistry* 20 (20), 5650–5655. <https://doi.org/10.1021/bi00523a002>.
40. Jia, B., Linh, L.T., Lee, S., Pham, B.P., Liu, J., Pan, H., et al. (2011). Biochemical characterization of glyceraldehyde-3-phosphate dehydrogenase from *Thermococcus kodakarensis* KOD1. *Extremophiles* 15, 337–346. <https://doi.org/10.1007/s00792-011-0365-4>.
41. Noor, E., Haraldsdóttir, H.S., Milo, R., and Fleming, R.M. (2013). Consistent estimation of Gibbs energy using component contributions. *PLoS Comput. Biol.* 9, e1003098. <https://doi.org/10.1371/journal.pcbi.1003098>.
42. Noor, E., et al. (2014). Pathway thermodynamics highlights kinetic obstacles in central metabolism. *PLoS computational biology* 10, e1003483. <https://doi.org/10.1371/journal.pcbi.1003483>.
43. Chander, M, Setlow, P, Lamani, E, and Jedrzejewski, M.J (1999). Structural studies on a 2,3-diphosphoglycerate independent phosphoglycerate mutase from *Bacillus stearothermophilus*. *J Struct Biol* 126, 156–165. <https://doi.org/10.1006/jsbi.1999.4112>.
44. Lotti, M., Pleiss, J., Valero, F., and Ferrer, P. (2018). Enzymatic Production of Biodiesel: Strategies to Overcome Methanol Inactivation. *Biotechnol. J.* 13, 1700155. <https://doi.org/10.1002/biot.201700155>.
45. Couderc, R. Baratti J. (1980). Oxidation of methanol by the yeast *Pichia pastoris* purification and properties of alcohol oxidase. *Agric. Biol. Chem.* 44, 2279–2289. <https://doi.org/10.1080/00021369.1980.10864320>.
46. Wait, A.F., Brandmayr, C., Stripp, S.T., Cavazza, C., Fontecilla-Camps, J.C., Happe, T., et al. (2011). Formaldehyde-A Rapid and Reversible Inhibitor of Hydrogen Production by [FeFe]-Hydrogenases. *J. Am. Chem. Soc.* 133 (5), 1282–1285. <https://doi.org/10.1021/ja110103p>.
47. Guterl, J.K., Garbe, D., Carsten, J., Steffler, F., Sommer, B., Reißer, S., et al. (2012). Cell-free metabolic engineering: production of chemicals by minimized reaction cascades. *ChemSusChem* 5, 2165–2172. <https://doi.org/10.1002/cssc.201200365>.
48. Xie, L., Wei, X., Zhou, X., Meng, D., Zhou, R., Zhang, Y.-H.P.J., et al. (2018). Conversion of D-glucose to L-lactate via pyruvate by an optimized cell-free enzymatic biosystem containing minimized reactions. *Synth. Syst. Biotechnol* 3 (3), 204–210. <https://doi.org/10.1016/j.synbio.2018.05.003>.
49. Jia, X., Liu, Y., and Han, Y. (2017). A thermophilic cell-free cascade enzymatic reaction for acetoin synthesis from pyruvate. *Sci. Rep.* 7, 4333. <https://doi.org/10.1038/s41598-017-04684-8>.
50. Gao, H., Tuyishime, P., Zhang, X., Yang, T., Xu, M., and Rao, Z. (2021). Engineering of microbial cells for L-valine production: challenges and opportunities. *Microb. Cell Fact.* 20, 172. <https://doi.org/10.1186/s12934-021-01665-5>.
51. Liu, P., Xu, H., and Zhang, X. (2021). Metabolic engineering of microorganisms for L-alanine production. *J. Ind. Microbiol. Biotechnol.* 49 (2), kuab057. <https://doi.org/10.1093/jimb/kuab057>.

Chem Catalysis, Volume 3

Supplemental information

Cell-free enzymatic L-alanine synthesis

from green methanol

Vivian Pascal Willers, Manuel Döring, Barbara Beer, and Volker Sieber

Supplemental Experimental Procedures

Chemicals, reagents, strains and enzymes

All chemicals were purchased from VWR, Roth, Serva, Roche, Sigma-Aldrich, Merck, Alfa Aesar, and Fisher Scientific. CO₂ and renewable hydrogen-based methanol was kindly provided by Fraunhofer-Institut für Grenzflächen- und Bioverfahrenstechnik IGB. *Escherichia coli* (*E. coli*) NEB® Turbo cells (New England Biolabs® inc.) were used as cloning strain. *E. coli* BL21 (DE3) F⁻ ompT gal dcm lon hsdSB(rB- mB-) λ(DE3 [lacI lacUV5-T7 gene 1 ind1 sam7 nin5]) (Novagen) were used for heterologous protein expression.

Pyruvate kinase/lactate dehydrogenase mix (PyK/LDH) from rabbit muscle was purchased from Sigma. Lactate dehydrogenase (LDH) from rabbit muscle was purchased from Roth. Alcohol oxidase (ppAOX) of *Pichia pastoris* was purchased from Sigma. Catalase (CAT) of *Corynebacterium glutamicum* was purchased from Sigma-Aldrich. Glyceraldehyde 3-phosphate dehydrogenase (GAPDH) from rabbit muscle was purchased from Sigma. 3-Phosphoglycerate-phosphokinase (3-PGK) from yeast was purchased from Sigma.

Cloning, expression, and purification of enzymes

Plasmids pET28a- and pET24a were provided by Novagen, and pCBRHisN were constructed on the basis of pET28a and prepared as published by Guterl and co-workers.^[S1] Phusion high fidelity polymerase (New England Biolabs GmbH) was used to amplify target genes with restriction sites from genomic DNA. The formolaseM3 (flsM3) gene variant was generated by mutagenesis using overlap extension PCR, similar to that published by Williams and co-workers.^[S2] Restriction ligation cloning was used for the integration of target genes into the plasmids. Restriction enzymes and constructs are presented in Table S1.

E. coli BL21 (DE3) functions as host strain for heterologous protein expression. Expression of proteins was carried out in two steps. First 20 ml of LB medium containing 100 µg/mL kanamycin were inoculated with a colony from a LB agar plate and incubated for 16 h at 37 °C and 300 rpm. Main cultures were cultivated in shaking flasks containing either 20% (v/v) ZYP-5052 auto induction medium^[S3] including 100 µg/mL kanamycin or terrific broth medium including also 100 µg/mL kanamycin. The main culture was inoculated to an OD₆₀₀ of 0.05 and incubated at 37 °C and 90 rpm until an OD₆₀₀ of 0.6. By using terrific broth medium expression

was induced by adding 0.5 mM of IPTG. Temperature was reduced to 25 °C or 16 °C (Table S1). After 20 h of cultivation, *E. coli* cells were centrifuged and stored at -20 °C until purification.

Cell lysates were prepared on ice using ultra sonication (Ultraschallprozessor UIS250V Hielscher Ultrasonic GmbH) and centrifuged afterward (20 °C, 40000 g, 30 min).

All proteins containing a His₆-tag and were purified using an ÄKTApurifier system (GE Healthcare) equipped with a 5 mL HiTrapFF Crude column. First, the column was equilibrated with binding buffer (50 mM HEPES pH 8.0, 20 mM Imidazol, 500 mM NaCl). Then the supernatant was applied. A washing step with binding buffer was used to remove unbound proteins. To elute the His₆-tagged proteins from the column, the imidazole concentration was raised from 20 mM to 500 mM. The eluate was fractionated and protein-containing fractions were collected. The buffer was exchanged via HiPrep 26/10 desalting column to 50 mM HEPES pH 7.5. Purified protein solution was stored at -80 °C.

Enzyme kinetic measurements

Enzyme kinetics (Table S4) were determined in 200 µl reactions at 30 °C with 100 mM HEPES pH 7.5, 5 mM MgCl₂, if not stated otherwise. Additionally, further cofactors and additives were used according to the analyzed enzymes and coupling enzymes. Reactions were started by addition of the target enzyme and measured by using a Biotek epoch-2 microplate spectrophotometer (Biorad).

ATP depended reactions were coupled to pyruvate kinase and lactate dehydrogenase (rabbit muscle, from Sigma) with the use of phosphoenolpyruvate (PEP) as co-substrate. Activity was measured by following the oxidation of NADH at 340 nm.

NAD(P)⁺/NAD(P)H depended reactions were directly measured by following the reduction/oxidation of NAD(P)⁺/NAD(P)H at 340 nm.

All other reactions were coupled to ATP depended reactions and monitored as described for ATP dependent reactions or coupled to NAD(P)⁺ or NAD(P)H consuming reactions by following reduction of NAD(P)⁺ or oxidation of NAD(P)H at 340 nm.

Dihydroxyacetone kinase

Dihydroxyacetone kinase (DhaK) activity was assayed in a coupled approach with pyruvate kinase and lactate dehydrogenase by measuring oxidation of NADH^[S4] in 382 μ l. Standard reaction containing additional 1.25 mM PEP, 0.3 mM NADH, 2 mM ATP, 5 – 0.005 mM dihydroxyacetone (DHA) and 3.8 μ l Pyk/LDH mix. Reaction was started by addition of DHA to the reaction mixture.

Triosephosphate isomerase

Triosephosphate isomerase activity (TpI) was assayed in a modified coupled approach similar to Zhai and co-workers with GAPDH by measuring the reduction of NAD⁺.^[S5] Standard reaction containing additional 10 mM potassium phosphate pH 7.5, 2.5 mM NAD⁺, 1 mM ADP, 50 – 0.05 mM dihydroxyacetone phosphate (DHAP), 3.2 U/ml GAPDH and 4.6 U/ml 3-PGK. Reaction was started by addition of DHAP to the reaction mixture.

Glyceraldehyde 3-phosphate dehydrogenase (GapN)

Glyceraldehyde 3-phosphate dehydrogenase (GapN) activity was assayed by direct measuring the reduction of NAD⁺.^[S6] Standard reaction containing additional 0.1 mM glucose 1-phosphate (G1P), 5 mM NAD⁺, and 2.5 – 0.01 mM glyceraldehyde 3-phosphate (GAP). The reaction was started by the addition of GAP to the reaction mixture.

Phosphoglycerate mutase

Phosphoglycerate mutase (PgM) activity was assayed in a coupled approach with enolase (tmENO) and PyK/LDH mix by measuring the oxidation of NADH.^{[S7],[S8]} Standard reaction containing additional, 2 mM ADP, 0.1 mM MnCl₂, 0.3 mM NADH, 2.5 – 0.06 mM 3-phosphoglycerate, 0.06 mg/mL tmENO, and 2 μ l PyK/LDH mix. The reaction was started by addition of 3-phosphoglycerate (3-PG) to the reaction mixture.

Enolase

Enolase (ENO) activity was assayed in a coupled approach with PyK/LDH mix by measuring the oxidation of NADH.^[S9] Standard reaction containing additional, 2 mM ADP, 0.3 mM NADH, 1.5 – 0.006 mM 2-phosphoglycerate (2-PG) and 2 μ l pyruvate kinase/lactate dehydrogenase mix. The reaction was started by addition of 2-PG to the reaction mixture.

Pyruvate kinase

Pyruvate kinase (PyK) was assayed in a coupled approach with LDH by measuring the oxidation of NADH.^[S10] Standard reaction containing additional, 2 mM ADP, 0.3 mM NADH, 20 – 0.04 mM PEP and 6 U/mL LDH. The reaction was started by addition of PEP to the reaction mixture.

Alanine dehydrogenase

Alanine dehydrogenase (AlaDH) was assayed by directly measuring the oxidation of NADH.^[S11] Standard reaction containing additional, 200 mM (NH₄)₂SO₄, 0.3 mM NADH and 10 – 0.02 mM pyruvate. The reaction was started by addition of pyruvate to the reaction mixture.

Enzyme activity in cascade conditions

Enzyme activity was determined in 200 µl reactions at 30 °C with 100 mM HEPES pH 7.5, 200 mM (NH₄)₂SO₄, 5 mM MgCl₂, 0.1 mM MnCl₂, 0.5 mM TPP and 0.5 mM G1P to mirror the cascade conditions. Additionally, further cofactors and additives were used according to the analyzed enzymes and coupling enzymes (Table S5). Assays were prepared as described before. Reactions were started by addition of the target enzyme and measured by using a Biotek epoch-2 microplate spectrophotometer (Biorad).

Formolase/FormolaseM3

FLS/FLSM3 activity was assayed in a coupled approach with kbDhaK, PyK/LDH mix by measuring the oxidation of NADH. Standard reaction containing additional 1 mM PEP, 0.3 mM NADH, 5 mM formaldehyde (FALD), 2 µl PyK/LDH mix and 3 U/mL dihydroxyacetone kinase. The reaction was started by addition of FLS to the reaction mixture.

Regulation and inhibition of kbDhaK and taPyK

ATP/ADP regulation and Mn²⁺ inhibition studies were performed by measuring the activities of kbDhaK and taPyK with additional MnCl₂ concentration of 0 – 5 mM and in a different approach with addition of 0 – 5 mM ATP or ADP to the reaction. taPyK activities with additional MnCl₂ and additional ATP was assayed as mentioned above. However, kbDhaK activity for the regulation of ADP and inhibition of MnCl₂ was measured in a different set up, because the assay system from above is not suitable. The activity was assayed with a modified

coupled system described by Garcia-Alles and co-workers,^[S12] with gsTpI and ccGapN. DHA is phosphorylated by kbDhaK, DHAP is isomerized to GAP by gsTpI and then GAP is oxidized by ccGapN by reduction of NADP⁺ to 3-PG. Activity was assayed in cascade conditions with additional 1 mM NADP⁺, 1 mM ATP, 5 mM DHA, 0.8 mg/ml ccGapN and 0.2 mg/ml gsTpI. The reaction was started by the addition of kbDhaK to the reaction mixture. Mn²⁺ activation of gsPgM was performed similarly to the activity measurements of gsPgM with a variation of MnCl₂ concentration of 0 - 1 mM and a set concentration of 4 mM 3-PG.

Enzyme activity with additional formaldehyde and methanol

Enzyme activity was determined as described above. This time, 5 or 10 mM FALD and 60 or 150 mM methanol (MeOH) were added to the mixture. The activity was measured by the addition of the target enzyme.

Alcohol oxidase

Activity of ppAOX was determined in a coupled approach with HRP by measuring the reduction of ABTS at 418 nm. Standard reaction containing additional 1.25 mM ABTS, 150 mM MeOH, and 1 µl HRP (1 mg/mL). The reaction was started by addition of ppAOX to the reaction mixture.

Stability analysis

Thermostability analysis

Melting point analysis was performed in 25 µL reaction volume with 2 µL SYPROTM Orange (1:80 dilution) 2 µl of protein, and 5 mM or 10 mM FALD or 60 mM, 90 mM or 150 mM MeOH in the cascade matrix. Measurements were performed with a CFX96 Touch Real-Time PCR detection system (Biorad). The temperature was increased in increments of 1 °C from 25 °C to 100 °C with 1 kelvin per minute increase. The melting curves were prepared as described in the manufacturer's instructions (Biorad). Melting point data were derived from the minimum of the negative derivative of the fluorescence curve versus temperature (Biorad).

Formaldehyde stability analysis

FALD stability of kbDhaK was determined by assaying the activity of kbDhaK by using the coupled PyK/LDH assay system described before. 1 mg/mL kbDhaK was incubated with 1 mM, 2.5 mM, 5 mM and 10 mM FALD in the cascade matrix at 30 °C by using a nutating

shaker (VWR Rocking Platform, VWR, Germany).^[S13] Samples were taken after 0 h, 1 h and 3 h of incubation. Samples were pre diluted 1:100 and 20 μ l of this dilution were used to start the reaction in a final volume of 200 μ l. For FALD separation experiment, samples were incubated as described before for 2 h. After this incubation, samples were centrifuged for 10 min (10000 g) using centrifugal filters modified PES 10 kDa (VWR). Enzymes were re-diluted in cascade matrix and further incubated as before. Sampling and reaction measurement was conducted as described before.

Thermodynamic pathway analysis

Analysis of the thermodynamic driving force of the cascade was performed using max-min driving force (MDF) calculations. To generate estimates of the change in Gibbs energy values, the eQuilibrator (3.0) pathway analysis web tool with default settings was used (Figure S2).^[S14] Metabolite concentrations ranged from 1 μ M to 10 mM, a pH of 7.5, an ionic strength of 0.25 M, and a $-\log[\text{Mg}^{2+}]$ (pMg) of 3, as well as the reaction definitions. The derived values were then used in the MDF framework using the eQuilibrator (3.0) pathway analysis web tool (Figure S2).

Cascade reactions

Dihydroxyacetone cascade

Initial cascade reactions for optimization of enzyme composition were set up in 50 μ l scale in 2 ml tubes. 100 mM HEPES pH 7.5, 200 mM ammonium sulphate, 2 mM ATP, 5 mM NAD^+ , 5 mM MgCl_2 , 0.1 mM MnCl_2 , 0.5 mM TPP and 0.5 mM G1P as well as 20 mM of DHA were mixed. Enzymes were concentrated using centrifugal filters modified PES 10 kDa (VWR). Reactions were started with addition of the target enzyme composition (Table S3) and incubated at 30 °C with an Eppendorf shaker (600 rpm, ThermoMixer C, Eppendorf, Germany).

Alanine cascade optimization

Initial cascade reactions for optimization were set up in 50 μ l scale in 2 ml tubes. 100 mM HEPES pH 7.5, 200 mM ammonium sulphate, 2 mM ATP, 5 mM NAD^+ , 5 mM MgCl_2 , 0.1 mM MnCl_2 , 0.5 mM TPP and 0.5 mM G1P as well as 60 mM, 90 mM or 150 mM of MeOH were mixed. Enzymes were concentrated using centrifugal filters modified PES 10 kDa (VWR). Reactions were started with addition of target enzyme composition (Table S3) and incubated at

30 °C. To provide sufficient oxygen during the reaction time, tubes were incubated by using a nutating shaker.

Final alanine cascade setup

Final cascade reactions were set up in 500 µl scale in 50 ml tubes. 100 mM HEPES pH 7.5, 200 mM ammonium sulphate, 2 mM ATP, 5 mM NAD⁺, 5 mM MgCl₂, 0.1 mM MnCl₂, 0.5 mM TPP and 0.5 mM G1P and 60 mM or 150 mM MeOH were mixed. Enzymes were concentrated using centrifugal filters modified PES 10 kDa (VWR). Reactions were started with addition of target enzyme composition and incubated at 30 °C (Table S3). To counteract the high K_m of alcohol oxidase to oxygen induced by 150 mM MeOH,^[S15] we gassed the 50 ml tubes with oxygen for 20 minutes before starting the reaction. To provide sufficient oxygen during the reaction time, tubes were incubated by using a nutating shaker.

Quantification of metabolites

Methanol quantification

MeOH was quantified by headspace GC-FID (Thermo Scientific Trace GC Ultra, equipped with a flame ionization detector (FID) and a Headspace Tri Plus auto sampler) equipped with a Stabilwax column (30 m, 0.25 mm internal diameter, 0.25 µm film thickness (Restek, Bellefonte, USA)) with helium as carrier gas similar to Guterl and co-workers.^[S1] The oven temperature was held at 50 °C for 2 min and raised with 10 °C/min to 80°C held for 1 min. Cascade samples were diluted 1:10 in water and filtered using modified PES 10 kDa (VWR) centrifugal filters. 200 µL of the dilution was added to a 5 ml headspace vial for analysis. Prior to injection samples were incubated at 40 °C for 15 min. Injection was carried out via split mode with 10 ml/min flow, with an injection volume of 700 µl using headspace mode. The methanol standard curve (30 - 0.1 mM) was prepared in the cascade matrix and treated similarly to the cascade samples.

Alanine quantification

Alanine quantification was carried out in two different ways. For optimization of enzyme load, a fluorescence assay based on Gmelch and co-workers was used.^[S16] Samples were diluted 1:10 in water and filtered using centrifugal filters modified PES 10 kDa (VWR). After filtration samples were again diluted 1:10. 5 µl of sample were combined with 8 µl of 1 M borate buffer

pH 10.0, 45 μ l of 0.1% fluorescamin in dry acetonitrile and 100 μ l of water. Fluorescence was measured with a Varioscan spectral scanning multimode reader (Thermo electron corporation) (λ_{em} : 486 nm, λ_{ex} : 396 nm). Alanine standard (0 – 50 mM) in cascade matrix was prepared and measured in a similar way.

Alanine detection of cascades with final parameters was carried out as described by Begander and co-workers^[S17] using an HPLC (Ultimate300 HPLC-system, Dionex Softron GmbH, Germering, Germany) system. For the quantification, derivatisation with OPA/3-MPA reagent was used, as recommended by the manufacturers of Dr. Maisch GmbH (Ammerbuch-Entringen, Germany). As column, a GromSil OPA-3, 3 μ M, 125 mm \times 4.0 mm from Dr. Maisch GmbH (Ammerbuch-Entringen, Germany) was used. Samples were diluted 1:10 or 1:20 in water and filtered using centrifugal filters modified PES 10 kDa (VWR). After filtration, 8 μ l of sample were combined with 40 μ l of 1 M borate buffer pH 10.7, 8 μ l of l-norvaline (1.02 mM) as internal standard and 184 μ l of water. For derivatisation and monitoring 14 μ l of this mixture were mixed with 6 μ l of OPA-reagent 1:10 diluted in 1 M borate buffer pH 10.7.

Alanine standard curve was prepared in a similar way with a maximum concentration of 2.5 mM alanine in the matrix of the cascade with 200 mM ammonium sulphate, 2 mM ATP, 5 mM NAD⁺, 100 mM HEPES pH 7.5, 200 mM ammonium sulphate, 2 mM ATP, 5 mM NAD⁺, 5 mM MgCl₂, 0.1 mM MnCl₂, 0.5 mM TPP and 0.5 mM G1P.

Formaldehyde quantification

Quantification of FALD was performed by the acetylacetone method.^[S18] For this purpose, Nash reagent was prepared by mixing 0.1 M acetic acid, 0.2% (v/v) acetylacetone and 3.89 M ammonium acetate. 50 μ L of this solution was added to 50 μ L of the appropriately diluted sample and incubated for 30 min at 37 °C in a 96-well plate. After incubation, absorbance was immediately measured at 412 nm with a Biotek epoch-2 microplate spectrophotometer (Biorad). FALD concentration was determined from a standard curve of formaldehyde (0 - 1 mM) in the cascade matrix on the same plate.

Dihydroxyacetone quantification

DHA was quantified by the diphenylamine (DPA) method.^[S19] The DPA reagent consists of DPA (0.3 g), 10% H₂SO₄ (v/v) and acetic acid. 135 μ L of the DPA reagent was mixed with 15

μL of the appropriately diluted sample in a 96-well PCR plate without skirt (Brand). The plate was sealed with a 96-well plate sealing mat (Brand) and fixed by two metal plates. The samples were incubated for 30 min in a sand bath previously heated to 105 °C for at least 90 min. After incubation, the samples were cooled at room temperature for 15 minutes. Immediately after cooling, 100 μl of the sample was placed in a 96-well plate and absorbance was measured at 615 nm with a Biotek epoch-2 microplate spectrophotometer (Biorad). DHA concentration was determined using a standard curve of dihydroxyacetone (0 - 3 mM) in the cascade matrix on the same plate.

HEPES detection

HEPES was detected using an HPLC (Ultimate300 HPLC-system, Dionex Softron GmbH, Germering, Germany) system coupled to an ELSD detector, equipped with a Triart Diol-HILIC column (100 x 2.0 mm, 1.9 μm , YMC). Separation was conducted at 7 °C with a flow rate of 0.4 mL/min, by using a gradient elution: Buffer A: 0.1% formic acid pH 4.5 titrated with ammoniac, Buffer B: 0.1% (v/v) formic acid in acetonitrile. Elution started with 2 minutes of isocratic elution with 15% (v/v) buffer A and 85% (v/v) buffer B. After 2 minutes a linear gradient was applied for 3 minutes which reached 30% (v/v) buffer A and 70% (v/v) buffer B. This following isocratic elution for further 4 minutes. After these 4 minutes buffer ratio was set back to 15% (v/v) buffer A and 85% (v/v) buffer B followed by 7 minutes of isocratic elution. Signal analysis was conducted by using Chromeleon Software (ThermoFisher Scientific). Samples were diluted to have a maximum concentration of 1.5 mM HEPES in 70% acetonitrile. HEPES standard curve was prepared in a similar way with a maximum concentration of 3 mM HEPES. Injection volume was 0.5 – 10 μL .

Supplementary figures and tables

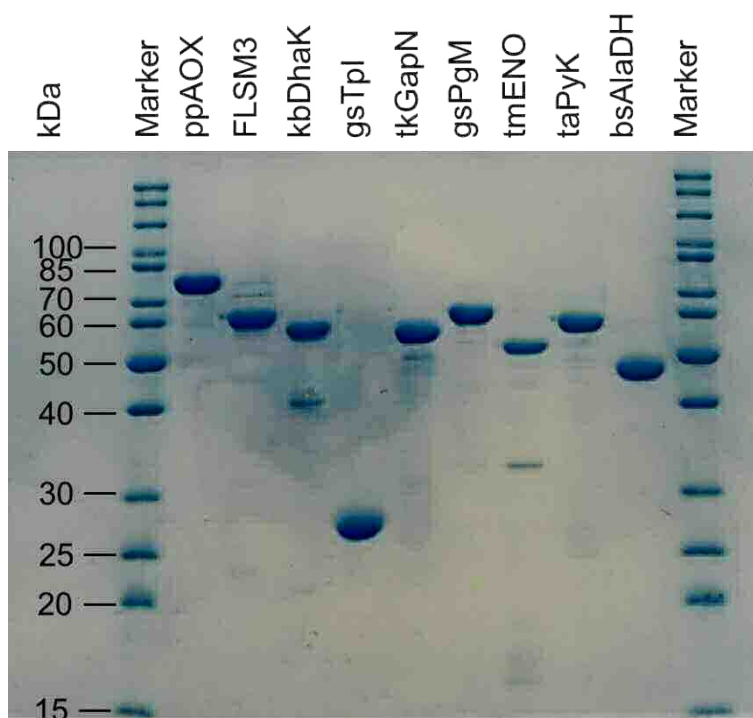


Figure S1.

SDS-gel of cascade enzymes normalized to 3 μg protein. As protein marker PageRuler™ unstained protein ladder was used.

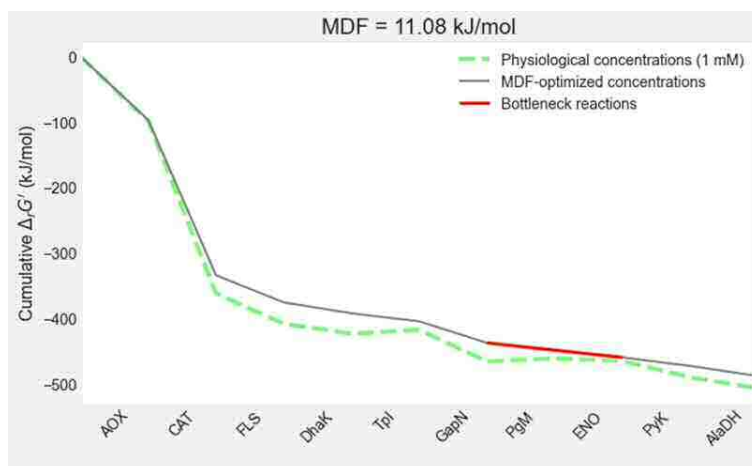
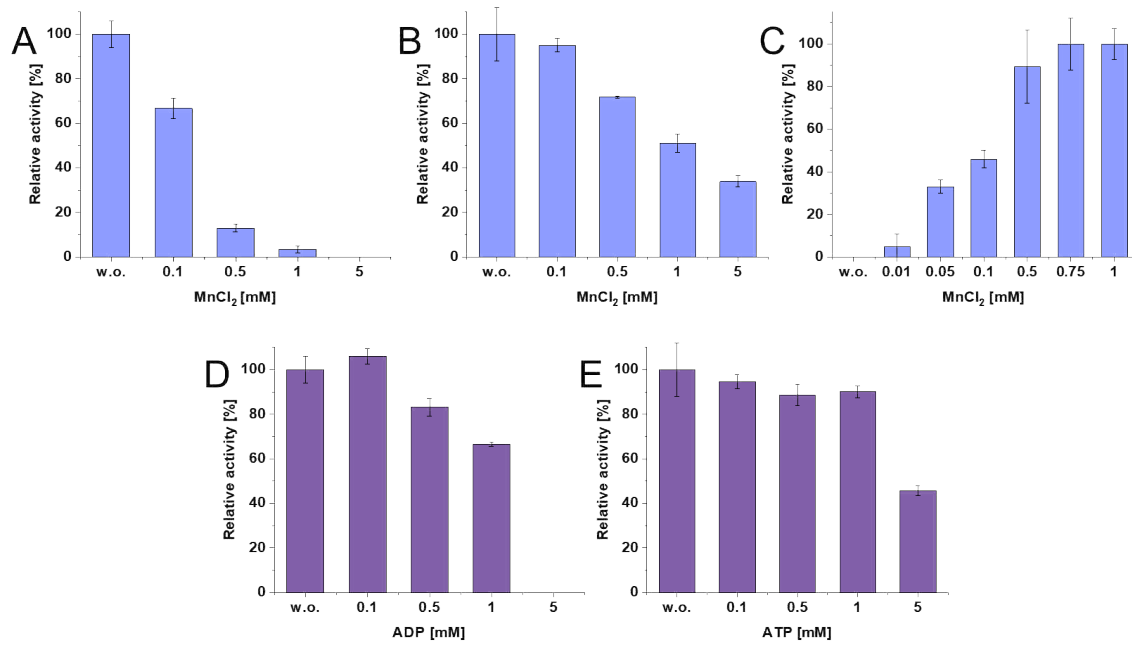


Figure S2.

Max-min driving force analysis of methanol to alanine pathway with $\Delta_r G'^0$ values in green corresponding to default conditions of eQuilibrator pathway tool with physiological concentrations pH: 7.5, ionic strength: 0.25, pMg: 3. Grey line represents optimized metabolite concentrations regarding maximal MDF. Red line represents estimated thermodynamical bottleneck reactions.^[S14]

**Figure S3.**

Change in activity of dihydroxyacetone kinase (kbDhaK), pyruvate kinase (taPyK) and phosphoglycerate mutase (gsPgM), upon addition of manganese, ATP and ADP. Effect of Mn²⁺ on activity of A: kbDhaK, B: taPyK and C: gsPgM. Regulatory effect of ATP/ADP on D: kbDhaK and E: taPyK. Reactions were performed in triplicate (n = 3) and analyzed as described in the methods. Error bars represent SD.

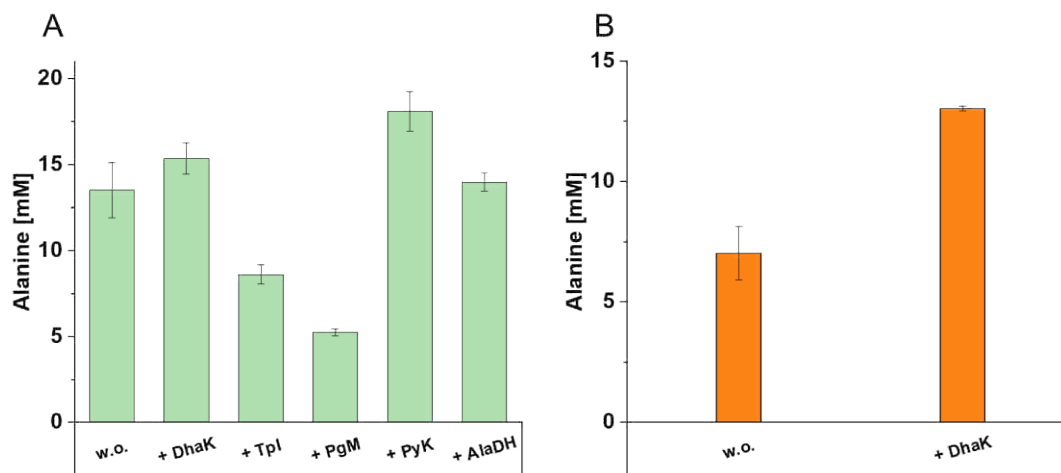


Figure S4.

Variation of cascade enzyme concentration for the production of L-alanine. A: L-alanine titers of the DHA cascade starting from 20 mM DHA. The enzyme composition is similar in all six approaches except for the named enzyme of which the concentration was significantly increased in each approach. B: L-alanine titers of the MeOH cascade starting from 60 mM methanol. The enzyme composition is similar in both approaches except for the kbDhaK. The concentration of kbDhaK was significantly increased in the second approach. Reactions were performed in duplicates ($n = 2$) and analysed as described in the methods. Error bars represent SD.

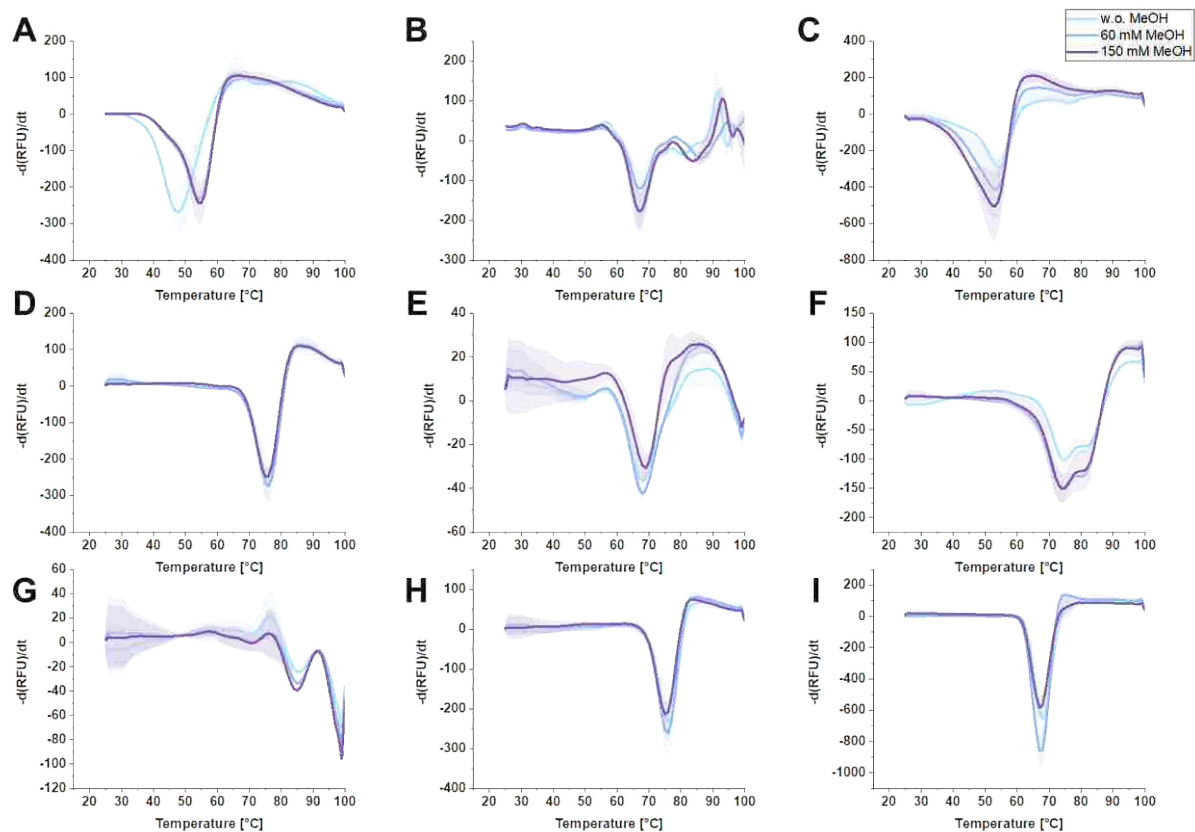


Figure S5.

Melting curves of cascade enzymes in cascade matrix without, with 60 mM and 150 mM methanol addition. A: ppAOX, B: FLSM3, C: kbDhaK, D: gsTpI, E: tkGapN, F: gsPgmM, G: tmENO, H: taPyK, I: bsAlaDH. Measurements were performed in triplicate ($n = 3$) and analysed as described in the Methods. Error clouds represent SD.

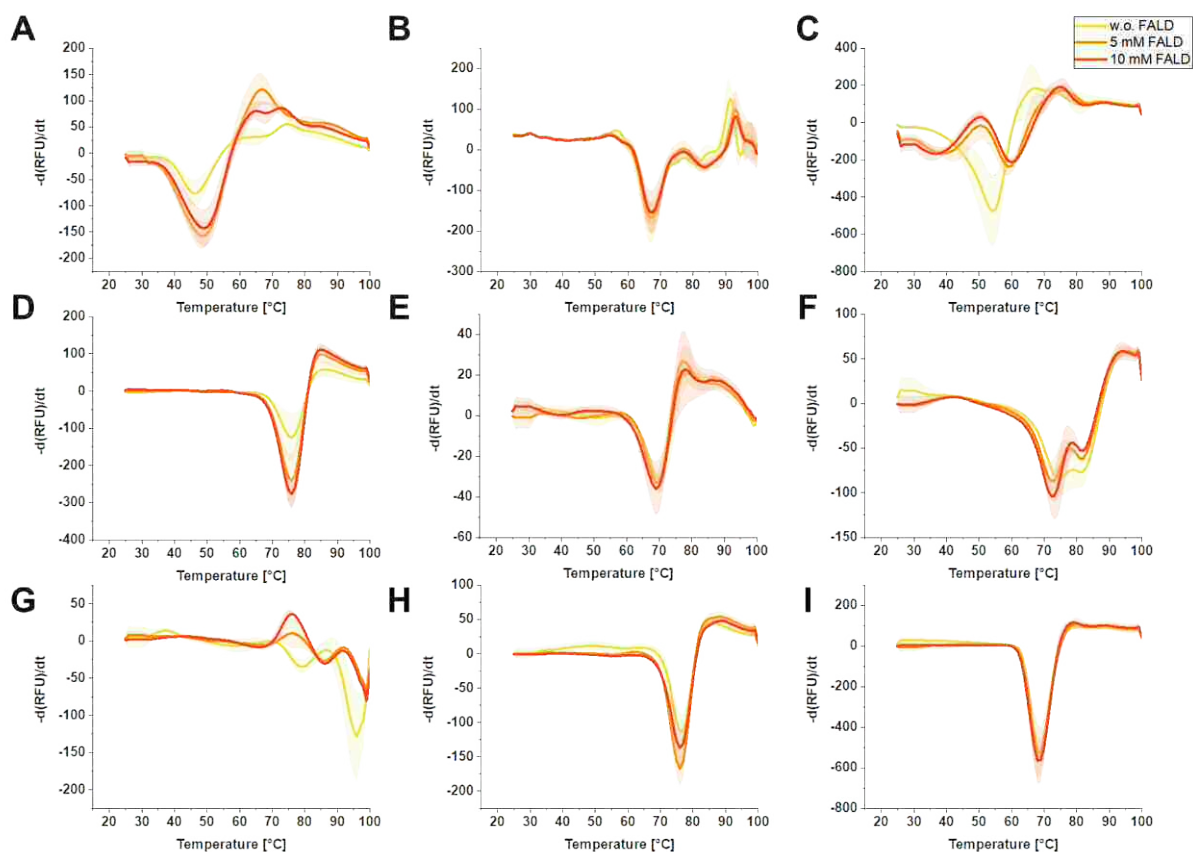
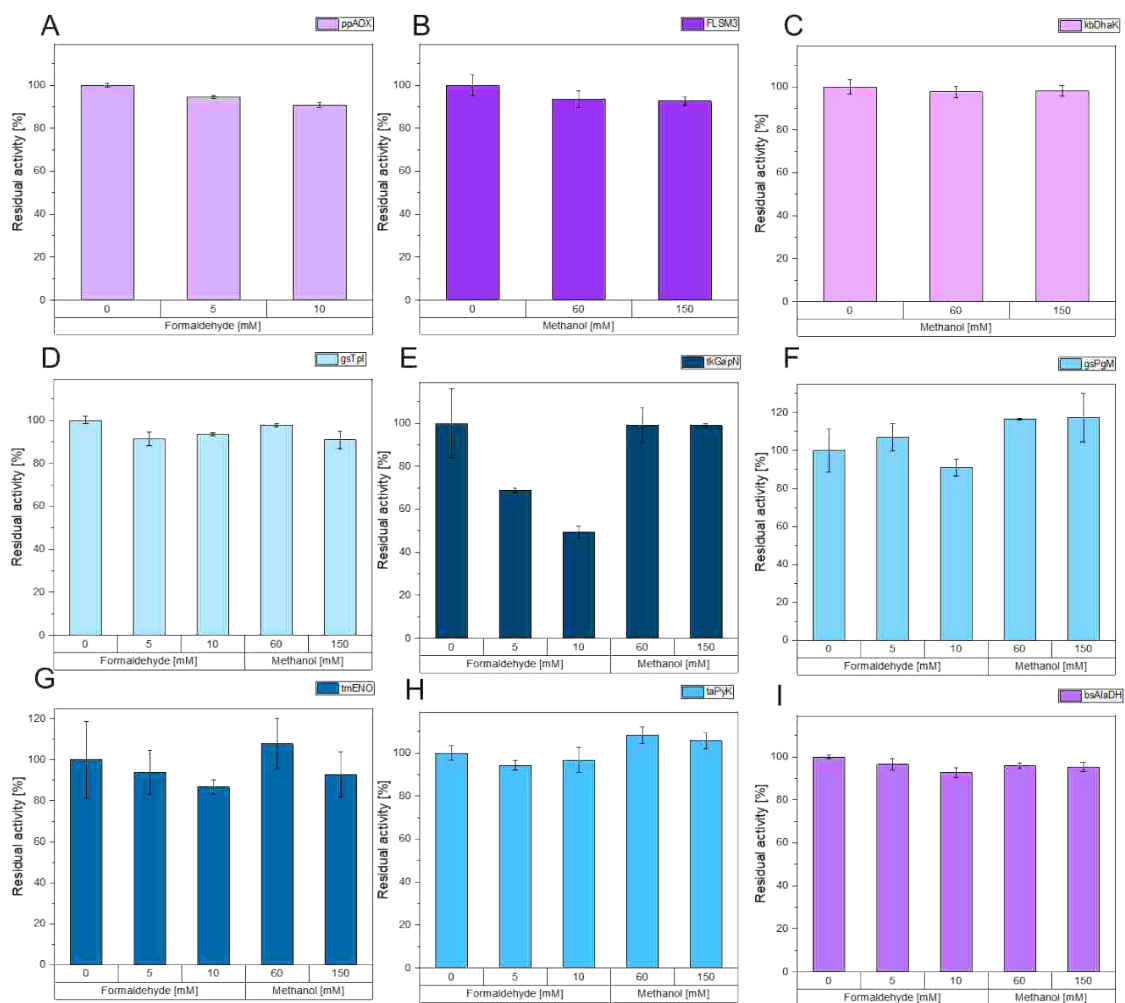


Figure S6.

Melting curves of cascade enzymes in cascade matrix without, with 5 mM and 10 mM formaldehyde addition. A: ppAOX, B: FLSM3, C: kbDhaK, D: gsTpI, E: tkGapN, F: gsPgm, G: tmENO, H: taPyK, I: bsAlaDH. Measurements were performed in triplicate ($n = 3$) and analysed as described in the methods. Error clouds represent SD.

**Figure S7.**

Activity of cascade enzymes with addition of various formaldehyde and methanol concentrations at 30 °C. A: ppAOX, B: FLSM3, C: kbDhaK, D: gsTpI, E: tkGapN, F: gsPgm, G: tmENO, H: taPyK, I: bsAlaDH. Measurements were performed in triplicate (n = 3) and analysed as described in the methods. Error bars represent SD.

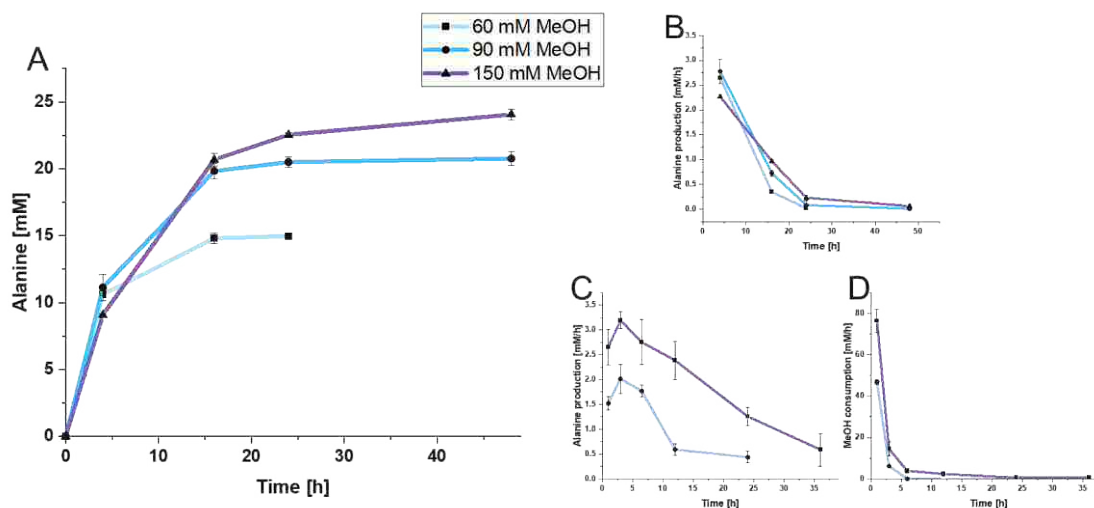


Figure S8.

Analysis of L-alanine production of MAP 1.0 as well as L-alanine production and methanol consumption rates of MAP 1.0 and MAP 2.0. A: Time course of L-alanine production of MAP 1.0 in mM with 60 mM, 90 mM and 150 mM substrate concentration. L-alanine production was monitored using HPLC detection by derivatisation with OPA. B,C,D: Rates of L-alanine production and methanol consumption with 60 mM, 90 mM and 150 mM substrate concentration B: MAP 1.0 L-alanine production rates, C: MAP 2.0 L-alanine production rates, D: MAP 2.0 methanol consumption rates. Reactions were performed in triplicate ($n = 3$) and analyzed as described in the methods. Error bars represent SD.

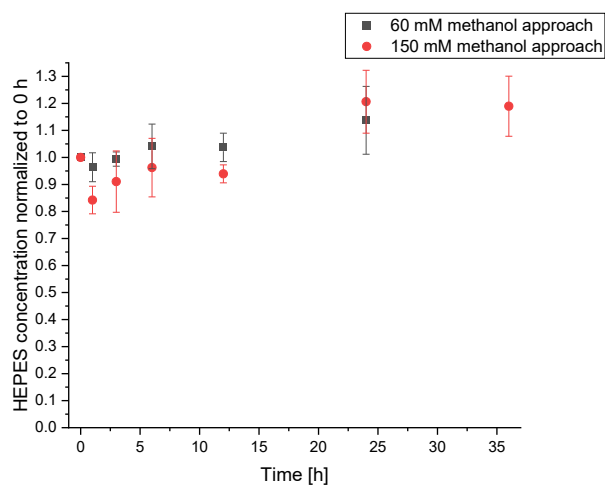


Figure S9.

Time course of HEPES buffer during the cascade. HEPES concentrations are normalized to the 0 h sample to detect evaporation effects. Reactions were performed in triplicate ($n = 3$) and analyzed as described in the methods. Error bars represent SD.

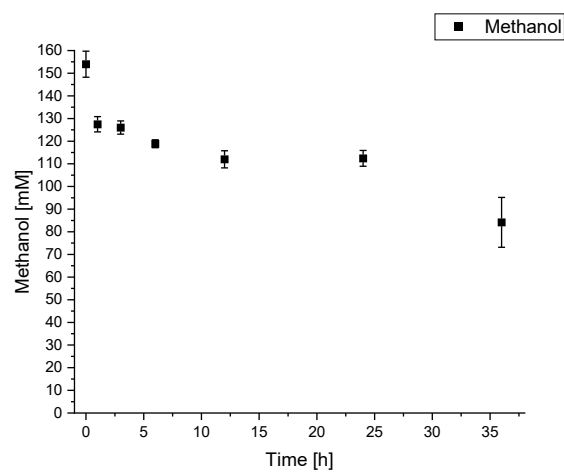


Figure S10.

Time course of methanol consumption of MAP 2.0 control experiment without addition of ppAOX and FLS. Reactions were performed in triplicate ($n = 3$) and analysed as described in the methods. Error bars represent SD.

Table S1.

Enzyme list with expression conditions, enzyme yield, cloning method, and origin organism.

Enzyme	Abb.	Molecular weight [Da]	NCBI Accession code	Organism	Restriction enzymes	Plasmid	Expression conditions	Enzyme yield [mg _{protein} /L _{cellculture}]
Alcohol oxidase	AOX	73898	XP_002494271.1	<i>Pichia pastoris</i>				
Catalase	CAT	57220	BAV22054.1	<i>Corynebacterium glutamicum</i>				70
Formolase/FormolaseM3	FLS/FLSM3	60313		Computational designed protein originated from <i>Pseudomonas fluorescens</i>	NdeI/XhoI	pET24a	TB-media. 25 °C	
Dihydroxyacetone kinase	DhaK	58475	WP_029604097.1	<i>Kozakia baliensis</i>	NdeI/XhoI	pET28a	ZY-media. 25 °C	128
Triosephosphate isomerase	TpI	29345	WP_033015090.1	<i>Geobacillus stearothermophilus</i>	NdeI/SacI	pET28a	ZY-media. 25 °C.	144
Glyceraldehyde-3-phosphate dehydrogenase	GapN	55488	BAD84894.1	<i>Thermococcus kodakarensis</i>	NdeI/XhoI	pET28a	ZY-media. 25 °C	6
Phosphoglycerate mutase	PgM	59166	WP_033015095.1	<i>Geobacillus stearothermophilus</i>	NdeI/SacI	pET28a	ZY-media. 25 °C	136
Enolase	ENO	49033	WP_004080719.1	<i>Thermotoga naphthophila</i>	BsaI/Klenow...	pET28a	ZY-media. 25 °C	4
Pyruvate kinase	PyK	61310	WP_010901306.1	<i>Thermoplasma acidophilum</i>	BsaI/Klenow...	pET28a	ZY-media. 25 °C	43
Alanine dehydrogenase	AlaDH	39684	NP_391071.1	<i>Bacillus subtilis</i>	XbaI/XhoI	pET28a	ZY-media. 16 °C	70
Assay enzyme	Abb.	Molecular weight [Da]	Accession code	Organism	Restriction enzymes	Plasmid	Expression conditions	
Glyceraldehyde-3-phosphate dehydrogenase	GapN	54950	ADL50400.1	<i>Clostridium cellulovorans</i>	NdeI/SacI	pET28a	ZY-media. 16 °C	111

Table S2.

Enzymatic reactions, estimated Gibbs energy and shadow price provided by MDF-Analysis by using default conditions of eQuilibrator pathway tool (pH 7.5, ionic strength: 0.25 M, pMg: 3.0). $\Delta_rG'^{\circ}$: Gibbs free energy of reaction at particular pH and ionic strength. $\Delta_rG'^m$: Reaction Gibbs energy in physiological conditions of 1 mM reactant concentrations. Δ_rG' : Reaction Gibbs energy after reactant concentration optimization. Shadow price: Measure of how a change in constraint change the MDF.^[S14]

Enzyme	Reaction formula	Relative flux	$\Delta_rG'^{\circ}$	$\Delta_rG'^m$	Δ_rG'	Shadow price
Alcohol oxidase	Methanol + O ₂ <=> H ₂ O ₂ + Methanal	3	-98.9	-98.8	-96.7	0.0
Catalase	3 H ₂ O ₂ <=> 1.5 O ₂ + 3 H ₂ O	1	-287.8	-262.2	-236.7	0.0
Formolase/FormolaseM3	3 Methanal <=> Glycerone	1	-80.6	-46.4	-41.3	0.0
Dihydroxyacetone kinase	Glycerone + ATP <=> Glycerone phosphate + ADP	1	-14.9	-14.9	-16.6	0.0
Triosephosphate isomerase	Glycerone phosphate <=> D-Glyceraldehyde 3-phosphate	1	5.6	5.6	-12.3	0.0
Glyceraldehyde-3-phosphate dehydrogenase	NAD ⁺ + D-Glyceraldehyde 3-phosphate + H ₂ O <=> NADH + D-Glycerate-3-phosphate	1	-48.0	-48.0	-32.8	0.0
Phosphoglycerate mutase	D-Glycerate-3-phosphate <=> D-Glycerate-2-phosphate	1	4.5	4.5	-11.1	> 0
Enolase	D-Glycerate-2-phosphate <=> Phosphoenolpyruvate + H ₂ O	1	-3.8	-3.8	-11.1	< 0
Pyruvate kinase	ADP + Phosphoenolpyruvate <=> Pyruvate + ATP	1	-25.0	-25.0	-12.9	0.0
Alanine dehydrogenase	Pyruvate + NH ₃ + NADH <=> L-Alanine + NAD ⁺ + H ₂ O	1	-33.6	-16.5	-15.5	0.0

Note: The thermodynamic data derived from the web interface of eQuilibrator (<https://equilibrator.weizmann.ac.il/>)

Table S3.

Final enzyme compositions and substrate concentrations for different cascade versions.

	DAP 1.0	MAP 1.0	MAP 2.0
Enzyme	Conc. [mg/ml]	Conc. [mg/ml]	Conc. [mg/ml]
Alcohol oxidase		0.10	0.10
FormolaseM3			13.20
Formolase		27.78	
Dihydroxyacetone kinase	0.11	3.30	3.30
Triosephosphate isomerase	0.03	7.50	0.03
Glyceraldehyde-3-phosphate dehydrogenase	3.00	3.00	3.00
Phosphoglycerate mutase	2.55	2.55	2.55
Enolase	0.30	0.30	0.30
Pyruvate kinase	4.10	4.10	4.10
Alanine dehydrogenase	0.02	0.02	0.02
Additional enzymes	Conc. [U/mL]	Conc. [U/mL]	Conc. [U/mL]
Catalase		10000	10000
Substrates	Conc. [mM]	Conc. [mM]	Conc. [mM]
DHA	20		
MeOH		150	150
ATP	2	2	2
NAD⁺	5	5	5
(NH₄)₂SO₄	200	200	200

Table S4.Enzyme kinetics of cascade enzymes.* enzyme kinetics calculated as described by Jia et al.^[S6]

Enzyme	k_{cat} [s^{-1}]	K_m [mM]	K_i [mM]	n	Source
ppAOX	5.7	0.6			[S20]
FLSM3	0.2375	23.59			[S21]
kbDhaK	15.91 \pm 3.86	0.03 \pm 0.01			This study
gsTpfI	154.05 \pm 3.39	3.60 \pm 0.11			This study
tkGapN	0.78 \pm 0.07	0.24 \pm 0.03*	6.84 \pm 1.78	0.52 \pm 0.03	This study
gsPgM	7.56 \pm 0.40	0.76 \pm 0.11			This study
tmENO	9.28 \pm 0.47	0.15 \pm 0.01			This study
taPyK	17.00 \pm 1.39	1.17 \pm 0.27			This study
bsAlaDH	58.24 \pm 3.75	0.12 \pm 0.01	2.59 \pm 0.29		This study

Table S5.

Enzyme activities in cascade matrix with additional substrates and cofactors used in activity assay.

Enzyme	Coupled enzyme	Cofactors	Substrate	Activity [U/mg]
ppAOX				12 -40 [Sigma]
FLSM3	DhaK. PyK. LDH	1 mM ATP. 1 mM PEP. 0.3 mM NADH	5 mM Formaldehyde	0.02 ± 0.0
kbDhaK	PyK. LDH	1 mM ATP. 1 mM PEP. 0.3 mM NADH	1 mM Dihydroxyacetone	8.4 ± 0.2
gsTpi	GAPDH, 3-PGK	2.5 mM NAD ⁺ , 5 mM Kpi, 1 mM ADP	1 mM Dihydroxyacetone phosphate	32.7 ± 1.3
tkGapN		5 mM NAD ⁺ .	1 mM Glyceraldehyde- 3-phosphate	0.3 ± 0.0
gsPgM	Eno. PyK. LDH	1 mM ADP. 0.3 mM NADH	1 mM 3- Phosphoglycerate	0.4 ± 0.0
tmENO	PyK. LDH	1 mM ADP. 0.3 mM NADH	1 mM 2- Phosphoglycerate	3.0 ± 0.0
taPyK	LDH	1 mM ADP. 0.3 mM NADH	1 mM PEP	7.2 ± 0.1
bsAlaDH		0.3 mM NADH	2.5 mM Pyruvate. 200 mM (NH ₄) ₂ SO ₄	40.5 ± 2.6.

Supplemental Reference and notes

- [S1]. Guterl, J.K., Garbe, D., Carsten, J., Steffler, F., Sommer, B., Reiß, S., Philipp, A., Haack, M., Rühmann, B., and Koltermann, A. (2012). Cell free metabolic engineering: production of chemicals by minimized reaction cascades. *ChemSusChem* 5, 2165-2172, doi:10.1002/cssc.201200365.
- [S2]. Williams, E.M., Copp, J.N., and Ackerley, D.F. (2014). Site-saturation mutagenesis by overlap extension PCR. In *Directed Evolution Library Creation*, (Springer), 1179, New York, NY, doi:10.1007/978-1-4939-1053-3_6.
- [S3]. Studier, F.W. (2005). Protein production by auto-induction in high-density shaking cultures. *Protein Expression Purif.* 41, 1, 207-234, doi:10.1016/j.pep.2005.01.016.
- [S4]. Gauss, D., Sánchez-Moreno, I., Oroz-Guinea, I., García-Junceda, E., and Wohlgemuth, R. (2018). Phosphorylation catalyzed by dihydroxyacetone kinase, *Eur. J. Org. Chem.* 2018: 2892-2895 doi:10.1002/ejoc.201800350.
- [S5]. Zhai, X., Amyes, T.L., and Richard, J.P. (2015). Role of loop-clamping side chains in catalysis by triosephosphate isomerase. *J. Am. Chem. Soc.* 137, 15185-15197, doi:10.1021/jacs.5b09328.
- [S6]. Jia, B., Linh, L.T., Lee, S., Pham, B.P., Liu, J., Pan, H., Zhang, S., and Cheong, G.-W. (2011). Biochemical characterization of glyceraldehyde-3-phosphate dehydrogenase from *Thermococcus kodakarensis* KOD1. *Extremophiles* 15, 337-346, doi:10.1007/s00792-011-0365-4.
- [S7]. Johnsen, U., and Schönheit, P. (2007). Characterization of cofactor-dependent and cofactor-independent phosphoglycerate mutases from Archaea. *Extremophiles* 11, 647-657. doi:10.1007/s00792-007-0094-x.
- [S8]. Currie, D.H., Guss, A.M., Herring, C.D., Giannone, R.J., Johnson, C.M., Lankford, P.K., Brown, S.D., Hettich, R.L., and Lynd, L.R. (2014). Profile of secreted hydrolases, associated proteins, and SlpA in *Thermoanaerobacterium saccharolyticum* during the degradation of hemicellulose. *Appl. Environ. Microbiol.* 80(16), 5001-5011. doi:10.1128/AEM.00998-14.

- [S9]. Rider, C., and Taylor, C. (1974). Enolase isoenzymes in rat tissues: Electrophoretic, chromatographic, immunological and kinetic properties. *Biochim. Biophys. Acta, Protein Struct.* *365*, 1, 285-300, doi:10.1016/0005-2795(74)90273-6, .
- [S10]. Potter, S., and Fothergill-Gilmore, L.A. (1992). Purification and properties of pyruvate kinase from *Thermoplasma acidophilum*. *FEMS Microbiol. Lett.* *94*, 3, 235-239, doi:10.1111/j.1574-6968.1992.tb05324.x.
- [S11]. Ye, W., Huo, G., Chen, J., Liu, F., Yin, J., Yang, L., and Ma, X. (2010). Heterologous expression of the *Bacillus subtilis* (natto) alanine dehydrogenase in *Escherichia coli* and *Lactococcus lactis*. *Microbiol. Res.* *165*, 268-275, doi:10.1016/j.micres.2009.05.008.
- [S12]. Garcia-Alles, L.F., Siebold, C., Nyffeler, T.L., Flükiger-Brühwiler, K., Schneider, P., Bürgi, H.-B., Baumann, U., and Erni, B. (2004). Phosphoenolpyruvate- and ATP-dependent dihydroxyacetone kinases: covalent substrate-binding and kinetic mechanism. *Biochemistry* *43*, 41, 13037-13045, doi:10.1021/bi048575m.
- [S13]. Sutiono, S., Pick, A., and Sieber, V. (2021). Converging conversion—using promiscuous biocatalysts for the cell-free synthesis of chemicals from heterogeneous biomass. *Green Chem.*, *23*, 3656-3663 doi:10.1039/D0GC04288A.
- [S14]. Noor, E., Bar-Even, A., Flamholz, A., Reznik, E., Liebermeister, W., and Milo, R. (2014). Pathway thermodynamics highlights kinetic obstacles in central metabolism. *PLoS Comput Biol.* *10*, e1003483, doi:10.1371/journal.pcbi.1003483.
- [S15]. Couderc, R., and Baratti, J. (1980). Oxidation of methanol by the yeast, *Pichia pastoris*. Purification and properties of the alcohol oxidase. *Agric. Biol. Chem.* *44:10*, 2279-2289, doi:10.1080/00021369.1980.10864320.
- [S16]. Gmelch, T.J., Sperl, J.M., and Sieber, V. (2019). Optimization of a reduced enzymatic reaction cascade for the production of L-alanine. *Sci Rep.*, *9*, 11754, doi:10.1038/s41598-019-48151-y.
- [S17]. Begander, B., Huber, A., Sperl, J., and Sieber, V. (2021). Development of a Cofactor Balanced, Multi Enzymatic Cascade Reaction for the Simultaneous Production of L-Alanine and L-Serine from 2-Keto-3-deoxy-gluconate. *Catalysts* *11*, 31, doi:10.3390/catal11010031.
- [S18]. Jo, H.-J., Kim, J.-H., Kim, Y.-N., Seo, P.-W., Kim, C.-Y., Kim, J.-W., Yu, H.-n., Cheon, H., Lee, E.Y., and Kim, J.-S. (2022). Glyoxylate carbonylase-based whole-cell biotransformation of formaldehyde into ethylene glycol via glycolaldehyde. *Green Chem.*, *24*, 218-226, doi:10.1039/D1GC03549E.
- [S19]. Dikshit, P.K., and Moholkar, V.S. (2016). Optimization of 1,3-dihydroxyacetone production from crude glycerol by immobilized *Gluconobacter oxydans* MTCC 904. *Bioresour. Technol.* *216*, 1058-1065. doi:10.1016/j.biortech.2016.01.100.
- [S20]. Koch, C., Neumann, P., Valerius, O., Feussner, I., and Ficner, R. (2016). Crystal Structure of Alcohol Oxidase from *Pichia pastoris*. *PLOS ONE* *11*, e0149846. 10.1371/journal.pone.0149846, doi:10.1371/journal.pone.0149846.
- [S21]. Cai, T., Sun, H., Qiao, J., Zhu, L., Zhang, F., Zhang, J., Tang, Z., Wei, X., Yang, J., Yuan, Q., et al. (2021). Cell-free chemoenzymatic starch synthesis from carbon dioxide. *Science* *373*, 1523-1527. doi:10.1126/science.abh4049.

7. Abbreviations

$(\text{NH}_4)_2\text{SO}_4$	Ammonium sulfate
°C	Degree celsius
μL	Micro liter
μm	Micro meter
ABTS	2,2'-Azino-di(3-ethylbenzthiazolin-6-sulfonsäure)
ADH	Alcohol dehydrogenase
ADP	Adenosine-5'-diphosphate
AI	Artificial intelligence
AlaDH	L-Alanine dehydrogenase
ALDH	Aldehyde dehydrogenase
AlsS	Acetolactate synthase
ATP	Adenosine-5'-triphosphate
bp	Base pair
C1	One carbon molecule
C3	Three carbon molecule
C4	Four carbon molecule
C5	Five carbon molecule
C6	Six carbon molecule
CaCl_2	Calcium chloride
CIP	alkaline phosphatase
CO	Carbon monoxide
CO_2	Carbon dioxide
CoA	Coenzyme A
Cu	Copper
Cu-ZnO	Copper-zinc oxide
CV	Column volume
DHA	Dihydroxyacetone
DhaK	Dihydroxyacetone kinase
DHAP	Dihydroxyacetone phosphate
DHAS	Dihydroxyacetone synthase
DMSO	Dimethyl sulfoxide
DNA	Deoxyribonucleic acid

Abbreviations

dNTP	Desoxyribonukleosidtriphosphate
<i>e.g.</i>	For example
<i>E. coli</i>	<i>Escherichia coli</i>
EDTA	Ethylenediaminetetraacetic acid
ENO	Enolase
FALD	Formaldehyde
FID	Flame ionization detector
FLS	Formolase
FLSM3	Formolase variant M3
FRET	Förster resonance energy transfer
FSA	Fructose-6-phosphate aldolase
g	gram
GA	Glycolaldehyde
GALS	Gycolaldehyde synthase
GapDH	Glyceraldehyde 3-phosphate dehydrogenase
GapN	Glyceraldehyde 3-phosphate dehydrogenase non-phosphorylating
GC	Gas chromatography
gDNA	Genomic DNA
Gt	Giga tonne
h	hours
H ₂	Hydrogen
H ₂ O	Water
H ₂ O ₂	Hydrogen peroxide
H ₂ SO ₄	Sulforic acid
HCl	Hydrochloric acid
HEPES	4-(2-hydroxyethyl)-1-piperazineethanesulfonic acid
HF-Buffer	High-Fidelity DNA Polymerase buffer
HILIC	Hydrophilic interaction chromatography
His ₆ Tag	Polyhistidin-Tag with six histidin
HPLC	High-performance liquid chromatography
IEA	International Energy Agency
IlvC	ketol-acid reductoisomerase
IlvD	dihydroxy-acid dehydratase
IMAC	immobilized metal ion affinity chromatography

iPROBE	In vitro prototyping and rapid optimization of biosynthetic enzymes
IPTG	Isopropyl β -D-1-thiogalactopyranoside
K ₂ HPO ₄	Dipotassium phosphate
kB	Kilo base
k _{cat}	Turnover number
KCl	Potassium chloride
kDA	Kilo Dalton
KDC	alpha-keto-acid decarboxylase
K' _{eq}	Equilibrium constant
KH ₂ PO ₄	Monopotassium phosphate
K _m	Michaelis Menten Konstant
KOH	Potassium hydroxide
kPa	Kilo pascal
L	Liter
LB	lysogeny broth
LC Column	Liquid chromatography column
LDH	Lactate dehydrogenase
MAP	Methanol to L-Alanine pathway
MDF	max-min driving force
MgCl ₂	Magnesium chloride
MgCl ₂ * 6H ₂ O	Magnesium chloride hexahydrate
MgSO ₄	Magnesium sulfate
MgSO ₄ * 7H ₂ O	Magnesium sulfate heptahydrate
Milli-Q water	Ultrapure water
min	Minute
mL min ⁻¹	Mili Liter per minute
mM	Milli molar
MnCl ₂	Manganese chloride
MnCl ₂ * 4H ₂ O	Manganese chloride tetrahydrate
Na ₂ HPO ₄	Disodium phosphate
NaCl	Sodium chloride
NAD ⁺	β -Nicotinamidadenindinucleotid
NADH	β -Nicotinamidadenindinucleotid reduced
NADP ⁺	β -Nicotinamidadenindinucleotidphosphat

Abbreviations

NADPH	β-Nicotinamidadeninucleotidphosphat reduced
NaH ₂ PO ₄	Monosodium phosphate
NaH ₂ PO ₄ * H ₂ O	Monosodium phosphate hydrate
NaOH	Sodium hydroxide
ng	Nano gram
nM	Nano molar
OD ₆₀₀	optical density measured at a wavelength of 600 nm
OPA	ortho-phthalaldehyde
PCR	Polymerase chain reaction
PEP	Phosphoenolpyruvate
PES	polyethersulfone
PgM	Phosphoglycerate mutase
pH	pH-Wert
PHB	Polyhydroxybuttersäure
PyK	Pyruvate Kinase
rpm	revolutions per minute
RT	Room temperature
RuMP	ribulose monophosphate pathway
SACA pathway	Synthetic Acetyl-CoA pathway
SAM	S-Adenosyl-Methionine
SBtab	SBtab is a set of syntax rules and conventions that simplify data processing and thereby facilitate data exchange
SDS-PAGE	Sodium dodecyl sulfate polyacrylamide gel electrophoresis
SEC	Size exclusion chromatography
slm	Standard liter per minute
SOB-medium	Super Optimal Broth-Medium
SOC-medium	Super Optimal broth with Catabolite repression-Medium
SOP	standard operating procedures
TAE-buffer	Tris-acetate-EDTA-buffer
TB	Terrific broth
TCA cycle	tricarboxylic acid cycle

Abbreviations

TEMED	Tetramethylethylenediamine
TktA	Transketolase
T_M	Melting temperature
T_m	Melting point
TpI	Triosephosphate isomerase
TPP	Thiamine pyrophosphate
Tris	Tris(hydroxymethyl)aminomethane
TTN	total turnover number
TUM	Technical University of Munich
U	Unit
UV	Ultraviolet
V	Voltage
$v\% v^{-1}$	Volume% per volume
$w v^{-1}$	Weight per volume
$w w^{-1}$	Weight per weight
X1P	xylulose-1-phosphate
g	G force
XI pathway	xylose Isomerase pathway
XR/XDH pathway	xylose reductase/ xylose dehydrogenase pathway
XuMP	Xylulose monophosphate pathway
XylA	Xylulose isomerase
XylB	Xylulokinase
YahK	Alcohol dehydrogenase of <i>Escherichia coli</i>
YjgB	Alcohol dehydrogenase of <i>Escherichia coli</i>
YqhD	Alcohol dehydrogenase of <i>Escherichia coli</i>
ZnO	Zinc oxide

8. List of Tables

Table 1: Differences between in vitro and in vivo enzymatic cascade reactions	10
Table 2: List of devices	20
Table 3: Software and databases used in this study.....	25
Table 4: Chemicals used in this study	26
Table 5 Commercial Kits	30
<i>Table 6: Commercial enzymes for assays used in this study</i>	<i>31</i>
Table 7: Commercial Enzymes used in this study.....	32
<i>Table 8: Microorganisms carry genes of interest</i>	<i>33</i>
Table 9: Oligonucleotides used in this study. The highlighted segment represents the cutting site for the restriction enzymes used. The annealing temperature (T_a) of oligonucleotides was calculated via the NEB Tm Calculator web application for Phusion® High-Fidelity DNA Polymerase with Phusion® High-Fidelity DNA Polymerase buffer (HF-Buffer) and an oligonucleotide concentration of 500 nM.....	34
Table 10: Plasmids used in this study	36
Table 11: Standard PCR scheme.....	41
<i>Table 12: Colony PCR scheme.....</i>	<i>42</i>
Table 13: Primer combinations for overlap extension PCR to create FLSM3.	42
<i>Table 14: Buffers and solutions for agarose gel electrophoresis.....</i>	<i>44</i>
Table 15: Buffers and media for the preparation of chemically competent Escherichia coli cells	46
<i>Table 16: Buffer, media and solutions used in the transformation of chemically competent cells.</i>	<i>47</i>
<i>Table 17: Buffers and Media used for protein production</i>	<i>48</i>
Table 18: Preparation of auto-induction medium and TB-medium.....	48
Table 19: Buffers for the cell lysis	49
Table 20: Buffers for the ÄKTA™ purifier system	50
Table 21: Buffers and solutions used for SDS-PAGE.....	53
<i>Table 22: Preparation of SDS-gels</i>	<i>55</i>
Table 23: Concentration of enzymes during incubation and final dilution of enzymes in Assay	63
Table 24: Concentration of enzymes during incubation and final dilution of enzymes in Assay	64
Table 25: Buffers used for quantification of metabolites via HPLC	67
Table 26: Buffers used for quantification of metabolites via HPLC	68
Table 27: Buffers for L-alanine quantification via fluorescamine	70
Table 28: SBtab file for the MDF analysis of the methanol to L-alanine pathway	107

9. List of Figures

Figure 1: Comparison of Earth Overshoot Days and German Overshoot Days continuous between 1971 and 2018 plus the dates for 2022 and 2023. Thereby the dates for the German Overshoot Days were calculated based on day numbers extracted from the public data package of National Footprint and Bio-capacity Accounts 2022 Public Data Package and the data for 2023. Earth Overshoot Days were extracted from overshootdays.com based on National Footprint and Bio-capacity Accounts 2022 dataset and the data for 2023 ¹⁻⁵	2
Figure 2: Natural pathways of xylose utilization adapted from Zhao et al. ¹⁰ . The gray arrow indicates the metabolism of xylose via the pentose phosphate pathway. The red arrow indicates the metabolism of xylose via the phosphoketolase reaction. The green arrow indicates the metabolism of xylose via the xylulose monophosphate pathway (XuMP) involving formaldehyde. The blue arrow indicates the metabolism of xylose via the Dahms pathway and the yellow arrow indicates the metabolism of xylose via the Weimberg pathway.	4
Figure 3: Schematic representation of concepts of biocatalysis, electrocatalysis, photocatalysis, homogenous- and heterogenouscatalysi for the production of methanol from CO ₂ adapted from Navarro-Jaén et al. ⁵⁰	6
Figure 4: Concepts of enzymatic cascade systems adapted from Benítez-Mateos et al. ⁹³ , whereby S is the substrate, I is an intermediate, P is the product and E is an enzyme. A: Linear cascade. B: Cyclic cascade. C: Parallel cascade. D: Orthogonal cascade. E: Triangular cascade	12
Figure 5: Schematic representation of the production of biofuels from CO ₂ and lignocellulosic biomass (A) as well as L-alanine production from CO ₂ (B).	17
Figure 6 Correlation between melting point (T _m) and isobutanol tolerance of different cascade enzymes represented as activity of the enzymes after 24 h incubation in isobutanol at 37 °C. Activity after 24 h was normalized to activity at 0 h without the addition of isobutanol.	78
Figure 7: Schematic representations of equilibria between dihydroxyacetone, glycerol and D-glyceraldehyde adapted from Walgode et al. ¹⁸⁰ Equilibrium constants were calculated via the Equilibrator web tool (eQuilibrator 3.0 with a pH of 7.5, a pMG of 3.0 and an ionic strength of 0.25 ¹⁴²).	80
Figure 8: Formaldehyde conversion via cyclic xylulose monophosphate pathway (XuMP), ribulose monophosphate pathway (RuMP) and serine pathway together with linear formaldehyde assimilation pathways via formolase (FLS), glycolaldehyde synthase (GALS), glyoxylate carboligase (GCL) and fructose-6-phosphate aldolase (FSA).	82
Figure 9: Proposed valine pathway from methanol alone or in combination with xylose	91
Figure 10: Activity of ccGapN on glyceraldehyde 3-phosphatase from fructose 1,6-bisphosphate in a coupled assay system with aldolase over a time period of 20 h. The assay was conducted as described in Section 2.2.3 and 2.2.4.	105
Figure 11: Activity of ccGapN on glyceraldehyde 3-phosphatase from fructose 1,6-bisphosphate in a coupled assay system with aldolase with addition of either NADP ⁺ or NAD ⁺ as cofactor.. The assay was conducted as described in Section 2.2.3 and 2.2.4.	105
Figure 12: Formaldehyde tolerance (Section 2.2.6.3) over a time period of 24 h at 37 °C of A: taPyK, B: tmENO, C: kbDhaK. Activity was measure as described in Section 2.2.3.	106
Figure 13: Isobutanol tolerance (Section 2.2.6.5) over a time period of 32 h at 37 °C of A: pfXylA, B: kbDhaK, C: tmTpi_fusPgK, D: tkGapN, E: gsPgM, F: tmENO. Activity was measure as described in Section 2.2.3.	106
Figure 14: Isobutanol tolerance (2.2.6.5) over a time period of 32 h at 37 °C of A: taPyK, B: bsAlsS, C: gslIvC D: llKDC, E: ecYjgB. Activity was measure as described in 2.2.3.	107

10. List of Formulas

Formula 1: $\epsilon_{\text{prot}280} = N_{\text{Tyr}} * \epsilon_{\text{Tyr}280} + N_{\text{Trp}} * \epsilon_{\text{Trp}280} + N_{\text{Cystine}} * \epsilon_{\text{Cystine}280}$	51
Formula 2: $c_{\text{prot}} = A_{280d} * \epsilon_{\text{prot}(280)} * MW_{\text{prot}}$	52
Formula 3: $v = a * V_{\text{ges}} * D_f / (V_{\text{enz}} * \epsilon_{\text{NADH}} * d * \text{cenz})$	56
Formula 4: $y = v_{\text{max}} * x / (K_m + x)$	61
Formula 5: $y = v_{\text{max}} * x_n / (k_n + x_n)$	61
Formula 6: $y = A_1 * \exp(-x/t_1) + y_0$	66
Formula 7: $IC_{50} = (LN_{50} - y_0) / A_1 * t_1$	66